A sedimentological and structural analysis

of the Proterozoic Uncompahgre Group,

Needle Mountains, Colorado

by

Charles William Harris

Dissertation submitted to the Faculty of the

Virginia Polytechnic Institute and State University

in partial fulfillment of the requirements for the degree of

Doctor of Philosophy

in

Geology

APPROVED:

Kenneth A. Eriksson, Chairman

Carol Simpson

Lynn Glover, III

J. Fred Read

J. Alexander Speer

October, 1987

Blacksburg, Virginia

A sedimentological and structural analysis of the Proterozoic Uncompahgre Group, Needle Mountains, Colorado

by

Charles William Harris

Kenneth A. Eriksson, Chairman

Geology

(ABSTRACT)

Siliciclastic sediments of the Proterozoic Uncompahgre Group can be subdivided into stratigraphic units of quartzite (Q) and pelite (P); these units include a basal, fining- and thinning-upward retrogradational sequence (Q1-P1) that records the transition from an alluvial to a shallow-marine setting. Overlying the basal sequence are three thickening- and coarsening-upward progradational sequences (P2-Q2, P3-Q3 and P4-Q4) that were influenced by tide-, storm- and wave-processes. The progradational units are subdivided into the following facies associations in a vertical sequence. Outer- to inner-shelf mudstones, Bouma sequence beds and storm beds of association A are succeeded by inner-shelf to shoreface cross-stratified sandstones of association B. Conglomerates and cross-bedded sandstones of upper association B represent alluvial braid-delta deposits. Tidal cross-bedded facies of the inner shelf/shoreface (association C) gradationally overlie association B. Interbedded within the tidal facies in upper association C are single pebble layers or <1 m-thick conglomerate beds and trough cross-bedded pebbly sandstones. Single pebble layers could be due to storm winnowing whereas conglomerates and pebbly sandstones may record shoaling to an alluvial/shoreface setting.

A temporally separated storm/alluvial and tidal shelf model best explains the origin and lateral distribution of facies in the progradational sequences. The presence of

smaller progradational increments in the mudstone dominated units (P3) and the recurrence of facies associations in the thick quartzite/conglomerate units (Q2, Q3, Q4) suggests that external cyclic factors controlled sedimentation. A composite relative sea level curve integrating glacio-eustatic oscillations and long-term subsidence may account for the evolution of the thick progradational sequences of the Uncompahgre Group.

Sedimentary rocks of the Uncompahgre Group have been subjected to polyphase deformation and greenschist facies metamorphism. Phase 1 structures (localized to the West Needle Mountains) include bedding-parallel deformation zones, F_1 folds and an S_1 cleavage. Phase 2 coaxial deformation resulted in the development of upright, macroscopic F_2 folds and an axial-planar crenulation cleavage, S_2. In addition basement-cover contacts were folded. Phase 3 conjugate shearing generated strike-parallel offset in stratigraphic units, a macroscopic F_3 fold, and an S_3 crenulation cleavage. In addition, oblique-slip, reverse faults were activated along basement-cover contacts.

The Uncompahgre Group unconformably overlies and is inferred to be parautocthonous upon ca. 1750 Ma gneissic basement that was subjected to polyphase deformation (D_B) and amphibolite facies metamorphism. Basement was intruded by ca. 1690 Ma granitoids. Deformation of gneissic and plutonic basement together with cover (D_{BC}) postdates deposition of the Uncompahgre Group. The structural evolution of the Uncompahgre Group records the transition from a ductile, north-directed, fold-thrust belt to the formation of a basement involved "megamullion" structure which was subjected to conjugate strike-slip faulting to accommodate further shortening. D_{BC} deformation may be analogous to the deep foreland suprastructure of an orogenic belt that developed from ca. 1690 to 1600 Ma in the southwestern U.S.A..

Acknowledgements

"Mountains should be climbed with as little effort as possible and without desire. The reality of your own nature should determine the speed. If you become restless, speed up. If you become winded, slow down. You climb the mountain in an equlibrium between restlessness and exhaustion. Then, when you're no longer thinking ahead, each footstep isn't just a means to an end but a unique event in itself. *This* rock looks loose. From *this* place the snow is less visible, even though closer. These are things you should notice anyway. To live only for some future goal is shallow. It's the sides of the mountain which sustain life, not the top. Here's where things grow.

But of course, without the top you can't have any sides. It's the top that *defines* the sides. So on we go . . . we have a long way . . . no hurry . . . just one step after the next"

from *Zen and the Art of Motorcycle Maintenance*
by Robert M. Pirsig; William Morrow and Co., Publishers.

Maturation often comes with difficulty and hardship but proves to be the real strength of a foundation for future growth. Dr. Ken Eriksson, my dissertation advisor, provided encouragement and guidance that helped to aid in the completion of this project. Ken and I, despite our strong wills, stubbornness and emotional volatility, were able to forge ahead and grow, both in our science and personalities. Nonetheless between the two of us there pervades an aura of respect and subtle friendship. Dr. Carol Simpson encouraged my expansion of the dissertation to include structural geology and helped clarify a major aspect of this study. In addition, Carol's criticisms kept me on my toes regarding fundamental concepts in structural geology. Dr. Fred Read planted the seed for the idea of trying to apply cycle stratigraphy to siliciclastic sediments, when it had been purported "it could never be done!". Drs. Lynn Glover, III and J. Alex Speer

generously supplied their review time and expertise in evaluating the final versions of the dissertation. Dr. Jack Ellingson first introduced me to the Needle Mountains area in 1976. Later, both he and Drs. Rob Blair and Jack Campbell of Ft. Lewis College in Durango, Colorado, provided both logistical support and welcome moments of conversation during my summers in the field. I thank Dr. Barbara Tewksbury of Hamilton College, Clinton, New York, for sharing her dissertation work and ideas with me during the initial phase of this study. Becky Houston (Exxon Production Co.), generously provided a copy of her Master's thesis work on the Uncompahgre Group in the Lime Creek area. Finally, I would like to thank Dr. Dave Wones, posthumously, for his willingness to gamble on me, in spite of my detractors, during the first and second summers of this project. He would have been pleased to know the debt has been paid.

Special thanks and gratitude are extended to my many graduate student colleagues and in particular to my friends Ed Simpson, Judy Patterson and Rich Gibson. Judy and Ed provided philosophical and scientific feedback and valuable emotional support. Rich gave very freely of his ideas both in the field and office and greatly benefitted the portion of this dissertation related to structural geology. Other colleagues I would like to recognize include: Hank and Debbie Randall, Jim and Ginnie de Luca, Kris Soegaard, Fred Wehr, Roger Barnaby, John Hogan, Mark Crowell, Dave Weary, Julie Herman, Mike Wizevich, Isabel Montanez and Janet Schweitzer Gibson.

Field assistants Jeff Stein and Dave Cole are thanked for their time and effort in dealing with the vagaries of sedimentology and structural geology. I especially admire Jeff Stein's patience and willingness to suffer through the exaceberations of insects, cool, damp-wet! weather and the sometimes intractable behaviour of his supervisor during two summers.

Technical assistance was provided by Llyn Sharp (photographic laboratory), Kathy Hawkins and Sharon Chiang (drafting expertise), and Marge Dellers (GML, Script).

As a note of professional recognition, the third paper of this dissertation represents an equal collaborative effort of Rich Gibson and myself, improved by reviews of K.A. Eriksson, C. Simpson, P.F. Hoffman and K. Karlstrom. This paper is now completed and published in the scientific journal, *Geology*.

Funding for this project was provided by the Virginia Tech Educational Foundation and National Science Foundation Grant no. EAR 8507811 awarded to Dr. K.A. Eriksson.

In conclusion, I dedicate this effort to the family members who supported me in every facet of my life; my mother, Margaret T. Harris, my aunt and uncle, Edna and Frank Britton, and to the memories of my stepfather, William Reed Harris, Jr. and my father Charles Mark Meyers.

Table of Contents

List of Illustrations

List of Tables

Chapter 1: Progradational Sequences in the Early Proterozoic Uncompahgre Group, southwest Colorado: Cyclic Controls on Shallow-marine Sedimentation in a Storm- to Tide-dominated Shelf

ABSTRACT

Siliciclastic sediments of the early Proterozoic Uncompahgre Group include three (500 to 800 m thick) thickening- and coarsening-upward sequences (P2-Q2, P3-Q3, and P4-Q4) that were influenced by tide-, storm-, and wave-processes. The progradational units are subdivided into the following facies assocations in a vertical sequence. Outer- to inner-shelf mudstones, Bouma sequence beds and storm beds of association A are succeeded by inner-shelf to shoreface cross-stratified sandstones of association B. Conglomerates and cross-bedded sandstones of the upper part of association B are inferred to have been deposited on an alluvial braid delta. Tidal cross-bedded facies of the inner shelf/shoreface (association C) gradationally overlie association B. Interbedded with the tidal facies in upper association C are single pebble layers or <1 m thick, conglomerate beds and trough cross-bedded pebbly sandstones. Single pebble layers could be due to storm winnowing on the inner shelf whereas conglomerates and pebbly sandstones may record shoaling to alluvial/shoreface conditions.

Two models of sedimentation may explain the origin and lateral distribution of facies in the progradational sequences: 1) a coeval storm and tidal shelf or 2) a temporally separated storm/alluvial and tidal shelf. The first model has been employed as a viable means for explaining the vertical transistion of facies in prograding shallow-marine shelf

sequences overprinted by tides, waves and storms. However several factors are not accounted for in this model, such as variable subsidence rates, eustasy, sediment supply and offshelf sediment transport paths. In the Uncompahgre Group it is not possible to trace tidal sand bodies laterally into storm beds. In addition, shoreface and alluvial facies in upper associations A and B, which both underlie association C, precludes application of Walther's Law and invalidates the coeval storm and tidal shelf model. A temporally separated storm/alluvial and tidal shelf model is thus preferred. The presence of smaller progradational increments in the mudstone dominated units (P3) and the recurrence of facies associations in the thick quartzite/conglomerate units (Q2, Q3, Q4) suggests that external cyclic factors are controlling sedimentation. A composite relative sea level curve incorporating glacio-eustatic effects and episodic long-term subsidence may account for the evolution of the thick, shallow-marine to alluvial sequences of the Uncompahgre Group.

INTRODUCTION

Thick sequences of quartz-rich siliciclastic sedimentary rocks have been interpreted as shallow-marine to alluvial sediments and range from Phanerozoic to Archean in age (see for example, Anderton, 1976; Hobday and Tankard, 1978; Levell, 1980b; Watchorn, 1980; Eriksson *et al.*, 1981; Cotter, 1983; Dott, 1983; Soegaard and Eriksson, 1985; Simpson and Eriksson, 1986). The majority of these units were deposited in marine environments under the influence of tides, storms and waves. Other processes which may entrain sediment but so far have not been documented in the rock record include intrabasinal wind-driven and thermo-haline currents or intruding oceanic currents (Harms *et al.*, 1982; Walker, 1984; Reading, 1986). Hydraulic processes cannot always adequately explain the distribution of facies in modern or ancient sedimentary se-

quences. Problems not clearly resolved in terms of process alone include: 1) the contemporaneous lateral transition from a tide- to storm-dominated shelf (Anderton, 1976; Soegaard and Eriksson, 1985) versus a temporal change from a storm- to a tide-dominated shelf (Klein, 1982; Nummedal, 1986a,b); 2) the efficacy of storm-induced currents to transport sediment great distances offshore (Hayes, 1967; Nelson, 1982; Aigner and Reineck, 1982; Allen, 1984; Walker, 1984; Hobday and Morton, 1984; Niedoroda *et al.*, 1984; Aigner, 1985); and 3) the presence of extensive conglomerates and/or sand bodies in shallow-marine settings as either part of, or detached from the shoreface (Leckie and Walker, 1982; Leithold and Bourgeois, 1984; Tillman and Martinsen, 1984; Bergman and Walker, 1986). In light of the recognition of eustatic variation through geologic time (Vail *et al.*, 1977) and its influence upon carbonate (Read *et al.*, 1986; Grotzinger, 1986) and siliciclastic (Frazier, 1974; Weimer, 1984; Bergman and Walker, 1986; Nummedal, 1986a,b; Plint *et al.*, 1986) sedimentary packages, eustatic changes may account for features not explained by hydraulic processes. The duration and magnitude/rate of tectonic subsidence may be an equally important factor in controlling the evolution and preservation potential of a sedimentary package (Aigner, 1985; Ettensohn, 1985).

Two important problems in Precambrian sedimentological studies are: 1) discriminating alluvial from marine environments, and 2) recognizing unconformities. In Phanerozoic sedimentary rocks, facies and paleoenvironments can often be linked with specific biogenic structures and/or fossils (Thayer, 1983; Ekdale *et al.*, 1984). Precambrian rocks greater than 700 million years-old do not contain body or trace fossils but do provide a superb record of physical processes in all environments whereas in the Phanerozoic biological activity destroys primary structures in shelf environments (Bambach and Sepkoski, 1979; Miller and Byers, 1984). Unconformities are difficult to recognize without adequate lateral exposure, especially in transitional marine to alluvial

environments (Christie-Blick and Levy, 1985, 1986; Bergman and Walker, 1986; Plint *et al.*, 1986). The possible occurrence of unconformities in thick sedimentary packages requires that Walther's Law be used with caution when interpreting paleoenvironments from the vertical and lateral distribution of facies.

This study focuses on the Proterozoic Uncompahgre Group of southwest Colorado, an approximately 3 km-thick succession of mudstone, sandstone and conglomerate. Facies associations are recognized and related to specific marine or alluvial depositional regimes. Where process interpretations are equivocal, criteria are developed for discriminating marine from alluvial environments. Conceptual process-response models (synthetic cycles) are proposed which address the problem of variable relative sea level excursions or subsidence rates and their controls on facies sequences and likewise the distribution of paleoenvironments. The results of this study may be applicable to other thick shallow-marine successions of Precambrian age which span a large portion of the first 3 billion years of earth history.

REGIONAL GEOLOGY

Precambrian rocks in southwest Colorado are exposed as basement inliers (Fig. 1-1) surrounded by extensive Phanerozoic cover rocks. Basement to the Uncompahgre Group consists of *ca.* 1.75 Ga gneisses and amphibolites which were intruded by *ca.* 1.7 Ga granitic plutons and dikes (Silver and Barker, 1968; Barker, 1969; Bickford *et al.*, 1969). Deposition of the Uncompahgre Group upon the older basement rocks was followed by deformation and greenschist facies metamorphism of both basement and cover (Barker, 1969; Gibson and Simpson, 1986; Harris *et al.*, 1987). An upper age limit for the Uncompahgre Group and its deformation is defined by cross-cutting *ca.* 1.45 Ga granitic batholiths (Barker, 1969).

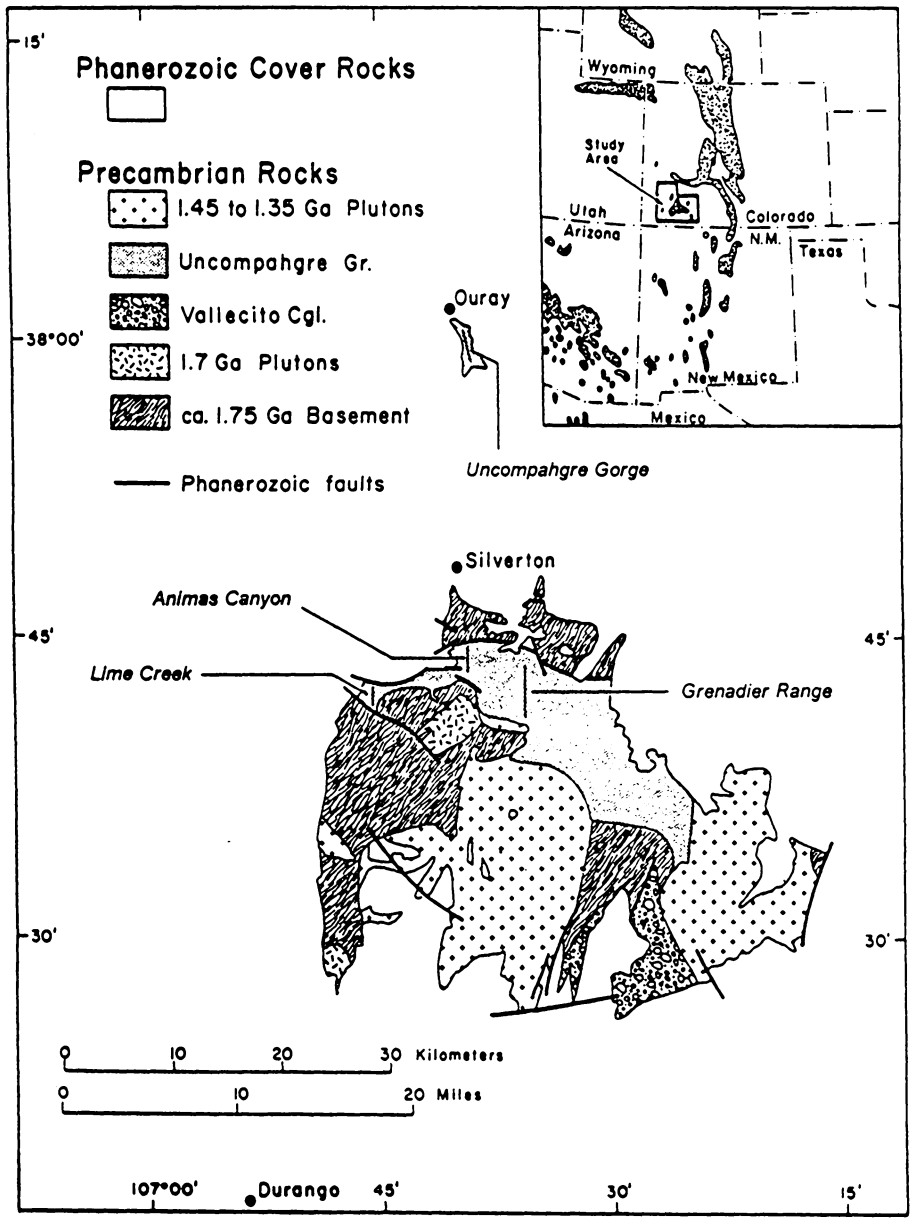

Figure 1-1: Distribution of Precambrian rocks in southwest Colorado. Inset shows location of study area in relation to exposures of other Precambrian rocks (shaded) in the southwest U.S.A.. Compiled from Barker (1969) and Condie (1982). Locations of compiled sections labeled on map.

The Uncompahgre Group is subdivided into lithostratigraphic units of quartzite ± conglomerate (Q) and pelite (P) (Fig. 1-2). A basal 500 m-thick fining-upward unit (Q1) is overlain by three, 600 to 300 m-thick, upward-coarsening and thickening units (Q2, Q3, Q4) separated from one another by 100 to 300 m-thick units of pelite (P1, P2, P3, P4 and P5). The basal retrogradational sequence of Q1-P1 records the transition from alluvial to shallow-marine environments (Harris and Eriksson, 1987). This paper will focus on the three progradational sequences (P2-Q2, P3-Q3, P4-Q4). Smaller-scale, 10 to 30 m-thick, upward-coarsening and -thickening sandstone units are present within the P3 unit. Because of deformation and metamorphism, the sedimentary rocks are now metaquartzites and metapelites. Nevertheless, the generally superb preservation of primary sedimentary structures, including detrital grains, permits description of these metasediments in terms of their protoliths, e.g. mudstone, siltstone, sandstone and conglomerate. Mudstones are both carbonaceous and aluminous. Quartz-rich sandstones and siltstones are quartz arenites and sublitharenites. Conglomerates are generally polymictic with a dominant vein quartz component and subordinate fraction of iron-formation, chert, quartzite and rhyolite.

The paleoslope of the basin is inferred to have been to the southwest based on a gradual thickening and increase in grain size of stratigraphic units to the north and east (Fig. 1-3). Localities of compiled sections are shown on Fig. 1-1.

SEDIMENTOLOGY: FACIES ANALYSIS

Progradational sequences in the Uncompahgre Group are subidvided into three generalized recurring facies associations A, B, and C which are recognized in a vertical sequence. These associations represent a transition from an outer-shelf to inner-shelf environment which may have periodically shoaled to alluvial/shoreface conditions.

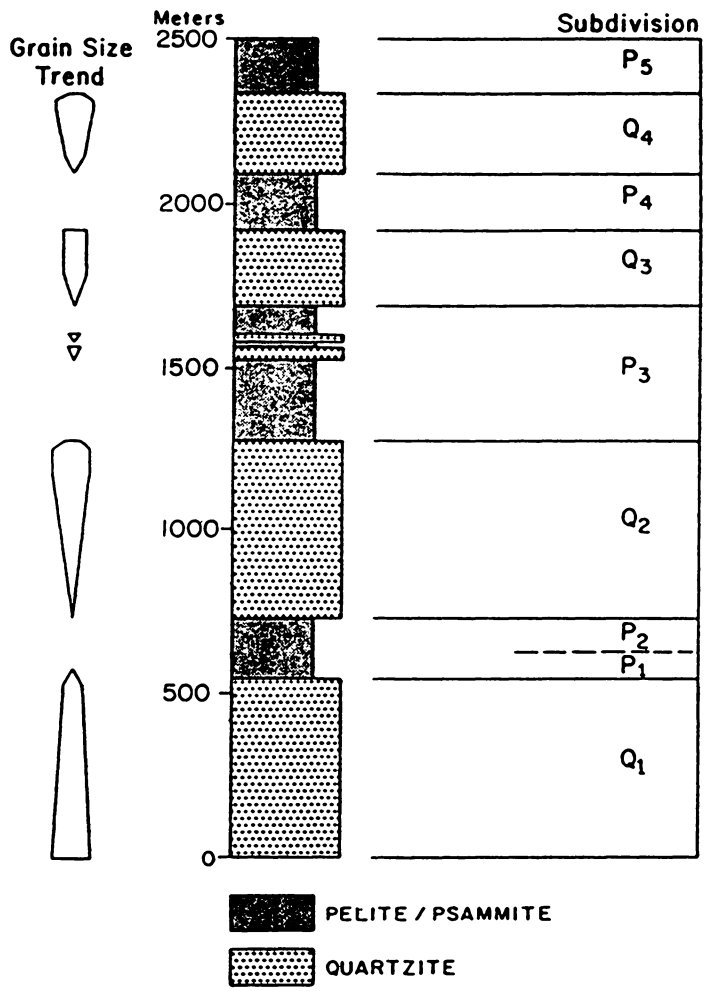

Figure 1-2: Stratigraphic subdivisions of the Uncompahgre Group.

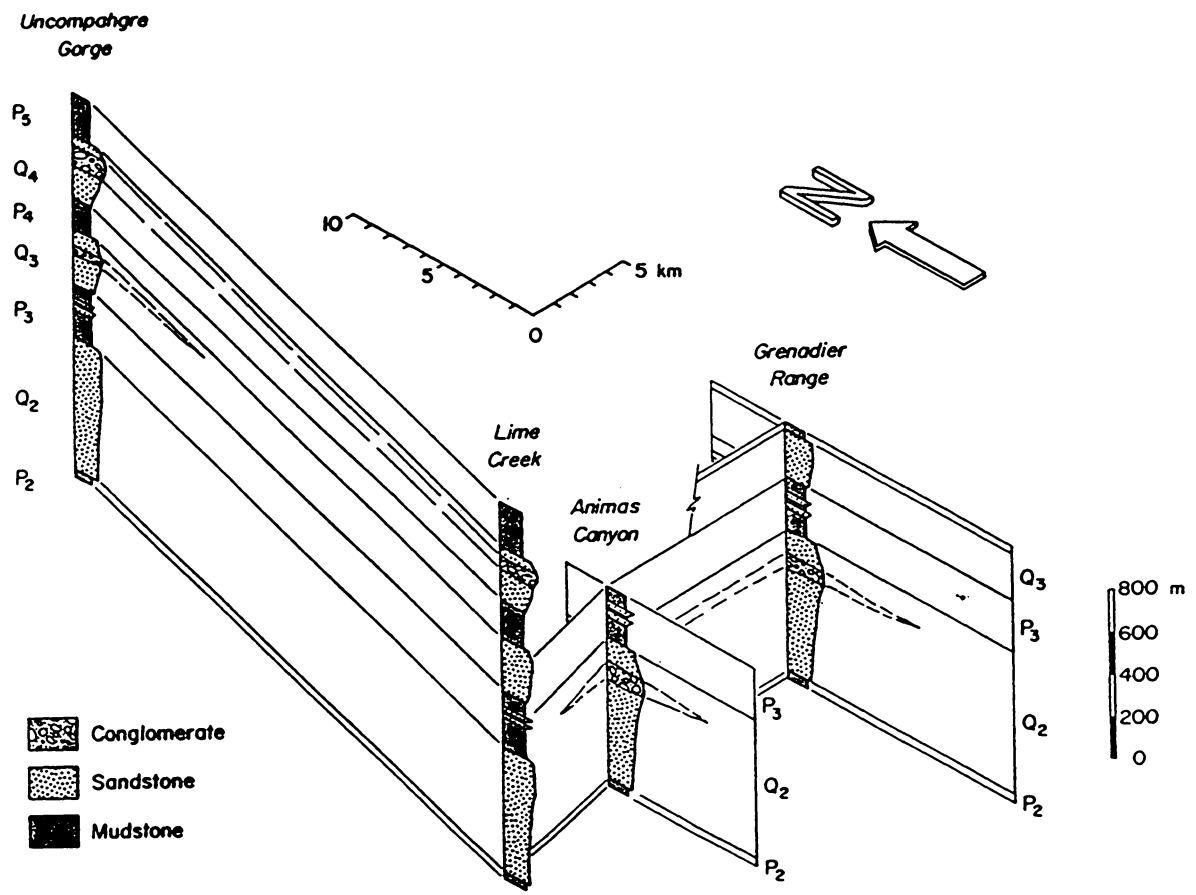

Figure 1-3: Fence diagram for Uncompahgre Group. Location of compiled sections shown on Fig. 1-1.

Facies Association A: Outer to Inner Shelf/Shoreface

Description

Four major facies groupings are recognized in association A; these consist of 1) mudstone and carbonaceous mudstone, 2) Bouma sequence beds with intercalated mudstone, 3) rippled- and parallel-laminated sandstone with interbedded mudstone, and 4) hummocky to trough cross-stratified sandstone (Fig. 1-4). This group of facies, in the order listed, is best exemplified by the P2-Q2 and P4-Q4 sequences. Most rocks of association A are thinly laminated to very thinly bedded mudstone. Internally mudstone beds contain laterally continuous 1 to 5 mm-thick laminae. In carbonaceous mudstone, 1 to 3 mm thick pyritiferous layers are present. In the vertical sequence there is a gradual increase in the abundance of siltstone and sandstone. These thinly laminated to thinly bedded units (0.2 to 5 cm thick) consist of fine-grained sandstone which may grade upward into siltstone capped by mudstone (Fig. 1-4a) Individual sandstone beds are sharp-based without pervasive loading structures or flute casts. Internal structures include parallel- or ripple cross-laminae, which are 1 to 2 mm thick and fine upward. When present, overlying siltstones may be either laminated or massive. Interbedded mudstones are 1 to 5 cm thick. The vertical succession of sedimentary structures is similar to that of a Bouma sequence (Bouma, 1962) in which the following subdivisions are recognized: Tbde, Tbcde and Tde.

Overlying the previous facies are thin- to medium-bedded sandstones which are separated by mudstone <2 cm thick (Fig. 1-4b). Beds of parallel-laminated sandstone contain thinning- and fining-upward, 1 to 3 mm-thick laminae, consisting of coarse- to very fine-grained sand and silt. Fine- to medium-grained, ripple cross-laminated sandstone contains a complex, often bidirectional internal stratification; ripples are

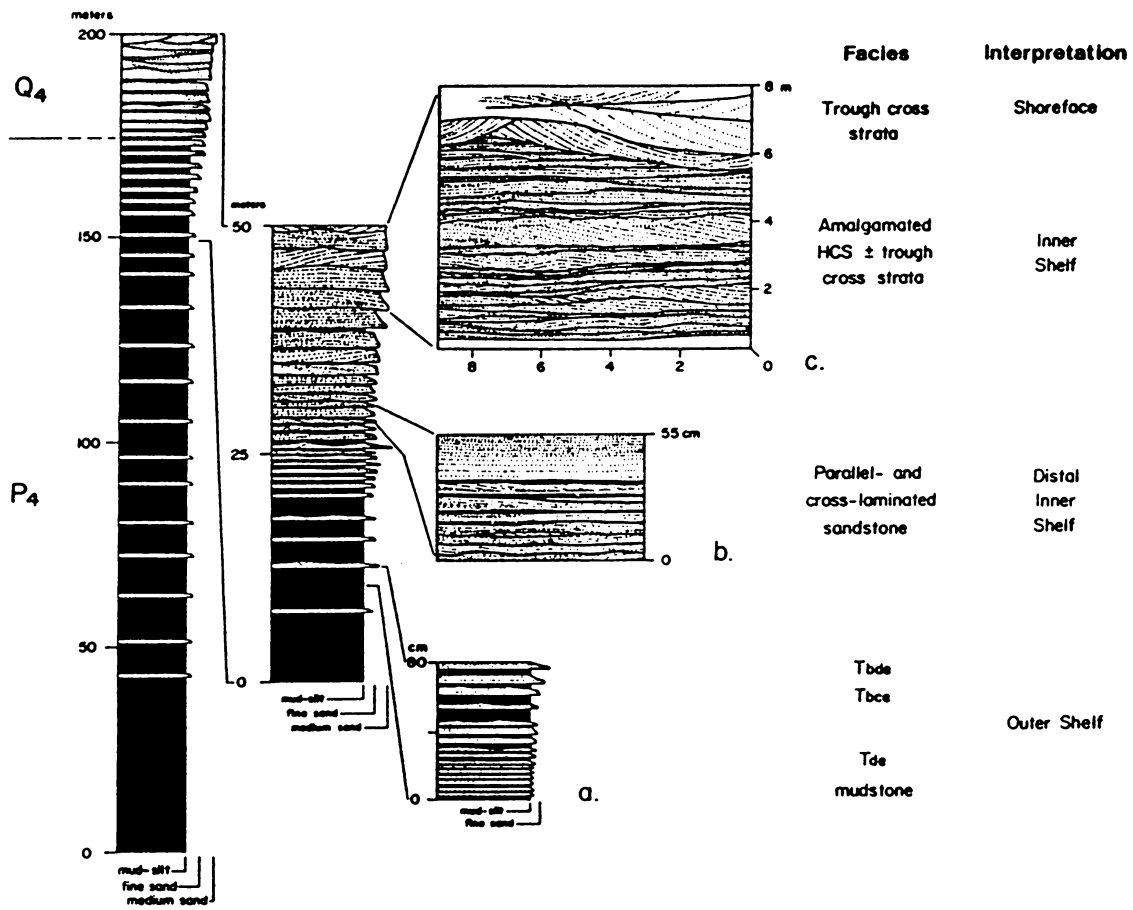

Figure 1-4: Facies association A of P4 and lower Q4 units, Lime Creek. Insets a, b, and c show details of facies from association A. Lower 150 m of P4 is schematic.

draped by nearly symmetrical, mm-thick parallel-laminae (Fig. 1-5a). Ripple amplitude and wavelengths are respectively, 1 to 5 cm and 10 to 20 cm. The internal morphology and draping laminae of the ripples are form discordant. Projecting from the base, and rarely from the top of the rippled sandstones are <1 cm wide, 1-3 cm deep, sand dikelets extending into and through the enclosing mudstones (Fig. 1-4b; Fig. 1-5b). Post depositional compaction and later tectonic deformation has resulted in ptygmatic folding of the sand dikelets. Similar features have been described by Donovan and Foster (1972), Plummer and Gostin (1981) and Soegaard and Eriksson (1985) and interpreted as synaeresis or subaqueous shrinkage cracks. Uncommon asymmetric, 1 to 3 cm deep, 10 to 15 cm wide, small channels cut into underlying mudstones are present in this part of association A (Fig. 1-5b). Channel fill consists of cross- to parallel-laminated, fine-grained sandstone. These small-scale channels are analogous to gutter casts described by Whitaker (1973) and Goldring and Aigner (1982).

The uppermost part of facies association A consists of 15 to 75 cm-thick beds of fine- to coarse-grained, parallel-laminated to hummocky cross-stratified sandstone (Fig. 1-4c; Fig. 1-5c). Hummocky beds contain internal low-angle discordant undulating and truncated laminae, which are 1 to 3 mm thick, and pinch and swell over lateral distances of 0.5 to 3.0 m. In contrast to the idealized depositional sequence recognized in hummocky bedded units (Dott and Bourgeois, 1982; Walker, 1984; Brenchley, 1985), wave ripples and mudstone do not usually cap this facies. The tops of beds may be scoured and capped by sets of low-angle, trough cross strata less than 10 cm thick.

Trough cross-stratified, medium- to coarse-grained sandstones sharply overlie and truncate the hummocky cross-stratified to parallel-laminated sandstones (Fig. 1-4c). Erosional relief of troughs varies from 10 to 50 cm. Cosets of trough cross-strata define meter-thick beds which contain 20 to 50 cm thick sets. Individual trough sets are 0.5 to

Figure 1-5: Sedimentary structures from Facies association A.

a) Form-discordant, wave-rippled fine-grained sandstone - Upper P4, Uncompahgre Gorge. b) Synaeresis cracks in mudstone and sandstone-filled gutter casts - Lower Q3, Uncompahgre Gorge. c) Amalgamated sets of hummocky cross-stratified sandstone - Lower Q4, Lime Creek.

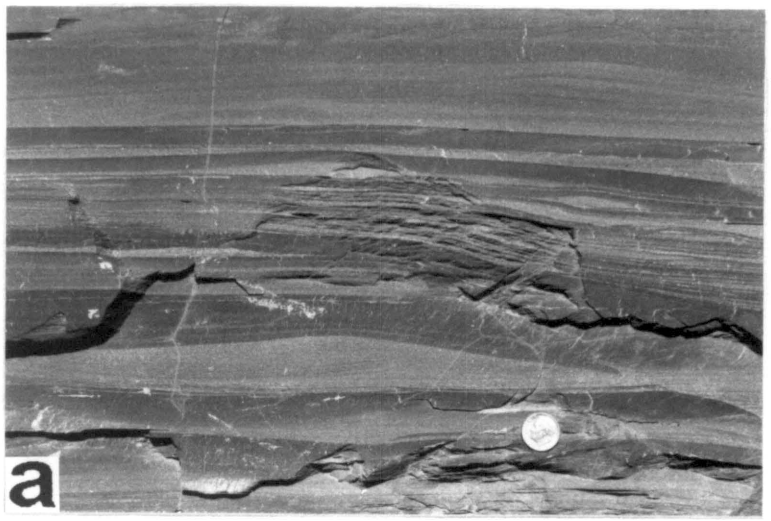
a

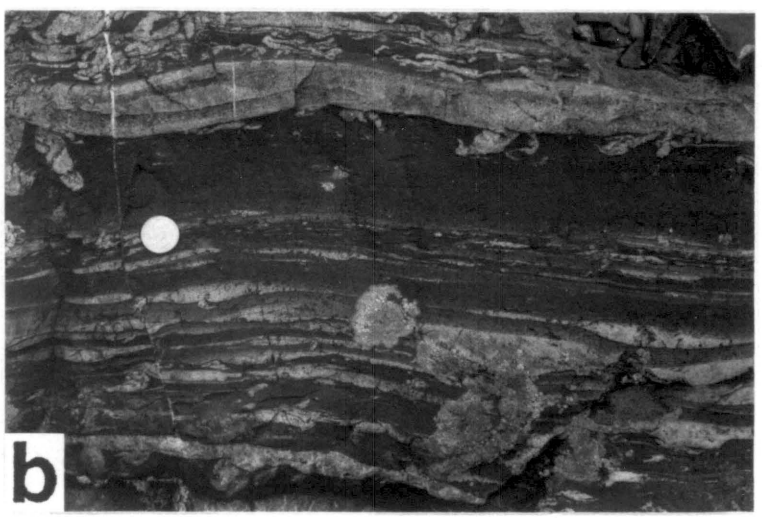
b


CENTIMETRE
INCH
c

1.5 m wide and contain 1 to 2 cm thick foresets. Foresets are defined by changes in grain size and heavy mineral segregations.

Interpretation

Mudstone and carbonaceous mudstone present in the lower one-third to one-half of association A record deposition of mud by suspension settling in a quiet-water, low-energy setting (Fig. 1-4). Abundant carbon (graphite) and pyrite present in this facies suggests that sedimentation occurred in an oxygen-deficient environment. The transition to Bouma sequence beds is similar to that documented from Mesozoic sequences in Canada and the southwest U.S.A. (Hamblin and Walker, 1979; Leckie and Walker, 1982; Swift et al., 1987); introduction of sediment is attributed to storm events. The sequence of structures in Bouma sequence beds Tde, Tbde and Tbcde are inferred to have been deposited by waning flow from suspension or geostrophic currents. Parallel lamination of the Tb interval traditionally has been interpreted as a product of deposition on a plane bed (Blatt *et al.*, 1972) but could also be generated by the migration of low-amplitude bedforms, as a function of bedload traction and sediment fallout during passage of an overriding turbulent suspension current (Paolo *et al.*, 1986). Mudstone capping and separating Bouma sequence beds represents fallout from dilute suspension currents or suspension settling of clays during fairweather conditions (*cf.* Stow and Shanmugam, 1980; Nelson, 1982).

Continuing studies on the modern Atlantic and Gulf coastal shelves (Niedoroda *et al.*, 1984; Snedden and Nummedal, 1986) suggests that storm-generated geostrophic currents, modified by the Coriolis force, might be a viable mechanism for generating depositional units resembling Bouma sequence beds. However, the transport of sediment for tens to hundreds of kilometers across the shelf perpendicular to the

shoreline is doubtful (Niedoroda *et al.*, 1984; Snedden and Nummedal, 1986). Nelson (1982), Aigner and Reineck (1982), and Aigner (1985) have appealed to storm-surge, ebb-return or gradient currents to transport sediment up to 100 km offshore. In macrotidal estuaries, like the Helgoland Bight (Aigner and Reineck, 1982; Aigner, 1985), tidal amplification at peak spring tides, in conjunction with a storm-generated geostrophic current, might prove to be a more reasonable mechanism for moving sediment great distances offshore.

The overlying parallel- to ripple-laminated sandstones in association A indicate a shift to a regime in which storm-wave orbitals impinged on the substrate. Abundant form-discordant symmetrical ripples are similar to those described by de Raaf *et al.*(1977) and Reineck and Singh (1980) and support this interpretation. Intercalated parallel-laminated sandstones are inferred to have formed by the migration of low-amplitude bedforms under oscillatory or combined flow (*cf.* Reineck and Singh, 1980; Swift *et al.*, 1983).

Thicker-bedded, hummocky cross-stratified sandstones in the upper part of association A suggest shoaling in conjunction with an increase in sand supply. Sedimentation is inferred to have occurred at or above storm-wave base. Hummocky cross stratification may be generated by aggradation and/or translation in a combined- or oscillatory-flow regime (Dott and Bourgeois, 1982; Swift *et al.*, 1983; Allen, 1985; Kreisa, 1986; Nottvedt and Kreisa, 1987). Amalgamation of hummocky beds is interpreted by Dott and Bourgeois (1982) and Leithold and Bourgeois (1984) to be caused by scouring and erosion above storm-wave base with the removal of fine-grained caps. Trough cross strata which scour into the top of hummocks (Fig. 1-4c) may reflect erosion by combined-flow currents with a stronger unidirectional component resulting in limited migration of megaripple bedforms (Nottvedt and Kreisa, 1987).

Trough cross-stratified sandstones overlying the hummocky facies probably record the evolution from combined or oscillatory flow to unidirectional tractive currents. Harms *et al.* (1982), Kreisa (1986), and Nottvedt and Kreisa (1987) infer that the transition from hummocky to trough cross-stratification is probably a function of an increase in grain size from fine to medium sand, such as that observed in lower to medial association B. The trough cross-stratified sandstones could be interpreted as either shoreface or alluvial deposits similar to facies described from Mesozoic rocks of Canada (Hamblin and Walker, 1979). A marine interpretation is preferred for this uppermost facies of association A because characteristics diagnostic of subaerial exposure and alluvial sedimentation are not observed (refer to Table 1-1).

Facies present in association A are comparable to those documented from Holocene environments and the geologic record and are attributed to storm, wave and fair-weather processes. The vertical arrangement of facies is similar to the gradational outer- to inner-shelf to shoreface configuration of Harms *et al.* (1982; their Fig. 8-9). Mudstone succeeded by Bouma sequence beds in the lower portion of association A records deposition of sediment in an outer-shelf setting below effective storm wave base. Gradual shoaling to a distal inner-shelf environment is indicated by the presence of wave-produced sedimentary structures. Storm beds in the upper portion of association A reflect the transition to an inner-shelf environment. The trough cross-stratified sandstones may signify the advent of sedimentation in a shoreface setting, based on comparison with Phanerozoic examples (*cf.* Hamblin and Walker, 1979; Leckie and Walker, 1982).

Table 1-1

Criteria for differentiating alluvial from marine settings based on physical features of depositional units (adapted from Reading, pers. comm.,1980)

	Alluvial	Shallow-marine
Sedimentary Structures:		
1. Compound cross-bedding	r*	c
2. Reactivation surfaces	p	c
3. Simple tabular-planar cross bedding with mudstone/siltstone drapes	r	p
4. Subordinate-flow ripples climbing up base of foresets	r	p
5. Periodic bundling of foresets with or without mudstone/siltstone drapes	a/r	p
6. Single pebble layers capping sets/cosets	a/r	p/c
7. Form discordant ripples (wave-generated) - symmetrical	r	c
8. Hummocky cross stratification	a	c
9. Synaeresis cracks	a/r	c
10. Desiccation structures	c	r
11. Ripped-up clasts of intrabasinal sediment	c	r
Sandstone/conglomerate body geometries:		
1. Deeply incised channels	r/c	r
2. Sheet-like geometry (including conglomerates)	r/p	c
3. Planar erosion surfaces (low-relief surfaces)	r/p	c
4. Lenticularity indices of conglomerates (cf. Clifton, 1973)	low to high values	high values
Paleocurrents:		
1. Bimodal-Bipolar	r	p
2. Unimodal with minor reversals	r	c
3. Unimodal	c	r
4. Orthogonal relationship between dominant paloecurrents and wave ripple crest orientations	a	p
Textures and Composition:		
1. Heavy mineral segregations	p	c
2. Sorting	poor	moderate/good
3. Quartz/Feldspar ratio	moderate to high	high
4. Rounding	poor	moderate/good

* a = absent; r = rare; p = present; c = common

Facies Association B: Inner Shelf to Alluvial Setting

Description

Five facies are recognized in association B: 1) mudstone and siltstone, 2) parallel-laminated sandstone, 3) trough cross-laminated sandstone, 4) trough to tabular-tangential cross-bedded, medium- to coarse-grained and pebbly sandstone, and 5) rare layers and stratified lenses of conglomerate (Fig. 1-6). The lower boundary of association B is gradational with the top of association A. Within facies association B there is an upward increase in grain size, bed thickness, sand/mud ratio and abundance of trough and tabular-tangential cross stratification. Channeling does not occur at the outcrop scale over tens of meters, and is not evident in exposures extending laterally for several kilometers. The general sequential arrangement of facies in association B is best exemplified in the lower to medial Q2 and Q4 units.

The basal and medial portions of association B consists of interbedded sandstone, siltstone and mudstone. Siltstone and mudstone units are 1 to 5 cm thick and decrease in abundance upwards. Sandstones in the lower portion of the association are either parallel laminated or trough cross-laminated (Fig. 1-6a). Parallel-laminated sandstone contains internal flat to undulating laminae which are 1 to 3 mm thick and exhibit low-angle discordances. Intercalated trough cross-laminated sandstones form discontinuous 5 to 20 cm-thick sets and extend laterally for 1 to 2 m. Foresets are 2 to 4 mm thick, normally graded and defined by opaque minerals or siltstone drapes. In the medial portion of association B the abundance of cross stratification increases relative to parallel lamination (Fig. 1-6b). Sandstones are medium- to coarse-grained and rarely pebbly. Cross-bed sets are 10 to 20 cm-thick with <1.5 cm-thick normally-graded foresets. Tabular to lenticular sets of cross-beds extend laterally for distances of 4 m.

Figure 1-6: Facies association B of Q2 unit.

Lower portion of section from Lime Creek and upper portion from Animas Canyon. Insets a, b, and c illustrate details of facies from association B.

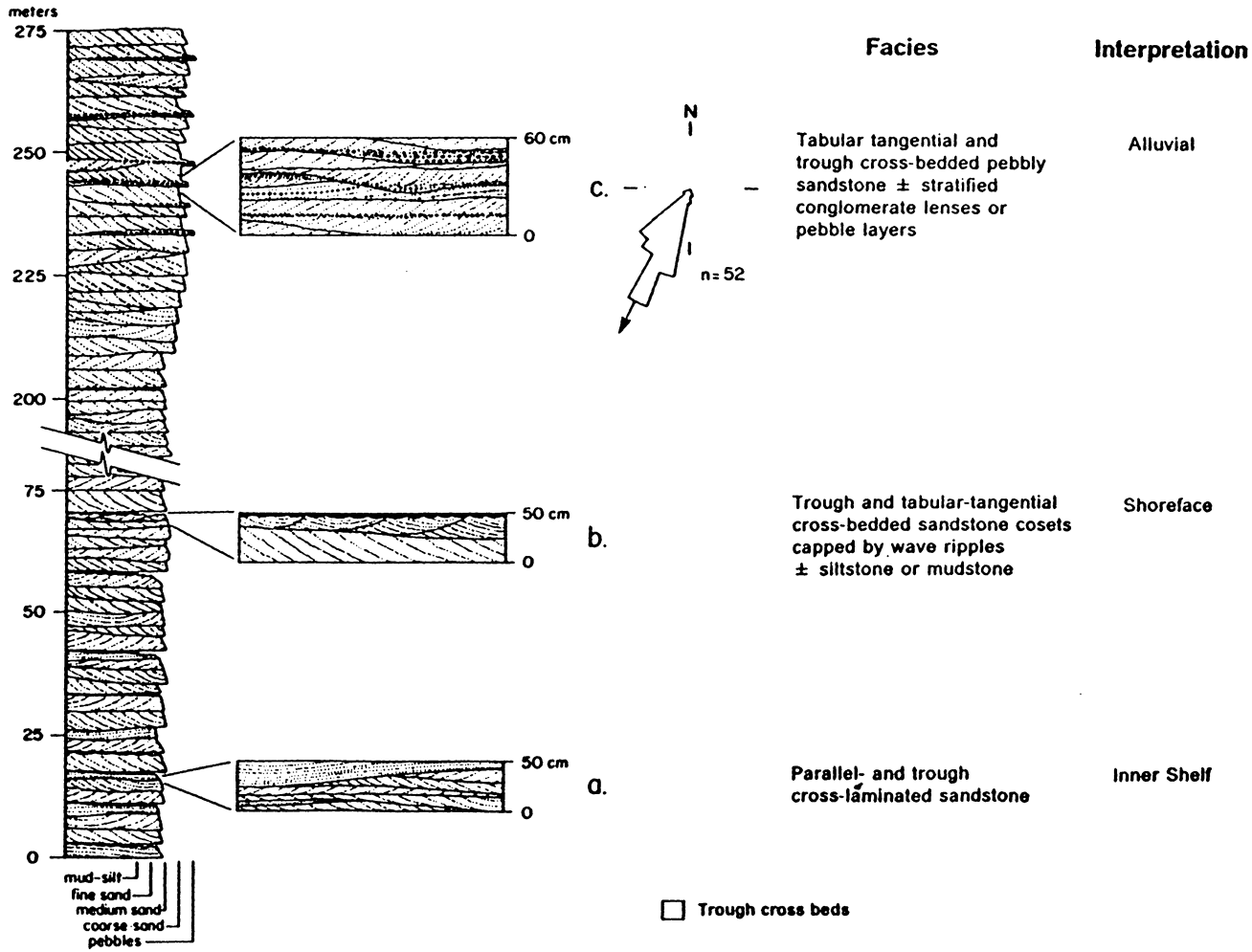
meters
275
250
225
200
75
50
25
0
60 cm
0
50 cm
0
50 cm
0
c.
b.
a.
N
n=52
Facies
Interpretation
Tabular tangential and trough cross-bedded pebbly sandstone ± stratified conglomerate lenses or pebble layers
Alluvial
Trough and tabular-tangential cross-bedded sandstone cosets capped by wave ripples ± siltstone or mudstone
Shoreface
Parallel- and trough cross-laminated sandstone
Inner Shelf
mud-silt
fine sand
medium sand
coarse sand
pebbles
Trough cross beds

Asymmetric to symmetric rounded-crest ripples, with straight to bifurcating crests, rarely cap beds of trough cross-stratified sandstone in the lower to medial portion of association B (Fig. 1-6b). Ripple symmetry indices (after Reineck and Singh, 1980) of 1.4 to 2.2 indicate that the ripples are of wave origin.

The uppermost portion of association B is comparable to the medial part except that cross-stratified sandstones are coarser and are intercalated with and scour into conglomerates (Fig. 1-6c; Fig. 1-7). Paleocurrents from trough cross-beds in this facies record a dominant south-southwest transport mode (Fig. 1-6). Two types of thinly to very thinly bedded conglomerate are present; these are lenticular-stratified, and single- or multiple-pebble layer conglomerate. Clasts are <1 cm in diameter and well rounded. Conglomerate lenses are <10 cm thick and extend laterally for up to 20 m; lenticularity indices (Clifton, 1973) thus are high. Vague stratification in the conglomerate lenses is defined by <2 cm-thick concentrations of pebbles separated by granules and sand. Stratification is inclined at very low angles. Single- or multiple-pebble layers, <5 cm-thick, either merge with or separate cross-bed sets.

Interpretation

Trough cross-laminated to parallel-laminated sandstones in the lower part of association B were probably generated by combined-flow processes and/or intense bed shear due to storm-wave activity (Nottvedt and Kreisa, 1987). The upward increase in abundance of trough cross stratification indicates that combined-flow processes were supplanted by purely unidirectional tractive currents. Wave ripples capping beds in the basal to medial portions of association B support the interpretation that all sandstone facies were modified by or were a product of wave activity. Analogous associations of facies have been described by Levell (1980a) from the late Precambrian Skaergardnes

Figure 1-7: Conglomerate and cross-bedded sandstone, Q2, Animas Canyon. Tabular-tangential cross-bedded sandstone with graded foresets. Note lenses of pebbly conglomerate separating cross-bedded sandstone sets (compare with detailed inset, Fig. 1-6c).

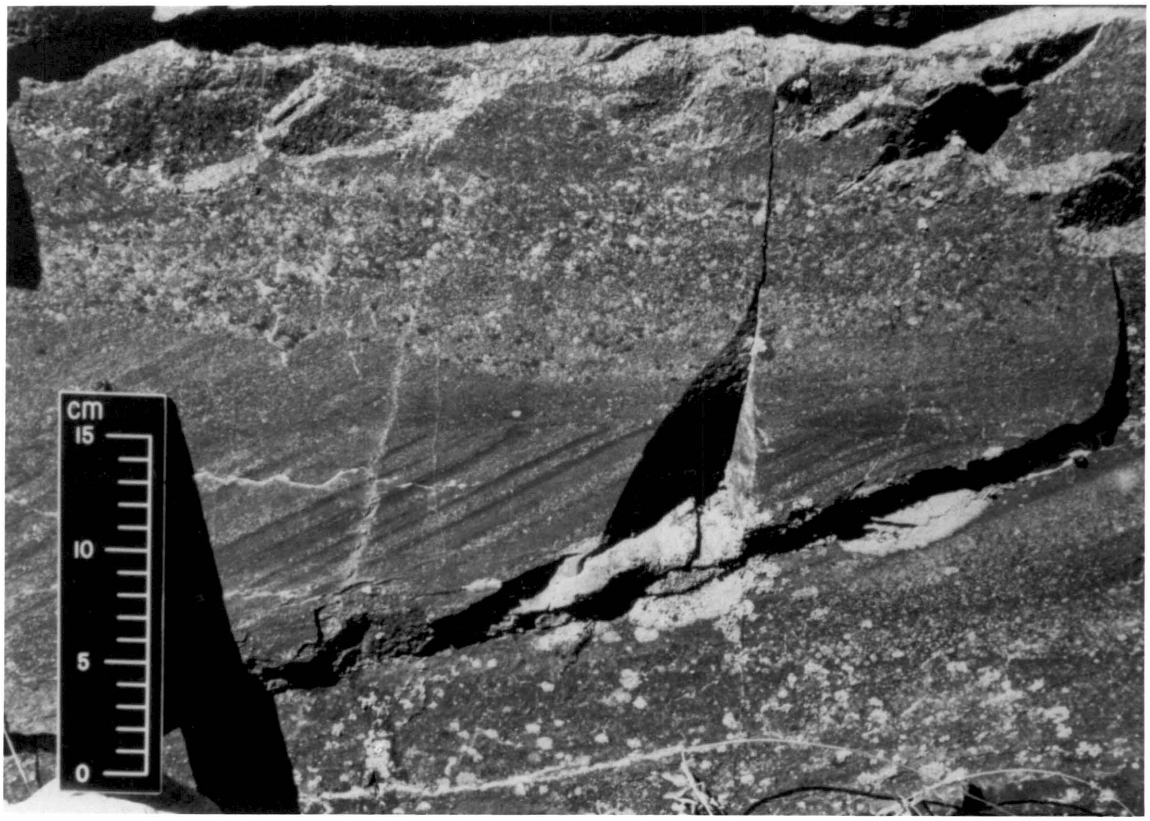
cm
15
10
5
0

Formation of Norway and attributed to a similar mechanism. The intercalated mudstone and siltstone layers represent deposition of fine-grained sediment during periods of low energy or fairweather conditions.

Cross-stratified sandstones and conglomerates comparable to those in the uppermost portion of association B have been interpreted as shoreface deposits (Bourgeois and Leithold, 1984; Leithold and Bourgeois, 1984). Shoreface environments are typically dominated by both shoreline perpendicular (onshore/offshore) and longshore currents (Clifton, 1976) whereas paleocurrents from trough cross-stratified sandstones document a southerly, offshore-directed paloecurrent mode. Based on this observation, an alluvial setting is preferred for the uppermost portion of association B. The cross-bedded sandstones are inferred to be the product of the migration of either megaripples (dunes) or sandwaves in unconfined channels as described by Miall (1977, 1985). Tabular-planar to tabular-tangential cross-bedded sandstones could also be the remnants of linguoid and transverse bars (*cf.* Miall, 1985). Single- or multiple-pebble layers represent 3-D scour trough lags or deflation lags (*cf.* Levell, 1980a). Lenses of stratified conglomerate are analogous to diffuse gravel sheets (Hein and Walker, 1977), sheetflood deposits or gravel-capped bars (Bluck, 1979).

In the lower to medial portion of association B the absence of desiccation structures in mudstones plus the occurrence of wave ripples capping beds indicates a subaqueous, subtidal setting of deposition. The upward change in sedimentary structures and inferred hydrodynamic processes suggests that shoaling from an inner shelf to shoreface environment occurred. Emergence and establishment of a distal alluvial braid plain or braid-delta setting is inferred for the uppermost portion of association B. Well-defined alluvial channels are not recognizable in this part of association B. However, Miall (1985) has stated that low-relief, channel-bounding surfaces would be difficult to discern

in distal coarse-grained alluvial systems because of the nearly flat margins of the channel and their exceedingly high width to height ratios of 90 to >100.

Facies Association C: Tidal Inner Shelf/Shoreface to Alluvial Setting

Facies association C gradationally overlies association B and is characterized by an increase in bed and cross-bed set thicknesses (Fig. 1-8, Fig. 1-9). Examples of facies from association C are taken from the Q3 and Q4 stratigraphic units. Stratigraphic units Q2 and Q4 exhibit a simple stepwise progression from associations A to B to C, but the Q3 unit is more complex (compare Fig. 1-8 and Fig. 1-9). A variety of cross-bedded sandstone facies are present in association C and are separated from one another by intercalated mudstone, siltstone and thinly bedded sandstone. In addition, distinctive thinly to very thickly bedded conglomerate and trough cross-bedded, pebbly sandstone are present in association C. For simplicity, groups of facies are described and interpreted separately, before presenting an integrated depositional model for association C.

Simple sandwave facies: Description

Simple cross-bedded sandstone units consist of 15 cm- to 1.5 m-thick, tabular cross-bed sets, which are lenticular over distances up to 300 meters. Grain size varies from fine to coarse sand; where present, pebbles are less than 1 cm in diameter. Examples of this facies in association C are taken from the Q3 unit (Fig. 1-8). Depositional units usually are separated abruptly from one another by thin intervals of mudstone, siltstone and sandstone.

Internally, the simple cross-bedded units consist of tabular-planar to tabular-tangential cross strata in which foresets vary from 0.5 to 8 cm thick (Fig. 1-8c). Pebbly

Figure 1-8: Interbedded Facies associations B and C, Q3 unit Lime Creek. Insets a, b, and c document detailed features of facies in association C.

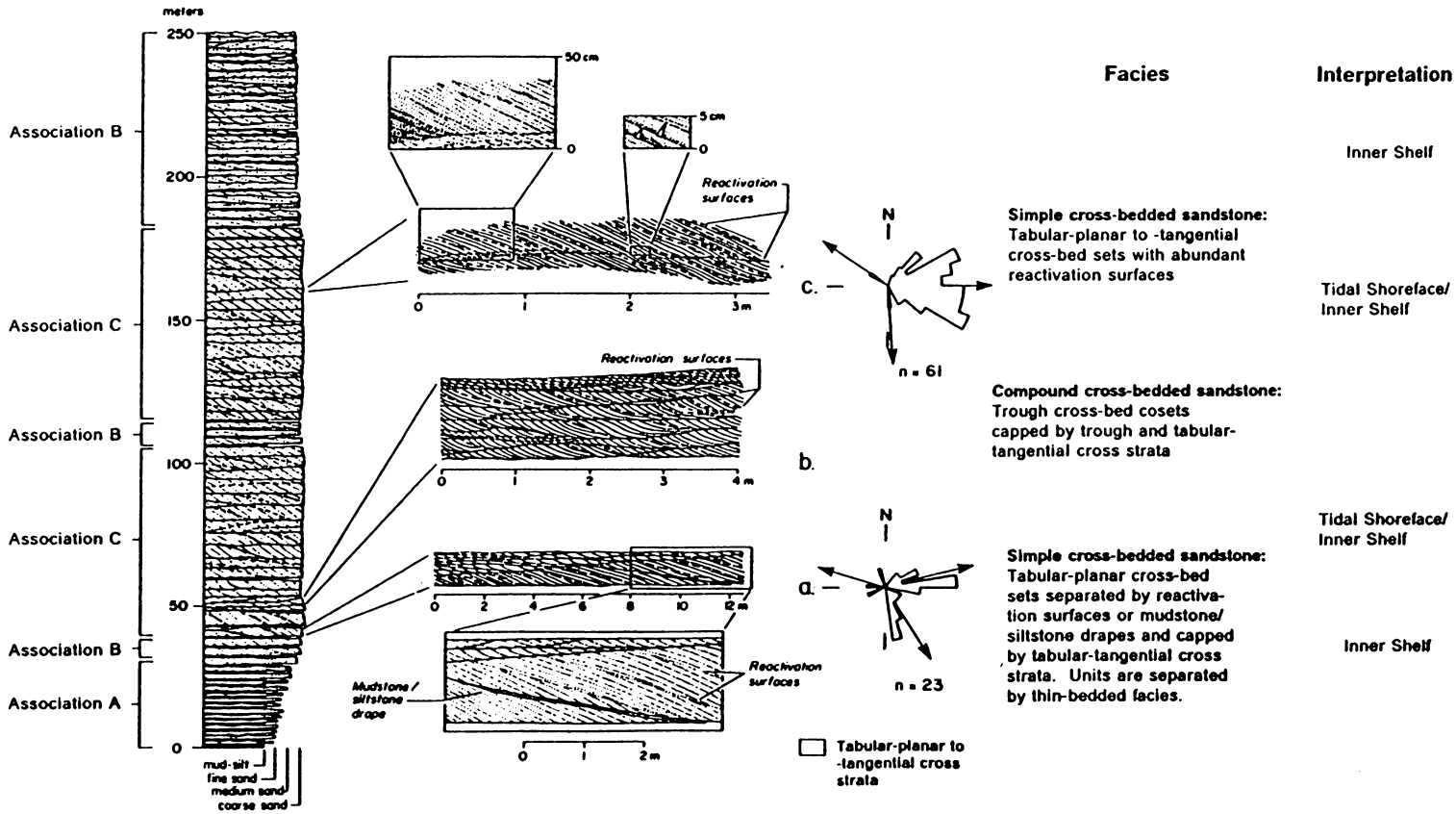
meters
250
200
150
100
50
0
Association B
Association C
Association B
Association C
Association B
Association A
mud-silt
fine sand
medium sand
coarse sand
50 cm
0
5 cm
0
Reactivation surfaces
0 1 2 3m
Reactivation surfaces
0 1 2 3 4m
b.
0 2 4 6 8 10 12m
Mudstone / siltstone drape
Reactivation surfaces
0 1 2m
a.
N
c.
n = 61
N
n = 23
Tabular-planar to -tangential cross strata
Facies
Interpretation
Inner Shelf
Simple cross-bedded sandstone: Tabular-planar to -tangential cross-bed sets with abundant reactivation surfaces
Tidal Shoreface/ Inner Shelf
Compound cross-bedded sandstone: Trough cross-bed cosets capped by trough and tabular-tangential cross strata
Tidal Shoreface/ Inner Shelf
Simple cross-bedded sandstone: Tabular-planar cross-bed sets separated by reactivation surfaces or mudstone/ siltstone drapes and capped by tabular-tangential cross strata. Units are separated by thin-bedded facies.
Inner Shelf

foresets are massive at the base but become inversely and/or normally graded up the foreset; grading defines a vague stratification in the foreset. Thinner foresets typically coarsen into the toeset and are normally to inversely graded, often with a distinct bimodality of grain size in the foresets (Fig. 1-8c). Along the length of cross-stratified sets, foresets change in thickness and orientation, varying from thicker tabular-planar foresets with <20° inclination to thinner tabular-tangential foresets with steeper dips (Fig. 1-8c). Separating and defining groups of foresets are convex-upward truncations; these are comparable to reactivation surfaces described by Visser (1980) and Boersma and Terwindt (1981). Groups of foresets between reactivation surfaces are similar to bundles recognized by Visser (1980). The bundles display a repetitive lateral thickening and thinning. One unique aspect of this facies is the prevalence of pebbly and coarse- to medium-grained sandstone with a paucity of mudstone and siltstone drapes separating bundles. These deposits thicken downward toward the toeset and merge with intervening mudstone, siltstone and sandstone (Fig. 1-8a). Paleocurrents from the simple cross-bedded facies document a dominant east-southeast mode with minor reversals to the west (Fig. 1-8). Commonly capping this facies are sets of 10 to 15 cm-thick, tabular-tangential and trough cross-bedded, medium- to fine-grained sandstone plus granule to pebble lags and rippled sandstone.

Interpretation

The simple cross-bedded sandstone facies were probably deposited in a strong time-velocity asymmetric tidal current regime such as that proposed by theoretical models for tidal sedimentation by Allen (1980, 1981a,b). The migration of relatively straight- to sinuous-crested sandwaves (Dalrymple *et al.*, 1978) comparable to the Type I and II dunes of Allen (1980), may have generated the observed depositional units. The repeti-

tive foreset bundles without abundant mudstone drapes, are similar to features described by Boersma and Terwindt (1981), Allen and Homewood (1984) and Dalrymple (1984) and attributed to daily inequalities of current velocities within the neap-spring tidal cycle. Subordinate-flow current ripples on toesets extending up reactivation surfaces (Visser, 1980) are not developed; their absence could be a function of the coarse grain size of sediment in the toeset. The rare mudstone-siltstone drapes in this facies probably were deposited during a temporary cessation in the migration of the tidal sandwaves. Tabular-tangential and trough cross strata (2-D and 3-D megaripples) capping the simple cross-bedded facies in association C could be attributed to a decrease in sediment supply to the sandwave field as proposed by Rubin and Hunter (1982). Granule and pebble lags plus rippled caps to the depositional units may have been generated by shoaling storm waves.

Composite sandwave facies: Description

Pebbly to fine-grained, compound cross-bedded sandstones consist of tabular to lenticular, 1 to 3 m-thick units, which are laterally continuous over tens to hundreds of meters. Depositional contacts are sharp, with the base of beds defined by coarse-grained sand, ± pebbles, ± ripped-up siltstone or mudstone clasts. Erosional relief averages <10 cm. If intercalated mudstones and siltstones are not present, contacts between beds are defined by either a pebble or granule lag or rippled coarse- to medium-grained sandstone.

Most commonly, the compound cross-bedded facies consists of 10 to 20 cm-thick sets of tabular-planar to tabular-tangential cross beds, which are stacked to form 1 to 3 m-thick depositional units (Fig. 1-9a). Foresets are 1 to 4 cm thick and either normally or inversely graded. Low-angle, gravel-floored surfaces, dipping from 5° to 10°, separate

Figure 1-9: Interbedded Facies associations C and B in Q4 unit. Composite section compiled from Lime Creek and Uncompahgre Gorge areas. Detailed insets of various facies from association C are shown in a, b, and c.

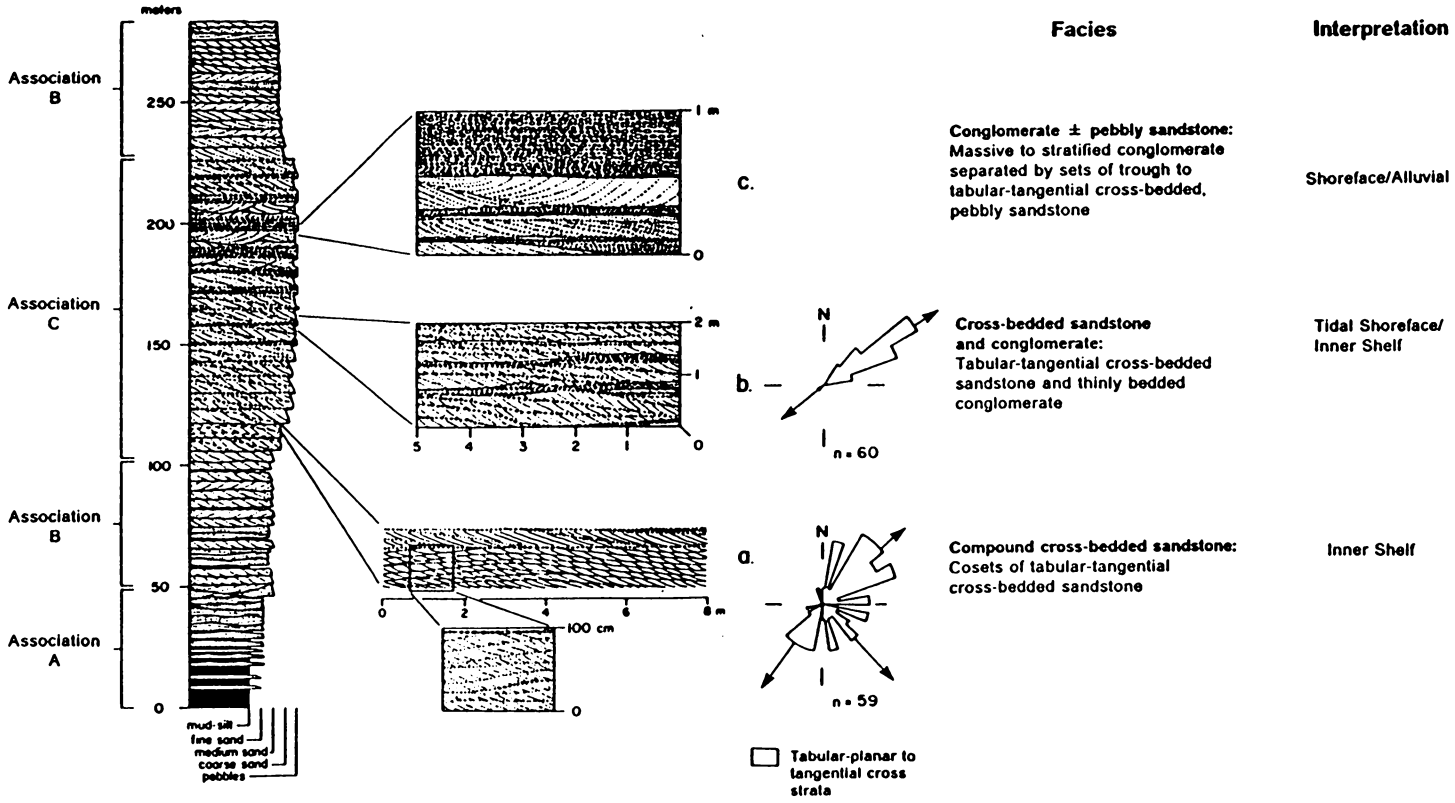
meters
Association B
Association C
Association B
Association A
250
200
150
100
50
0
mud-silt
fine sand
medium sand
coarse sand
pebbles
1 m
0
2 m
1
5 4 3 2 1 0
0 2 4 6 8 m
100 cm
0
c.
b.
a.
N
n = 60
N
n = 59
Tabular-planar to tangential cross strata
Facies
Interpretation
Conglomerate ± pebbly sandstone: Massive to stratified conglomerate separated by sets of trough to tabular-tangential cross-bedded, pebbly sandstone
Shoreface/Alluvial
Cross-bedded sandstone and conglomerate: Tabular-tangential cross-bedded sandstone and thinly bedded conglomerate
Tidal Shoreface/ Inner Shelf
Compound cross-bedded sandstone: Cosets of tabular-tangential cross-bedded sandstone
Inner Shelf

cross-bed sets; these surfaces are inclined in either an upcurrent or downcurrent direction and in rare instances form broadly convex-up surfaces within a composite bed (Fig. 1-9a; inset). The paleocurrent mode is primarily to the east and northeast, with a subordinate reversal to the southwest (Fig. 1-9).

Cosets of trough cross-bedded sandstones are also present in the compound cross-bedded facies. Cross-bed sets are 20 to 30 cm thick and define meter-thick depositional units. Individual sets are separated by very low angle (<5°) surfaces (Fig. 1-8b). Individual foresets are 1 to 5 cm thick and either normally or inversely graded. Foresets exhibit lateral variability in thickness and are periodically separated by reactivation surfaces (Fig. 1-8b).

Both types of compound cross-bedded units are capped by 10 to 20 cm-wide, 5 to 10 cm-thick trough cross beds, and ascending or descending sets of 5 to 10 cm thick, tabular-tangential cross-strata separated by flat to gently-inclined surfaces (Fig. 1-8b).

Interpretation

Ascending and descending sets of tabular-planar or tabular-tangential cross beds in composite depositional units can be attributed to the migration of sandwaves with superimposed Type 1 or 2-D and Type 2 or 3-D megaripples (Dalrymple *et al.*, 1978; Harms *et al.*, 1982; Dalrymple 1984; deMowbray and Visser, 1984). Migration of these bedforms could generate successive climbing sets in a net unidirectional tidal current regime with strong time-velocity asymmetry (Allen, 1980). In this regime, the subordinate current may be of sufficient strength to erode foresets on the crest to leeface of the sandwave during one phase of the tidal cycle (Allen, 1980; de Mowbray and Visser, 1984) and thus create the low-angle discordances or convex-up surfaces separating cross-bed sets in the composite sandwaves.

Ascending trough cross-bed sets are inferred to be caused by the successive migration of climbing 3-D megaripples (*cf.* Rubin and Hunter, 1982; Dalrymple, 1984). Periodically interspersed reactivation surfaces are attributed to tidal current variability and current reversals. High sedimentation rates may account for the net climb and aggradation of trough cosets (Rubin and Hunter, 1982).

Trough and tabular-tangential cross-strata which cap both of the previous facies are attributed to the late-stage development of 2-D megaripples and ripples migrating over the coarser and thicker depositional units. The change in grain-size and scale of cross-stratification may be caused by an upcurrent decrease in sediment supply as suggested by Rubin and Hunter (1982). Reworking by wave activity during shoaling may explain the granule lags and rippled sandstones capping the depositional units.

Inter-sandwave facies: Description

Sharply overlying the cross-bedded sandstone units in association C are 10 to 50 cm-thick units composed of <10 cm-thick beds of, coarse- to fine-grained, ripple- to parallel-laminated sandstone, plus interbedded siltstone and mudstone (Fig. 1-10). This group of facies is most commonly developed in the Q3 unit (Fig. 1-8a). Rippled sandstones are lenticular and contain internal form-discordant laminae. The discordant laminae, plus the symmetry and rounding of ripple crests, are analogous to wave-generated structures described by (de Raaf *et al.*, 1977). Projecting from the base of the sandstone beds, into underlying mudstones and siltstones are infrequent folded sand dikelets, <1 cm wide and <3 cm deep (Fig. 1-10). The rippled sandstone facies may merge laterally into the toesets of the enclosing thicker-bedded, compound and simple cross-bedded facies (Fig. 1-8a). Rarely, 10 to 20 cm-thick beds of parallel-laminated, medium- to fine-grained sandstone, minus interbedded siltstone and mudstone, separate

Figure 1-10: Interbedded siltstone and rippled sandstone. Example from lower Q3, Uncompahgre Gorge. Sand dikelets (synaeresis cracks) project into underlying siltstones.

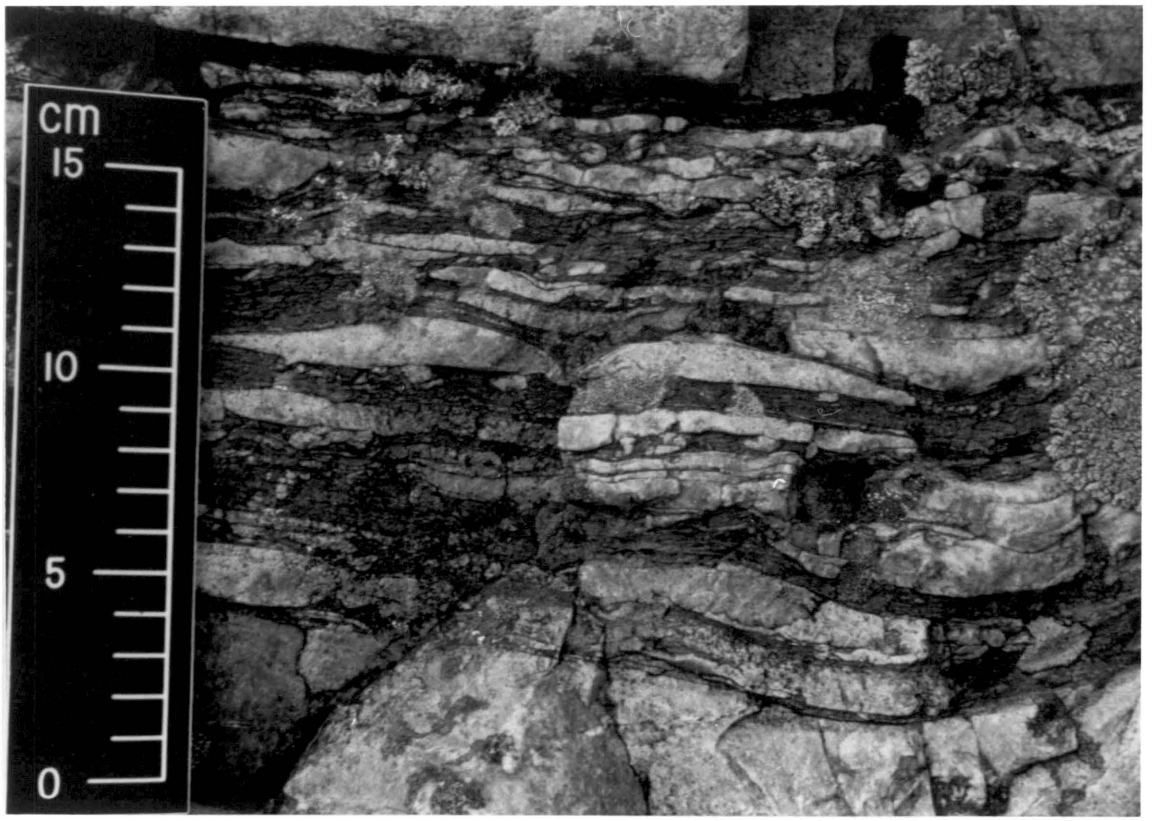
cm
15
10
5
0

the simple and compound cross-bedded facies. Internal parallel to gently undulating laminae are 1 to 3 mm thick.

Interpretation

Mudstone, siltstone and sandstone are inferred to have been deposited in the lee or down current direction of the advancing tidal sandwaves (*cf.* Homewood and Allen, 1981). This inference is supported by the fact that rippled sandstones merge with the toesets of the sandwaves, and mudstones rarely extend up and drape foresets in sandwaves. Mudstone and siltstone were produced by suspension fallout whereas intercalated wave-rippled and parallel-laminated sandstone were generated by fairweather or storm-wave orbitals impinging on the substrate. The mudstone, siltstone and sandstone facies together may be analogous to the very low-angle (<1°) to horizontal E1 surfaces of Allen (1980), over which the tidal sandwaves migrated. The sharp transition from the sandwaves to the overlying fine-grained facies is attributed to drowning of the tidal system and cutoff of sediment supply. A decrease in sediment supply could alternatively be linked to deflation of the sandwave field (Rubin and Hunter, 1982).

Braid delta and shoreface facies: Description

Pebble to cobble conglomerates and pebbly sandstones are restricted to the upper to medial portions of stratigraphic units Q2 and Q4. The descriptions presented are from the Q4 unit (Fig. 1-9). Thinly to very thickly bedded conglomerates vary from lenticular beds tens of meters in length to continuous sheets extending along strike for 3 to 4 km.

Packages of conglomerate in the stratigraphic units Q2 and Q4 can be correlated over distances of up to 40 km.

Thinly bedded conglomerates are 1 to 5 pebble diameters in thickness, massive to stratified, and <10 cm thick (Fig. 1-9b; Fig. 1-11). Pebbles are subangular to rounded and <3 cm in maximum diameter. The conglomerate deposits are clast-supported with the matrix between clasts consisting of granules and coarse sand.

Meter-thick conglomerates (Fig. 1-9c) are sheetlike in geometry, massive to vaguely stratified and rarely normally graded. Clasts are subangular to rounded and vary from 1 to 8 cm in diameter. Where present, stratification is horizontal to gently inclined (<5°) and defined by alignment of single pebbles. The thickly bedded conglomerates are clast- or matrix-supported. Matrix consists of smaller pebbles, granules and coarse sand. The base of conglomerate units is subhorizontal, with an erosional relief of less than 10 cm.

Intercalated with both conglomerate types are simple and trough cross-bedded sandstone facies. The simple cross-bedded sandstones are like those elsewhere in association C, with the exception of an increased component of pebbles and granule sands. Paleocurrents are to the east and reactivation surfaces are defined by concentrations of pebbles (Fig. 1-9b). Trough cross-bedded pebbly sandstones resemble those described in association B, although the grain size and set dimensions are different (Fig. 1-9c). Trough sets are 15 to 30 cm thick, 1 to 3 m wide, and scour into adjoining troughs. Foresets are 0.5 to 2.0 cm thick, normally graded and defined by concentrations of pebbles and granules. Isolated pebbles, <2 cm in diameter, are present on foresets.

Figure 1-11: Intercalated cross-bedded sandstone and conglomerate. Example from upper Q4, Lime Creek area (compare with inset in Fig. 1-9b).

Interpretation

The origin of the pebbly conglomerate and sandstone facies is problematic. Single-layer and thinly bedded pebbly conglomerates commonly have been interpreted as winnowed-pebble lags generated by either storm or fairweather wave activity (Table 1-1; Anderton, 1976; Levell, 1980a, 1980b; Leithold and Bourgeois, 1984; Cotter, 1985). Intercalated simple cross-bedded pebbly sandstones are interpreted to be similar to simple sandwaves in Q3 (Fig. 1-8a, c), thus supporting the marine origin for the thinly bedded conglomerates.

Meter-thick conglomerate beds are difficult to reconcile with the processes that generated the winnowed-pebble lags. Intercalated medium-bedded, trough cross-bedded pebbly sandstones could be alluvial deposits. Troughs may represent megaripples migrating in unconfined channels on a distal braidplain, whereas interbedded conglomerates may be analogous to gravel bar or sheetflood deposits; similar interpretations for this associations of facies have been proposed by Miall (1977, 1985). However, the broad sheetlike geometry of the conglomerates over several kilometers is not particularly compatible with an alluvial interpretation (compare with Table 1-1). The high lenticularity indices of the thickly bedded conglomerates (constant thickness versus extensive lateral continuity; Clifton, 1973) are similar to values for inferred shoreface conglomerates described by Bourgeois and Leithold (1984). If the conglomerates and pebbly sandstones are alluvial, transgressive reworking along ravinement surfaces (Swift, 1968) during a gradual eustatic rise could account for the widespread areal extent of the conglomerates. In this scenario, sea level rise was not sufficient to cut off sediment supply because the conglomerate units are not capped by wave-reworked surfaces (Leckie and Walker, 1982; Cotter, 1985) and mudstone (Bergman and Walker, 1986; Plint *et al.*,1986) but succeeded by sandstone or conglomerate. Another mechanism for

explaining the alternation of marine and alluvial facies is a hypothetical model proposed by Levell (1980b), which appeals to a shift in alluvial depositional loci. Abandonment in the alluvial system results in transgressive shoreface retreat coincident with basin subsidence. Marine reworking of the alluvial sediments could then generate the transgressive lags.

Summary

Facies association C is interpreted to have been deposited in a tidal inner shelf to shoreface setting which shoaled periodically to alluvial conditions. Tides were the dominant mechanism for generating the simple and compound cross-bedded facies. Wave modification of tidal sediments is indicated by the presence of: 1) intercalated wave-rippled sandstones between the tidal sandstone units, and 2) thinly bedded conglomerates (gravel lags) capping the sandstone bodies. Thickly bedded conglomerates and interbedded trough cross-bedded pebbly sandstones probably accumulated on a distal braid-plain or braid-delta. Marine reworking in response to episodic subsidence, switch in depositional loci or eustatic rise could explain the tabular nature of the thickly bedded conglomerates.

SEDIMENTOLOGY: SEQUENCE ANALYSIS

Facies associations A, B and C represent the generalized vertical arrangement of groups of facies in the progradational sequences. In detail there are significant deviations from this simplified pattern within the thickening- and coarsening-upward sequences of P2-Q2, P3-Q3, and P4-Q4. The following discussion summarizes the vertical arrangement, possible paleodepth ranges, and paleoenvironments for these sequences.

The lowermost pelite-quartzite sequence (P2-Q2) consists of facies associations A, B, and C in that order (Fig. 1-12). Association B is rarely developed in the uppermost part of Q2. Outer-shelf facies (A) are gradationally overlain by inner-shelf to shoreface and possible alluvial facies (A to B), followed by tidal inner-shelf/shoreface and alluvial facies (C). Outer-shelf siltstones and mudstones of lower P3 abruptly overlies association C. Symmetrical ripples of 1.2 to 1.4 m wavelength are preserved at the top of the Q2 unit in the Uncompahgre Gorge area (Fig. 1-1). The ripples yield maximum calculated water depths of 350 m (after Diem, 1985); this value represents the maximum possible depth associated with the terminal drowning of the Q2. Sedimentation of the overlying outer-shelf mudstones of association A thus may have begun at depths equal to or greater than 350 m.

P3-Q3 records a complex series of transitions in facies associations (Fig. 1-12). P3 is dominated by mudstone but three <25 m-thick, coarsening- and thickening-upward, outer-shelf to inner-shelf/shoreface packages of association A are present within this unit (Fig. 1-12). These packages are separated by mudstone. The basal portion of Q3 is defined by a thin interval of outer-shelf facies which are succeeded by a condensed interval of inner-shelf facies (A to lower B) capped by tidal inner-shelf/shoreface facies (C) (Fig. 1-12). Repetitive alternations of medial association B megaripples transitional to association C sandwaves and intersandwave deposits compose the lower to medial portion of the Q3 unit (Fig. 1-12). The overlying medial portion of Q3 in the Uncompahgre Gorge area (Fig. 1-1; Fig. 1-3) is represented by an abrupt change to shoreface and/or alluvial facies of upper association B (not shown on Fig. 1-12). Symmetrical ripples of 2 to 4 cm wavelength in sandstones of association B yield calculated water depths of <2 m (after Diem, 1985). In contrast outcrops in this portion of Q3 at Lime Creek (Fig. 1-1; Fig. 1-3) do not contain the small symmetrical ripples and are thus inferred to be more distal, subtidal inner-shelf deposits. A repeated sequence of tidal inner-

Figure 1-12: Sequence of facies associations in stratigraphic units. Detailed inset documents greater complexity in stratigraphic unit P3-Q3 which contains smaller-scale sequences. Triangles illustrate generalized grain-size trends in stratigraphic units and smaller-scale sequences.

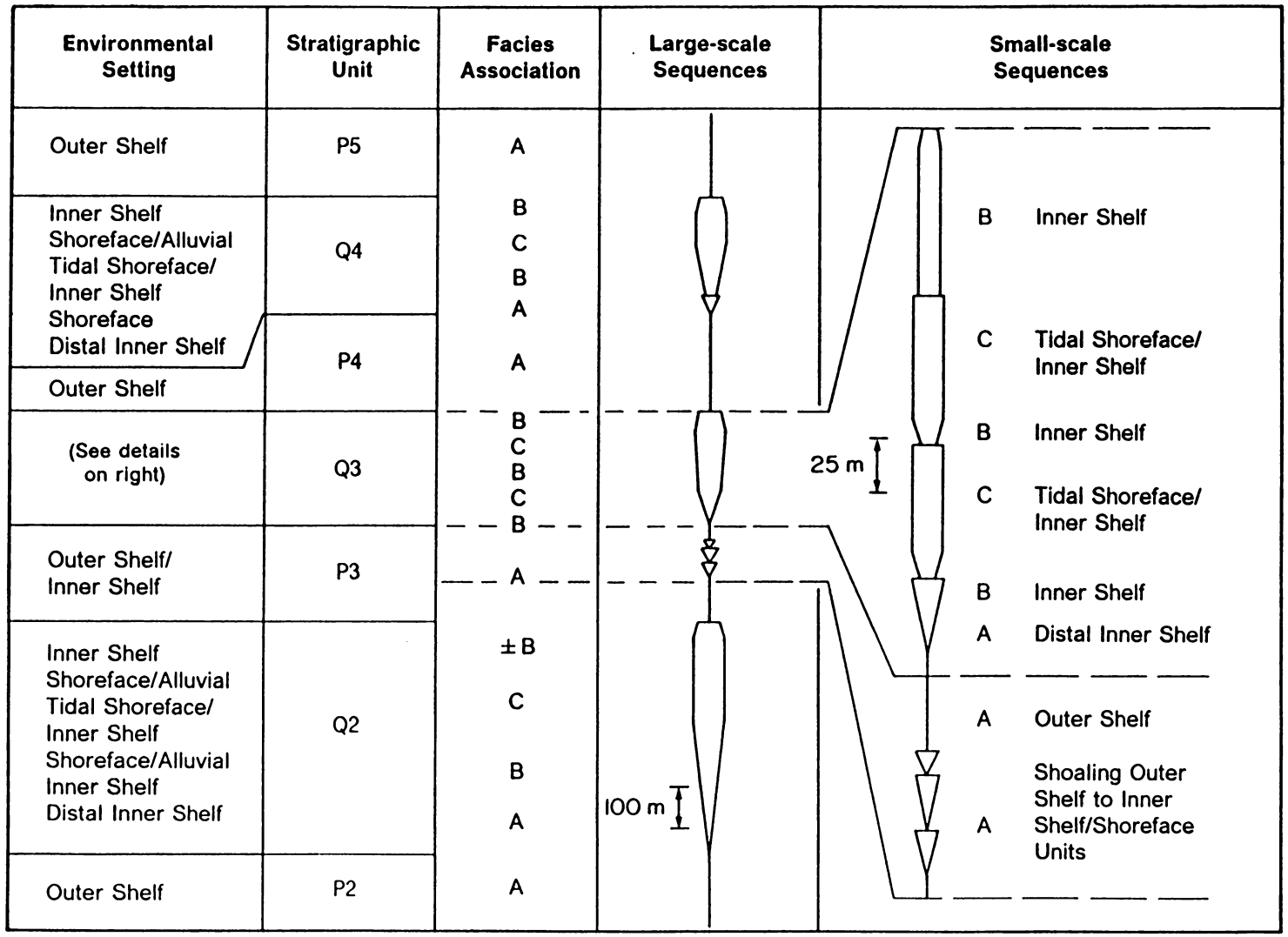
Environmental Setting
Stratigraphic Unit
Facies Association
Large-scale Sequences
Small-scale Sequences
Outer Shelf
P5
A
Inner Shelf
Shoreface/Alluvial
Tidal Shoreface/
Inner Shelf
Shoreface
Distal Inner Shelf
Q4
B
C
B
A
P4
A
Outer Shelf
(See details on right)
Q3
B
C
B
C
B
Outer Shelf/
Inner Shelf
P3
A
Inner Shelf
Shoreface/Alluvial
Tidal Shoreface/
Inner Shelf
Shoreface/Alluvial
Inner Shelf
Distal Inner Shelf
Q2
±B
C
B
A
Outer Shelf
P2
A
100 m
25 m
B Inner Shelf
C Tidal Shoreface/ Inner Shelf
B Inner Shelf
C Tidal Shoreface/ Inner Shelf
B Inner Shelf
A Distal Inner Shelf
A Outer Shelf
A Shoaling Outer Shelf to Inner Shelf/Shoreface Units

shelf/shoreface sandwaves and intersandwave deposits gradationally overlie inner-shelf facies (B)(Fig. 1-12). These facies are succeeded by a moderately thick interval of subtidal inner-shelf facies (B). Final drowning of Q3 is reflected by the deposition of outer shelf carbonaceous mudstones (A) above association B.

The stratigraphic sequence of P4-Q4 is similar to P2-Q2 (Fig. 1-12). A thick interval of outer-shelf facies (A) is overlain by inner-shelf to shoreface facies of upper association A to lower association B. Shoreface to alluvial facies of upper association B are supplanted by tidal inner-shelf to shoreface facies (C). Shoreface to alluvial conglomerates and sandstones are present in the upper part of association C. Conglomerate units in Q4 are thickest in Uncompahgre Gorge but thin and decrease in abundance to the south in the Lime Creek area (Fig. 1-1; Fig. 1-3). Inundation of the Q4 shelf is indicated by a gradual change to inner-shelf facies (B). Terminal drowning of the Q4 is evidenced by the abrupt transition to outer-shelf mudstones (A) of P5 (Fig. 1-12).

PALEOENVIRONMENTAL SYNTHESIS

A paleoenvironmental model that attempts to reconstruct the sedimentation history of the Uncompahgre Group in a time and space continuum must account for the sequential and lateral distribution of facies associations discussed in the previous section. Fundamental to the development of a depositional model are the concepts of autocyclic and allocyclic controls.

Allocyclic and Autocyclic controls

To understand and reconstruct the temporal and spatial evolution of the progradational sequences, four controls must be considered: sediment supply, intrabasinal

transport paths, eustasy and subsidence rates. Intrabasinal transport paths are considered to be autocyclic whereas sediment supply, eustasy and tectonic subsidence are allocyclic (Beerbower, 1964; Clifton, 1981).

Sediment supply to a basin is a product of the variability of the distribution system and the source area. Variables influencing these parameters include: composition of the source rocks, climate, and relief (Schumm and Lichty, 1965). Upon introduction of sediment into a marine setting, it may be distributed and entrained by storms, waves and geostrophic-gradient or tidal currents (autocyclic mechanisms). To preserve these sediments from further erosion and reworking, space must be created by either subsidence or eustasy. Subsidence rates and eustatic excursions are not easily differentiated in Precambrian siliciclastic shallow-marine sequences where time constraints are poor and paleodepth ranges are difficult to estimate. The effects of short term (10^3-10^6years) eustatic oscillations and subsidence rates cannot be differentiated, and thus are equated with relative changes in sea level (ΔR_{sl}). In a shallow-marine setting, such changes will have a dramatic effect on the three-dimensional geometry and slope of the depositional interface, thus strongly influencing processes active at this juncture.

Models of shelf sedimentation: tide- and storm-dominated

Depositional models for shallow-marine settings influenced by storms, fair-weather waves and tidal processes can be subdivided into two categories. In the first case the two processes are inferred to be coeval and spatially coexisting (Anderton, 1976; Levell, 1980b; Reineck and Singh, 1980; Aigner and Reineck, 1982; Aigner, 1985; Soegaard and Eriksson, 1985; Johnson and Baldwin, 1986) whereas in the second case they are visualized as being temporally separated (Nummedal 1986a, b; Wright, 1986). Either model could explain the facies sequences in the Uncompahgre Group (Fig. 1-12). The coeval

storm and tidal shelf model will be reviewed first because it has been more widely employed in previous studies.

Coeval storm and tidal shelf model

In this reconstruction, two phases of sedimentation closely followed one another in time. During fairweather, tidal processes were dominant. Composite and simple sandwaves (facies association C) of the inner shelf/shoreface migrated in a general easterly direction parallel to the paleoshoreline (Fig. 1-13). The distal inner shelf and outer shelf would have been draped by mud (Fig. 1-13).

With the onset of storm conditions, shoaling storm waves in conjunction with geostrophic curents would have degraded and eroded the tidal sandwaves of facies asssociation C, leaving behind residual lags (Fig. 1-9b) with transport of sediment obliquely offshore (Fig. 1-14; *cf.* Swift *et al.*, 1983; Niedoroda *et al.*, 1984). Three-dimensional megaripples transitional to hummocky storm beds (facies associations B and A) would have developed on the inner shelf/shoreface during offshore transport of sediment. As the sediment laden suspension clouds, driven by geostrophic currents, reached the outer shelf, Bouma sequence beds were deposited (lower association A; Fig. 1-14). With an abatement of storm activity, mudstone was deposited across the shelf. A return to fairweather conditions resulted in the elevation of wave base with repair and renewed migration of tidal sandwaves.

The vertical architecture of the progradational sequences in the coeval storm and tidal shelf model implies a simple long-term progression in external (allocyclic) controls. For this model the following scenario is proposed:

Figure 1-13: Coeval storm and tidal shelf, fair-weather conditions. During fair weather, tidal currents prevail, with the development of simple and composite sand waves on the inner shelf. Mud is deposited on the outer shelf.

Coeval storm- and tide-dominated shelf: Fairweather conditions

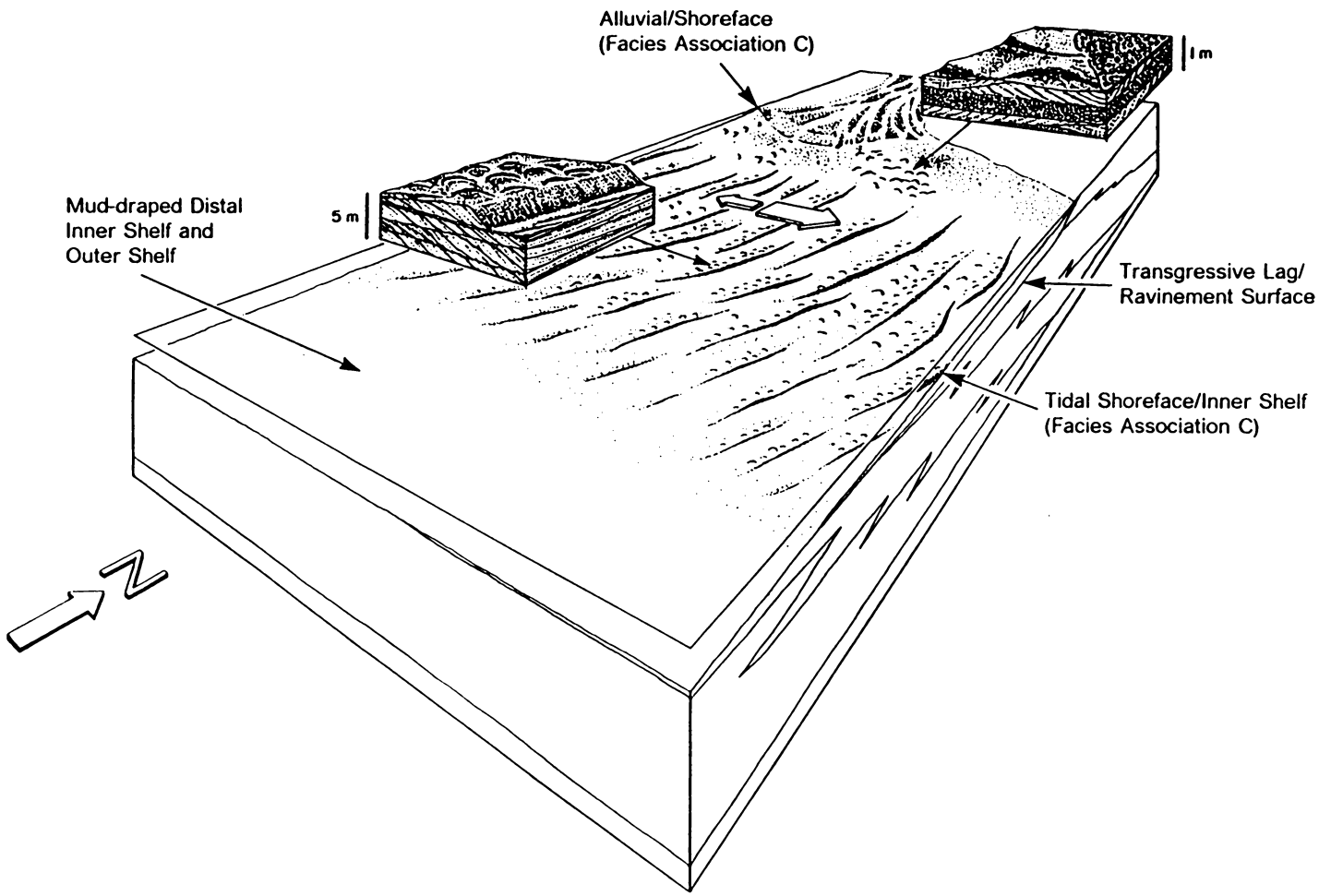

Figure 1-14: Coeval storm and tidal shelf, storm conditions. During storm conditions, the shoreface/inner shelf is degraded and eroded with deposition of sand extending from the inner shelf to the outer shelf. Arrows indicate inferred orientation of offshore flow produced by geostrophic currents.

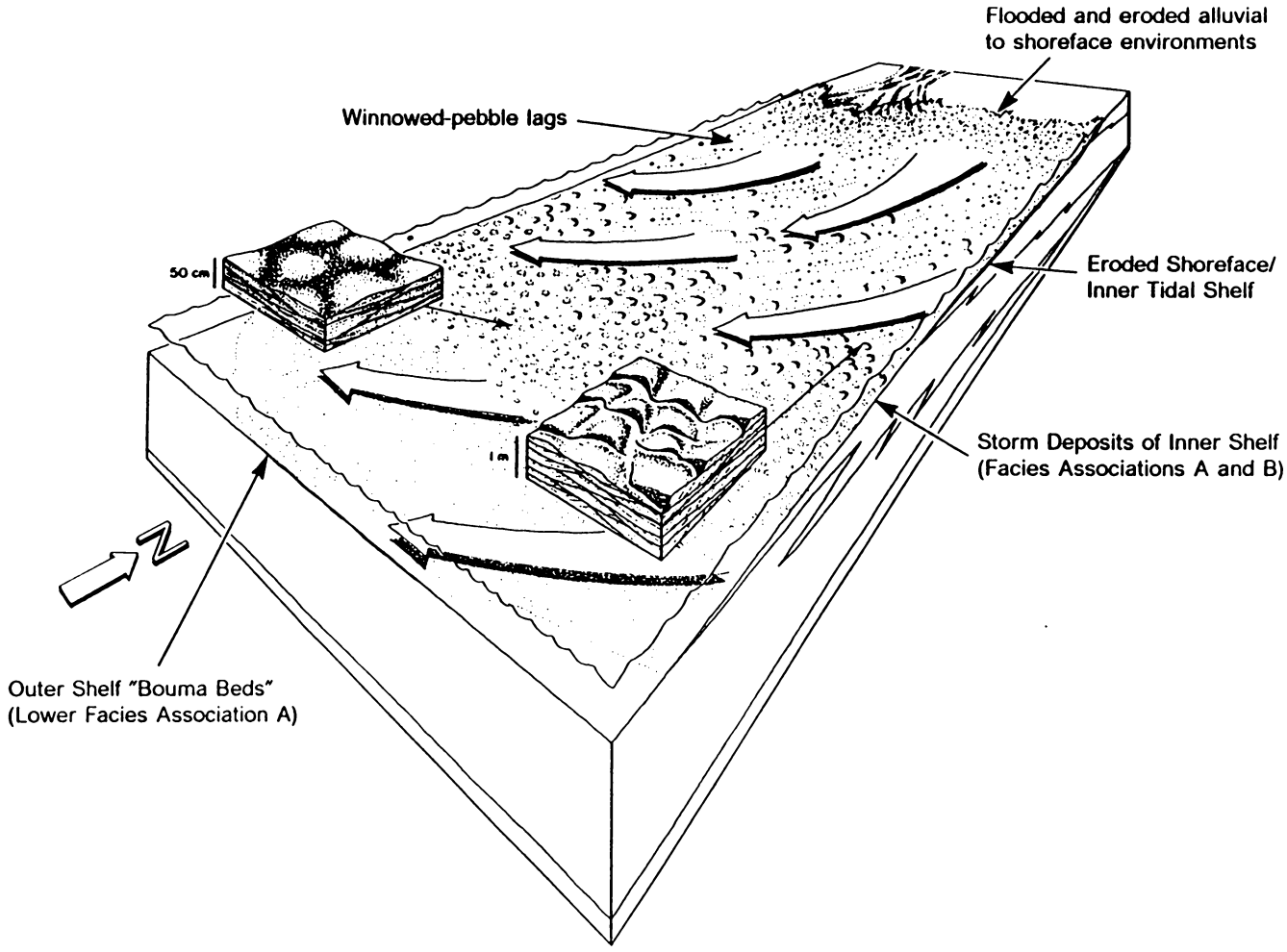

Coeval storm- and tide-dominated shelf: Storm conditions

1. An inital rapid rise in relative sea level (ΔR_{sl}) or a decrease in sediment supply to the basin coupled with a constant subsidence rate results in deposition of carbonaceous mudstones of the outer shelf (lower association A).
2. A relatively stationary sea level (ΔR_{sl}) with an increasing sediment supply led to combined aggradation and progradation of a graded shelf. The fair-weather, tide-dominated inner shelf/shoreface of association C was overprinted by periodic storm activity. Sediment entrained on the inner shelf by storm activity was transported onto the distal inner shelf and outer shelf.
3. A renewed rapid rise in relative sea level (ΔR_{sl}) or a decrease in sediment supply led to terminal drowning of the progradational sequence.

Although in a general sense the coeval storm and tidal shelf model partially explains the sequential ordering of facies associations, it has several shortcomings; these include:

1. Tidal facies cannot be traced laterally into coeval storm beds in the outcrop belt.
2. Trough cross-bedded sandstones in the upper part of facies association A which erosively overlie storm beds, are interpreted to record the transition from an inner-shelf to shoreface setting (Fig. 1-4). In addition, trough and tabular-tangential cross-bedded pebbly sandstones and flat lenses of conglomerate of upper association B may be alluvial rather than inner-shelf deposits (Fig. 1-6). An alluvial origin for the cross-bedded facies is in conflict with the model. The premise that vertically stacked facies are genetically related is thus invalid, because of possible unconformities and missing facies.

Other problems with the coeval storm and tidal shelf model which are not exclusive to the Uncompahgre Group include:

1. Variable amounts of subsidence and temporal scales of eustasy are not accounted for.
2. Long-distance sediment transport across a shelf, perpendicular to the shoreline, as suggested by paleocurrent data from the upper part of facies association B (Fig. 1-6) has not been documented from Holocene shelves. Rather, sediment is transported obliquely offshore by currents that evolve into shore-parallel geostrophic flows (Swift *et al.* , 1983; Niedoroda *et al.*, 1984).
3. The effect of storm overprint in a tidal setting has not been observed in siliciclastic Holocene settings (Stride *et al.*, 1982).
4. Facies distributions in modern shallow-marine settings may not be appropriate for comparison to the ancient because modern shelves are both sediment starved (in contrast with ancient coarse-grained systems) and not in dynamic equilibrium with the processes acting upon them due to the rapid post-glacial sea level rise (*cf.* Walker, 1984).

Temporally separated storm/alluvial and tidal shelf model

The shortcomings listed for the coeval storm- and tide-dominated shelf model in application to the Uncompahgre Group may be resolved by considering the effects of two allocyclic controls together, eustasy plus subsidence (ΔR_{sl}), as a function of time.

Relatively constant or episodic subsidence in a sedimentary basin is either tectonically driven (intra- or inter-plate compressional/extensional stresses; Cloetingh *et al.*, 1985 Karner, 1986) or related to thermal cooling following rifting (McKenzie, 1978; Heller and Angevine, 1985); these processes commonly act in combination with isostatic loading (sediment + water; Bloom, 1967; Matthews, 1984). The duration of the above events, 10^6 to 10^8 years, approximately corresponds to the 1st to 2nd order relative sea

level curves of Vail *et al.* (1977). Excursions in relative sea level (ΔR_{sl}) may vary by hundreds of meters. Shorter term Milankovich cycles of 10^3 to 10^6 years, could explain cyclic patterns in sedimentation attributed to eustatic oscillations or climatic changes (van Houten, 1964; Schwarzacher and Fischer, 1982). Cyclic variation in global insolation related to precession, tilt and eccentricity of the Earth's orbital parameters (Milankovich cycles) controls climate (precipitation patterns) and likewise the areal extent of continental/alpine glaciation (Covey, 1984). Changes in climate and glacial mass could strongly influence sediment supply and relative sea level. The last Pleistocene deglaciation produced a sea level oscillation of 100 m (Matthews, 1984). As a function of this scale of sea level excursion significant erosional relief (up to hundreds of meters) is evident in marginal- to shallow-marine settings of Pleistocene and Cretaceous age (Frazier, 1974; Weimer, 1984).

A model developed for upward-coarsening and -shoaling Cretaceous sequences is useful for explaining the evolution of progradational sequences in the Uncompahgre Group. This model, based on the work of Nummedal (1986a,b), Wright (1986) and partially on the studies of Bergman and Walker (1986) and Plint *et al.* (1986), suggests that the vertical seqeunce of facies (depositional environments) can be related to to external relative sea level changes (either subsidence or eustasy) which profoundly alter the three-dimensional geometry of the depositional system.

The Cretaceous examples from Canada and the southwest U.S.A. represent cycles of approximately 2×10^5 years maximum duration and exhibit a characteristic vertical sequence. After an initial rapid rise in relative sea level (ΔR_{sl}) a condensed section of limestone or carbonaceous mudstone was deposited due to a lag time in siliciclastic input relative to the steep slope of ΔR_{sl} (Fig. 1-15a). As the rate of relative sea level rise decreased and the sedimentation rate increased, the evolving progradational package shoaled to shoreface conditions (Fig. 1-15a). Exposure occurred during a fall in relative

Figure 1-15: Synthetic cycles for small-scale progradational sequences.

a) Example from Cretaceous sequences in San Juan Basin, New Mexico and Alberta Basin, Canada illustrating change in relative sea level and its effect on progradational packages. Time increment is approximately 2×10^5 years.

b) Example from Uncompahgre Group; progradational sequence within P3 unit. Note similarity to Cretaceous example; however unconformity, conglomerate and tidal facies are absent from the upper part of the sequence implying lack of exposure during relative sea level fall. Time interval of approximately 10^3 to 10^5 years is inferred.

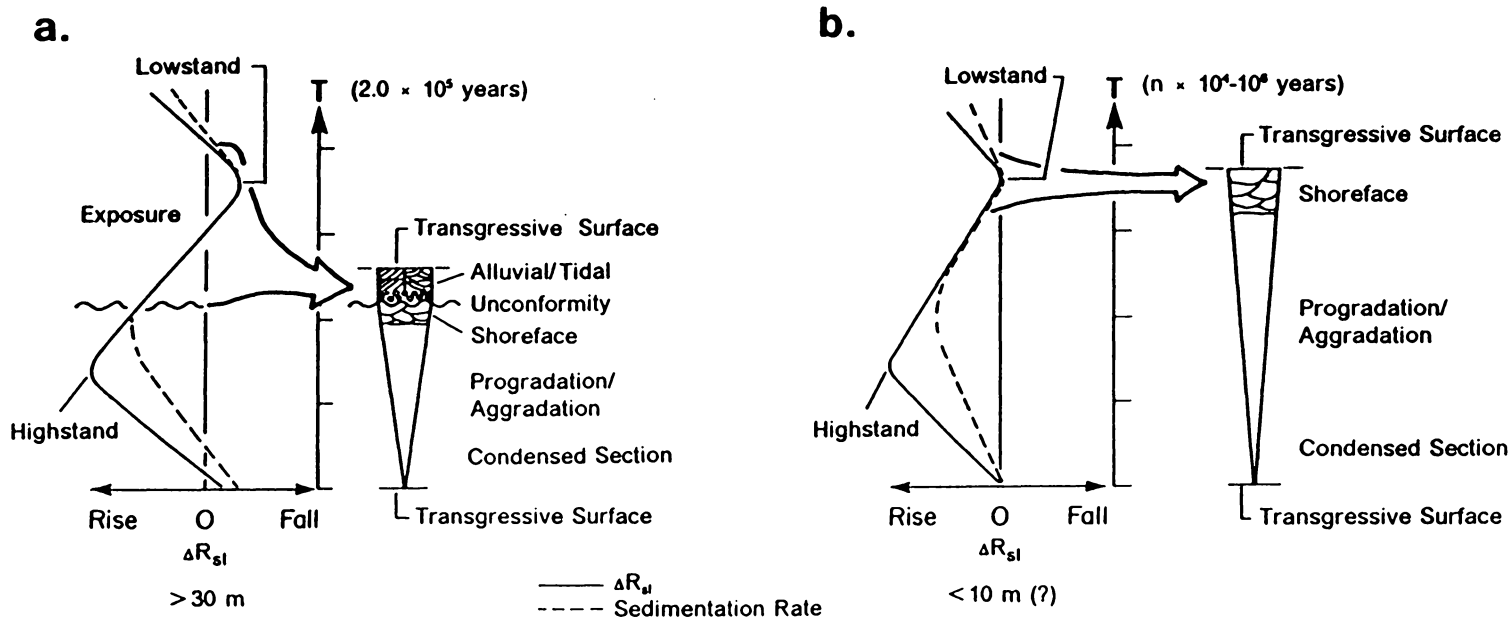
a.
Lowstand
T
(2.0 × 10⁵ years)
Exposure
Transgressive Surface
Alluvial/Tidal
Unconformity
Shoreface
Progradation/
Aggradation
Condensed Section
Transgressive Surface
Highstand
Rise
O
Fall
ΔRsl
>30 m
b.
Lowstand
T
(n × 10⁴-10⁶ years)
Transgressive Surface
Shoreface
Progradation/
Aggradation
Condensed Section
Transgressive Surface
Highstand
Rise
O
Fall
ΔRsl
<10 m (?)
ΔRsl
Sedimentation Rate

sea level and the marine sequence may have been eroded in the proximal part of the basin by alluvial channels. Degradation would have resulted in an unconformity or disconformity above the shoreface deposits (Fig. 1-15a). Sediment deposited above the disconformity or unconformity would bear no genetic relationship to the underlying shallow-marine progradational sequence; Walther's Law is thus only valid up to the unconformity or disconformity. Alluvial sediments may have been deposited on the erosional surface. During the ensuing gradual relative rise in sea level (ΔR_{sl}), the alluvial deposits along the shoreface disconformity commonly were reworked into a transgressive lag (Bergman and Walker, 1986; Plint *et al.*, 1986). Sediment trapped in embayments or on the inner shelf during sea level rise may have been reworked into tidal sandstone bodies (Nummedal 1986a,b). An accelerated relative sea level rise (ΔR_{sl}) resulted in drowning of the sequence and repetition of the cycle.

The Cretaceous model can be applied to the smaller progradational sequences in the P3 unit of the Uncompahgre Group (Fig. 1-3; Fig. 1-12; Fig. 1-15b). A similar scenario based on relative sea level change could account for the sequence of facies of the outer- to inner-shelf/shoreface transition of facies association A. The top of the progradational sequenes in P3 are not capped by alluvial, tidal or conglomeratic facies, but rather shoreface sandstones are overlain by outer-shelf mudstones (Fig. 1-15b). Unconformities are not present in these packages, suggesting that the magnitude of the relative sea level excursion was small (<10 m) and that sedimentation tracked this fall. The implied short time duration and widespread areal extent of small-scale progradational packages in the Uncompahgre Group suggests that these units were a product of short term (10^3 to 10^6 years) relative sea level changes probably attributable to eustatic effects. Similar progradational sequences of Late Cretaceous age have been documented by Swift *et al.* (1987). However these units are thought to be a product of varying sediment supply in conjunction with steady subsidence rates in the basin.

The thicker progradational sequences of the the Uncompahgre Group (P2-Q2, P3-Q3 and P4-Q4) represent greater time increments (10^6 to 10^7 years). Progradational sequences of equivalent thickness are present in the Archean Moodies Group, South Africa (Eriksson, 1979), the early Proterozoic Goulburn Group, Canada (Grotzinger and Gall, 1986), and the Devonian clastic wedges of the Appalachian Basin (Ettensohn, 1985).

By analogy with the Cretaceous example, it is possible to construct a model for a temporally separated storm/alluvial to tidal shelf for the thick sequences of the Uncompahgre Group. To create the necessary space to accommodate the 500 to 800 m-thick sequences relative sea level oscillations (ΔR_{sl}) of 100 to 300 m are required. The following scenario outlines the chronological and spatial evolution of these thick sequences.

1. Following an initial rapid relative sea level rise (ΔR_{sl}) mud was deposited on the outer shelf succeeded by a gradually increasing sand component related to aggradation and progradation of outer-shelf facies (Fig. 1-16; Fig. 1-17a). As sediment supply began to catch up with ΔR_{sl}, shoaling occurred and a graded storm-dominated outer to inner shelf was established. Ultimately shoaling led to emergence and alluvial sedimentation resulting in a rapid progradation of facies belts into the basin. As a consequence of progradational infill, the slope of the depositional interface was lowered (Fig. 1-16).

2. The second phase of sedimentation commenced during the succeeding gradual rise in relative sea level (Fig. 1-17a). As a product of shoreface retreat the depositional interface was beveled with the development of transgressive lags (Fig. 1-18). The former alluvial system was inundated and reworked. Coarse-grained sediment

Figure 1-16: Temporally separated storm/alluvial and tidal shelf. Prograding storm/alluvial shelf following a rapid relative rise in sea level. Shoreface is narrow with a sharp transition to alluvial setting. Note lack of tidal depositional units.

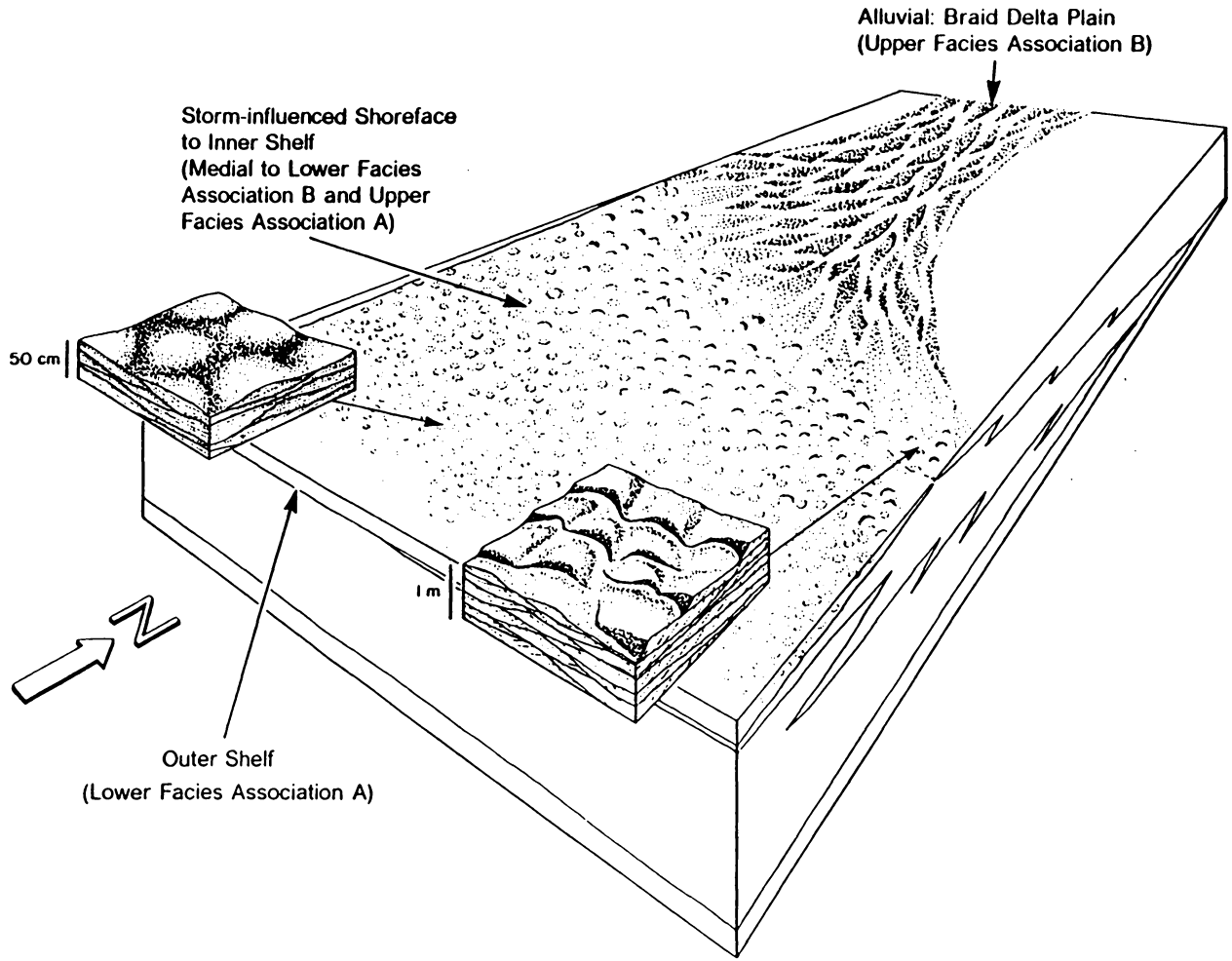

Prograding storm-dominated shelf following rapid sea level rise

Figure 1-17: Synthetic cycles, large-scale progradational sequences.

a) Large-scale oscillation (100 to 300 m (?)) in simple relative sea level curve over a time interval of approximately 10^6 to 10^7 years. Unconformities plus alluvial and tidal facies are confined to the upper one-half to one-third of the progradational sequence.

b) Composite relative sea level curve incorporating superimposed cycles of 10^5 years (glacio-eustatic) and 10^6 to 10^7 years (subsidence) with a net 100 to 300 m (?) oscillation in sea level. Note multiple unconformities or disconformities generated in the upper one-third to one-half of the sequence are represented by alternating alluvial and shallow-marine tidal deposits.

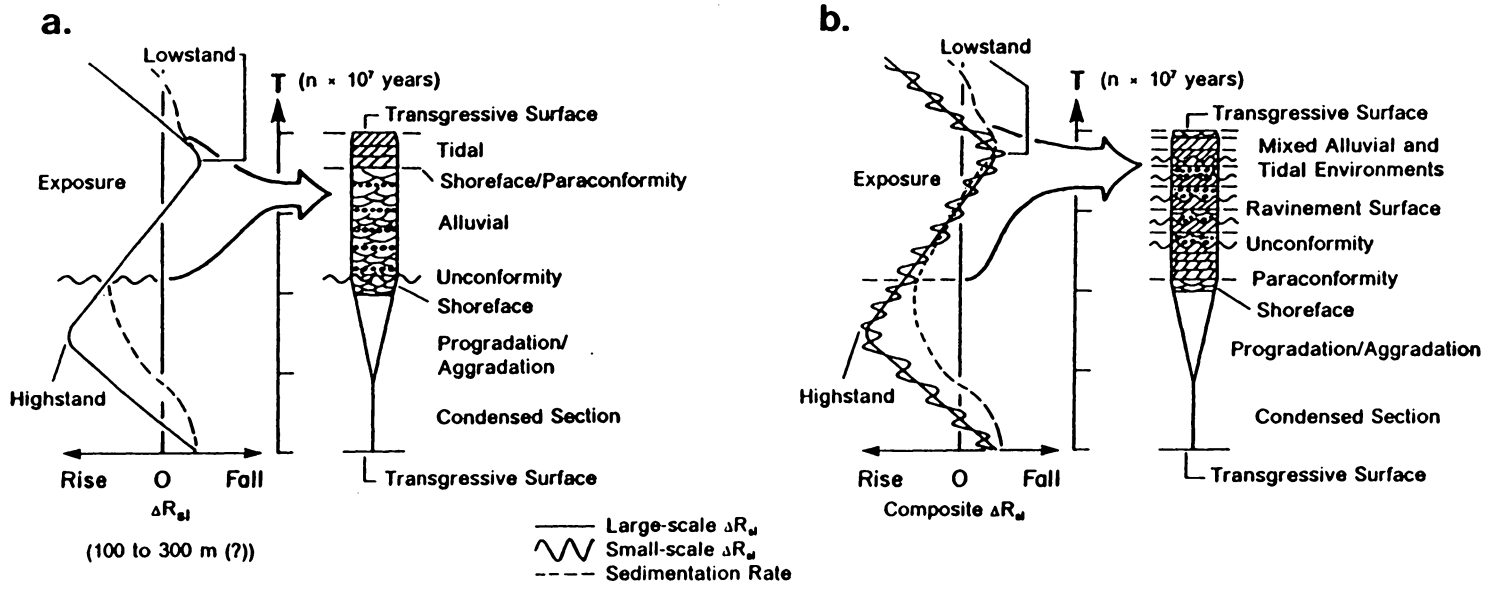
a.
Lowstand
T (n × 10⁷ years)
Transgressive Surface
Tidal
Shoreface/Paraconformity
Exposure
Alluvial
Unconformity
Shoreface
Progradation/
Aggradation
Highstand
Condensed Section
Rise
O
Fall
Transgressive Surface
ΔR_sl
(100 to 300 m (?))
Large-scale ΔR_sl
Small-scale ΔR_sl
Sedimentation Rate
b.
Lowstand
T (n × 10⁷ years)
Transgressive Surface
Mixed Alluvial and
Tidal Environments
Exposure
Ravinement Surface
Unconformity
Paraconformity
Shoreface
Progradation/Aggradation
Highstand
Condensed Section
Rise
O
Fall
Transgressive Surface
Composite ΔR_sl

Figure 1-18: Temporally separated storm/alluvial and tidal shelf. Development of a tide-dominated shelf, during stasis to a slow rise in relative sea level. Note mud deposition and absence of storm deposits on outer shelf.

Tide-dominated shelf following gradual sea level rise

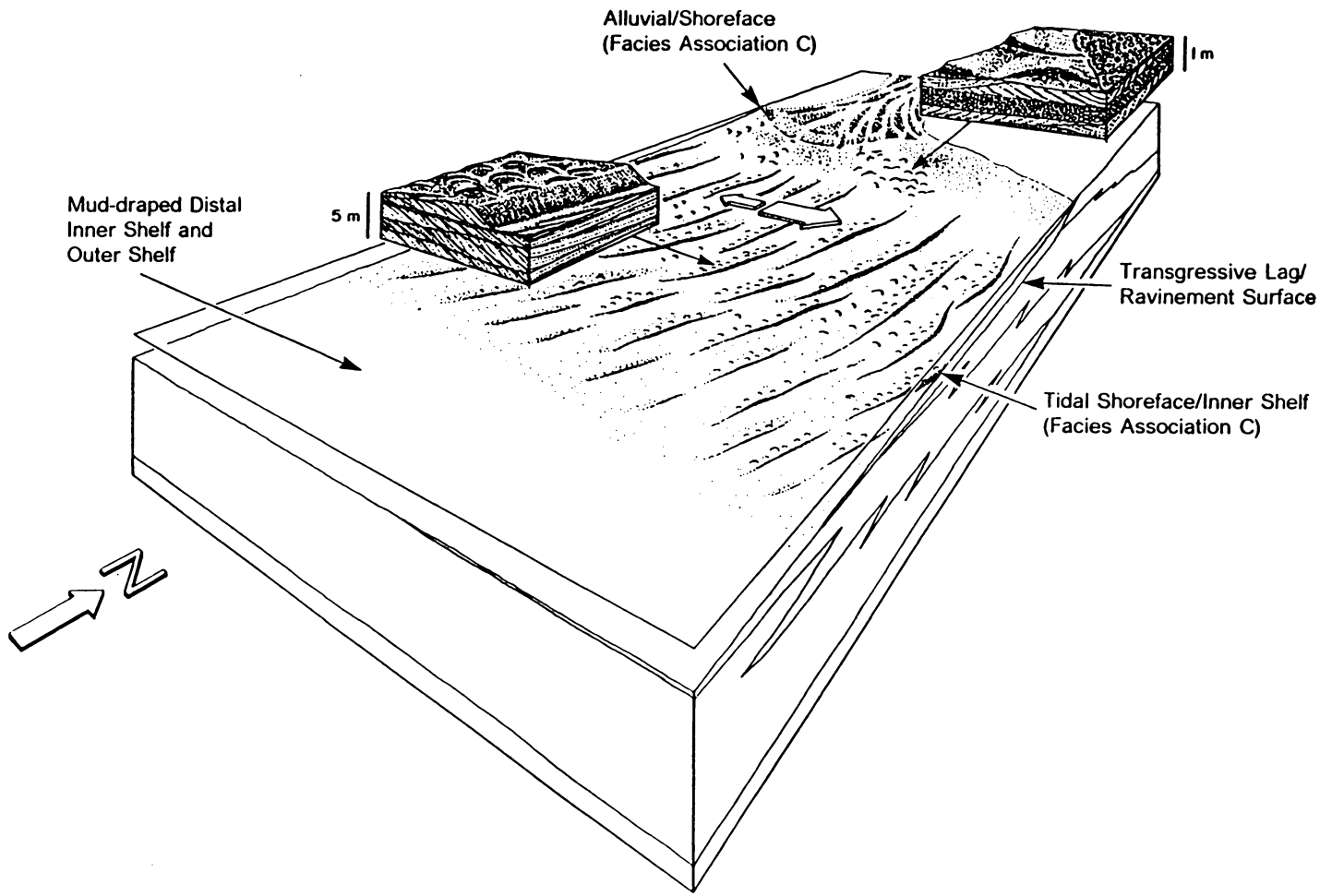

trapped in braid deltas was moved offshore during storm events. A wide, flat shelf developed during this phase of sedimentation would be conducive to tidal amplification and thus promoted the development of inner shelf-shoreface tidal facies (C) (Fig. 1-17a; Fig. 1-18). Mudstones were deposited beyond the depth and range of tidal reworking. Storm overprint in the tidal facies created gravel lags, but extensive thick sequences of storm-produced facies (hummocky cross-stratified sandstones) were not generated because of the coarse grain size of the sediment. With an accelerating rise in ΔR_{sl}, the tidal shelf was inundated and succeeded by the deposition of mudstone defining the base of the next progradational sequence (Fig. 1-17a).

The temporally separated storm/alluvial and tidal shelf model for the thick progradational sequences of the Uncompahgre Group does not explain the occurrence of the smaller-scale packages in the P3 unit; these were previously attributed to diminished relative sea level excursions of shorter time duration (10^5 years). Other lines of evidence pointing to the occurrence of smaller increments of relative changes in sea level within the large-scale progradational sequences include: 1) the periodic drowning and re-establishment of the tidal shelf/shoreface environments (association C; Fig. 1-8a), 2) the alternation between shoreface conglomerates and tidal pebbly sandstones (association C; Fig. 1-9b), 3) the transition from shoreface facies (association A) to inner-shelf sandstones (association B; Fig. 1-12) and 4) the alternation in Q3 of inner-shelf facies of association B and the tidal inner-shelf/shoreface facies (association C; Fig. 1-8; Fig. 1-12). In Fig. 1-17b a composite relative sea level curve (ΔR_{sl}) is shown which integrates two time scales of relative sea level oscillation, those of 10^5, and 10^6 to 10^7 years. Following a rapid rise in ΔR_{sl}, the same general type of progradational sequence was produced as in Fig. 1-17a but with one significant difference. As sedimentation resulted in shoaling near highstand, the shorter duration and smaller-scale oscillations led to the

development of thinner progradational packages. During a gradual fall in ΔR_{sl}, the effects of the small-scale excursions in relative sea level created rapid spatial changes in the paleoenvironments reflected in the alternation of alluvial and tidal facies in association C (Fig. 1-8; Fig. 1-9). Subtle unconformities or disconformities (ravinement surfaces) separated these facies from contrasting environments (Fig. 1-17b). Following lowstand, a gradual rise in ΔR_{sl} first resulted in re-establishment of an exclusively shallow-marine setting (Fig. 1-17b). With an accelerating ΔR_{sl} the shelf was terminally drowned and an outer shelf environment was developed.

What factors controlled the large-scale oscillations in relative sea level which generated the 500 to 800 m-thick progradational sequences in the Uncompahgre Group? Based on their probable minimum time duration of 10^7 years they cannot be related solely to glacio-eustatic effects of 10^3 to 10^6 years. Therefore, longer term secular controls must be appealed to, such as tectonic events of 10^7 years frequency. Analogous shallow-marine shelf to alluvial transitions to that in the Uncompahgre Group, are documented in the clastic wedges of Devonian age in the Appalachian basin (Ettensohn, 1985) and in the Goulburn Group of Early Proterozoic age in Canada (Grotzinger and Gall, 1986). In both of these examples, basin subsidence to accommodate the thick sedimentary sequences was attributed to tectonic activity marginal to the basin.

There are several problems which are not considered in the temporally separated storm/alluvial and tidal shelf model; these problems are identified and addressed in the points below:

1. The variable contribution of isostatic loading has not been accounted for in this model. This factor is not considered because it is not possible to determine the sedimentation rates.

2. Sediment supply and its variability due to external factors such as climatic and source area changes is not known. Transitions from alluvial to marine facies (association C) could reflect a variable sediment supply to the sedimentary basin during a constant rate of change in ΔR_{sl}.
3. The age constraints for deposition of the Uncompahgre Group are poor, thus it is difficult to clearly determine the time duration of periods of sediment starvation and enrichment. Only by analogy with Phanerozoic and other Proterozoic units with more precise time bracketing, can the assumed time intervals be applied to the Uncompahgre Group.
4. Autocyclic mechanisms, such as a shift in depositional loci in an alluvial system marginal to a shallow marine repository (Levell, 1980b), could explain the facies transitions evident in association C. However the broad sheetlike nature of depositional units and their relatively consistent spatial distribution suggests this may not be a valid criticism of the model.

CONCLUSIONS

1. Siliciclastic sedimentary rocks in the Uncompahgre Group were deposited primarily in a shallow-marine setting influenced by storms, waves and tides with periodic shoaling to an alluvial braid-delta or distal braid plain environment. The succession of facies in associations A to B and C record shoaling from: 1) outer shelf to storm- to wave-current dominated inner shelf or shoreface (association A) to; 2) inner shelf/shoreface to alluvial (association B) to; 3) tidal inner shelf/shoreface to alluvial (association C) environments of deposition. Terminal drowning at the top of the progradational sequences led to the development of a short increment of association B (inner shelf) followed abruptly by outer shelf mudstones of association A.

2. Two possible models exist for sedimentation in a shallow-marine shelf setting dominated by tides and storms: 1) a coeval storm to tidal shelf and 2) a temporally separated storm/alluvial and tidal shelf. The latter model is preferred to explain the evolution of the thick progradational sequences in the Uncompahgre Group, that are similar to smaller-scale Cretaceous analogs. The second model best explains the data base because: 1) tidal sandstone bodies cannot be traced in the outcrop belt laterally into storm beds, 2) tidal sandstone bodies are not in direct contact with the storm-dominated portions of the progradational units in vertical sequence, and 3) sediment transport across an inner tidal shelf orthogonal to the dominant, shoreline-parallel, tidal-current system, has not been documented from Holocene examples.
3. The inferred cyclic ordering of facies in the vertical sequences of the Uncompahgre Group may be explained by a composite eustatic/tectonic relative sea level curve. Small-scale cycles (tens of meters in thickness) of probable short time duration (10^5 to 10^6 years) may reflect changes in eustasy related to Milankovich cycles. Thick progradational cycles which are 500 to 800 m thick and compose the P2-Q2, P3-Q3 and P4-Q4 stratigraphic units are attributed to pulses of accelerated tectonic subsidence of probable 10^7 years duration. The composite cyclicity present in the Uncompahgre Group created subtle unconformities or disconformities in the shoaling portions of the progradational sequences. These discordances imply that vertically stacked facies are not genetically related to one another.

Chapter 2: Polyphase Deformation and Conjugate Shearing in Metasedimentary Rocks of the Uncompahgre Group: A Proterozoic Fold Belt in Southwest Colorado

ABSTRACT

Isolated remnants of cover rocks comprising the Uncompahgre Group in the Needle Mountains and Uncompahgre Gorge area have been subjected to polyphase deformation and greenschist facies metamorphism. Two phases of approximately coaxial deformation were succeeded by conjugate shearing. Phase 1 structures (recognized only in the West Needle Mountains) included bedding-parallel, ductile deformation zones and F_1 mesoscopic folds and an associated cleavage S_1. Continued compression during phase 2 resulted in upright folding of early structures and the development of macroscopic F_2 folds and an axial-planar cleavage S_2. Coincident with upright folding of cover, basement-cover contacts were folded. Further shortening during Phase 3 deformation resulted in conjugate shearing of cover rocks with the development of both a macroscopic F_3 fold and an S_3 crenulation cleavage. In addition, basement-cover contact zones were activated as phyllonitic, oblique-slip, reverse faults. Conjugate shearing produced strike-parallel offset of stratigraphic units, with loss of section. Conjugate reactivation of Phase 1 ductile deformation zones was manifested by oblique dextral and sinistral slip.

The structural evolution of the Uncompahgre Group records the transition from a ductile, north-directed, thin-skinned, fold-thrust belt to the formation of a basement-

involved "megamullion" structure which was subjected to conjugate strike-slip faulting to accommodate further shortening. The results of this study indicate that the basal unit of the Uncompahgre Group was parautocthonous on basement, thus implying that the metasedimentary cover rocks are younger than surrounding ca. 1750 Ma basement gneisses and ca. 1690 Ma granitoids. The overall style of deformation may be analogous to the deep foreland suprastructure of an orogenic belt which developed between ca. 1690 Ma and 1600 Ma in the southwestern U.S.A..

INTRODUCTION

Folded and faulted sequences of sedimentary cover rocks in Precambrian and Phanerozoic orogenic belts reached their final deformed state by a variety of different paths. Unraveling the deformation history of these units becomes more problematic when they occur as isolated fragments within or marginal to higher-grade amphibolitic, gneissic and plutonic basement. These remnants have been interpreted to be fold-thrust belts (Hoffman and others, 1984; Tirrul, 1985; King, 1986; Jackson and others, 1987), parautocthonous megamullions of former rift basins (Tricart and Lemoine, 1986) or wrench-faulted transpressional basins (Aspler and Donaldson, 1985). By analogy, a thick sequence of quartzites and pelites comprising the Early to Middle Proterozoic Uncompahgre Group in the Needle Mountains of southwest Colorado has been interpreted to be to be a remnant of a fold-thrust belt involved in south-directed tectonic transport (Tewksbury, 1985). In the regional context of deformation of approximately coeval cover sequences in the southwest U.S.A., the south-directed transport direction of metasedimentary rocks in the Needle Mountains is opposite to that recognized in New Mexico and Arizona (Grambling and Codding, 1982; Puls and Karlstrom, 1984; Karlstrom and Conway, 1986). A critical point for evaluating the fold-thrust belt model

for the Uncompahgre Group is to determine the original sequential and chronological arrangement of stratigraphic units. Previous studies (Cross and others, 1905; Barker, 1969; Tewksbury, 1985, 1986) failed to resolve this crucial problem within the Uncompahgre Group. With an established stratigraphic framework it is then possible to determine if the geologic structures are similar to those typical of fold-thrust belts (cf. Boyer and Elliott, 1982).

New structural and stratigraphic data, plus a re-examination of published data, indicates that previous interpretations for the evolution of the Uncompahgre Group need to be re-evaluated. A somewhat different deformation model is proposed that can be compared with other examples in which sedimentary cover occurs as deformed inliers within basement. It is also important for constraining models of the tectonic evolution of a portion of the Proterozoic Colorado Province (after Bickford and others, 1986) of the southwest U.S.A..

GEOLOGIC SETTING

Proterozoic metasedimentary rocks of the Uncompahgre Group are located in the Needle Mountains near Silverton and in Uncompahgre Gorge near Ouray in southwest Colorado (Fig. 2-1). Inferred basement to the Uncompahgre Group in the Needle Mountains consists of ca. 1750 Ma amphibolite grade mafic and felsic gneisses and ca. 1690 Ma weakly-foliated granitoid plutons which intrude and cross-cut earlier tectonic fabrics in basement gneisses (Gibson and Simpson, 1986; Harris and others, 1987). Basement is not exposed in the Uncompahgre Gorge area.

In the West Needle Mountains area, the Uncompahgre Group occupies an east-west trending, 3 to 8 km-wide synclinorium commonly bounded by basement on the north and south (Fig. 2-1). Metamorphic grade varies from middle to upper greenschist facies

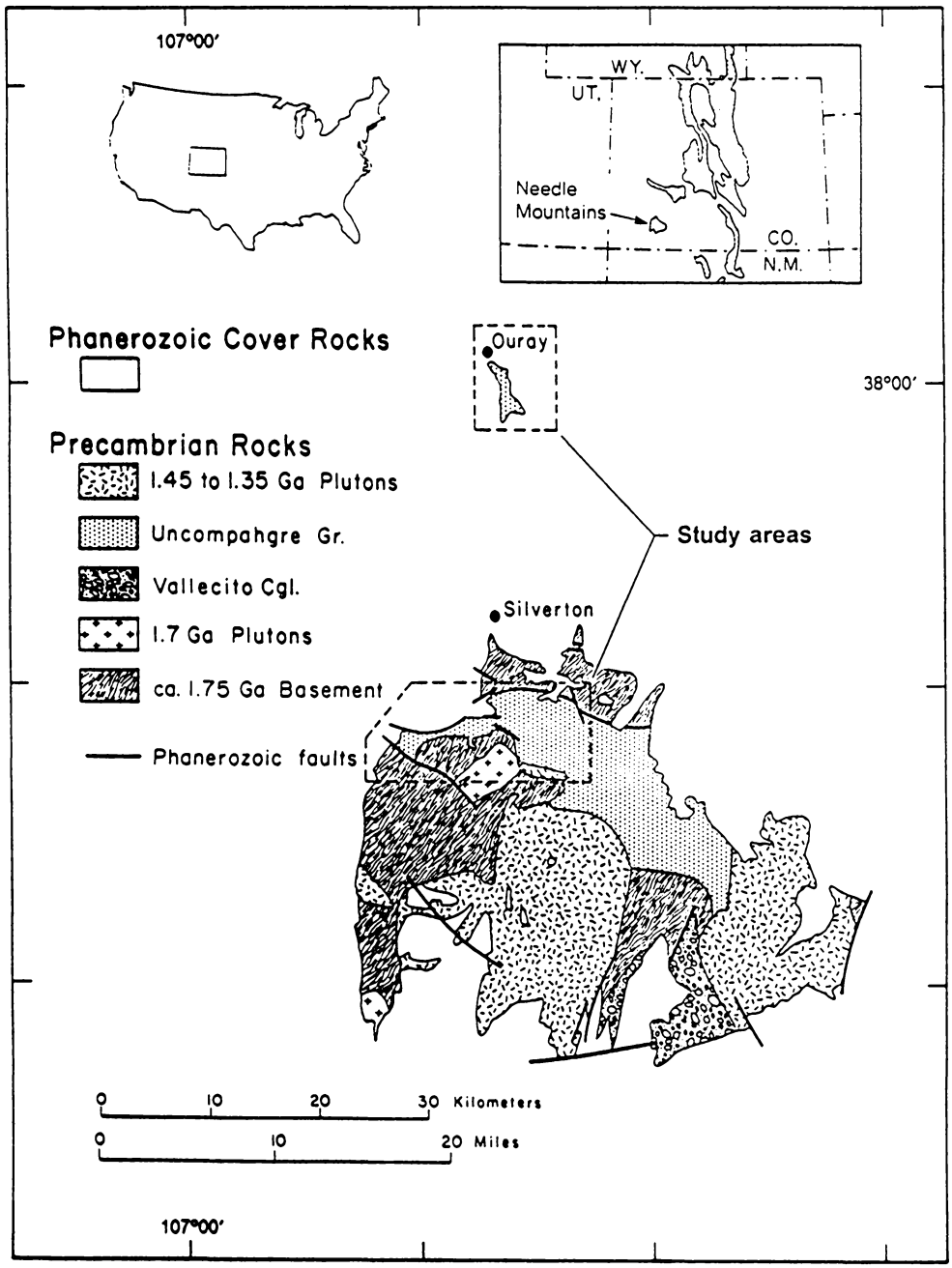

Figure 2-1: Generalized geologic map of the Needle Mountains. Geology modified from Barker (1969) and Steven and others (1974). Inset shows location of Needle Mountains in relation to other areas of Early to Middle Proterozoic outcrops (stippled).

based on the mineral assemblages present in pelites; white mica + quartz + chlorite ± biotite ± andalusite ± garnet ± chloritoid. The Uncompahgre Group consists of thick alternating units of quartzite and pelite in which abundant primary sedimentary structures provide excellent control on facing directions. Based on the work of Barker (1969) and Harris and others (1987) the Uncompahgre Group unconformably overlies surrounding basement and is therefore no older than the ca. 1690 Ma granitoids. A minimum age for the Uncompahgre Group and its associated deformation is provided by the cross-cutting, undeformed ca. 1450 Ma Eolus Granite (Silver and Barker, 1968; Barker, 1969; Bickford and others, 1969).

A generalized sequence of deformation for the Uncompahgre Group has been outlined by Tewksbury (1981, 1985, 1986) and consisted of the following phases : 1) an inferred layer-parallel translation of quartzite and pelite units to the south, based on a movement sense recognized on the southern basement/cover contacts, as thrust nappes generating meso- to microscopic F_1 folds and S_1 cleavage, 2) a later upright macroscopic F_2 folding and overprinting of the earlier S_1 cleavage by a spaced crenulation cleavage S_2, and 3) a final weak phase of north-trending microscopic to mesoscopic folding generating an S_3 crenulation cleavage which overprints S_1 and S_2. Where preserved and not truncated by Phanerozoic faults, contacts with basement are defined by 2 to 12 m-thick zones of phyllite and phyllonite interpreted as major north-dipping thrust faults merging with a basal decollement at depth (Tewksbury, 1985). The results of this study concur with the chronology of structures but not the deformation model proposed by Tewksbury (1981, 1985, 1986).

Post-Proterozoic brittle faults in the Uncompahgre Group are subparallel to and cross-cut Precambrian fabrics and structures. Brittle faults extend into and offset the adjoining Phanerozoic cover. In the Uncompahgre Group brittle faults are steeply dipping cm- to m-wide zones of iron-stained breccias of either quartzite or pelite and

psammite. Displacement on these faults varies from meters to possibly hundreds of meters, based on the measurable offset in adjoining Phanerozoic cover rocks.

STRATIGRAPHIC FRAMEWORK

Zones of relatively low strain, without evidence of tectonic duplication, were delineated by initial reconnaissance mapping. From measured sections of lithologic units in the Lime Creek and Snowdon Peak areas and the Uncompahgre Gorge area (Fig. 2-1) four quartzite/conglomerate units with distinctive associations of facies are recognized; these units are separated by thick intervals of pelite and psammite (Fig. 2-2). The basal unit of the Uncompahgre Group Q1, defines a retrogradational sequence which exhibits an overall upward-thinning and -fining of conglomerate/sandstone beds. Conglomerates at the base of Q1 are transitional upward to interbedded conglomerate and cross-bedded quartzite (Fig. 2-2). Q1 is gradational with psammite and pelite of the overlying P1 unit (Fig. 2-2). This retrogradational sequence is succeeded by three progradational sequences which record an upward-thickening and -coarsening of individual beds of pelite transitional to psammite, quartzite and conglomerate (P2-Q2, P3-Q3 and P4-Q4; Fig. 2-2). Q4 is capped by a final pelitic unit P5. Carbonaceous pelites are present in P3, P4 and P5 but not in P1 and P2. Thinner progradational units of interbedded psammites and thin- to medium-bedded quartzites in P3 (Fig. 2-2) define distinctive marker units that can be correlated over large areas of the Uncompahgre outcrop belt (Fig. 2-1). Similar units are absent in P1, P2, P4 and P5. The thick quartzite/conglomerate units Q2, Q3 and Q4 can be differentiated from one onother on the basis of a distinct sequential arrangement of facies; the detailed facies variations in these units are elaborated upon in Harris and Eriksson (1987).

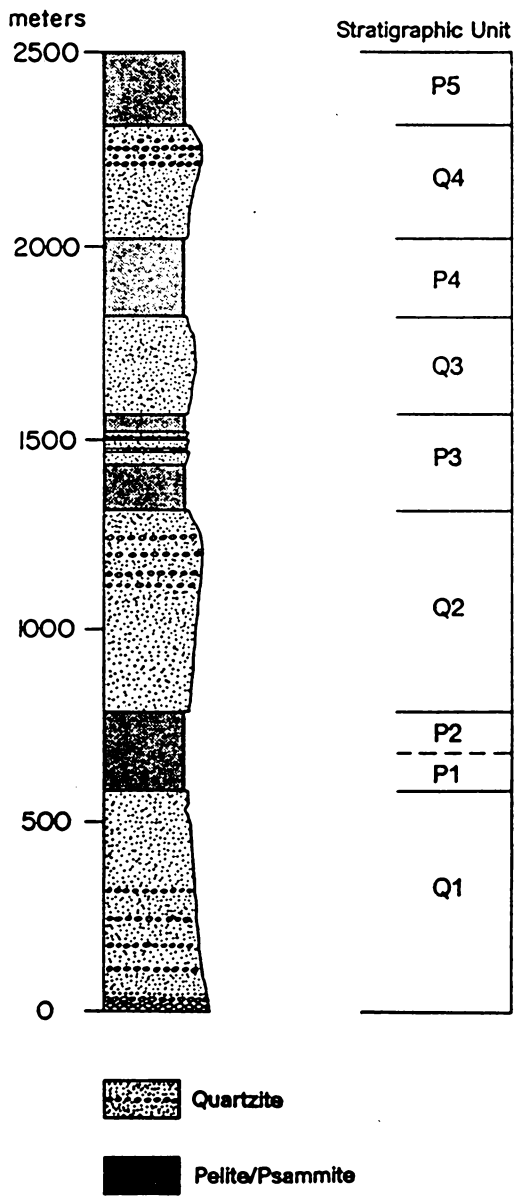

Figure 2-2: Stratigraphic subdivisions of the Uncompahgre Group.

STRUCTURAL GEOLOGY

Metasedimentary rocks of the Uncompahgre Group have undergone a compressional polyphase deformation history. Three phases of deformation are outlined in the ensuing discussion and Table 2-1. First phase structures are commonly the most difficult to recognize due to pervasive overprinting by the second and third phases of deformation. Between structural domains deformation is heterogeneous, as is evident in the map pattern extending from Lime Creek through Snowdon Peak into the Animas River areas (Fig. 2-3). Based on the data of this study, there is no strong evidence for large-scale duplication or inversion (recumbent nappes) within the Uncompahgre Group (Fig. 2-3, Fig. 2-4, Fig. 2-5). However duplication within stratigraphic units, in particular Q2, is prevalent in the north-central and northeast portions of the West Needle Mountains (Fig. 2-3, Fig. 2-4).

During polyphase deformation, ductile deformation zones of quartz mylonite or phyllonite <12 m thick developed in the vicinity of the contacts between pelites/psammites and thick units of quartzite and conglomerate and along basement/cover contacts. Because of successive structural overprinting on these zones it is difficult to constrain their development to a particular interval in the 3 phases of deformation. For this reason ductile deformation zones are discussed under a separate heading.

Cleavage terminology is from Powell (1979) whereas that for folds is from Ramsay (1967) and Hobbs and others (1976). The descriptive terminology for ductile deformation zones is from Simpson and Schmid (1983) and Simpson (1986).

Structures	Folds	Cleavages	Ductile deformation zones	Comments
Phase 1	a. Mesoscopic 1 m to 50 m wavelength, upright to recumbent, open to tight, subhorizontal F_1 folds. b. Mesoscopic, < 1 m wavelength, intrafolial, tight to isoclinal or rootless F_1 folds.	Axial planar, spaced anastomosing to continuous S_1 cleavage in psammites and pelites.	a. Bedding-parallel, 1 to 10 cm-thick zones, with internal sigmoidal foliation S_m or S_{m1} in pelites or psammites. b. 1 to 5 m-thick zones of quartz- to mica-rich mylonite or phyllonite with an internal sigmoidal, closely spaced to continuous foliation S_m.	Localized in Q1, Q2 and Q3 and in transition between Q1-P1 and Q2-P2. Dominated by layer-parallel thrusting in Needle Mountains area.
Phase 2	a. Macroscopic, 1 to 3 km wavelength, upright to steeply inclined, gently plunging open to tight F_2 folds. b. Mesoscopic, < 10 m wavelength, parasitic folds on limbs of F_2 folds	Axial planar, discrete to zonal, crenulation cleavage, S_2. Microlithon spacing varies from 0.5 to 5 mm. Microfolds are symmetric to asymmetric.	a. a. and b. above are overprinted during Phase 2. Microfolds and crenulation of S_{m1} by S_{m2}. Asymmetric, 5 to 10 cm-spaced crenulation of S_m by S_m'. b. Micaceous, 1 to 12 m-thick zones of quartz-rich phyllonite on Q1/basement contact. Spaced to continuous foliation S_m and S_m'.	Affects all units in Needle Mountains and Uncompahgre Gorge areas with refolding of Phase 1 structures. Crenulation cleavage confined to psammites and pelites.
Phase 3	a. Broad, 3 km wavelength, steeply south-plunging, open, macroscopic F_3 fold in Lime Creek area (Fig. 3). b. Mesoscopic, 10 to 30 cm wavelength, steeply plunging kink folds in psammites and pelites. c. Mesoscopic, 10 to 20 m wavelength, steeply plunging M-folds in hinge of macroscopic F_3 fold.	a. Cm- to mm-spaced zonal crenulation cleavage S_3 which folds S_1/S_2 cleavage. b. 5 to 20 cm-spaced pressure solution seams in quartzites with concentration of opaques along these surfaces (Lime Creek area).	Overprinting on Phase 2 S_m fabric by S_m'. Oblique dextral and sinistral offset with development of asymmetric, boudinaged fabric and extensional crenulations S_m'.	Structures localized in western one-third of map area (Fig. 3) in Needle Mountains. Not recognized in Uncompahgre Gorge area (Fig. 5), except for lateral displacement and attenuation of stratigraphic units. Note loss of section in vicinity of Snowdon Peak due to strike-parallel movement of units.

Table 2-1: Chronology of structures in the Uncompahgre Group.

Figure 2-3: Geology of the Uncompahgre Group, West Needle Mountains. Section lines correspond with cross sections in Fig. 2-4. Detailed inset map (outlined) is Fig. 2-7. Southeastern portion of map area from Barker (1969) and Tewksbury (1981,1985).

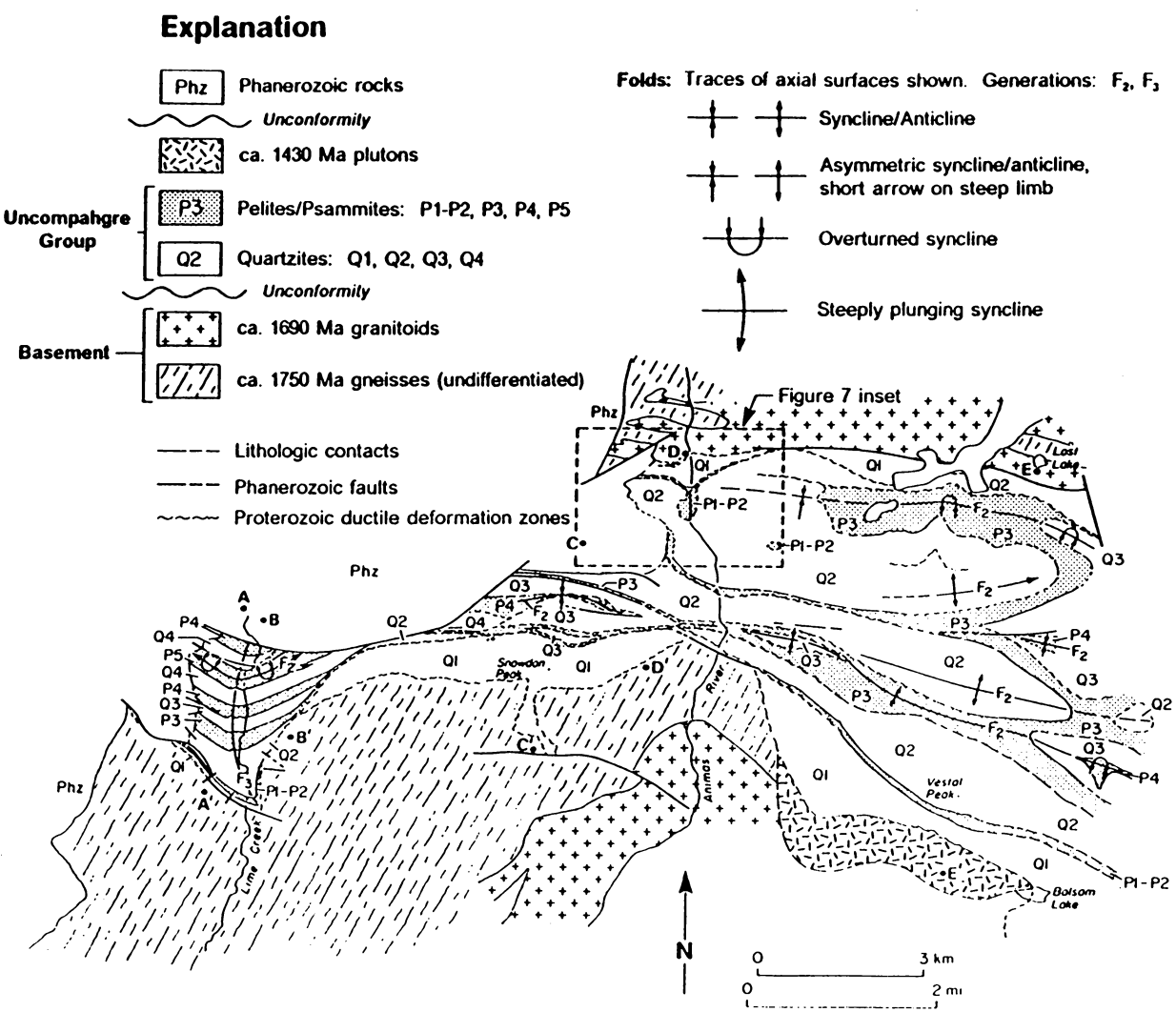
Explanation
Phz
Phanerozoic rocks
Unconformity
ca. 1430 Ma plutons
Uncompahgre Group
P3
Pelites/Psammites: P1-P2, P3, P4, P5
Q2
Quartzites: Q1, Q2, Q3, Q4
Unconformity
Basement
ca. 1690 Ma granitoids
ca. 1750 Ma gneisses (undifferentiated)
Lithologic contacts
Phanerozoic faults
Proterozoic ductile deformation zones
Folds: Traces of axial surfaces shown. Generations: F2, F3
Syncline/Anticline
Asymmetric syncline/anticline, short arrow on steep limb
Overturned syncline
Steeply plunging syncline
Figure 7 inset
Snowdon Peak
Vestal Peak
Bolsom Lake
Lost Lake
Animas River
Lime Creek
N
0 3 km
0 2 mi

Figure 2-4: Geologic cross sections of the Uncompahgre Group (UG). Arrows on post mid-Proterozoic brittle faults indicate high angle dip-slip displacement whereas arrows within stratigraphic units of the UG indicate movement sense on bedding-parallel ductile deformation zones.

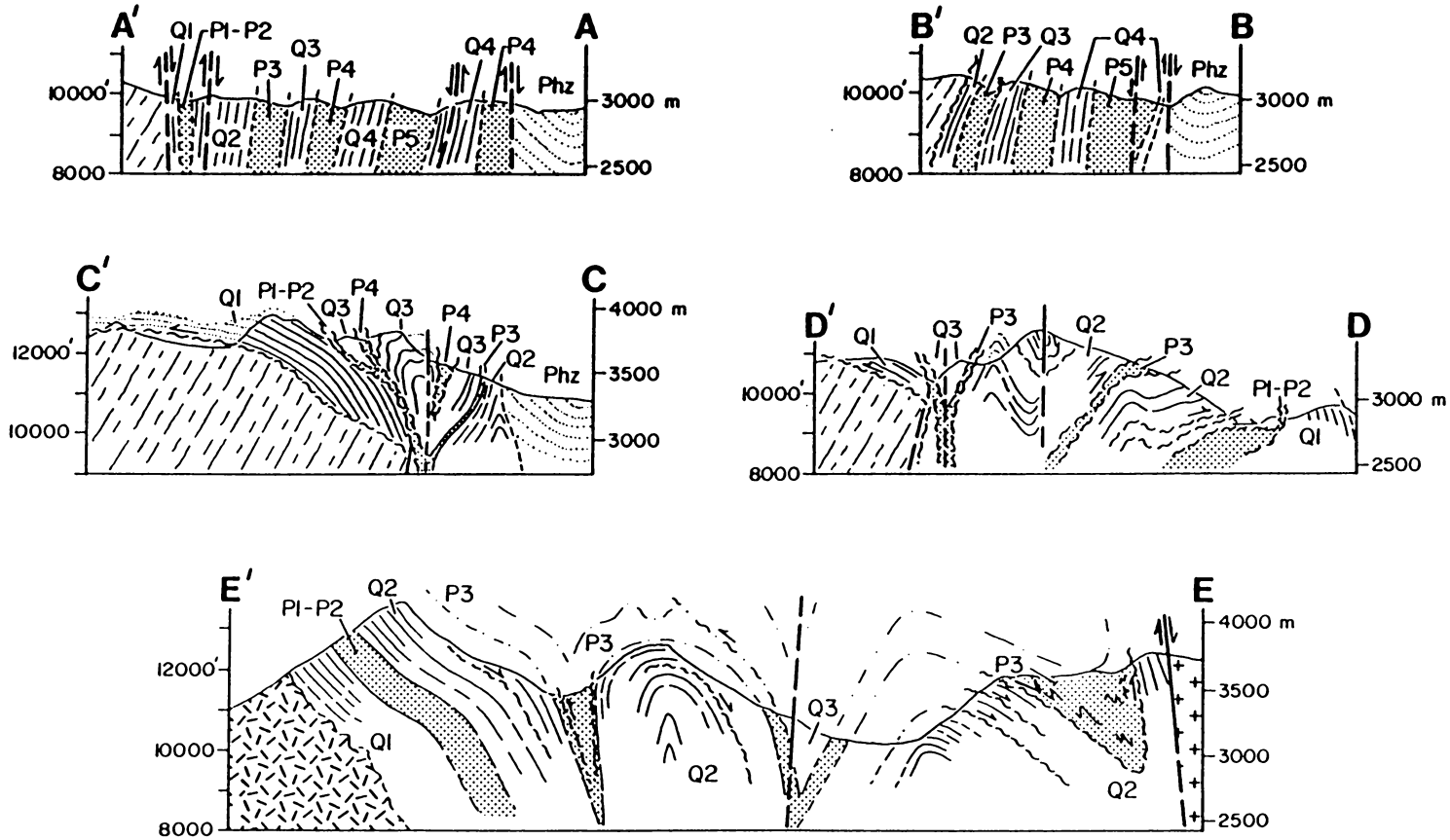
A'
A
Q1
P1-P2
P3
Q3
P4
Q4
P4
Phz
Q2
Q4
P5
10000'
8000
3000 m
2500
B'
B
Q2
P3
Q3
Q4
P4
P5
Phz
10000'
8000
3000 m
2500
C'
C
Q1
P1-P2
Q3
P4
Q3
P4
Q3
P3
Q2
Phz
12000'
10000
4000 m
3500
3000
D'
D
Q1
Q3
P3
Q2
P3
Q2
P1-P2
Q1
10000'
8000
3000 m
2500
E'
E
P1-P2
Q2
P3
P3
P3
Q3
Q1
Q2
Q2
12000'
10000
8000
4000 m
3500
3000
2500

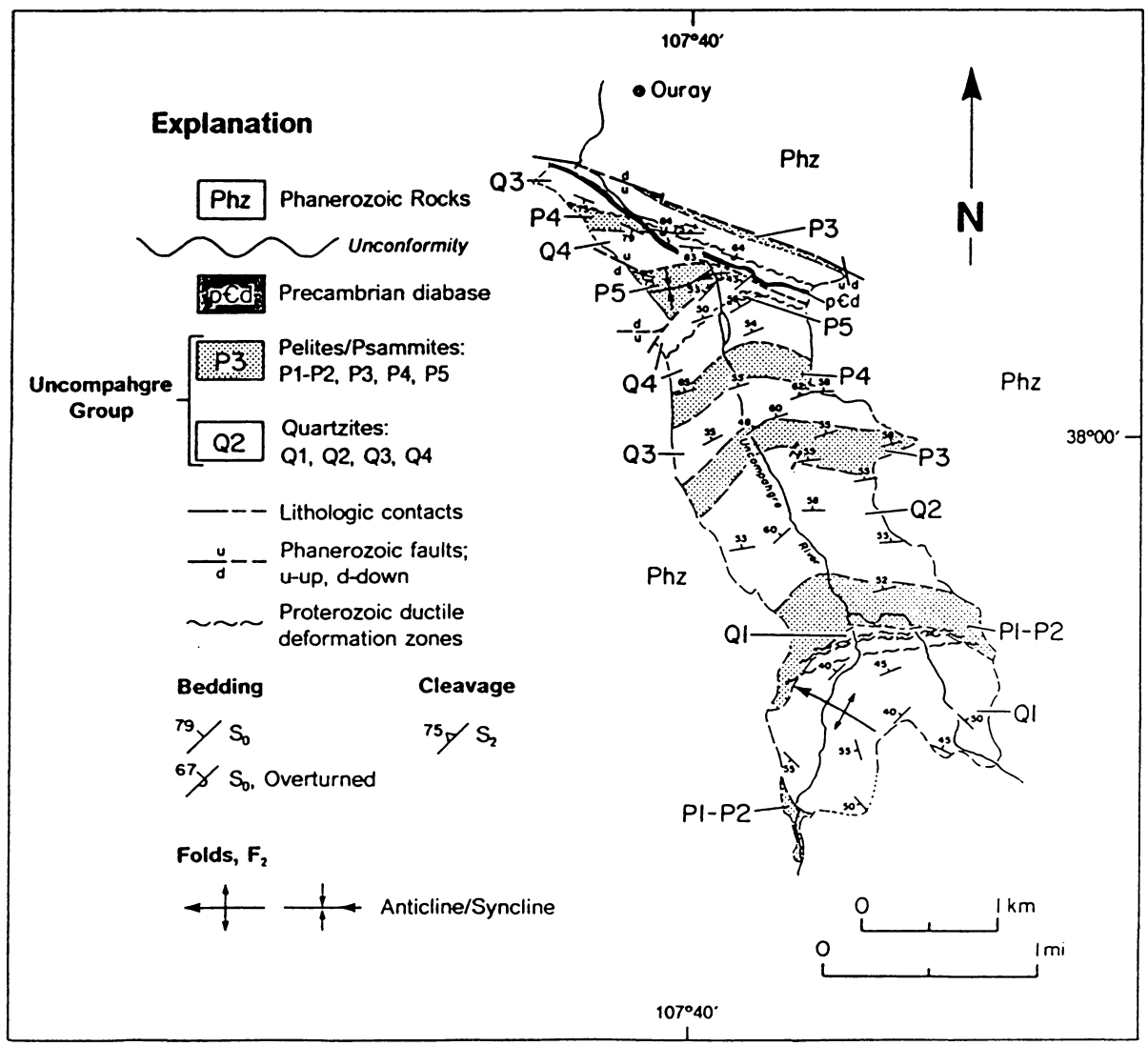

Figure 2-5: Geology of the Uncompahgre Group in Uncompahgre Gorge area. Geology modified from Luedke and Burbank (1962) and Burbank and Luedke (1964), incorporating additional mapping of this study.

Phase 1 Structures

Phase one structures consist of centimeter-scale, vein-quartz rich, bedding-parallel shear zones (Fig. 2-6) and mesoscopic F_1 folds with an associated axial-planar cleavage S_1. Bedding-parallel deformation zones are most common in stratigraphic units Q1, Q2, and Q3 east of the Lime Creek area in the West Needle Mountains (Fig. 2-3, Fig. 2-4) whereas in the Uncompahgre Gorge area they are uncommon. These zones typically result in disruption of the normal sequential facies ordering in stratigraphic units. Significant translation and repetition within the Uncompahgre Group is best exemplified in the Q2 unit, as graphically illustrated along the cliffs above the Animas River south of the basement/cover contact (Fig. 2-7, Fig. 2-8). Bedding-parallel shear zones that are 5 to 20 cm thick, are present in pelitic units between individual quartzite beds. Shear zones along these surfaces are defined by a sigmoidal, spaced foliation, S_m or S_{m1}, commonly emphasized by post-kinematic andalusite porphyroblasts and poikiloblasts. Relict bedding in pelites is obliterated and replaced by a pervasive fabric defined by quartz veins, elongate detrital grains, white mica and hematite (Fig. 2-6). Movement sense, based on the geometry of shear zone fabrics (S_m), associated quartz fibers (L_s) and mineral lineations (L_m, elongate white mica and hematite), is to the north (Fig. 2-7, Stereoplot 4). The magnitude of displacement on these zones is unknown, although individual beds are truncated over lateral distances of several hundred meters.

Mesoscopic F_1 folds and S_1 cleavage are developed in portions of stratigraphic units P1-P2, Q2, P3 and Q3. These early structures are typically associated with the previously described bedding-parallel faults. Mesoscopic subhorizontal, east-west trending folds vary from upright to recumbent and are open to rarely isoclinal (Fig. 2-7, stereoplot 3; Fig. 2-9; Fig. 2-10, Domain IV). Wavelengths of F_1 folds are less than 50 m (Fig. 2-8). Fold geometries are similar to those of class 1B, 1C and 2 of Ramsay

Figure 2-6: Bedding-parallel deformation zone in Q1 near Snowdon Peak.

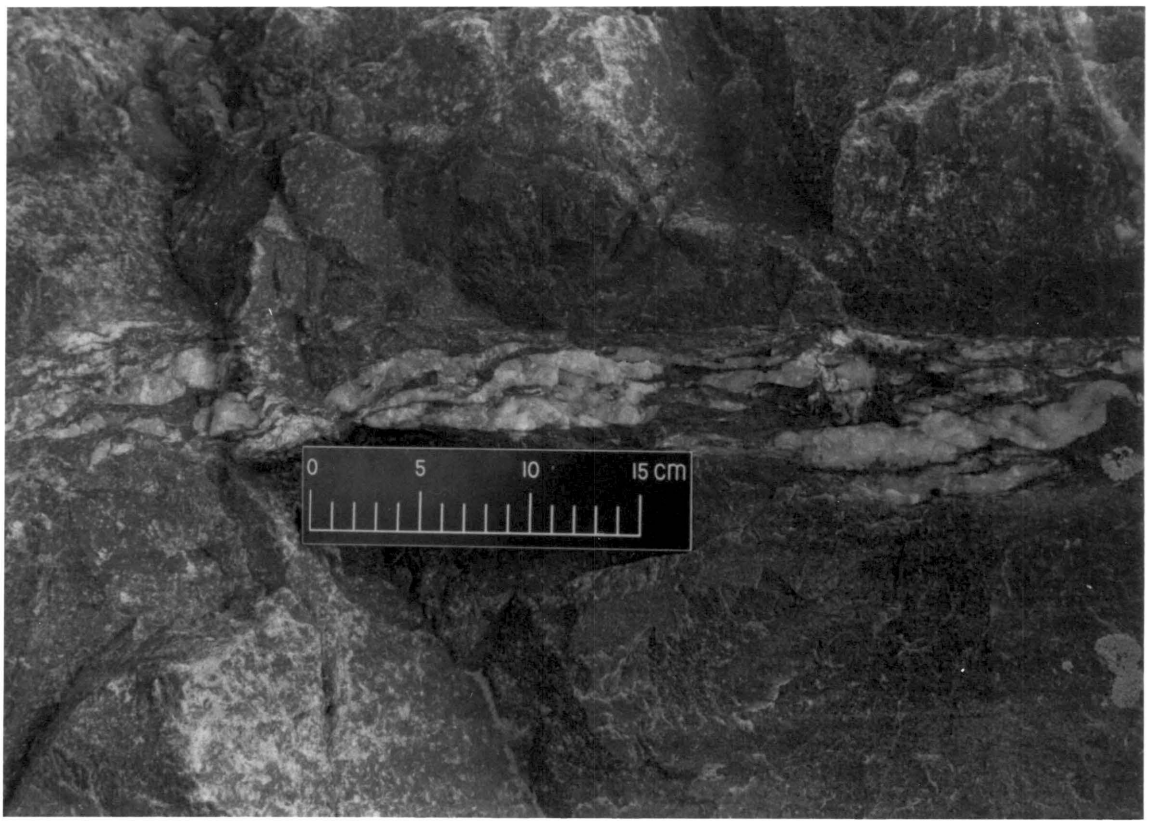
0
5
10
15 cm

Figure 2-7: Geologic map of Uncompahgre Group along the Animas River. Compare with location of inset in Fig. 2-3. Stereograms 1, 2, 3 and 4 are lower hemisphere equal area projections. Arrows on linear elements (mineral lineations, L_m, and quartz fibers, L_s) indicate apparent transport directions in corresponding shear zones.

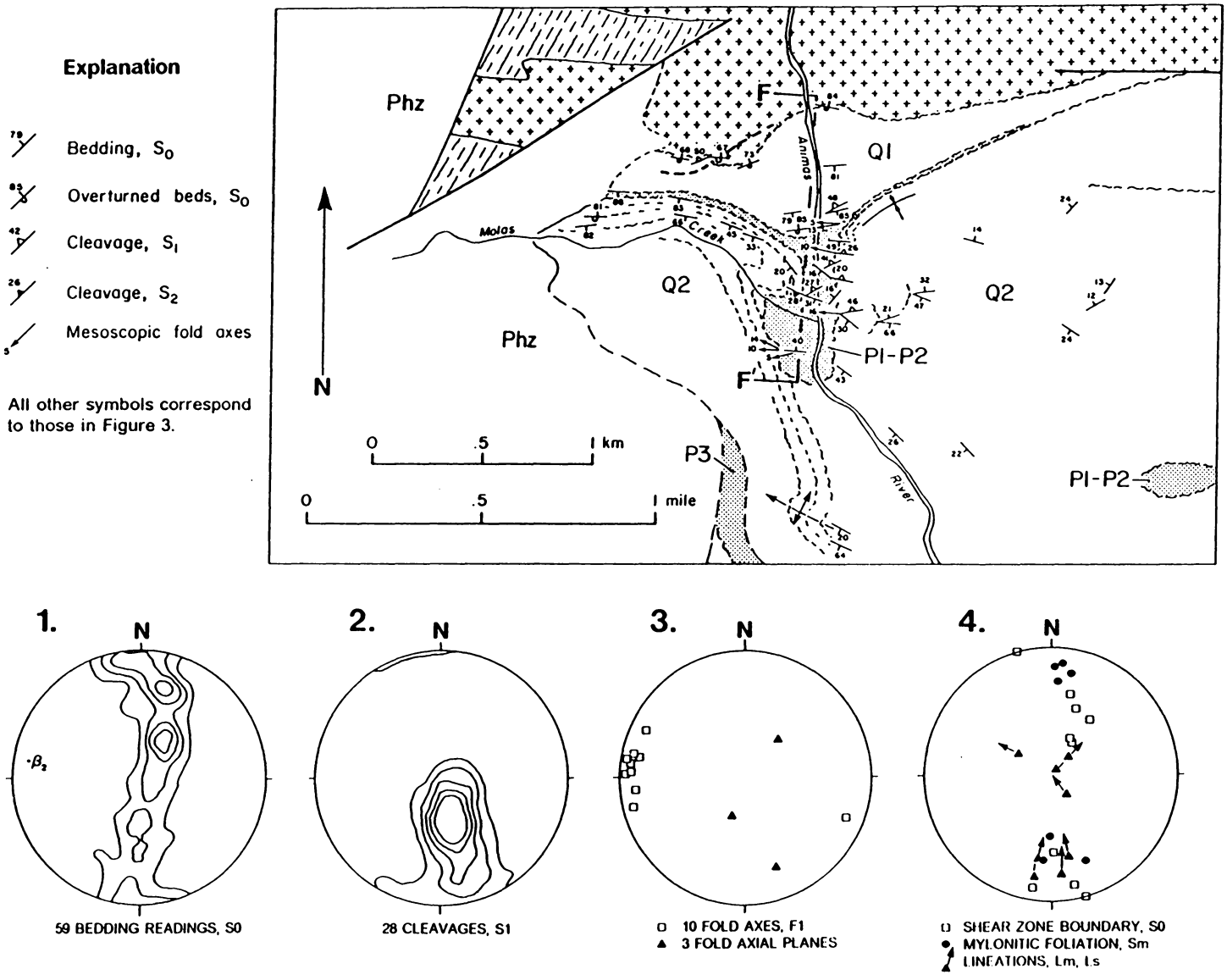
Explanation
Bedding, S_0
Overturned beds, S_0
Cleavage, S_1
Cleavage, S_2
Mesoscopic fold axes
All other symbols correspond to those in Figure 3.
Phz
F
Q1
Q2
Q2
Phz
F'
P1-P2
P3
P1-P2
N
0 .5 1 km
0 .5 1 mile
Molas
Animas
River
1.
N
59 BEDDING READINGS, S0
2.
N
28 CLEAVAGES, S1
3.
N
10 FOLD AXES, F1
3 FOLD AXIAL PLANES
4.
N
SHEAR ZONE BOUNDARY, S0
MYLONITIC FOLIATION, Sm
LINEATIONS, Lm, Ls

Figure 2-8: Geologic cross section along the Animas River. Section corresponds to line F-F′ in Fig. 2-7. Scale is not the same. Insets a. and b. illustrate deflection and truncation of S_1 by bedding-parallel faults. Q2 unit is duplicated and section is lost on Q2/P1-P2 deformation zone. Note truncation of Q1 unit both in cross section and map view (Fig. 2-7).

Q2
F'
S
Q2
Q1
F
N
P1-P2
Bedding-parallel shear zones
with internal Sm foliation
Cross bedding
in quartzites
0
100
200 m
S_0
0
10m
15 cm
a
S_2
S_1
S_0
b

Figure 2-9: Tight F_1 folds in lower Q2. F_1 folds are subhorizontal to gently inclined or recumbent. Note weak axial planar cleavage (arrow) S_1, in intercalated psammites and quartzites. Location of F_1 folds is along Animas River near southern basement-cover contact.


S_1

Figure 2-10: Domainal stereoplots emphasizing Phase 1 and 2 structures. Projections are equal area lower hemisphere. Stereoplots indicate approximately cylindrical, gently plunging, upright to steeply inclined nature of macroscopic F_2 folds.

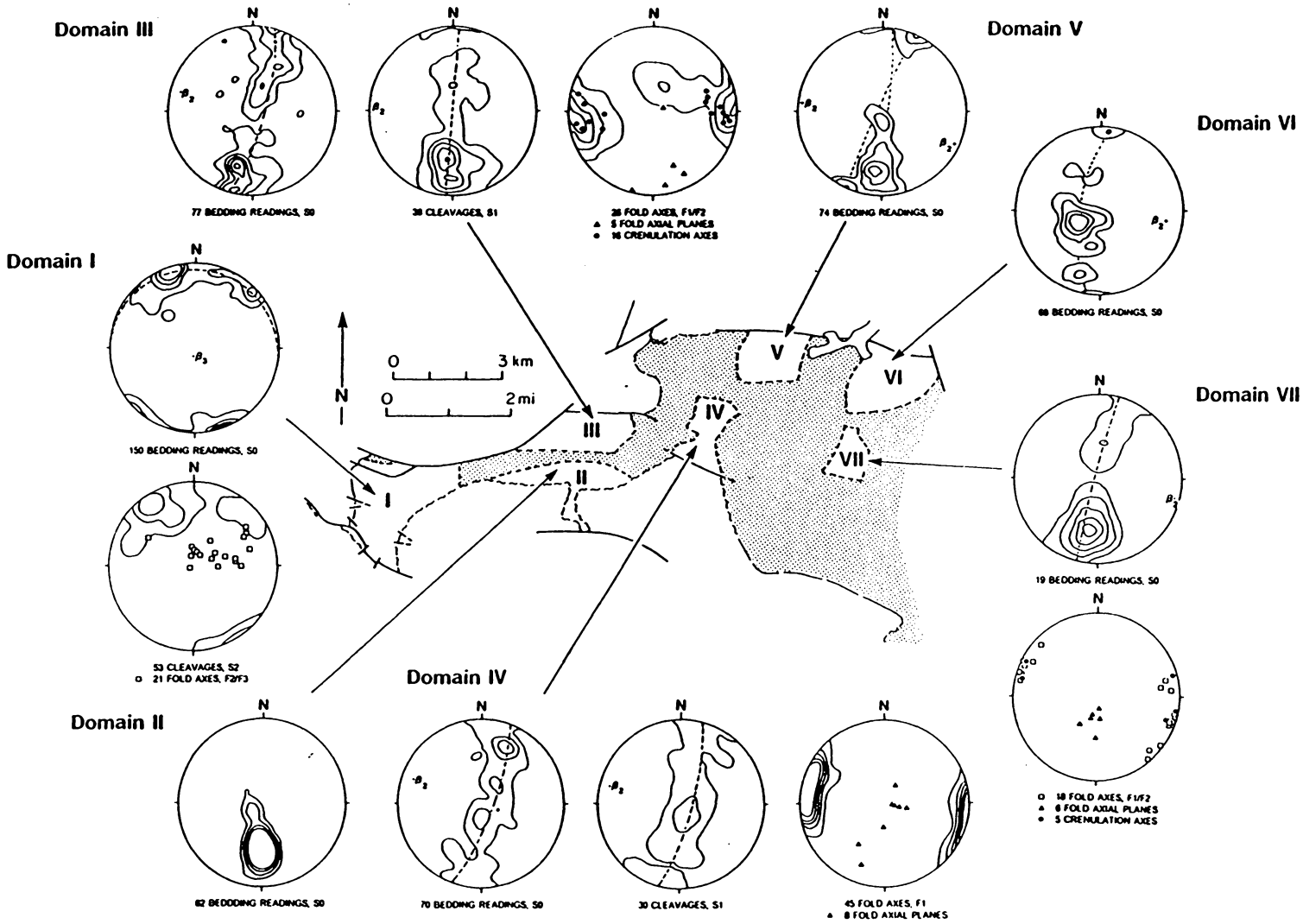
Domain III
77 BEDDING READINGS, S0
38 CLEAVAGES, S1
28 FOLD AXES, F1/F2
5 FOLD AXIAL PLANES
16 CRENULATION AXES
74 BEDDING READINGS, S0
Domain V
Domain VI
68 BEDDING READINGS, S0
Domain I
150 BEDDING READINGS, S0
53 CLEAVAGES, S2
21 FOLD AXES, F2/F3
0 3 km
0 2 mi
N
I
II
III
IV
V
VI
VII
Domain VII
19 BEDDING READINGS, S0
18 FOLD AXES, F1/F2
6 FOLD AXIAL PLANES
5 CRENULATION AXES
Domain IV
Domain II
62 BEDDING READINGS, S0
70 BEDDING READINGS, S0
30 CLEAVAGES, S1
45 FOLD AXES, F1
8 FOLD AXIAL PLANES

(1967). An axial planar cleavage, S_1 is associated with the F_1 folds and is present in psammitic to pelitic lithologies. S_1 is defined by a closely spaced, anastomosing to continuous cleavage in pelites with a wider spacing developed in psammites. Cleavage refraction between pelites and psammites is common.

Phase 2 Structures

Phase 2 structures are macroscopic and define the general map-scale F_2 folds in the Uncompahgre Group (Fig. 2-3, Fig. 2-5). F_2 folds are upright to gently inclined and plunge gently to moderately northwest, northeast and east-southeast (Fig. 2-7, stereoplot 1; Fig. 2-10, Domains I-VII). Fold wavelengths vary from 1 to 3 km. The limbs of F_2 folds are steep to overturned (Fig. 2-3, Fig. 2-4, Fig. 2-5, Fig. 2-11). Anticlines are cylindrical to chevron-shaped in profile view, whereas synclines are increasingly tight to keel-like in their apices (Fig. 2-4, C-C′, D-D′ and E-E′). Pelitic and psammitic units are thickened in the hinges of anticlines and thinned into the cores of synclines (Fig. 4). Phase 1 mesoscopic and microscropic structures (S_1, F_1, S_m, S_{m1}) are folded and overprinted as a product of Phase 2 deformation (Fig. 2-7, Stereoplots 2 and 4; Fig. 2-10, Domains III-IV). Associated with the macroscopic folds is the development of a spaced discrete to zonal crenulation cleavage, S_2 (Fig. 2-12), that is commonly axial planar to upright F_2 folds. Crenulation axes are approximately parallel to F_2 fold axes (Fig. 2-10, Domains III, IV and VII). Parasitic mesoscopic folds occur on the limbs of macroscopic F_2 folds. These <5 m wavelength folds are open to tight and verge steeply to moderately north and south. S_2 defines an axial planar to fanning cleavage in mesoscopic folds.

Phase 1 north-directed, bedding-parallel deformation zones and folds are folded, reactivated and then overprinted during Phase 2 (Fig. 2-7, stereoplot 4;

Figure 2-11: F_2 folds in the Uncompahgre Group.

a) Upright, gently plunging, F_2 fold in Q3 north of Snowdon Peak (Domain III, Fig. 2-10). Apparent recumbent nature is due to oblique section through fold. Relief in photograph is approx. 250m.

b) Upright, asymmetric, gently plunging, F_2 fold in Q2-P3 adjacent to northern basement-cover contact (Domain V, Fig. 2-10). Northern limb of F_2 fold is overturned to south. Relief in photograph is approx. 400 m.

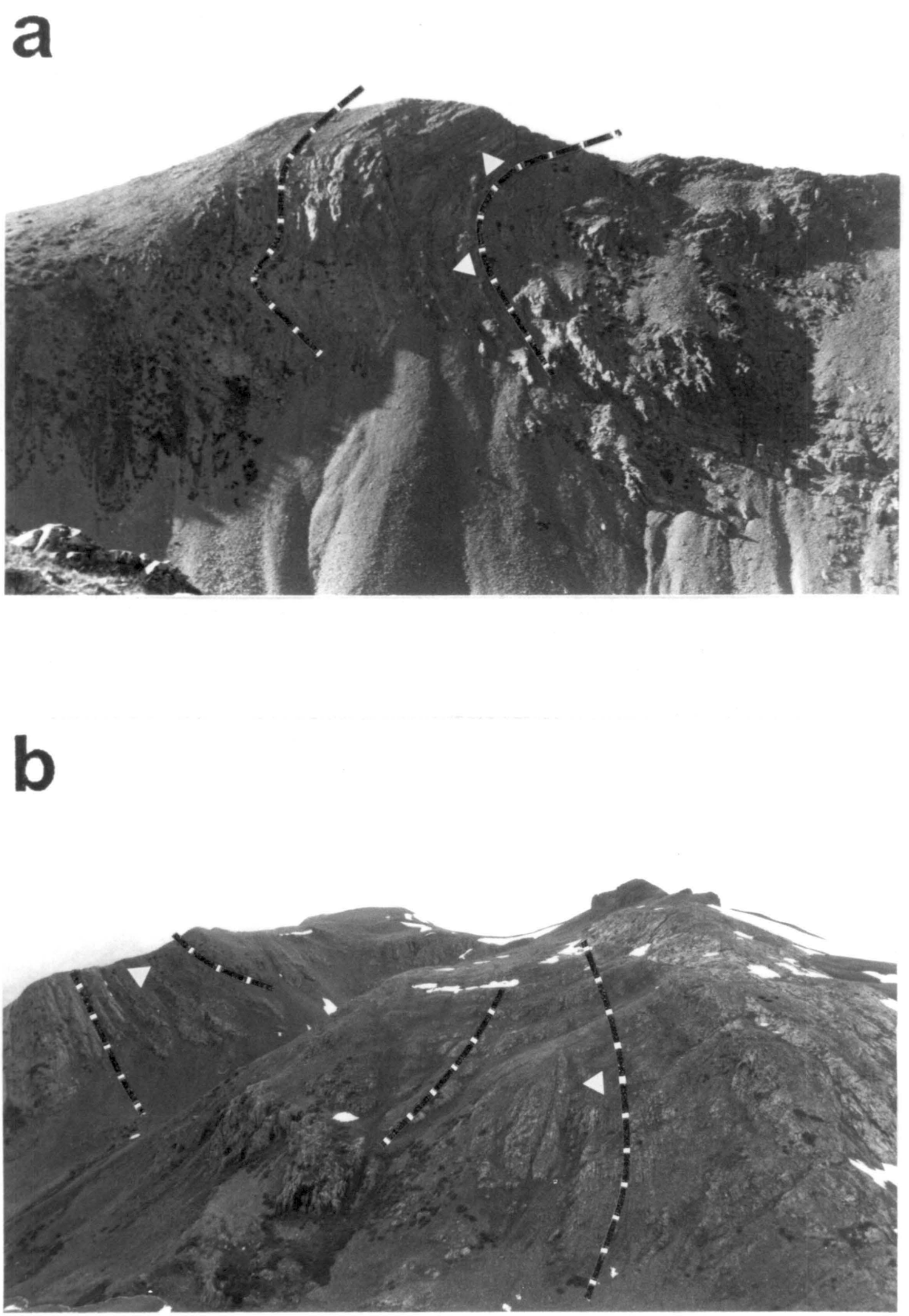
a
b

Figure 2-12: Spaced, discrete to zonal crenulation cleavage, S_2. S_1 is subhorizontal and subparallel to S0. (crossed nichols).

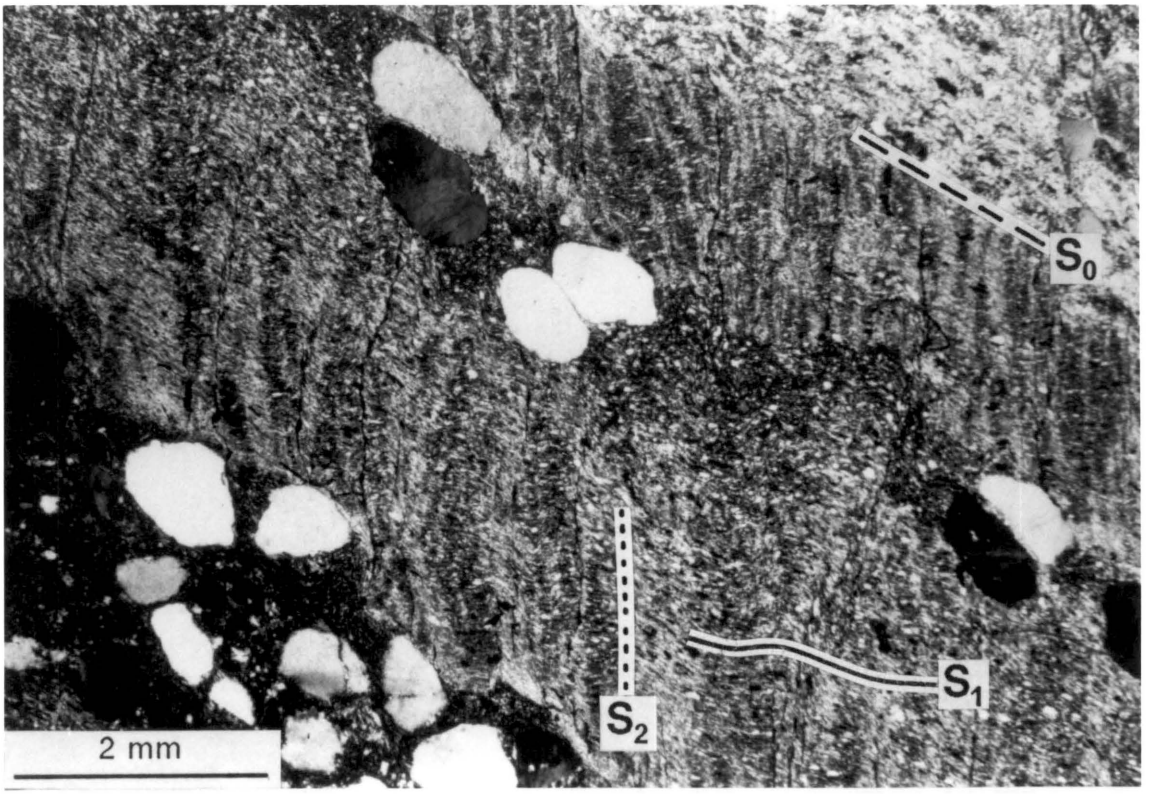
S_0
S_1
S_2
2 mm

Fig. 2-13, Domains B, C and D). Evidence for this folding is provided by a consistent asymmetry of the sigmoidal shear zone fabric around fold hinges (Fig. 2-4; Fig. 2-8, inset a). Fabrics that overprint these mesoscopic zones include an asymmetric, 1-5 mm spaced crenulation, S_{m2}, that microfolds the S_{m1} foliation (Fig. 2-14a, b). The vergence of S_{m2} is consistent with the approximate orientation of the axial planes of F_2 folds.

Inferred Phase 2 possibly transitional into phase 3 deformation results in renewed faulting in which for example the upper to medial portion of Q2 is displaced over the upper P2 unit, with a loss of section in the lower Q2 (Fig. 2-7; Fig. 2-8, inset a). The fault zone separating Q2 and Q1 cuts down section into the Q1 unit.

Phase 3 Structures

Structures generated during the final phase of deformation vary from microscopic to macroscopic in scale. Micro-structures are defined by a zonal crenulation cleavage, S_3, that refolds both S_1 and S_2 (cf. Tewksbury, 1981, 1986). Microfold axes trend north-south and dip steeply east or west whereas microfold wavelengths vary from 0.25 to 3 mm. Mesoscopic structures in quartzites in the Lime Creek area consist of a pervasive set of north-south oriented, steeply dipping, pressure solution seams that are emphasized by a black iron staining and weather out as fracture sets. Spacing on seams is variable but ranges from 10 to 30 cm. These seams are axial planar to a macroscopic, open, steeply south-plunging F_3 fold in the Lime Creek area (Fig. 2-3). This F_3 structure re-folds a macroscopic, east-west trending F_2 fold (Fig. 2-10, Domain I). As a consequence of refolding of earlier structures in the Lime Creek area (Fig. 2-3), steeply plunging, meso- to macroscopic, parasitic M-folds in quartzites and mesoscopic kink folds in psammites and pelites occur in the hinge of the macroscopic F_3 fold. Lateral offset of

Figure 2-13: Ductile deformation zones in the Uncompahgre Group.

Arrows on linear features (L_m, L_s) indicate direction of movement relative to corresponding shear-zone fabric. In northern domains (C and D) both dextral and sinsistral strike-slip and north-side up, dip-slip components are present. Note folding of north-directed kimematic indicators. Part of data in Domain A is from R.G. Gibson (personal communication, 1987).

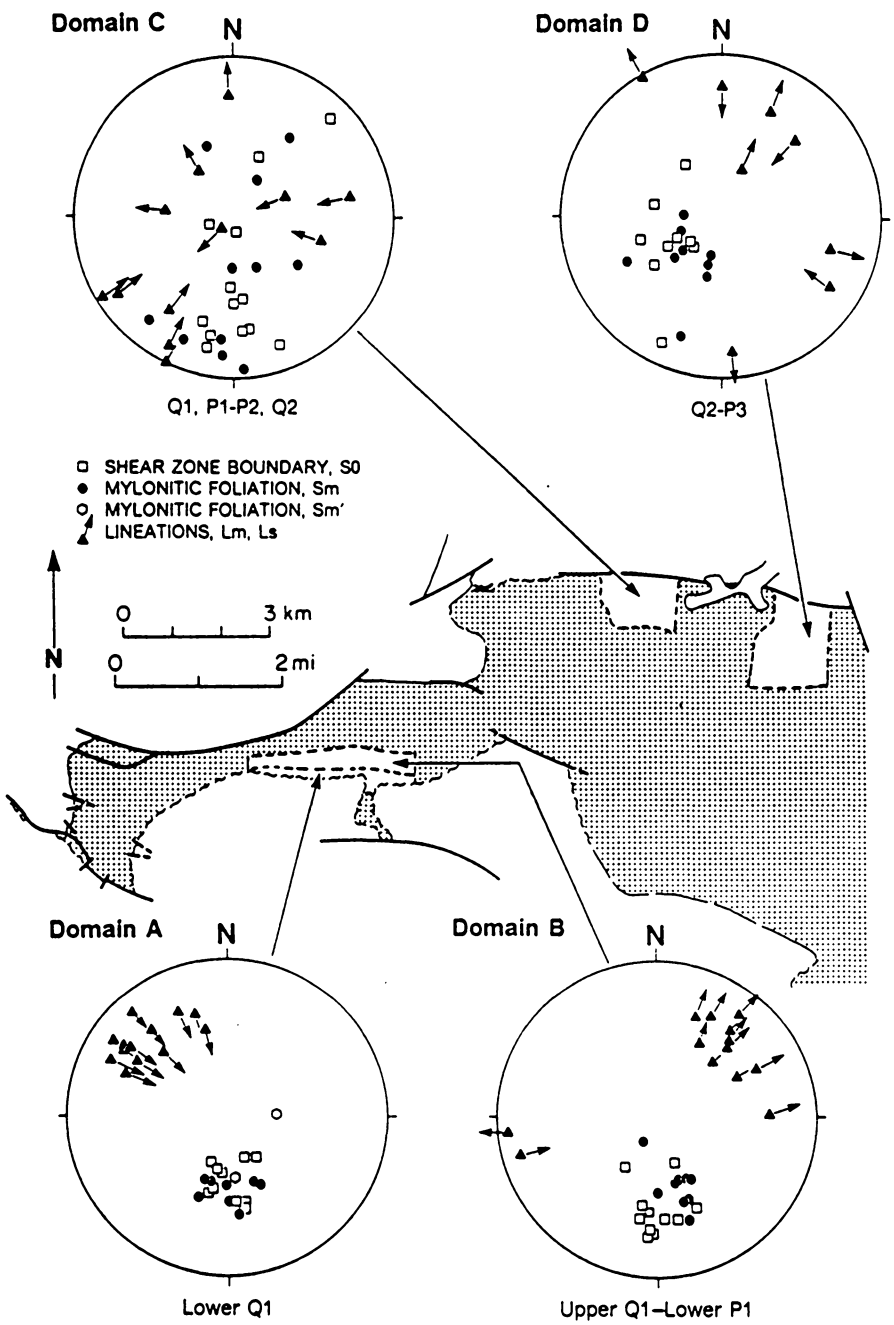
Domain C
N
Q1, P1-P2, Q2
Domain D
N
Q2-P3
SHEAR ZONE BOUNDARY, S0
MYLONITIC FOLIATION, Sm
MYLONITIC FOLIATION, Sm'
LINEATIONS, Lm, Ls
N
0
3 km
0
2 mi
Domain A
N
Lower Q1
Domain B
N
Upper Q1–Lower P1

Figure 2-14: Bedding-parallel deformation zone in Q2.

Sample from Domain VI, Fig. 2-10. S_{m1} foliation is overprinted and crenulated by S_{m2} foliation.

a) Photomicrograph (plane light) in which opaques + quartz ribbons ± mica defines S_{m1} fabric that is crenulated by S_{m2}.

b) Photomicrograph (crossed nichols) of same zone. Quartz ribbons (qz) are annealed and recrystallized. Post-kinematic, unstrained andalusite (and) overgrows S_{m1}/S_{m2} fabric (compare a and b).

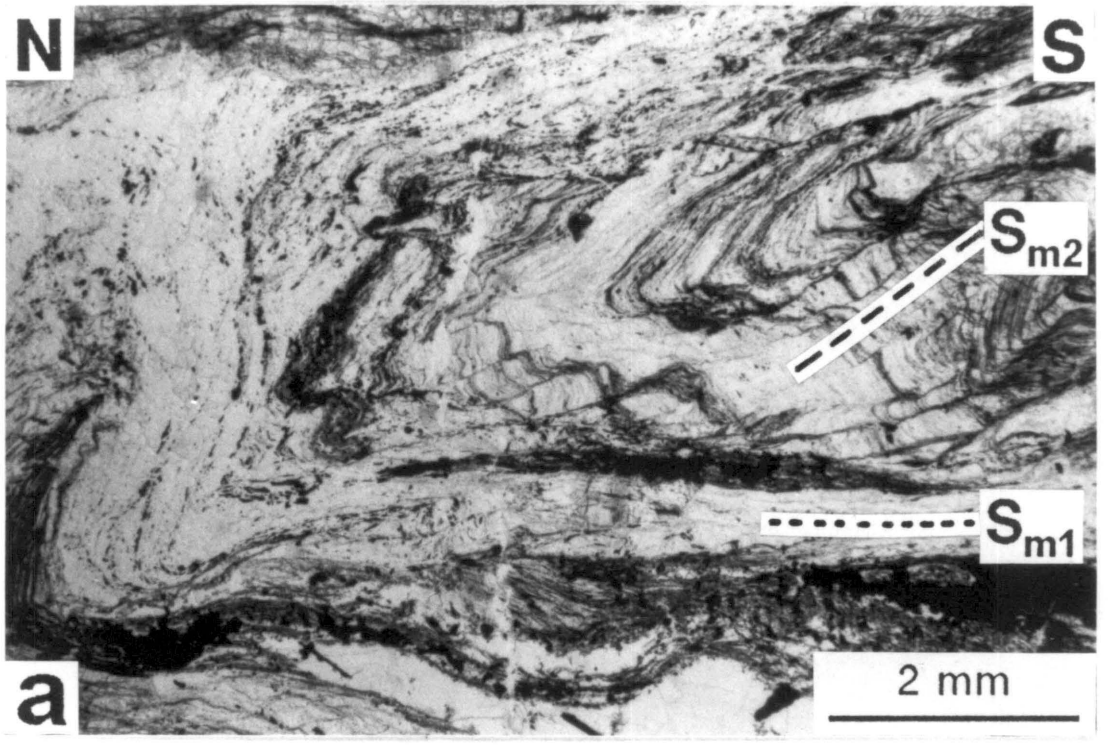
N
S
S_{m2}
S_{m1}
a
2 mm

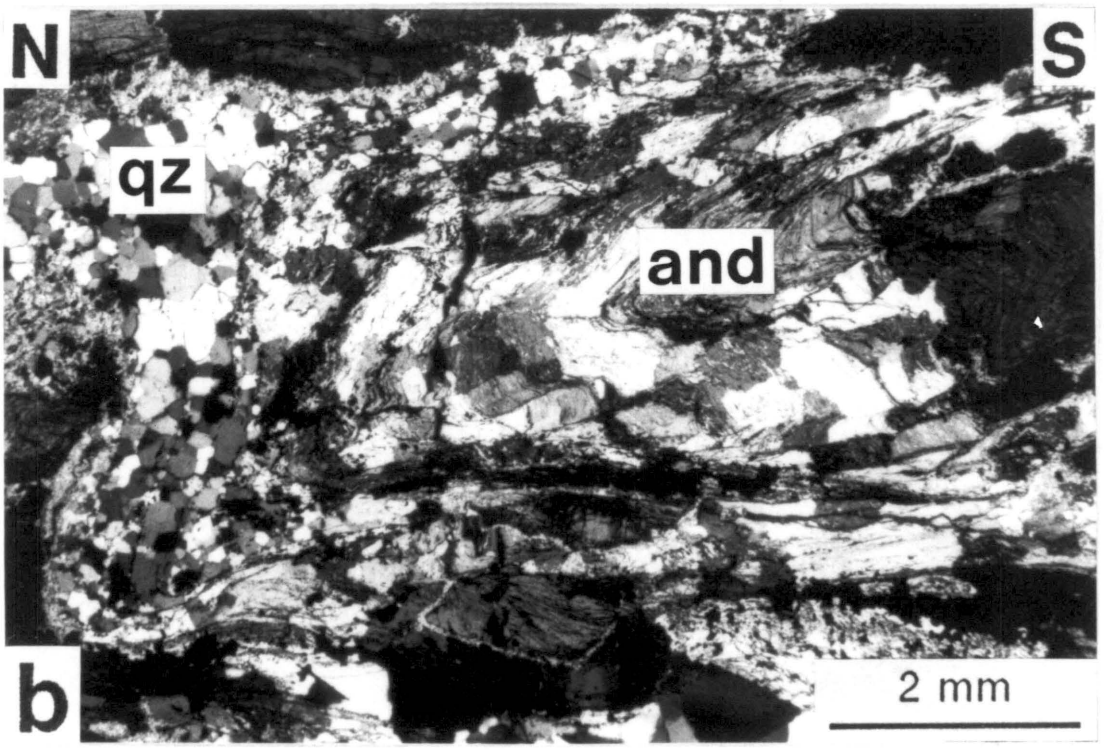
N
S
qz
and
b
2 mm

quartzite beds along bedding-parallel faults splaying into overlying pelites is present in the core of the macroscopic F_3 fold.

Ductile Deformation Zones

Discrete, areally extensive, 1 to 10 meter-wide zones of intensely deformed pelite, psammite and quartzite are developed in the Uncompahgre Group. These zones are described separately, as they exhibit features suggestive of continued reactivation and overprinting during the three phases of deformation.

Zones of quartz mylonite to mica-rich phyllonite occur at the transition between thick quartzite units and intervening psammites and pelites. One of these zones is best exemplified in the vicinity of the contact between Q1 and P1 (Fig. 2-3). There is a gradational change from intact thin beds of quartzite separated by thin zones (< 2 to 5 cm thick) of quartz-mica-hematite mylonite/schist with a strongly developed sigmoidal, continuous to closely-spaced, millimeter-scale foliation (S_m, Fig. 2-15a) to quartz-rich mylonites and phyllonites. Quartzite beds are dismembered and attenuated in proximity to this zone with a loss of relict sedimentary structures (Fig. 2-15b) There is an abrupt transition to a several meter-wide zone of quartz-rich mylonite and phyllonite (Fig. 2-15c). The mylonitic foliation (S_m) consists of a closely spaced to continuous, millimeter-scale fabric of quartz + white mica + hematite. Quartz augen and elongate quartz-rich domains are evident in outcrop (Fig. 2-15c). In thin section, quartz-rich domains are commonly recrystallized into polygonized aggregates, which in plane light define elongate ribbons separated by aligned opaques and mica-rich domains. In dynamically recrystallised quartz augen and adjoining quartz ribbons some lattice strain remains as indicated by the presence of deformation bands and undulatory extinction in quartz (Fig. 2-15d). Dynamic recrystallization is inferred because of the serrated or un-

Figure 2-15: Ductile deformation zone in transition from Q1 to P1.

Zone is located to north and east of Snowdon Peak (Fig. 2-13, Domain B). Movement sense is dextral north-side down.

a) Bedding-parallel deformation zone to right of scale with disruption of overlying quartzite bed by S_m

b) Increasing disruption and attenuation of quartzite beds by mylonitic foliation S_m.

c) Quartz-rich mylonite/phyllonite in Q1-P1. Note weak asymmetric crenulation of S_m by S_m' (pencil is approx. 12 cm long). Movement sense is top-to-the-north dextral.

d) Photomicrograph (crossed nichols) of quartz ribbons on margins of quartz augens. Ribbon enclosed in a fabric of white mica + quartz + hematite. Edges of ribbons defined by grain boundary migration and recrystallized subgrains.

S
N
S_m
S_0
a
S
N
cm
15
10
5
0
S_m
b
S
N
S_m
S_m'
c
S
N
S_m'
S_m
d
2 mm

even grain boundaries along the margins of curving quartz ribbons. These ribbons are subparallel to the enclosing quartz-mica-hematite foliation (S_m, Fig. 2-15d). In pelitic lithologies that are now phyllonites, relict bedding is obliterated and replaced by a closely spaced, continuous, mica-rich fabric (S_m), that is usually micro-folded.

Movement indicators (Fig. 2-13, Domain B) based on the geometry of the S_m foliation in addition to mineral elongation (L_m) and quartz-fibre alignment (L_s), record oblique north-side down movement on the southern Q1-P1 mylonite whereas an identical zone at the same stratigraphic level on the north (Fig. 2-13, Domain C) records south-side up movement. This consistent movement pattern and a similar style of deformation and displacement of the same stratigraphic units at the locus of this zone, suggests that it may be a first phase north-directed thrust fault plane. Similar zones of relatively intense deformation are developed at the Q2-P3 and P3-Q3 transitions. In these units there is a continuous to phacoidal cleavage (S_1) that encloses intrafolial tight to isoclinal, mesoscopic F_1 folds that may be rootless. These structures are similar to those described in detail by Tewksbury (1981, 1986). Movement sense on these zones was not documented by Tewksbury (1981, 1985, 1986), although they were interpreted to be probable loci of thrusting.

Later overprinting of these mylonitic/phyllonitic zones probably occurred during the second and third phases of deformation. Phase 2 overprint on early ductile deformation zones is associated with a reorientation and steepening during development of F_2 folds. In pelitic units phyllonitic deformation zones are localized along F_2 fold limbs. These zones are confined to the upper P2, upper and lower P3 and upper P4. Phacoidal to transposed cleavage fabrics are developed in these units. Movement sense, based on fabric asymmetry and quartz fibre orientations, is to the north and south, essentially perpendicular to F_2 fold axis orientations.

Phyllonites occur at the base of Q1 on the northern and southern basement/cover contacts and are inferred to have developed during phase 2 deformation (Fig. 2-3, Fig. 2-4, C-C′, D-D′). These 1 to 12 meter-thick zones of mica or quartz-rich phyllonite contain an internal sigmoidal anastomosing to continuous fabric of quartz + mica and opaques (S_m) which is offset by a gently inclined spaced foliation (S_m', extensional crenulation cleavage) (Fig. 2-16a). In proximity to these zones sedimentary structures and bedding are obliterated and there is an intense flattening of clasts contained in basal conglomerates of Q1. In cross section the southern deformation zone steepens with decreasing elevation (Fig. 2-4, C-C′). The northern basal deformation zone varies from vertical to overturned with increasing elevation (Fig. 2-4, D-D′; Fig. 2-8). Shear zone fabrics on the southern phyllonite record oblique top-to-the-south movement Fig. 2-13, Domain A), whereas those on the north are equivocal in their movement sense (Gibson and Simpson, 1986; Harris and others, 1987). Northern phyllonite zones are much thinner (<1 m) than those on the south and in one locality west of the Animas River on the northern basement/cover contact, Uncompahgre Group conglomerates directly overlie basement lithologies without an intervening deformation zone (Harris and others, 1987). Bedding-parallel deformation zones in quartzites of Q1 immediately south of this unconformable contact record south-side up movement (Fig. 2-7, stereoplot 4; Fig. 2-13, Domain C).

Final overprinting on individual mylonite zones and bedding-parallel deformation zones, probably during Phase 3 deformation, results in oblique sinsistral or dextral offset of an earlier mylonitic foliation (S_m), and concomitant extension and boudinage of bedding in proximity to these zones. East of a line striking 340, approximately 2 km west of Snowdon Peak (Fig. 2-3), ductile deformation zones reflect dextral movement whereas west of this line they record sinistral offset. The internal S_m foliation of oblique dextral mylonites and phyllonites is asymmetrically crenulated into 2 to 10 cm-wide do-

Figure 2-16: Basement-cover and Q1-P1 deformation zones.

a) Photomicrograph (crossed nichols) of dextral, top-to-the-south, ductile deformation zone on basement-cover contact immediately south of Snowdon Peak (Fig. 2-10, Domain II; Fig. 2-13, Domain A). Quartz-rich phyllonites consist of lenticular, relatively unstrained quartz augen or detrital grains (?) exhibiting weak undulose extinction and deformation bands, enclosed by an anastomosing fabric of white mica + opaques. S_m is offset by S_m'.

b) Asymmetrically boudinaged bedding S0 and internal fabric, S_m or S_i(?) in P1-P2 east of the Animas River (Fig. 2-10, Domain V; Fig. 2-13, Domain C). In plan view, north to top of photo, boudins are rotated in an anticlockwise direction in a bulk oblique dextral, south-side up shear zone (compare with kinematic indicators in Fig. 2-13, Domain C).

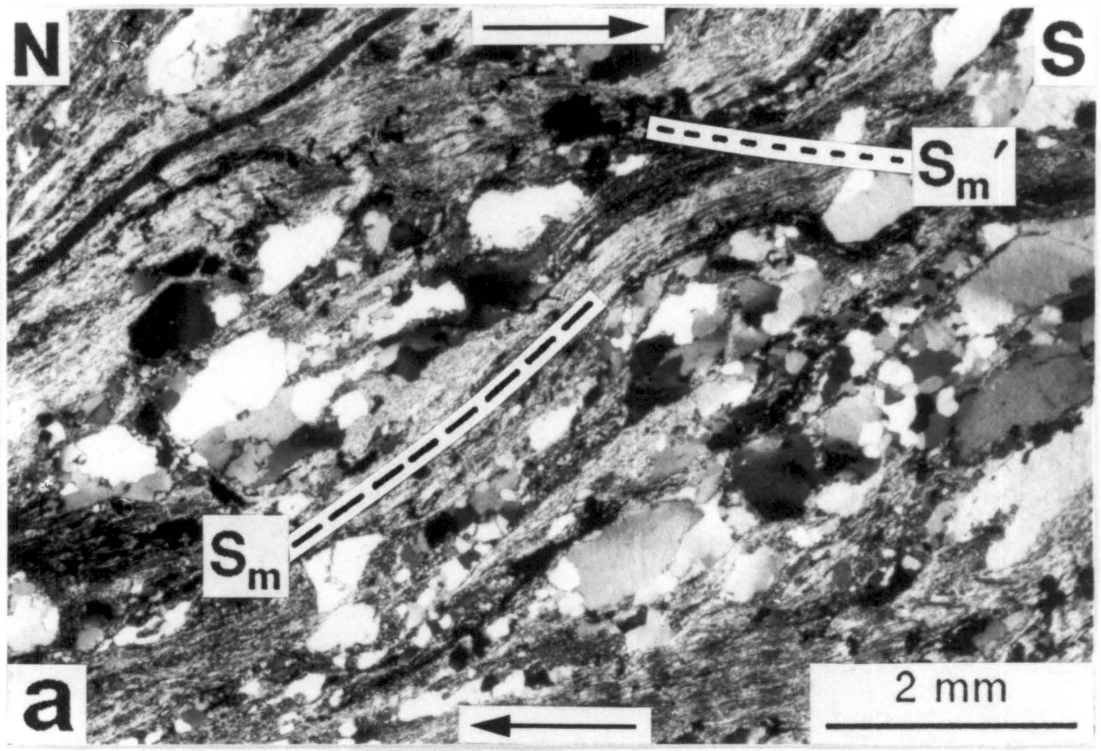
N
S
S_m'
S_m
a
2 mm

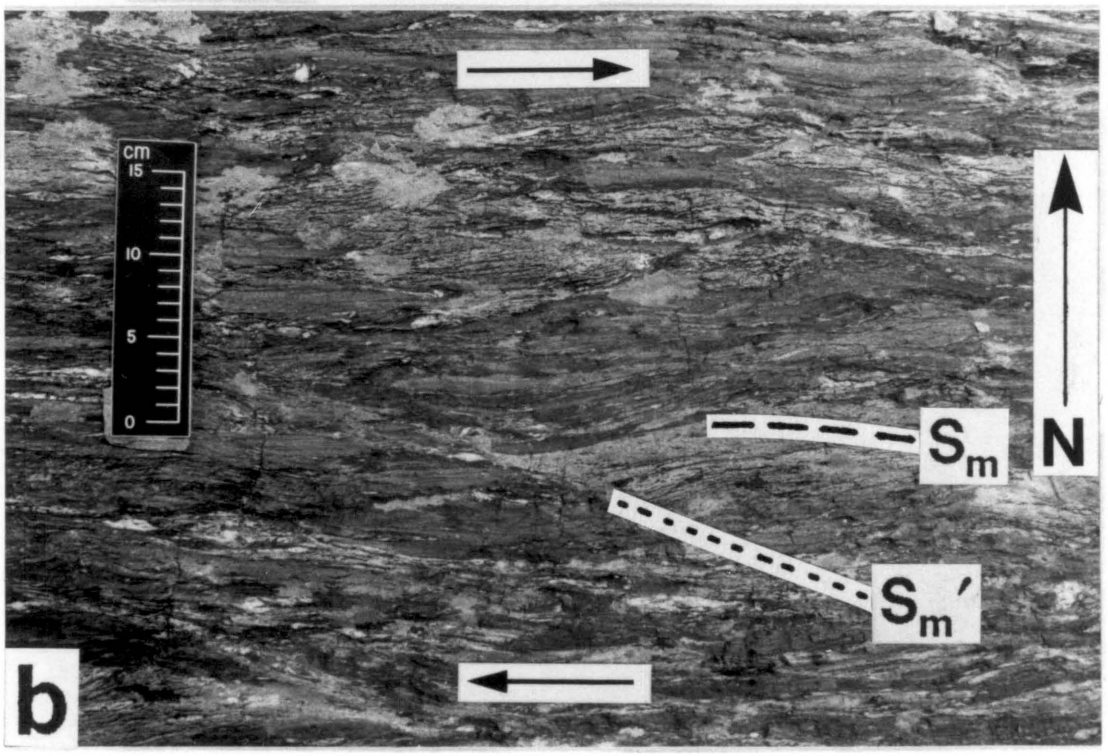
cm
15
10
5
0
N
S_m
S_m'
b

mains (S_m') that produce discontinuities in the S_m fabric. In thin section, quartz ribbons and aligned micas + hematite are asymmetrically warped, although features such as pressure solution fabrics and seams on microfold limbs, similar to those described by Gray and Durney (1979), are not present. In addition bedding and relict S_1 or S_m? is offset and rotated in an anticlockwise sense along discrete inclined planes (S_m') spaced every 10 to 20 cm (Fig. 2-16). A dextral movement sense thus is inferred. Fabric rotation and discontinuities are similar to Type 1 asymmetric pull-aparts described by Hanmer (1986). Psammitic and pelitic lithologies in the cores and limbs of tight synclines reflect the overprint of dextral offset. Discrete zones from 10 cm to 1 m wide, contain a spaced sigmoidal fabric that deflects both cleavage, quartz veins and relict bedding. A sinistral movement sense is inferred for deformation zones in the vicinity of Lime Creek (Fig. 2-3). Section is lost and stratigraphic units are attenuated and displaced southward. The presence of sinistral bedding-parallel deformation zones in Q2 corroborates this observation. The geometry and opposed sense of movement of cover rocks to the east and west in the vicinity of Snowdon Peak, in addition to the strike-parallel offset of stratigraphic units, suggests that a conjugate shear system developed during phase 3 deformation.

STRUCTURAL EVOLUTION

The structural style of the Uncompahgre Group mimics that of a fold-thrust belt during phase 1 of the deformation history but was distinctively different during phases 2 and 3. The following discussion reviews the deformational phases and inferred mechanisms and compares the structural evolution of the Uncompahgre Group with possible analogues.

Phase 1

The overall style of deformation during Phase 1 (Fig. 2-17a) involved north-directed, thrust-nappe emplacement with stacking and imbrication localized within stratigraphic units P1-P2, Q2 and Q3. Associated with early thrusting was the development of F_1 folds and an S_1 cleavage. Major thrust faults (ductile deformation zones) between thick stratigraphic units of pelite/psammite and quartzite were localized along mechanically weak surfaces separating these units of high viscosity and strength contrast. Strain was inferred to have been inhomogeneous in these sheets with the locus of deformation concentrated along shear zones subparallel to bedding. Quartzite units between faults recorded minimal deformation based on the superb preservation of primary sedimentary structures.

Coincident with the beginning of north-directed, layer-parallel thrusting was the detachment of Q2 and P1-P2 from the upper Q1 which remained parautocthonous on basement (Fig. 2-17a). Stratigraphic units Q1 and Q2 form a relatively intact sequence on the south with increasing repetition to the north, localized in Q2 and P1-P2. It is difficult to estimate displacements on phase 1 faults, such as the Q1-P1 mylonite zone, because their terminations are not exposed in the present outcrop belt and distinctive marker units that are offset by these faults are not recognizable. Applying the "bow and arrow" rule of Elliott (1976) to the northern Q-P1 deformation zone of 5 km strike length results in a minimum displacement estimate of 0.35 km. The significant repetition in the overlying Q2 unit in the northern Animas River area suggests that the amount of movement in the vicinity of this zone is much greater (Fig. 2-3, Fig. 2-4, Fig. 2-8).

Although Q1 is inferred to have been parautochthonous on basement, evidence indicates that there is an increasing strain gradient distributed through this unit along north-directed, bedding-parallel deformation zones up to the Q1-P1 mylonite zone. A

Figure 2-17: Deformation model for the Uncompahgre Group.

Model is developed for rocks exposed in the West Needle Mountains area (refer to text for description). Diagrams a. and b. do not include extensive overburden which would have been present during the first two phases of deformation. Diagram c. portrays existing structural level. Post middle-Proterozoic brittle faults define northern boundaries of part of outcrop belt and correspond with those in the geologic map of Fig. 2-3.

a. **Phase 1: Thrust-nappe emplacement**

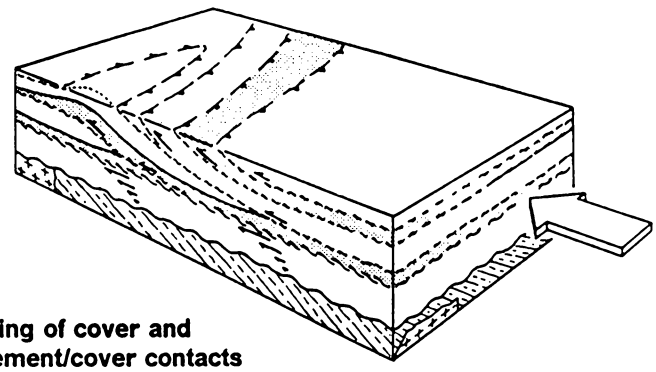

b. **Phase 2: Folding of cover and basement/cover contacts**

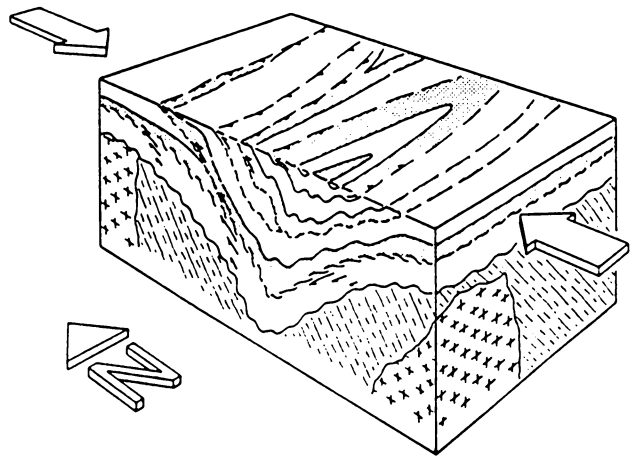

c. **Phase 3: Vertical and lateral escape of cover during conjugate shearing**

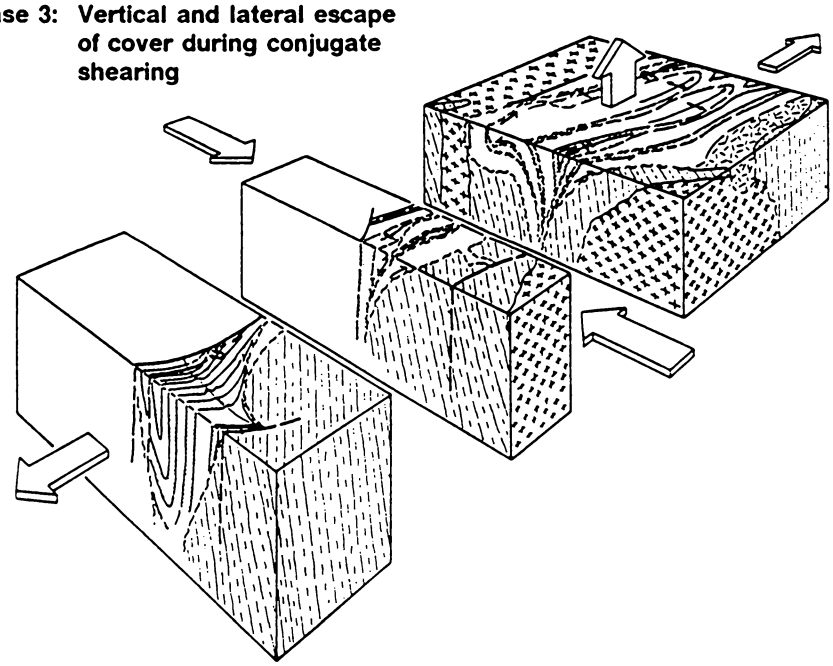

similar relationship has been documented in Wopmay Orogen, Canada, where a major detachment surface is localized 100 to 300 m above the unconformable contact between basement and autochthonous cover (King, 1986). An upward increase in the strain gradient was observed between the unconformity and the overlying detachment surface. In both examples, the strain gradient resembles that of simple-shear deformation of a thrust sheet, as predicted by the theoretical studies of Sanderson (1982). Unlike a typical thrust sheet, the deformation and displacement gradient is reversed with the least deformation occurring in the basal autochthonous portion in the Proterozoic examples.

Phase 1 deformation of the Uncompahgre Group is inferred to have been different to that of many Phanerozoic, shallow-level, fold-thrust belts such as those described by Harris and Milici (1977) and Price (1981). The Uncompahgre Group is representative of a deeper strucural level, typical of that of Precambrian orogenic belts. A pervasive cleavage in psammites and pelites and the presence of ductile deformation zones at various scales is used to infer that deformation occurred in a ductile regime as proposed by Elliott (1976). Structures generated during Phase 1 are similar to those of the "suprastructure" of a compressional orogenic belt as first defined by De Sitter and Zwart (1960) and later employed by Murphy (1987). The "suprastructure" represented the zone of upright folding and low-grade metamorphism in an orogenic belt (De Sitter and Zwart, 1960).

Phase 2

Phase 2 marks the advent of a different style of deformation, in which thrusting in cover rocks was supplanted by macroscopic folding and likewise the basement/cover interface was folded (Fig. 2-17b). Initiation and amplification of upright folds was accompanied by flexural-slip along bed-to-bed contacts in quartzites. As a consequence

of fold tightening and room problems, material was thinned in synclines and thickened in anticlines (Fig. 2-4, C-C′, D-D′, E-E′; cf. Dahlstrom, 1977). The replacement of early thrusting by folding and an overprinting cleavage may have been due to the infolding of the parautocthonous Q1 quartzite concomitant with folding of basement lithologies (Gibson and Simpson, 1986; Harris and others, 1987) which prevented further movement on phase 1 deformation zones. Macroscopic F_2 fold geometries may be attributed to non-Newtonian behaviour (buckling instabilities) of materials with high viscosity contrasts (quartzite and pelite) as proposed by Ramsay (1967) and Smith (1979). In detail, there is some deviation from this idealized and simplified model. In map view and cross section (Fig. 2-3; Fig. 2-4) the deformation related to folding is heterogeneous, with intense deformation localized east of Lime Creek extending into the Animas River area. In this zone of constriction, stratigraphic section is duplicated on the north (Q2 over P3) and section is lost (Q2) in the vicinity of Snowdon Peak (Fig. 2-3).

As a function of flexural-slip along bedding planes coincident with F_2 fold development, psammites, pelites, and thin-bedded quartzites between thick quartzite units, in addition to early bedding-parallel deformation zones, were overprinted by secondary fabrics. Simple shear deformation along bedding planes during flexural-slip placed these lithologies and zones in either compression or extension. Thus material lines or planes may be either folded or extended as predicted by Ghosh (1966), Sanderson (1979), and Ramsay (1980). Based on these theoretical models, crenulation of Phase 1 S_{m1} in ductile deformation zones by S_{m2}, would be limited to the northern limbs and cores of anticlines and the cores and southern limbs of synclines (Fig. 2-8, inset a and b; microfabrics, Fig. 2-14a, b).

Early, north-directed, bedding-parallel deformation zones and mylonite zones (e.g. Q1-P1 mylonite zone) were reactivated and probably record a continuum of evolution from Phase 1 into Phases 2 and 3. Along the northern Animas River structures present

in the P1-P2 and Q2 units suggest that out-of-sequence thrusting occurred (Fig. 2-8). In this model (Searle, 1985), younger thrusts overlap or truncate older underlying duplexes or thrust slices in a hindward sequence of imbrication. Several lines of evidence support this interpretation: 1) loss of section at the Q2-P2 contact, 2) truncation of F_1(?) folds by faults, 3) folded faults, and deflection of S_1 cleavage in P1-P2. Initial thrusting and folding in the the Q2 and P1-P2 units was inferred to predate out-of-sequence thrusting. The fault zone separating Q1 and Q2 in the Animas River area (Fig. 2-8) cuts downsection into Q1. This style of faulting may be attributed to late phase 2 fault decapitation of an upright F_2 fold in Q1 related to out-of-sequence thrusting.

To accomodate folding and shortening along the basement/cover contacts, former unconformities are variably activated as ductile deformation zones. In addition, opposed senses of movement, top-to-the-north (northern contact) and top-to-the-south (southern contact), are superimposed on quartzites of the Uncompahgre Group in the vicinity of these contacts (This study; Harris and others, 1987).

Folding of cover and the basement/cover interface during phase 2 may have been due to crustal thickening linked to the overburden of overriding thrusts sheets or a thick sedimentary prism above the Uncompahgre Group. A thick overburden may have led to crustal loading and ensuing thermal blanketing of the underlying basement and cover rocks increasing their ductility and relative plasticity (?). Compressional forces would have then been distributed through the thickness of the lithosphere leading to the development of "megamullions" in the basement. Cusp development on the basement/cover interface may be analogous to the perturbations of folding of an infinite half-space (Ramberg, 1967; 1981). Contrasts in viscosity between basement and cover rocks may have served also to amplify the development of the cusp (cf. Ramsay, 1967; Smith, 1979). A similar scenario has been proposed for the development of basement/cover folds in the Tumas dome of the Damara orogen (Jacob and others,

1983), the Tree River foldbelt (Hoffman and others, 1984), the Cape Smith foldbelt (Hoffman, 1985), and Wopman orogen (King, 1986). This phase of deformation in the Uncompahgre Group is dissimilar to the "infrastructure" of compressional orogenic belts in that large-scale, subhorizontal, high-metamorphic grade nappe structures are not present (cf. Sanderson, 1979; Murphy, 1987).

Phase 3

From structures preserved in the study area it is difficult to clearly discriminate the development of phase 2 structures from those of phase 3, except in the area west of Snowdon Peak extending into the Lime Creek area (Fig. 2-3). The transition from phase 2 upright folding to phase 3 conjugate shearing was probably due to further shortening during a progressive deformation in which cover is sandwiched between basement domes (Fig. 2-17c). Cross-folding in the Lime Creek area was caused by passive bending of an earlier F_2 fold, in a conjugate shear system developed in the basement (Gibson and Simpson, 1986; Harris and others, 1987) and adjoining cover rocks. Analogous mesoscopic, pseudofolds of gneissic foliation recognized by Jacob and others (1983) were attributed to conjugate shearing in a ductile regime.

Earlier Phase 1 mylonite zones and bedding-parallel deformation zones which were folded and steepened during Phase 2 were then subjected to varying degrees of oblique dextral and sinistral movement generating S_m' fabrics. Further shortening was accomodated by the strike-parallel movement of lithologic units. The overall movement pattern is interpreted to have been related to north-northwest/south-southeast compression with apparent maximum constriction concentrated in the vicinity of Snowdon Peak (Fig. 2-3). As a product of conjugate shearing, the southern basement-cover deformation zone near Snowdon Peak records an oblique sense of displacement to the

southeast (this study; Harris and others, 1987). In the Uncompahgre Group, the inferred maximum compression direction bisects the obtuse angle of the conjugate shear set. Ramsay (1980) and Jacob and others (1983) interpreted that this particular configuration of a conjugate shear system would develop in a ductile regime.

Comparison with contemporaneous cover sequences of the southwest U.S.A.

Is the deformation and tectonic transport direction of cover rocks in the Uncompahgre Group compatible with that of contemporaneous metasedimentary sequences in the southwestern U.S.A.? The initial phase of north-directed thrusting in the Uncompahgre Group matches the transport directions recognized in Arizona in the Mazatzal Group (Puls and Karlstrom, 1985; Karlstrom and Conway, 1986) and that of north verging recumbent nappes documented in New Mexico in the Ortega Group (Grambling and Codding, 1982). The second phase of upright folding is also present in New Mexico (Grambling and Codding, 1982) but not recognized in Arizona (Karlstrom and Conway, 1986; Brady and others, 1987). The cover sequences in Arizona record a lower metamorphic grade than the Uncompahgre Group and are therefore inferred to represent a shallower level of deformation in a thin-skinned, fold-thrust belt (Puls and Karlstrom, 1985; Karlstrom and Conway, 1986) whereas the Ortega Group probably was metamorphosed and deformed at a deeper crustal level based on the style of deformation and amphibolite facies metamorphism (Grambling and Codding, 1982). It thus appears that the Uncompahgre Group represents an intermediate case between the other two examples. It may suggest that the deformation of cover in the Needle Mountains is at a moderate to deep "suprastructural" level transitional to an "infrastructural" level to the south in New Mexico (cf. De Sitter and Zwart, 1960; Murphy, 1987). Phase 1, north-directed thrusting is not evident in the Uncompahgre Gorge area, although up-

right folding and lateral displacement of stratigraphic units does occur. The occurrence of the same mineral assemblage in pelites of the Uncompahgre Gorge area implies a similar degree of metamorphism and likewise crustal burial to that of the West Needle Mountains area. Because phase 1 thrust faults are not present in this area it is inferred that these outcrops represent a more distal portion of the orogenic belt.

Stratigraphic relationships between basement and cover in the Needle Mountains

Tewksbury (1985) proposed that the Uncompahgre Group was allocthonous thus creating problems in resolving its age relationship with surrounding basement rocks. However, the Uncompahgre Group is not a remnant of a south-directed, fold-thrust belt as proposed by Tewksbury (1981, 1985, 1986) although the structures documented along the southern basement-cover contact resembles the ramp-flat geometry of Phanerozoic fold-thrust belts. Based on this study and the work of Harris and others (1987), major detachment and north-directed transport was localized to those units above the Q1-P1 mylonite zone. The basal quartzite, Q1, remained attached to basement until deformational phases 2 and 3. Therefore the Uncompahgre Group is interpreted to be younger than adjoining basement lithologies that were deformed later, together with the cover rocks (Gibson and Simpson, 1986; Harris and others, 1987).

CONCLUSIONS

Three phases of deformation have affected the cover rocks of the Uncompahgre Group. An initial early phase of ductile, north-directed, thin-skinned thrusting was followed by cuspate infolding of cover into basement gneisses and amphibolites. Continued shortening and amplification of this structure led to the lateral and vertical escape

of cover rocks in a conjugate shear system. The general style of deformation is suggestive of progressive coaxial flattening in which cover initially deformed independent of basement, followed by folding of basement and cover. Infolding of cover into basement produced cuspate "megamullions" similar to those of the Alpine external massifs and their sedimentary cover (Ramsay, 1967; Gratier and Vialon, 1981; Tricart and Lemoine, 1986), the Tree River foldbelt (Hoffman and others, 1984), the Cape Smith foldbelt (Hoffman, 1985) and the internal zone of Wopmay orogen (King, 1986). In contrast to Phanerozoic orogens, the structures preserved in the Uncompahgre Group provide a window into the deeper parts of an orogenic belt, presumably the deep "suprastructure" of a foreland region undergoing compression and greenschist facies metamorphism.

Chapter 3: Proterozoic Cuspate Basement-Cover Structure, Needle Mountains, Colorado

ABSTRACT

Deformation zones along basement-cover contacts, which are commonly loci of significant displacement, may also be zones of limited movement when cover and basement are folded together. Proterozoic basement gneisses and siliciclastic cover rocks of the Uncompahgre Group in the Needle Mountains, Colorado, are in contact along steeply dipping deformation zones. Analysis of structures in the basement and cover, and along their contacts, provides evidence for (1) deformation of the basement prior to deposition of the Uncompahgre Group, (2) north-directed,thin-skinned thrusting, and (3) cuspate infolding of cover into basement accompanied by upward and outward movement of the cover. Opposed senses of movement along basement-cover contacts on opposite limbs of the synclinorium generated during cuspate infolding imply that the Uncompahgre Group is parautocthonous on basement. Conjugate strike-slip shear zones in both units accommodated north-northwest shortening. Deformation of basement and cover into cuspate structures may explain the presence of some cover sequences as isolated remnants within gneissic basement.

INTRODUCTION

In many compressional orogenic belts, decollement zones of significant displacement are present within lithologic units along or near basement-cover contacts (Price and Mountjoy, 1970; Gee; 1980; Tirrul, 1983). However, in other settings where basement is folded together with its autochthonous to parautochthonous cover (Ramsay, 1967; Platt, 1980; Hoffman et al., 1984), zones of locally intense deformation also may occur near basement-cover interfaces (Gratier and Vialon, 1980; Jacob et al., 1983; Tricart and Lemoine, 1986). The distinction between deformation zones that result from large-scale translation of rock units and those that may form as a mechanical response to folding is critical to evaluation of basement-cover relations. In Precambrian terranes, where cover sequences commonly occur as deformed remnants surrounded by basement, this distinction is especially important for developing tectonic models.

Deformed, post-1700 Ma siliciclastic cover sequences in southwestern North America are present as inliers within older, volcano-plutonic basement complexes. A variety of basement-cover relations have been recognized throughout this region (Barker, 1969; Grambling and Codding, 1982; Tewksbury, 1985; Karlstrom and Conway, 1986). In central Arizona, the Mazatzal Group unconformably overlies ca. 1740 Ma basement and was involved in north-directed, thin-skinned thrusting (Puls and Karlstrom, 1985; Karlstrom and Conway, 1986). Metasedimentary rocks of the Ortega Group in north-central New Mexico were deformed with basement into north-directed fold nappes (Grambling and Codding, 1982). Within the Needle Mountains of southwest Colorado, the area of this detailed study (Fig. 3-1), the cover rocks of the Uncompahgre Group have been interpreted to either (1) unconformably overlie ca. 1750 Ma basement (Barker, 1969) or (2) be in contact with basement along major south-directed thrusts (Tewksbury, 1985).

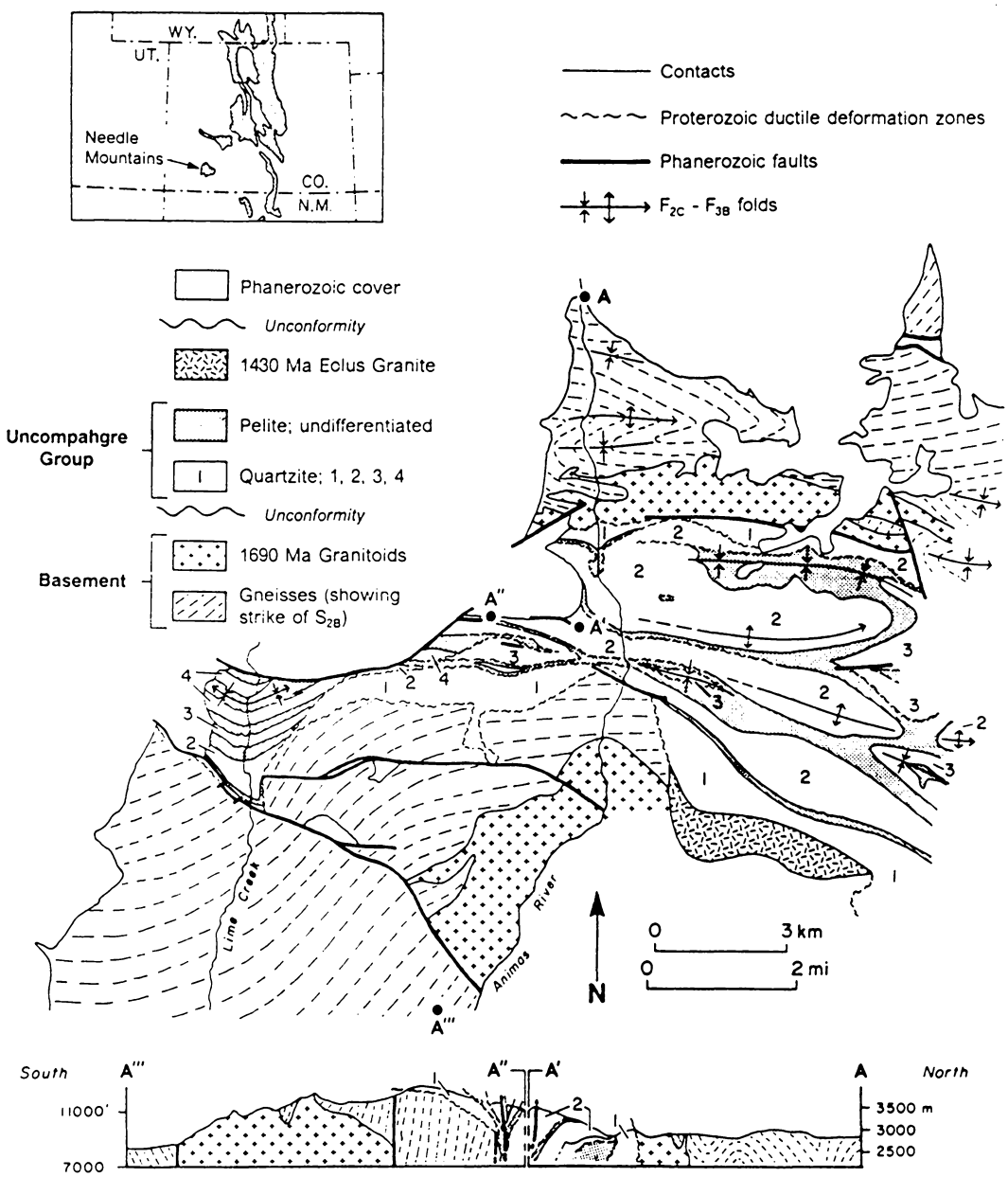

Figure 3-1: Geologic map and cross section of study area. Eastern and southeastern margins of map area from Barker (1969) and Tewksbury (1985). Inset shows location of Needle Mountains and other areas of Early to Middle Proterozoic outcrops (stippled).

In the northwestern Needle Mountains (Fig. 3-1), we undertook a detailed stratigraphic and structural analysis of Proterozoic basement and cover rocks in order to place constraints on their contact and age relations and resolve the apparent conflict in tectonic transport direction relative to terranes of similar age in New Mexico and Arizona. Evaluation of new and previously published data leads to a reinterpretation of the structural evolution of this area. The model presented in this paper may be applicable to other terranes where similar basement-cover relations exist.

STRATIGRAPHIC UNITS

The basement complex in the northwestern Needle Mountains (Fig. 3-1) is composed of (1) amphibolite-grade, compositionally layered and non-layered gneisses derived from mafic to felsic volcanogenic and plutonic rocks and (2) weakly foliated quartz diorite to granite intrusive rocks that cross-cut a prominent foliation within the gneisses (Barker, 1969). Rb-Sr and U-Pb isotopes yield ages of 1740-1760 Ma for the protoliths of the gneiss complex and 1680-1700 Ma for the granitoid plutons (ages recalculated from Silver and Barker, 1968; Barker et al., 1969; Bickford et al., 1969).

The Uncompahgre Group occupies an east-trending belt bounded by basement and consists of four alternating packages of quartzite and pelite; the total thickness is approximately 3 km (Fig. 3-1; stratigraphic subdivisions defined in Harris and Eriksson, 1987). Individual quartzite and pelite units, which are distinguishable from one another based on a sequential ordering of facies, may be correlated throughout the map area. Abundant primary sedimentary structures provide control on younging directions within stratigraphic units. The age of the Uncompahgre Group relative to basement is uncertain because of localized deformation along basement-cover contacts and the absence of clasts of the underlying basement in the cover rocks. If the Uncompahgre Group

unconformably overlies basement, as suggested by Barker (1969), then its maximum age would be equivalent to the ca. 1690 Ma granitoids. However, if basement-cover contacts are major thrusts, as proposed by Tewksbury (1985), then the Uncompahgre Group may be as old or older than basement gneisses. A minimum age for the Uncompahgre Group is provided by the cross-cutting, undeformed, 1410-1450 Ma Eolus Granite (Silver and Barker, 1968; Barker, 1969; Bickford et al., 1969).

STRUCTURAL GEOLOGY

Two polyphase pre-1430 Ma deformational events (D_B and D_{BC}) can be distinguished within the study area. D_B is exclusive to basement whereas D_{BC} structures are the product of an event that affected both basement and cover (Gibson and Simpson, 1986; Harris et al., 1986). An early phase of metamorphism (M_1) resulted in the growth of synkinematic garnets during D_B. Post-D_{BC}, M_2 metamorphism produced muscovite + chlorite ± andalusite ± chloritoid within the Uncompahgre Group and along basement-cover contacts, and retrograde assemblages within the basement (Barker, 1969). The chronology of tectonic features and metamorphism is outlined in Figure 3-2.

D_B Structures Within Basement

A well-developed planar mineral alignment (S_{1B}) is parallel to lithologic contacts everywhere except in mesoscopic, isoclinal F_{1B} fold hinges. F_{2B} folds are close to isoclinal, have a weak axial planar S_{2B} mineral alignment, deform S_{1B}, and are cross-cut by the ca. 1690 Ma granitoids. D_B structures are truncated along contacts with the Uncompahgre Group.

D_{BC} Structures Within Basement and Cover

The oldest structures within the Uncompahgre Group are deformation zones localized within stratigraphic intervals of interbedded pelite and quartzite up to 50 m thick or individual pelitic beds <15 cm thick. Structures in the thicker deformation zones include mesoscopic, tight to isoclinal, locally rootless folds (F_{1C}) that have axial-planar slaty cleavage, S_{1C} (Tewksbury, 1981, 1985; Harris et al., 1986). Narrower bedding-parallel deformation zones exhibit a sigmoidal foliation (S_{1C}) defined by elongate detrital grains, quartz ribbons, and aligned white mica + hematite. Shear zone geometry and local stratigraphic duplication within individual quartzite units indicate that north-directed thrusting produced these structures.

Macroscopic, upright, subhorizontal, east-trending, tight to open folds (F_{2C} and F_{3B}; Figs. 3-1 and 3-2) deform D_B structures in basement (Gibson and Simpson, 1986) and the bedding-parallel deformation zones within the Uncompahgre Group (Tewksbury, 1981, 1985). Circa 1690 Ma granitoids in the basement contain a subvertical, east-striking, S_{3B} foliation parallel to F_{3B} axial surfaces. In the cover, an axial-planar spaced cleavage (S_{2C}) is associated with F_{2C} folds.

Foliation surfaces (S_{1B}-S_{3B}) in basement gneisses and ca. 1690 Ma granitoids contain a subhorizontal mineral lineation that is parallel to the long axes of deformed clasts in metavolcaniclastic rocks. Asymmetric quartz *c*-axis fabrics and rare subvertical, mesoscopic shear zones or shear bands indicate predominantly dextral, noncoaxial flow in domains of east-striking foliation, and sinistral shear in zones of northeast-striking foliation (see map pattern of S_{2B} foliation in Fig. 3-1). These directions and senses of movement resemble those observed in conjugate ductile shear zones (cf. Ramsay, 1980) and imply north-northwest to south-southeast shortening.

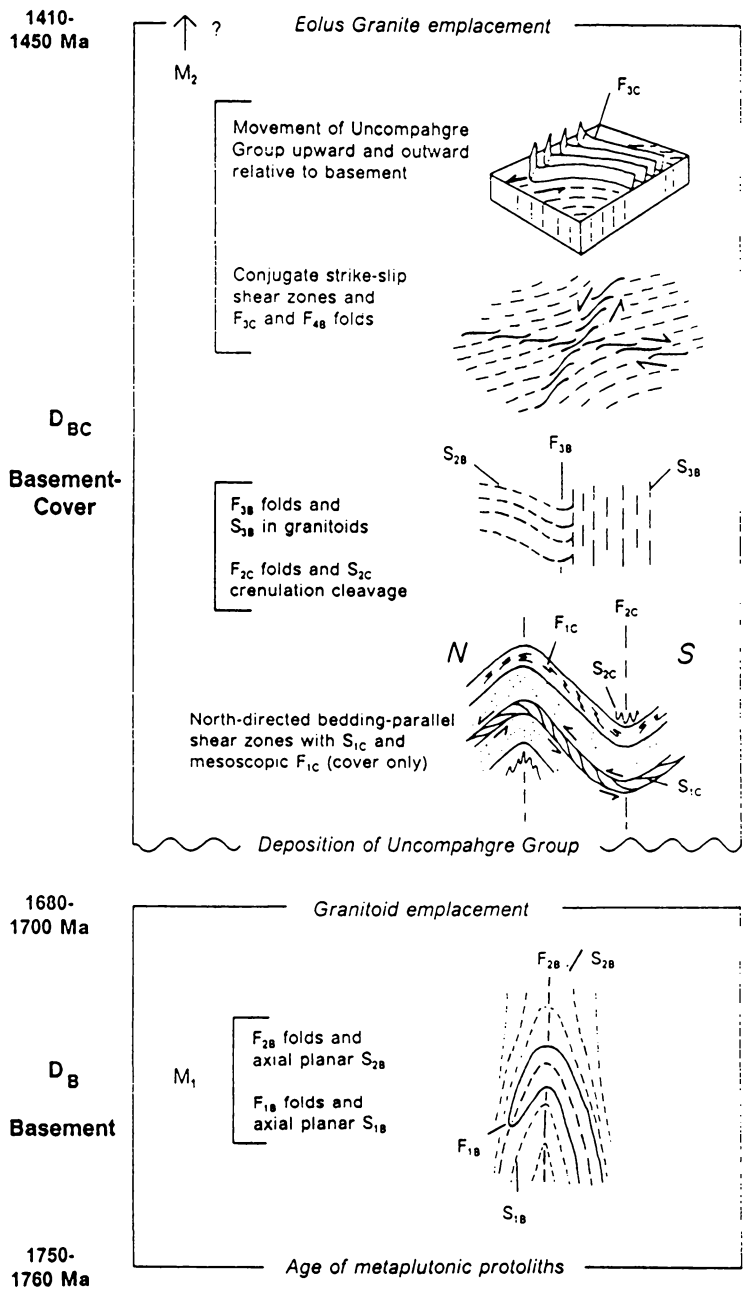

Figure 3-2: Chronology of deformation, plutonism, and metamorphism in the study area. Time scale is nonlinear. Peak of M_2 postdates D_{BC}, but minimum age is uncertain.

Steeply dipping, east- and northeast-striking zones of localized deformation within the Uncompahgre Group (Fig. 3-1) are characterized by attenuated and truncated stratigraphic units and phacoidal or crenulation fabrics in pelites. Asymmetrically pulled-apart psammitic beds, shear bands, and gently to moderately plunging mineral lineations indicate dextral oblique movement along east-striking zones and sinistral oblique slip within northeast-striking zones (Fig. 3-1). These senses of movement concur with the pattern observed in the basement.

Steeply plunging, macroscopic F_{3C} and mesoscopic F_{4B} folds in the vicinity of Lime Creek (Fig. 3-1) geographically coincide with zones of sinistral shearing in both the basement and cover. These structures are interpreted to be the product of reorientation of older structural elements into a northeast-striking, sinistral shear zone.

D_{BC} Structures Along Basement-Cover Contacts

Contacts between the basement and Uncompahgre Group are marked by a zone of quartz-muscovite phyllite or phyllonite that is generally less than 2 m thick but locally up to 12 m thick (Barker, 1969; Tewksbury, 1985). Within the adjacent Uncompahgre Group, conglomerates and pebbly sandstones become increasingly foliated and grade into these micaceous lithologies. In basement gneisses and granitoids, mineral assemblages are altered to phyllosilicates + Fe-Ti oxides; relict foliations (S_{1B} or S_{2B}) are either deflected into parallelism with the contact or overprinted by a spaced to continuous muscovite foliation that is subparallel to the contact.

The northern basement-cover contact is vertical to steeply north-dipping, whereas the southern contact is convex upward, and subhorizontal at topographically highest elevations (Fig. 3-1, cross section). Cover rocks, typically of the basal unit (quartzite 1; Fig. 3-1), always young away from the contacts. On the southern contact east of Lime

Creek, Proterozoic sinistral offset of stratigraphic units in the cover resulted in the juxtaposition of quartzite 2 and basement (Fig. 3-1). Along the northern contact east of the Animas River, a Phanerozoic fault places granitoids against quartzite 2 of the Uncompahgre Group (Fig. 3-1).

Shear bands within phyllonites along the southern contact record north-side-up, dip-slip motion; <10 cm-thick shear zones within the basal 50 m of the Uncompahgre Group quartzites show oblique dextral and north-side-up movement. Fabrics in phyllites along the northern contact usually display a lack of consistent asymmetry. At one locality along the northern contact west of the Animas River (Fig. 3-1), a basal quartz-pebble conglomerate of the Uncomaphgre Group is in direct contact with retrograded gneiss and granite. The outcrop exhibiting this probable unconformable contact is bounded on the north and south by south-side-up deformation zones.

DEFORMATION MODEL

Previous deformation models for the Needle Mountains have implied that the Uncompahgre Group is either parautocthonous (Barker, 1969) or allochthonous (Tewksbury, 1985) relative to basement. Tewksbury (1985) inferred a south-directed sense of tectonic transport from the apparent ramp-flat geometry of the phyllonite zone that defines the southern basement-cover contact (Fig. 3-1, cross section). Bedding-parallel deformation zones refolded about upright folds (F_{2C}) were interpreted by Tewksbury (1981) to be the product of progressive south-directed thrusting. This model requires a consistent north-side-up sense of movement on both the northern and southern basement-cover contacts. Major inconsistencies between Tewksbury's (1981, 1985) model and our data include (1) predominantly north-directed movement on pre-F_{2C} de-

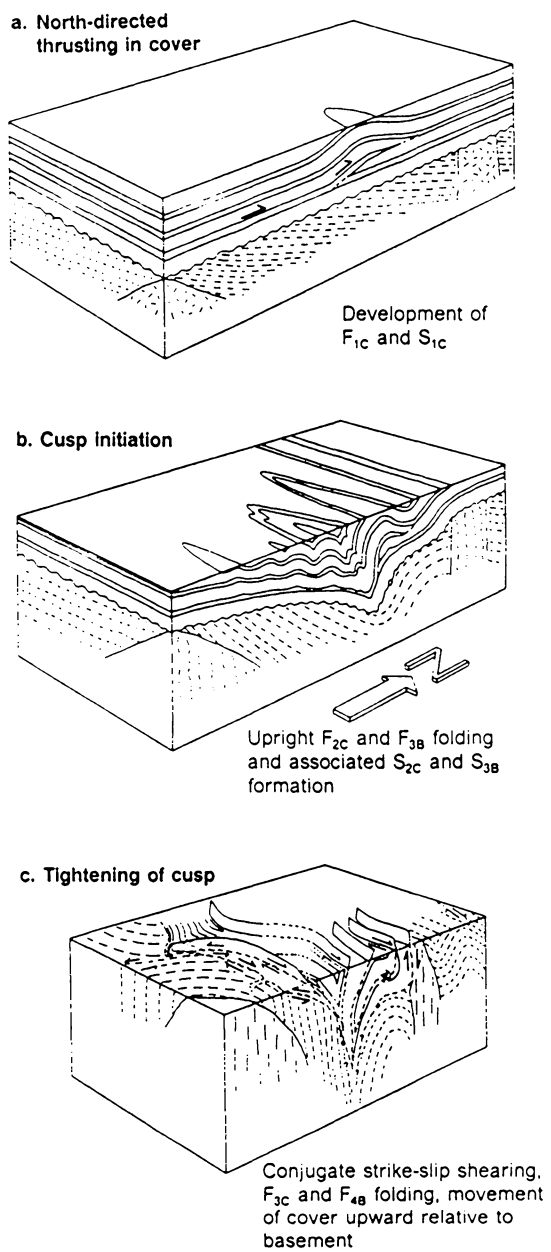

Figure 3-3: Interpretive model for D_{BC} deformation in northwestern Needle Mountains. North-directed thrusting (a) was preceded by deposition of Uncompahgre Group unconformably upon basement. Pre-D_{BC} basement fabric orientation is unknown. Cover structures in (b) patterned after observed deformation style in eastern part of map area.

formation zones within the Uncompahgre Group and (2) opposing senses of dip-slip movement along the northern and southern basement-cover contacts.

An alternative model for D_{BC} in the northwestern Needle Mountains is illustrated in Figure 3-3. The Uncompahgre Group was deposited unconformably on a previously deformed gneiss complex intruded by ca. 1690 Ma granitoids. Subsequent deformation was initially thin-skinned and produced north-directed, bedding-parallel deformation zones and local stratigraphic duplication (Fig. 3-3a). The preservation of intact stratigraphic order within the Uncompahgre Group, especially in the western and eastern parts of the study area (Fig. 3-1), suggests that this deformation did not involve large-scale stratigraphic duplication at the scale of the map area. With further compression, upright folding (F_{2C}, F_{3B}) of basement and cover began and the unconformity surface was deformed into a cusp-shaped geometry with convex-upward limbs (Fig. 3-3b). This type of structure is typically interpreted to reflect the greater viscosity of one unit (basement) relative to the other (cover) during folding (Ramsay, 1967; Dieterich, 1970). The final increments of deformation involved strike-slip shearing within all lithologic units and tightening of the cusp with upward movement of the Uncompahgre Group relative to basement (Fig. 3-3c). Decoupling of cover from basement during cuspate folding probably occurred because of contrasting rheological properties and the presence of a mechanically weak micaceous layer along the contact (probable unconformity). This process may be analogous to the detachment along lithologic contacts that is necessary to accommodate space problems during concentric folding of layered sequences (cf. Dahlstrom, 1977).

Although our data are consistent with the Uncompahgre Group being deposited unconformably on basement, few clasts in the basal Uncompahgre Group can be linked to a local basement provenance. However, potential source rocks for chert and iron formation clasts in the Uncompahgre Group (Harris and Eriksson, 1987) do exist in

basement terranes in southwest Colorado (e.g. Barker, 1969; Afifi, 1981). The absence of locally derived felsic gneiss and amphibolite clasts may be due to a distant provenance and/or deep weathering of these lithologies to sand- and clay-sized fractions (e.g. Stallard, 1986). A weathered horizon is a possible protolith for the hydrated aluminous rocks found along the basement-cover contacts.

Cross sections of the Uncompahgre Group outcrop belt (Figs. 3-1 and 3-3c) cannot be restored to their undeformed state by using standard section balancing techniques (e.g., Dahlstrom, 1969) because of the movement of stratigraphic units into and out of the plane of section during the final phase of D_{BC}. It is also not possible to estimate the magnitude of displacement along basement-cover contacts because they are parallel to bedding in the Uncompahgre Group and no other marker units are present at this interface.

The age of D_{BC} deformation can only be bracketed between pluton emplacement at approximately 1690 and 1430 Ma. It is possible, therefore, that the various phases of D_{BC} do not represent a continuum of deformation. However, a single progressive event most simply explains the observed relationships.

IMPLICATIONS

Basement-cover contacts in the northwestern Needle Mountains, previously interpreted as south-directed thrusts (Tewksbury, 1985), are reinterpreted as unconformities that localized deformation during cuspate infolding of cover into basement following limited north-directed, thin-skinned thrusting. This movement pattern is consistent with north-directed tectonic transport documented in approximately coeval rocks of northern New Mexico (Grambling and Codding, 1982) and central Arizona (Puls and Karlstrom, 1985; Karlstrom and Conway, 1986). The style of Proterozoic deformation in the Needle

Mountains is apparently analogous to that of the Alpine external massifs and their cover (Ramsay, 1967; Gratier and Vialon, 1980; Tricarte and Lemoine, 1986) and the Tree River fold belt and internal zone of the Wopmay Orogen (Hoffman et al., 1984; King, 1986).

Cuspate structures may be more common than previously recognized in geologic terranes where cover sequences occur as isolated remnants within basement. Deformation zones along basement-cover interfaces in such settings may form as a geometrical product of folding, and may not necessarily represent loci of large-scale tectonic translation.

References Cited

Afifi, A.M., 1981, Stratigraphy, petrology, and structure of Precambrian metavolcanic rocks in the Iris District, Gunnison and Saguache Counties, Colorado: New Mexico Geological Society Guidebook, V. 32, p. 287-292.

Aigner, T., 1985, Storm Depositional Systems, Dynamic stratigraphy in modern and ancient shallow-marine sequences, from Lecture Notes in Earth Sciences, Friedman, G.M, Neugebauer, H.J. and Seilacher, A., eds.: Berlin, Springer-Verlag, 174 p.

Aigner, T. and Reineck, H.-E., 1982, Proximality trends in modern storm sands from the Helgoland Bight (North Sea) and their implications for basin analysis: Senckenbergiana Maritima, V. 14, p. 183-215.

Allen, J.R.L., 1980, Sandwaves: A model of origin and internal structure: Sedimentary Geology, V. 26, p. 281-328.

_____1981a, Lower Cretaceous tides revealed by cross-bedding with mud drapes: Nature, V. 289, p. 579-581.

_____1981b, Paleotidal speeds and ranges estimated from cross-bedding sets with mud drapes: Nature, V. 293, p. 394-396.

_____1984, Sedimentary structures: Their character and physical basis, unabridged one volume edition: Amsterdam, Elsevier Science Publishers, 1256 p.

Allen, P.A., 1985, Hummocky cross-stratification is not produced purely under progressive gravity waves: Nature, V. 313, p. 562-564.

Allen, P.A. and Homewood, P., 1984, Evolution and mechanics of a Miocene tidal sandwave: Sedimentology, V. 31, p. 63-81.

Anderton, R., 1976, Tidal-shelf sedimentation: An example from the Scottish Dalradian: Sedimentology, V. 23, p. 429-458.

Aspler, L.B., and Donaldson, J.A., 1985, The Nonacho Basin (Early Proterozoic), Northwest Territories, Canada: Sedimentation and deformation in a strike-slip setting, in Biddle, K.T. and Christie-Blick, N., eds., Strike-slip deformation, basin formation, and sedimentation: Society of Economic Paleontologists and Mineralogists Special Publication no. 37, p. 193-209.

Bambach, R.K. and Sepkoski, J.J., 1979, The increasing influence of biologic activity on sedimentary stratification through time: Geological Society of America, Abstracts with Programs, V. 11, p. 383.

Barker, F., 1969, Precambrian geology of the Needle Mountains, southwestern Colorado: U.S. Geological Survey Professional Paper 644-A, p. A1-A35.

Barker, F., Peterman, Z.E., and Hildreth, R.A., 1969, A rubidium-strontium study of the Twilight Gneiss, West Needle Mountains, Colorado: Contributions to Mineralogy and Petrology, V. 23, p. 271-282.

Beerbower, J.R., 1964, Cyclothems and cyclic depositional mechanisms in allluvial plain sedimentation, in Merriam, D.F., ed., Symposium on Cyclic Sedimentation, V. 1: Kansas Geological Survey Bull. 169, p. 31-41.

Bergman, K. and Walker, R.G., 1986, Cardium Formation conglomerates at Carrot Creek Field: Offshore linear ridges or shoreface deposits?, in Moslow, T.F. and Rhodes, E.G., eds., Modern and Ancient Shelf Clastics: A Core Workshop, SEPM Core Workshop no.9: Soc. Econ. Paleont. and Mineral., Tulsa, OK., p. 217-268.

Bickford, M.E., Van Schmus, W.R., and Zietz, I., 1986, Proterozoic history of the midcontinent region of North America: Geology, V. 14, p. 492-496.

Bickford, M.E., Wetherill, G.W., Barker, F. and Lee-Hu, C.-N., 1969, Precambrian Rb/Sr chronology in the Needle Mountains, southwestern Colorado: Journal of Geophysical Research, V. 74, p. 1660-1676.

Blatt, H., Middleton, G., and Murray, R., 1972, Origin of Sedimentary Rocks: Englewood Cliffs, New Jersey, Prentice-Hall, Inc., 634 p.

Bloom, A.L., 1967, Pleistocene shoreline: A new test of isostasy: Geological Society of America Bulletin, V.78, p. 1477-1494.

Bluck, B.J., 1979, Structure of coarse-grained braided stream alluvium: Transactions Royal Society Edinburgh, V. 70, p. 181-221.

Boersma, J.R. and Terwindt, J.H.J., 1981, Neap-spring tide sequences of intertidal shoal deposits in a mesotidal estuary: Sedimentology, V. 28, p. 151-170.

Bouma, A.H., 1962, Sedimentology of some flysch deposits, a graphic approach to facies interpretation: Amsterdam, Elsevier Science Publishers, 168 p.

Bourgeois, J. and Leithold, E.L., 1984, Wave-worked conglomerates - Depositional processes and criteria for recognition, in Koster, E.H. and Steel, R.J., eds., Sedimentology of Gravels and Conglomerates: Canadian Society Petroleum Geologists, Memoir 10., p. 331-343.

Boyer, S.E. and Elliott, D., 1982, Thrust Systems: The American Association of Petroleum Geologists Bulletin, V. 66, p. 1196-1230.

Brady, T.B., Sherlock, S.M., and Karlstrom, K.E., 1987, Early Proterozoic crustal shortening by tectonic wedging, northern Sierra Anchas, central Arizona: Geological Society of America, Abstracts with Programs, V. 19, p. 262.

Brenchley, P.J., 1985, Storm influenced sandstone beds: Modern Geology, V. 9, p. 331-343.

Burbank, W.S., and Luedke, R.G., 1964, Geology of the Ironton Quadrangle, Colorado: U.S. Geological Survey Map GQ-291, Scale 1:24,000.

Christie-Blick, N. and Levy, M., 1985, A new approach to time correlation in Proterozoic rocks: Sequence boundaries in the Brigham Group, Utah: Geological Society of America, Abstracts with Programs, V. 17, no. 7, p. 546.

Christie-Blick, N. and Levy, M., 1986, Sequence boundaries in Proterozoic successions: Examples from western United States: Abs., Sediments Down Under, 12th International Sedimentological Congress, Canberra, Australia, p. 60.

Clifton, H.E., 1973, Pebble segregation and bed lenticularity in wave-worked versus alluvial gravel: Sedimentology, V. 20, p. 173-187.

Clifton, H.E., 1976, Wave-formed sedimentary structures - A conceptual model, in Davis, R.A., Jr. and Ethington, R.L., eds., Beach and Nearshore Sedimentation: Society of Economic Paleontologists and Mineralogists, Special Publication no.24, p. 126-148.

Clifton, H.E., 1981, Progradational sequences in Miocene shoreline deposits, southeastern Caliente Range, California: Journal of Sedimentary Petrology, V. 51, p. 165-184.

Cloetingh, S., McQueen, H. and Lambeck, K., 1985, On a tectonic mechanism for regional sealevel variations: Earth and Planetary Science Letters, V. 75, p. 157-166.

Cotter, E., 1983, Shelf, paralic, and fluvial environments and eustatic sea level fluctuations in the origin of the Tuscarora Formation (Lower Silurian) of central Pennsylvania: Journal of Sedimentary Petrology, V. 53, p. 25-49.

Cotter, E., 1985, Gravel-topped offshore bar sequences in the Lower Carboniferous of southern Ireland: Sedimentology, V. 32, p. 195-213.

Covey, C., 1984, The earth's orbit and the ice ages: Scientific American, p. 58-66.

Cross, W., Howe, E., Irving, J.D. and Emmons, W.H., 1905, Description of Needle Mountains Quadrangle, Colorado: U.S. Geological Survey Geologic Atlas, Folio 131, 14 p.

Dahlstrom, C.D.A., 1969, Balanced cross sections: Canadian Journal of Earth Sciences, V. 6, p. 743-757.

_____, 1977, Structural Geology in the eastern margin of the Canadian Rocky Mountains, in Heisey, E.L., Lawson, D.E., Norwood, E.A., Wach,P.H., and Hale, L.A., eds., 29th Annual Field Conference Guidebook, Rocky Mountain Thrust Belt Geology and Resources: Wyoming Geological Association, p. 407-439.

Dalrymple, R.W., 1984, Morphology and internal structure of sandwaves in the Bay of Fundy: Sedimentology, V. 31, p. 365-382.

Dalrymple, R.W., Knight, R.J., and Lambiase, J.J., 1978, Bedforms and their hydraulic stability relationships in a tidal environment, Bay of Fundy, Canada: Nature, V. 275-A, p. 100-104.

de Mowbray, T. and Visser, M.J., 1984, Reactivation surfaces in subtidal channel deposits, Oosterschelde, southwest Netherlands: Jour. Sedimentary Petrology, V. 54, p. 811-824.

de Raaf, J.F.M., Boersma, J.R., and van Gelder, A., 1977, Wave-generated structures and sequences from a shallow-marine succession, Lower Carboniferous, County Cork, Ireland: Sedimentology, V. 24, p. 451-483.

de Sitter, L.V., and Zwart, H.J., 1960, Tectonic development in supra and infrastructure of a mountain chain: Proceedings 21st International Geological Congress Copenhagen, V. 18, p. 248-256.

Diem, B., 1985, Analytical method for estimating palaeowave climate and water depth from wave ripple marks: Sedimentology, V. 32, p. 705-720.

Dieterich, J.H., 1970, Computer experiments on mechanics of finite amplitude folds: Canadian Journal of Earth Sciences, V. 7, p. 467-476.

Donovan, R.N. and Foster, R.J., 1972, Subaqueous shrinkage cracks from the Caithness Flagstone Series (Middle Devonian) of north Scotland: Journal of Sedimentary Petrology, V. 42, p. 309-317.

Dott, R.H., Jr., 1983, The Proterozoic red quartzite enigma in the north central United States: Resolved by plate collision?, in Medaris, L.G., Jr., ed., Early Proterozoic Geology of the Great Lakes Region: Geological Society of America Memoir 160, p. 129-141.

Dott, R.H., Jr. and Bourgeois, J., 1982, Hummocky stratification: Significance of its variable bedding sequences: Geol. Soc. America Bulletin, V. 93, p. 663-680.

Elliott, D., 1976, The energy balance and deformation mechanisms of thrust sheets: Philosophical Transactions of the Royal Society of London, V. A.283, p. 289-312.

Eriksson, K.A., 1979, Marginal marine depositional processes from the Archaean Moodies Group, Barberton Mountain Land, South Africa: Evidence and significance: Precambrian Research, V. 8, p. 153-182.

Eriksson, K.A., Turner, B.R. and Vos, R.G., 1981, Evidence of tidal processes from the lower part of the Witwatersrand Supergroup, South Africa: Sedimentary Geology, V. 29, p. 309-325.

Ekdale, A.A., Bromley, R.G. and Pemberton, S.G., 1984, Ichnology: The use of trace fossils in sedimentology and stratigraphy: SEPM Short Course no. 15, Society of Economic Paleontologists and Mineralogists, Tulsa, OK., 317 p.

Ettensohn, F.R., 1985, Controls on development of Catskill Delta complex basin-facies, in Woodrow, D.L. and Sevon, W.D., eds., The Catskill Delta: Geological Society of America, Special Paper no. 201, p. 65-75.

Frazier, D.E., 1974, Depositional-episodes: Their relationship to the Quaternary stratigraphic framework in the northwestern portion of the Gulf Basin: Geol. Circular 74-1, Bureau of Economic Geology, Univ. of Texas, Austin, Austin, TX., 28 p.

Gee, D.G., 1980, Basement-cover relationships in the central Scandinavian Caledonides: Geologiska Foreningens Stockholm Forhandlingar, V. 102, p. 455-474.

Ghosh, S.K., 1966, Experimental tests of buckling folds in relation to strain ellipsoid in simple shear deformations: Tectonophysics, V. 3, p. 169-185.

Gibson, R.G. and Simpson, C., 1986, Kinematic analysis and implication of Proterozoic strike-slip shear zones, West Needle Mountains, Colorado: Geological Society of America Abstracts with Programs, V. 18, p. 613.

Goldring, R. and Aigner, T., 1982, Scour and fill in the significance of event separation, in Einsele, G. and Seilacher, A., eds., Cyclic and Event Stratification: Berlin, Springer-Verlag, p. 355-362.

Grambling, J.A., and Codding, D.B., 1982, Stratigraphic and structural relationships of multiply deformed Precambrian metamorphic rocks in the Rio Mora area, New Mexico: Geological Society of America Bulletin, V. 93, p. 127-137.

Gratier, J.-P., and Vialon, P., 1980, Deformation patterns in a heterogeneous material: Folded and cleaved sedimentary cover immediately overlying a crystalline basement (Oisans, French Alps): Tectonophysics, V. 65, p. 151-180.

Gray, D.R., and Durney, D.W., 1979, Crenulation cleavage differentiation: Implications of solution deposition processes: Journal of Structural Geology, V. 1, p. 73-80.

Grotzinger, J.P., 1986, Cyclicity and palaeoenvironmental dynamics, Rocknest platform, northwest Canada: Geological Society of America Bulletin, V. 97, p. 1208-1231.

Grotzinger, J.P. and Gall, Q., 1986, Preliminary investigations of Early Proterozoic Western River and Burnside River Formations: Evidence for foredeep origin of Kilohigok Basin, District of Mackenzie: Current Research, Part A, Geol. Survey of Canada, Paper 86-1A, p. 95-106.

Hamblin, A.P. and Walker, R.G., 1979, Storm-dominated shallow marine deposits: The Fernie-Kootenay (Jurassic) transition, southern Rocky Mountains: Canadian Journal of Earth Sciences, V. 10, p. 1673-1690.

Hanmer, S., 1986, Asymmetrical pull-aparts and foliation fish as kinematic indicators: Journal of Structural Geology, V. 8, p. 111-122.

Harms, J.C., Southard, J.B. and Walker, R.G., 1982, Structures and sequences in clastic rocks: SEPM Short Course no.9, Society of Economic Paleontologists and Mineralogists, Tulsa, OK., 249 p.

Harris, C.W., and Eriksson, K.A., 1987, Tide-, storm-, and wave-influenced shelf sedimentation in a tectonically active intracratonic basin: the Proterozoic Uncompahgre Group, southwest Colorado: Geological Society of America Abstracts with Programs, V. 19, p. 281-282.

Harris, C.W., Gibson, R.G., Simpson, C. and Eriksson, K.A., 1986, Early to Middle Proterozoic polyphase deformation West Needle Mountains, southwest Colorado: Preliminary results: Geological Society of America, Abstracts with Programs, V. 18, p. 360.

Harris, C.W., Gibson, R.G., Simpson, C. and Eriksson, K.A., 1987, Proterozoic cuspate basement-cover structure, Needle Mountains, Colorado: Geology, V. 15, p. 950-953.

Harris, L.D., and Milici, 1977, Characteristics of thin-skinned style of deformation in the Southern Appalachians, and potential hydrocarbon traps: U.S. Geologicaly Survey Professional Paper 1018.

Hayes, M.O., 1967, Hurricanes as geologic agents, south Texas coast: American Association of Petroleum Geologists Bulletin, V. 51, p. 937-942.

Hein, F.J. and Walker, R.G., 1977, Bar evolution and development of stratification in the gravelly, braided, Kicking Horse River, British Columbia: Canadian Journal of Earth Sciences, V. 14, p. 562-570.

Heller, P.L. and Angevine C.L., 1985, Sea-level cycles during the growth of Atlantic-type oceans: Earth and Planetary Science Letters, V. 75, p. 417-426.

Hobbs, B.E., Means, W.D., and Williams, P.F., 1976, An outline of structural geology: New York, John Wiley & Sons, Inc., 571 p.

Hobday, D.K. and Morton, R.A., 1984, Lower Cretaceous shelf storm deposits, northeast Texas, in Tillman, R.W. and Siemers, C.T., eds., Siliciclastic Shelf Sediments: Society of Economic Paleontologists and Mineralogists Special Publication no.34, p. 205-213.

Hobday, D.K. and Tankard, A.J., 1978, Transgressive-barrier and shallow-shelf interpretation of the Lower Paleozoic Peninsular Formation, South Africa: Geological Society of America Bulletin, V. 89, p. 1733-1744.

Hoffman, P.F., 1985, Is the Cape Smith Belt (northern Quebec) a klippe?: Canadian Journal of Earth Sciences, V. 22, p. 1361-1369.

Hoffman, P.F., Tirrul, R., Grotzinger, J.P., Lucas, S.B., and Eriksson, K.A., 1984, The externides of Wopmay orogen, Takijuk Lake and Kikerk Lake Map area, district of Mackenzie, in Current Research, Part A: Geological Survey of Canada, Paper 84-1A, p. 383-395.

Homewood, P. and Allen, P.A., 1981, Wave-, tide-, and current-controlled sandbodies of Miocene Molasse, Western Switzerland: American Association Petroleum Geologists Bulletin, V. 65, p. 2534-2545.

Jackson, M.P.A., Eriksson, K.A. and Harris, C.W., 1987, Early Archean Foredeep sedimentation related to crustal shortening: A reinterpretation of the Barberton Sequence, Southern Africa: Tectonophysics, V. 136, p. 197-221.

Jacob, R.E., Snowden, P.A. and Bunting, F.J.L., 1983, Geology and Structural Development of the Tumas basement dome and its cover rocks, in Miller, R.McG., ed., Evolution of the Damara orogen of Southwest Africa/Namibia: Special Publication Geological Society of South Africa, V. 11, p. 157-172.

Johnson, H.D. and Baldwin, C.T., 1986, Shallow Siliciclastic Seas, in Reading, H.G., ed., Sedimentary Environments and Facies: Oxford, Blackwell Scientific Publ., Chap. 9, p. 229-282.

Karlstrom, K.E., and Conway, C.M., 1986, Deformational styles and contrasting lithostratigraphic sequences within an early Proterozoic orogenic belt, central Arizona: in Nations, J.D., Conway, C.M., and Swann, G.A., eds., Geology of central and northern Arizona (Geological Society of America Rocky Mountain Section meeting guidebook): Flagstaff, Northern Arizona Creative Printers, p. 1-25.

Karner, G.D., 1986, Effects of lithospheric in-plane stress on sedimentary basin stratigraphy: Tectonics, V. 5, p. 573-588.

King, J.E., 1986, The metamorphic internal zone of Wopmay orogen (Early Proterozoic), Canada: 30 km of structural relief in a composite section based on down-plunge projection: Tectonics, V. 5, p. 973-994.

Klein, G. de Vries, 1982, Probable sequential arrangement of depositional systems on cratons: Geology, V. 10, p. 17-22.

Kreisa, R.D., 1986, Hummocky cross-stratification is trough cross-bedding: Society of Economic Paleontologists and Mineralogists, Annual Midyear Meeting Abstracts, V. III, p. 63.

Leckie, D.A. and Walker, R.G., 1982, Storm- and tide-dominated shorelines in Cretaceous Moosebar-Lower Gates interval - Outcrop equivalents of deep basin gas trap in western Canada: American Association of Petroleum Geologists Bulletin, V. 66, p. 138-157.

Leithold, E.L. and Bourgeois, J., 1984, Characteristics of coarse-grained sequences deposited in nearshore, wave-dominated environments - Examples from the Miocene of southwest Oregon: Sedimentology, V. 31, p. 749-775.

Levell, B.K., 1980a, Evidence for currents associated with waves in Late Precambrian shelf deposits from Finnmark, north Norway: Sedimentology, V. 27, p. 153-166.

Levell, B.K., 1980b, A late Precambrian tidal shelf deposit, the Lower Sandfjord Formation, Finnmark, north Norway: Sedimentology, V. 27, p. 539-557.

Luedke, R.G. and Burbank, W.S., 1962, Geology of the Ouray Quadrangle, Colorado: U.S. Geological Survey Map GQ-152, Scale 1:24,000.

Matthews, R.K., 1984, Dynamic Stratigraphy: An Introduction to Sedimentation and Stratigraphy, Second Edition: Englewood Cliffs, New Jersey, Prentice-Hall, Inc., 489 p.

McKenzie, D., 1978, Some remarks on the development of sedimentary basins: Earth and Planetary Science Letters, V. 40, p. 25-32.

Miall, A.D., 1977, A review of the braided-river depositional environment: Earth-Science Reviews, V. 13, p. 1-62.

Miall, A.D., 1985, Architectural-element analysis: A new method of facies analysis applied to fluvial deposits: Earth-Science Reviews, V. 22, p. 261-308.

Miller, M.F. and Byers, C.W., 1984, Abundant and diverse Early Paleozoic infauna indicated by the stratigraphic record: Geology, V. 12, p. 40-43.

Murphy, D.C., 1987, Suprastructure/infrastructure transition, east-central Cariboo Mountains, British Columbia: geometry, kinematics and tectonic implications: Journal of Structural Geology, V. 9, p. 13-29.

Niedoroda, A.W., Swift, D.J.P., Hopkins, T.S. and Ma, C.-M., 1984, Shoreface morphodynamics on wave-dominated coasts: Marine Geology, V. 60, p. 331-354.

Nelson, C.H., 1982, Modern shallow-water graded sand layers from storm surges, Bering Shelf: A mimic of Bouma sequences and turbidite systems: Journal of Sedimentary Petrology, V. 52, p. 537-545.

Nottvedt, A. and Kreisa, R.D., 1987, Model for the combined-flow origin of hummocky cross-stratification: Geology, V. 15, p. 357-361.

Nummedal, D., 1986a, Shallow marine depositional sequence boundaries - Composite and simple: Society of Economic Paleontologists and Mineralogists, Annual Midyear Meeting Abstracts, V. III, p. 85.

_____, 1986b, Storm- versus tide-dominated structures in the Tocito Sandstone, Coniacian of the San Juan Basin, New Mexico: Geological Society of America, Abstracts with Programs, V. 18, p. 709.

Paolo, C., Wiele, S.M. and Reinhart, M.A., 1986, Upper-regime parallel lamination as the result of turbulent sediment transport and low-amplitude bed forms: Society of Economic Paleontologists and Mineralogists, Annual Midyear Meeting Abstracts, V. III, p. 87.

Platt, J.P., 1980, Archean greenstone belts: A structural test of tectonic hypotheses: Tectonophysics, V. 65, p. 127-150.

Plint, A.G., Walker, R.G. and Bergman, K., 1986, Cardium Formation 6. Stratigraphic framework of the Cardium in subsurface: Bulletin of Canadian Petroleum Geologists, V. 34, p. 213-225.

Plummer, P.S. and Gostin, V.A., 1981, Shrinkage cracks: desiccation or synaeresis?: Journal of Sedimentary Petrology, V. 51, p. 1147-1156.

Powell, C. McA., 1979, A morphological classification of rock cleavage, in Bell, T.H. and Vernon, R.H., eds., Microstructural processes during deformation and metamorphism: Tectonophysics, V. 58, p. 21-34.

Price, R.A., 1981, The Cordilleran foreland thrust and fold belt in the southern Canadian Rocky Mountains, in McClay, K.R., and Price, N.J., eds., Thrust and Nappe Tectonics: The Geological Society of London, Blackwell Scientific Publications, p. 427-448.

Price, R.A., and Mountjoy, E.M., 1970, Geologic structure of the Canadian Rocky Mountains between Bow and Athabasca rivers - A progress report: Geological Association of Canada Special Paper 6, p. 7-26.

Puls, D.D. and Karlstrom, K.E., 1985, Proterozoic foreland thrusting in the Mazatzal Mountains of central Arizona: Geological Society of America Abstracts with Programs, V. 17, p. 261.

Ramberg, H., 1981, Gravity, Deformation and The Earth's Crust: London, Academic Press, 452 p.

Ramsay, J.G., 1960, The deformation of early linear structures in areas of repeated folding: Journal of Geology, V. 68., p. 75-93.

_____, 1961, The effects of folding on the orientation of sedimentation structures: Jounal of Geology, V. 69, p. 84-100.

_____, 1967, Folding and Fracturing of Rocks: New York, McGraw-Hill, 568 p.

_____, 1980, Shear zone geometry: A review: Journal of Structural Geology, V. 2, p. 83-99.

Read, J.F., Grotzinger, J.P., Bova, J.A. and Koerschner, W.F., 1986, Models for generation of carbonate cycles: Geology, V. 14, p. 107-110.

Reading, H.G., 1986, Sedimentary Environments and Facies, Second Edition: Oxford, Blackwell Scientific Publications, 615 p.

Reineck, H.-E. and Singh, I.B., 1980, Depositional Sedimentary Environments, Second Edition: Berlin, Springer-Verlag, 549 p.

Rubin, D.M. and Hunter, R.E., 1982, Bedform climbing in theory and nature: Sedimentology, V. 29, p. 121-138.

Sanderson, D.J., 1979, The transition from upright to recumbent folding in the Variscan fold belt of southwest England: A model based on the kinematics of simple shear: Journal of Structural Geology, V. 1, p. 171-180.

_____, 1982, Models of strain variation in nappes and thrust sheets: A review: Tectonophysics, V. 88, p. 201-233.

Schumm, S.A. and Lichty, R.M., 1965, Time, space and causality in geomorphology: American Journal of Science, V. 265, p. 110-119.

Schwarzacher, W. and Fischer, A.G., 1982, Limestone-shale bedding and perturbations of the earth's orbit, in Einsele, G. and Seilacher, A., eds., Cyclic and Event Stratification: Berlin, Springer-Verlag, p. 72-95.

Searle, M.P., 1985, Sequence of thrusting and origin of culminations in the northern and central Oman Mountains: Journal of Structural Geology, V. 7, p. 129-143.

Silver, L.T. and Barker, F., 1968, Geochronology of Precambrian rocks of the Needle Mountains, southwestern Colorado: Part I., U-Pb zircon results: Geological Society of America Special Paper 115 (Abstracts), p. 204-205.

Simpson, C., 1986, Determination of movement sense in mylonites: Journal of Geological Education, V. 34, p. 246-261.

Simpson, C. and Schmid, S.M., 1983, An evaluation of criteria to deduce the sense of movement in sheared rocks: Geological Society of America Bulletin, V. 94, p. 1281-1288.

Simpson, E.L. and Eriksson, K.A., 1986, Wave-dominated and storm-dominated sedimentation in Lower Cambrian Hampton and Erwin Formation of Chilhowee Group, central and southern Virginia: Abstracts, American Association of Petroleum Geologists Bulletin, V. 70, no. 5, p. 648.

Smith, R.B., 1979, The folding of a strongly non-Newtonian layer: American Journal of Science, V. 279, p. 272-287.

Snedden, J. and Nummedal, D., 1986, Storm-deposited sand beds in modern sands of the Texas continental shelf: Society of Economic Paleontologists and Mineralogists, Annual Midyear Meeting Abstracts, V. III, p. 104.

Soegaard, K. and Eriksson, K.A., 1985, Evidence of tide, storm and wave interaction on a Precambrian siliciclastic shelf: The 1700 m.y. Ortega Group, New Mexico: Journal of Sedimentary Petrology, V. 55, p. 672-684.

Stallard, R.G., 1986, Weathering and erosion in the humid tropics, in Lerman, A., Meybeck, M. and Drever, J.I., eds., Physical and chemical weathering in geochemical cycles: Netherlands, D. Reidel, p. 1-30.

Steven, T.A., Lipman, P.W., Hail, W.J., Jr., Barker, F., and Luedke, R.G., 1974, Geologic map of the Durango Quadrangle, Southwestern Colorado: U.S. Geological Survey, Miscellaneous Investigations Series Map I-764, Scale 1:250,000.

Stow, D.A.V. and Shanmugam, G., 1980, Sequence of structures in fine-grained turbidites: Comparison of recent deep-sea and ancient flysch sediments: Sedimentary Geology, V. 25, p. 23-42.

Stride, A.H., 1982, Offshore Tidal Sands: Processes and Deposits: London, Chapman and Hall, 222 p..

Swift, D.J.P., 1968, Coastal erosion and transgressive stratigraphy: Journal of Geology, V. 76, p. 444-456.

Swift, D.J.P., Figueiredo, A.G., Jr., Freeland, G.L. and Oertel, G.F., 1983, Hummocky cross-stratification and megaripples: A geological double standard?: Journal of Sedimentary Petrology, V. 53, p. 1295-1317.

Swift, D.J.P., Hudelson, P.M., Brenner, R.L., and Thompson, P., 1987, Shelf construction in a foreland basin: storm beds, shelf sandbodies, and shelf-slope depositional sequences in the Upper Cretaceous Mesaverde Group, Book Cliffs, Utah: Sedimentology, V. 34, p. 423-457.

Tewksbury, B.J., 1981, Polyphase deformation and contact relationships of the Precambrian Uncompahgre Formation, Needle Mountains, Southwestern Colorado [Ph.D. Thesis]: Boulder, University of Colorado, 372 p.

_____, 1985, Revised interpretation of the age of allochthonous rocks of the Uncompahgre Formation, Needle Mountains, Colorado: Geological Society of America Bulletin, V. 96, p. 224-232.

_____, 1986, Conjugate crenulation cleavages in the Uncompahgre Formation, Needle Mountains, Colorado: Journal of Structural Geology, V. 8, p. 145-155.

Thayer, C.W., 1983, Sediment-mediated biological disturbance and the evolution of marine benthos, in Tevesz, M.J.S. and McCall, P.L., eds., Biotic Interactions in Recent and Fossil Benthic Communities: New York, Plenum Press, p. 480-625.

Tillman, R.W. and Martinsen, R.S., 1984, The Shannon shelf-ridge sandstone complex, Salt Creek anticline area, Powder River Basin, Wyoming, in Tillman, R.W. and Siemers, C.T., eds., Siliciclastic Shelf Sediments: Society of Economic Paleontologists and Mineralogists, Special Publication no.34, p. 85-142.

Tirrul, R., 1983, Structure cross-sections across Asiak foreland thrust and fold belt, Wopmay orogen, District of Mackenzie: in Current Research, Part B: Geological Survey of Canada Paper 83-1B, p. 253-260.

Tricart, P. and Lemoine, M., 1986, From faulted blocks to megamullions and megaboudins: Tethyan heritage in the structure of the western Alps: Tectonics, V. 5, p. 95-118.

Turner, F.V., and Weiss, L.E., 1963, Structural analysis of metamorphic tectonites: New York, McGraw-Hill, 545 p.

Vail, P.R., Mitchum, R.M.,Jr. and Thompson, S.,III, 1977, Seismic stratigraphy and global changes of sea level, part 4: Global cycles of relative changes of sea level, in Payton, C.E., ed., Seismic Stratigraphy - Applications to Hydrocarbon Exploration: American Association of Petroleum Geologists Memoir 26, p. 83-97.

van Houten, F.B., 1964, Cyclic lacustrine sedimentation, Upper Triassic Lockatong Formation, New Jersey and adjacent Pennsylvania, in Merriam, D.F., ed., Symposium on Cyclic Sedimentation, V. 1: Kansas Geological Survey Bulletin 169, p. 497-531.

Visser, M.J., 1980, Neap-spring cycles reflected in Holocene subtidal large-scale bedform deposits: A preliminary note: Geology, V. 8, p. 543-546.

Walker, R.G., 1984, Shelf and shallow marine sands, in Walker, R.G., ed., Facies Models, Second Edition, Geoscience Canada Reprint Series 1: Toronto, Geological Association of Canada, p. 141-170.

Watchorn, M.B., 1980, Fluvial and tidal sedimentation in the 3000 Ma Mozaan basin, South Africa: Precambrian Research, V. 13, p. 27-42.

Weimer, R.J., 1984, Relation of unconformities, tectonics and sea-level changes, Cretaceous of western interior, U.S.A., in Schlee, J.S., ed., Interregional Unconformities and Hydrocarbon Accumulation: American Association of Petroleum Geologists Memoir 36, p. 7-35.

Whitaker, J.H. McD., 1973, "Gutter casts", a new name for scour-and-fill structures: With examples from the Llandoverian of Ringerike and Malmoya, southern Norway: Norsk. Geol. Tidsskrift, V. 53, p. 403-417.

Wright, R., 1986, Cycle stratigraphy as a paleogeographic tool: Point Lookout Sandstone, southeastern San Juan basin, New Mexico: Geological Society of America Bulletin, V. 96, p. 661-673.

Appendix A. Paleowave Reconstructions

Equations
(after Diem, 1985)

Bottom orbital diameter; d_0

$$d_0 = \frac{\lambda}{0.65} \quad provided \ \lambda \ < 0.0028 \cdot D^{1.68}$$

Threshold velocity; U_t

$$U_t^2 = 0.21(\frac{d_0}{D})^{1/2}(\rho_s - \rho)gD/\rho, \ D < 0.5mm$$

$$U_t^2 = 0.46\pi(\frac{d_0}{D})^{1/4}(\rho_s - \rho)gD/\rho, \ D \geq 0.5mm$$

Bottom orbital velocity; U_m

$$U_t \ < \ U_m \ \leq \ \sqrt{0.112gd_0}$$

Wave period; T

$$\pi\sqrt{8.9d_0/g} \ \leq \ T \ < \pi d_0/U_t$$

Maximum possible deep water wavelength; $L_{t,\infty}$

$$L_{t,\infty} = (\pi g d_0^2)/(2U_t^2)$$

Wavelength; L

$$L_{max,min} \ = \ (L_{t,\infty})\sqrt{1 \pm \sqrt{1 - 80.4 \cdot U_t^4/(g^2 d_0^2)}}$$

Water depth; h

$$h < (l_{\max}/2\pi) \ arcosh \ (0.142L_{\max}/d_0)$$

Table A-1: Wave Calculations

Station Number/ Strati-graphic unit	Grain Size D (mm)	Wavelength λ (cm)	Orbital Diameter d_0 (m)	Threshold Velocity U_t (cm/sec)	Bottom Orbital Velocity (maximum) U_m (cm/sec)
CH-103b-84;					
Q3	0.199	3.0	0.04615	13.47	22.51
	0.199	4.0	0.06154	13.96	25.99
CH-108-84;					
Q3	0.0835	4.5	0.06923	10.23	27.56
	0.0835	3.5	0.05385	9.915	24.31
CH-274-85;					
Q2	0.840	120	1.846	36.68	142.34

Lower Wave Period T (sec)	Upper Wave Period T (sec)	Maximum Deep Water Wavelength $L_{t,\infty}$ (m)	Wavelength L_{max} (m)	L_{min} (m)	Maximum Water Depth h (m)
0.643	1.07	1.804	0.330	1.774	0.6724
0.748	1.38	2.990	0.440	2.960	1.280
0.788	2.12	7.060	0.489	7.040	3.760
0.695	1.71	4.540	0.381	4.520	2.280
4.070	15.81	389.75	12.93	389.53	253.72

Appendix B. Measured Sections

Key to Sections

Vertical axis: Thickness in meters

Horizontal axis: Grain size

G	Gravel
S	Sand
M	Mud

Hcs Hummocky cross stratification

 Covered Interval

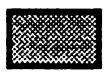 Mudstone

 Fine-grained sandstone/siltstone: massive to graded beds

 Rippled fine-grained sandstone/siltstone

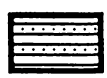 Parallel-laminated fine-grained sandstone/siltstone

 Rippled and parallel-laminated sandstone

 Parallel-laminated to horizontally stratified sandstone

 Hummocky cross-stratified sandstone

 Trough cross-bedded/ -laminated sandstone

Tabular-planar to -tangential cross-bedded sandstone

Compound tabular-tangential cross-bedded sandstone

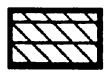

Compound tabular-planar cross-bedded sandstone

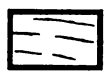

Reactivation surfaces in cross-bedded sandstones

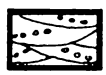

Trough cross-bedded pebbly sandstone

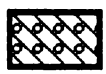

Pebbly, tabular-planar to -tangential cross-bedded sandstone

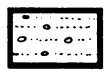

Horizontally stratified granule sandstone

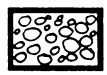

Massive conglomerate

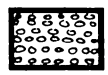

Stratified conglomerate

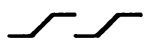

Fault

West Needle Mountains area:

Location Map and UTM Grid Coordinates

of Measured Sections

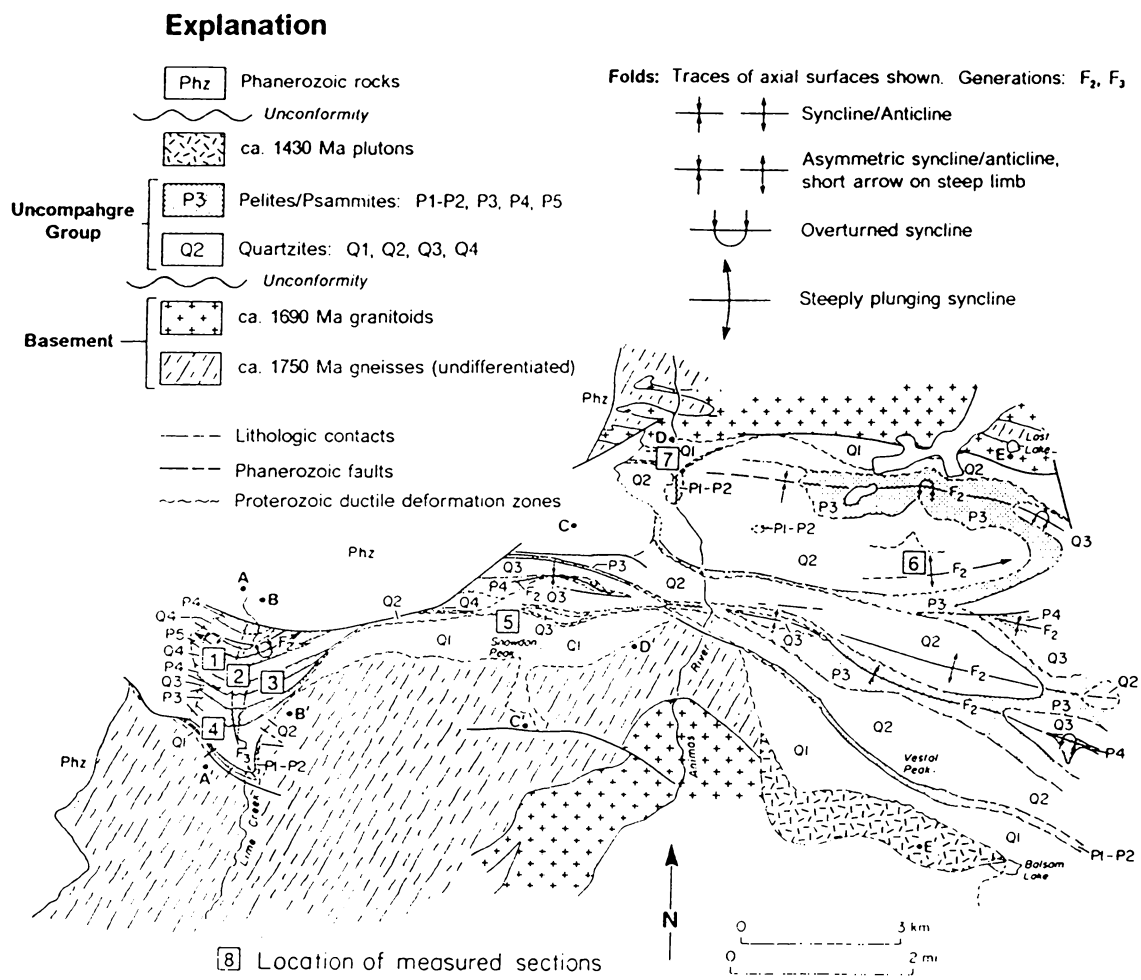

Figure B-1: Locations of measured sections in the West Needle Mountains.

Table B-1: UTM Grid Coordinates of Measured Sections.

Location	Station Number	7 1/2′ Quadrangle	UTM Grid Coordinates
1.	CH-17-84	Engineer Mountain	13SBM56837648
	CH-22-84	Engineer Mountain	13SBM56967646
2.	CH-06-84	Engineer Mountain	13SBM57357606
	CH-35-84	Engineer Mountain	13SBM57537617
3.	CH-09-84	Snowdon Peak	13SBM58087579
	CH-05-84	Snowdon Peak	13SBM57977608
	CH-83-84	Snowdon Peak	13SBM57837608
4.	CH-36-84	Engineer Mountain	13SBM56937526
	CH-87-84	Engineer Mountain	13SBM56567526
	CH-88-84	Engineer Mountain	13SBM57017488
5.	CH-413-86	Snowdon Peak	13SBM62067692
	CH-576-86	Snowdon Peak	13SBM62407648
6.	CH-567-86	Storm King Peak	13SBM69867820
7.	CH-150-85	Snowdon Peak	13SBM65598052

Q1 - Animas Canyon Section CH-150-85

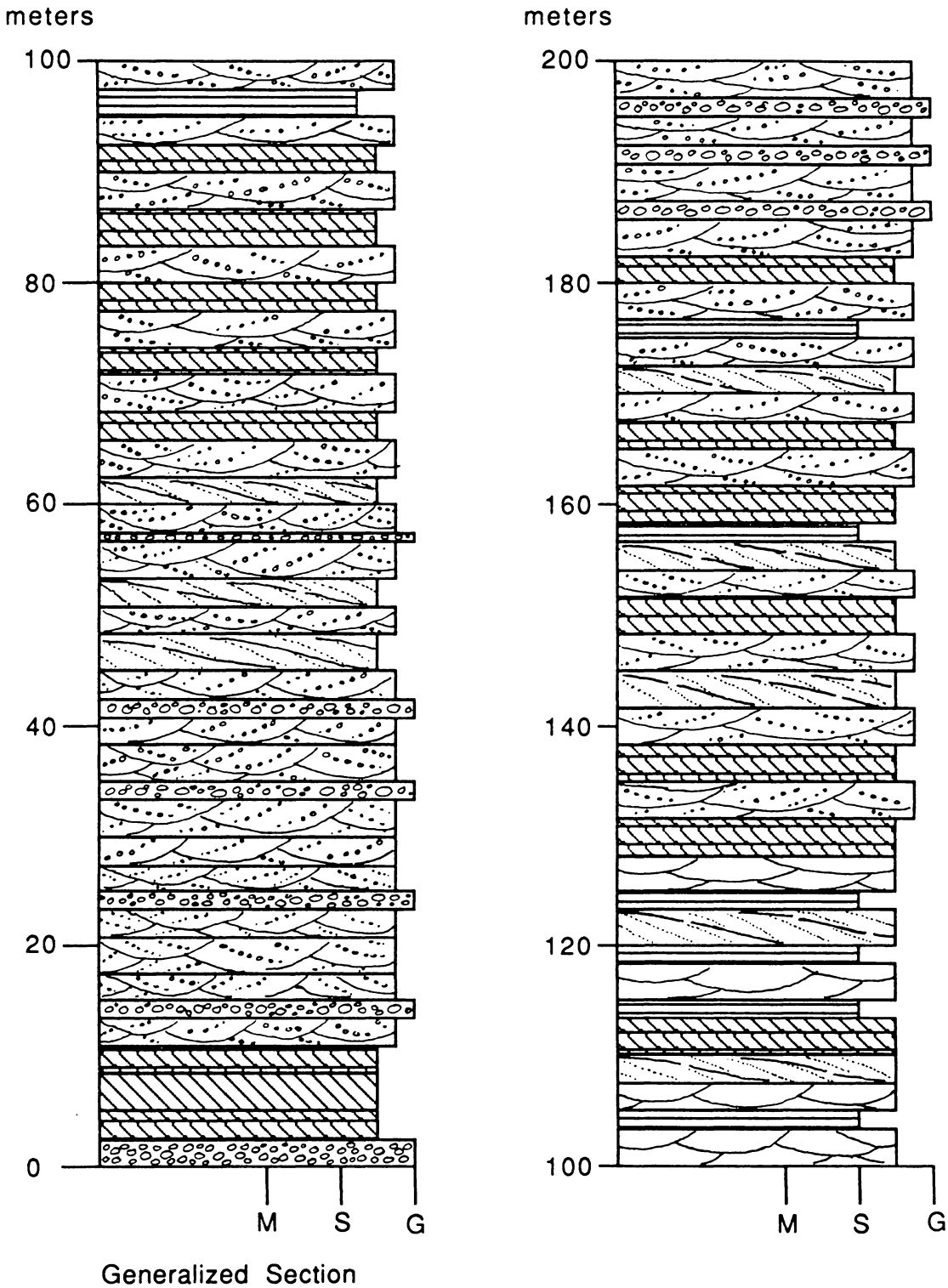

Generalized Section

Q1 - Animas Canyon Section CH-150-85

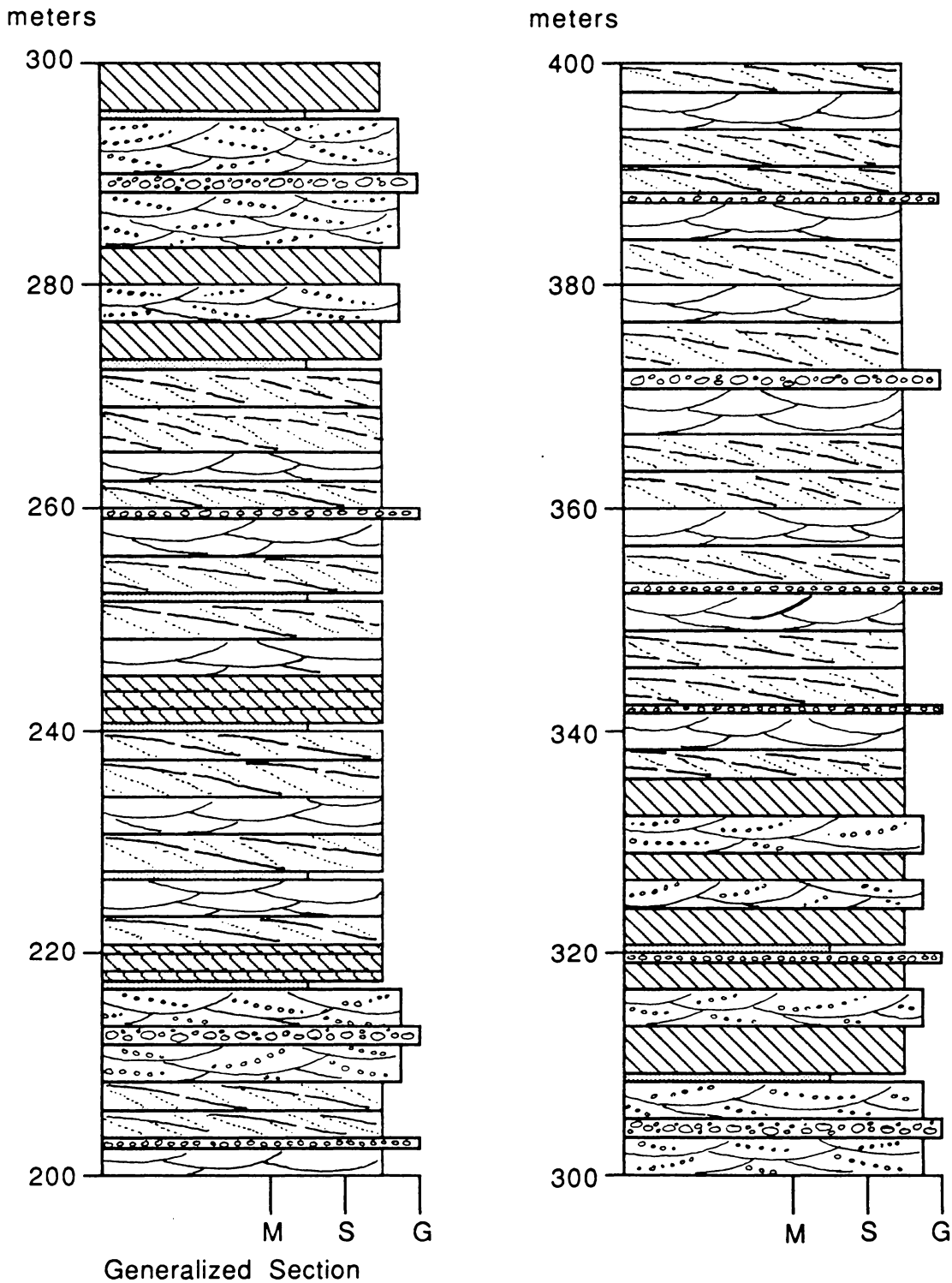

Generalized Section

Q1 - Animas Canyon Section CH-150-85

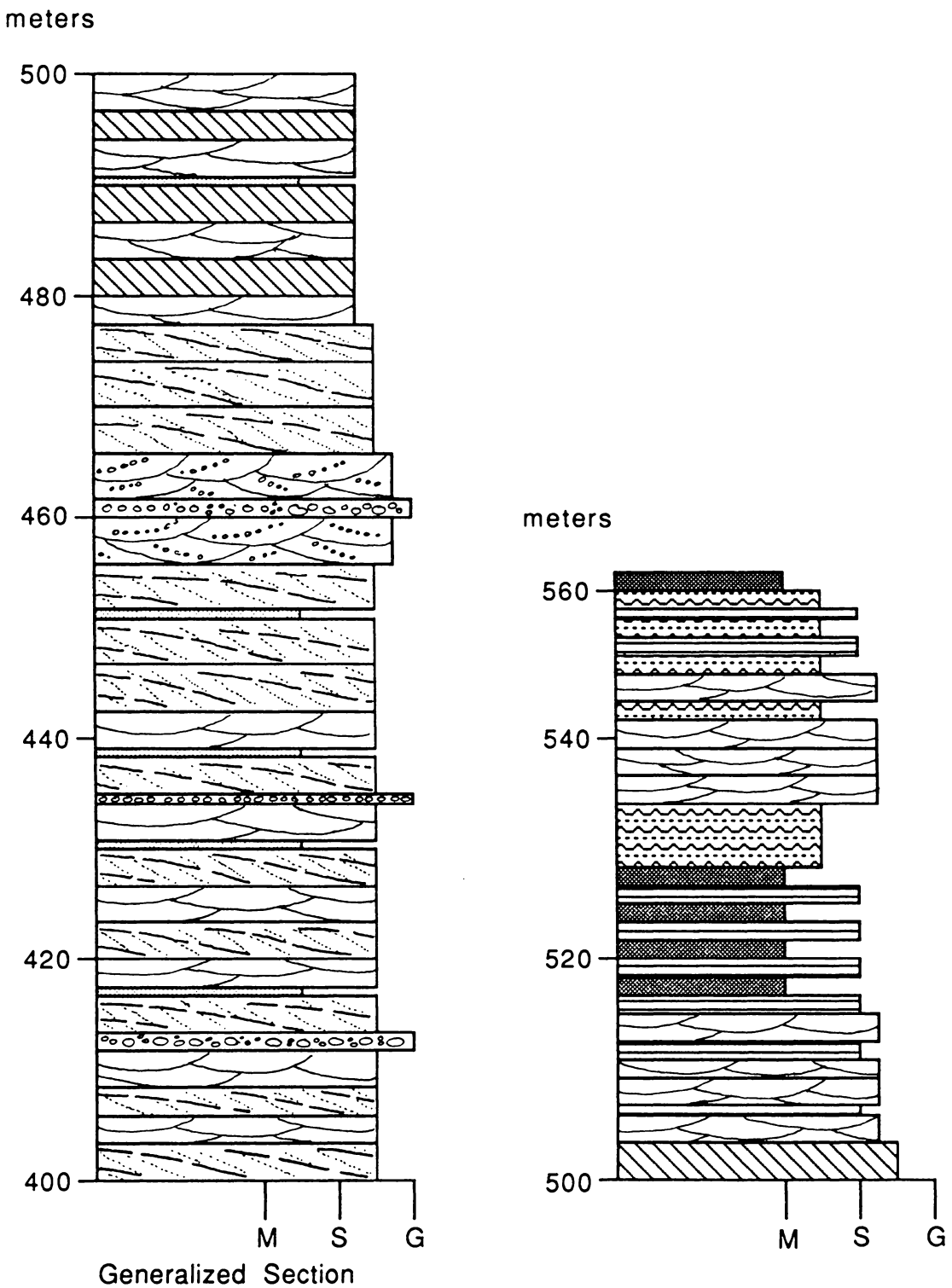

Upper Q1 - Snowdon Peak Section CH-413-86

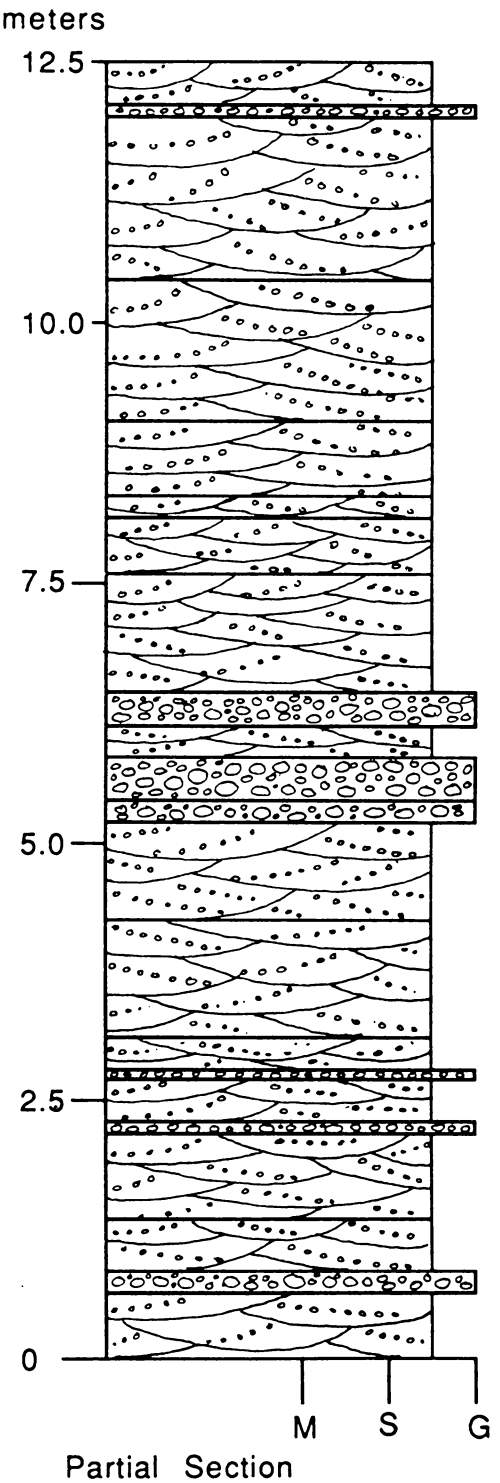

Q1 - Snowdon Peak Section CH-576-86

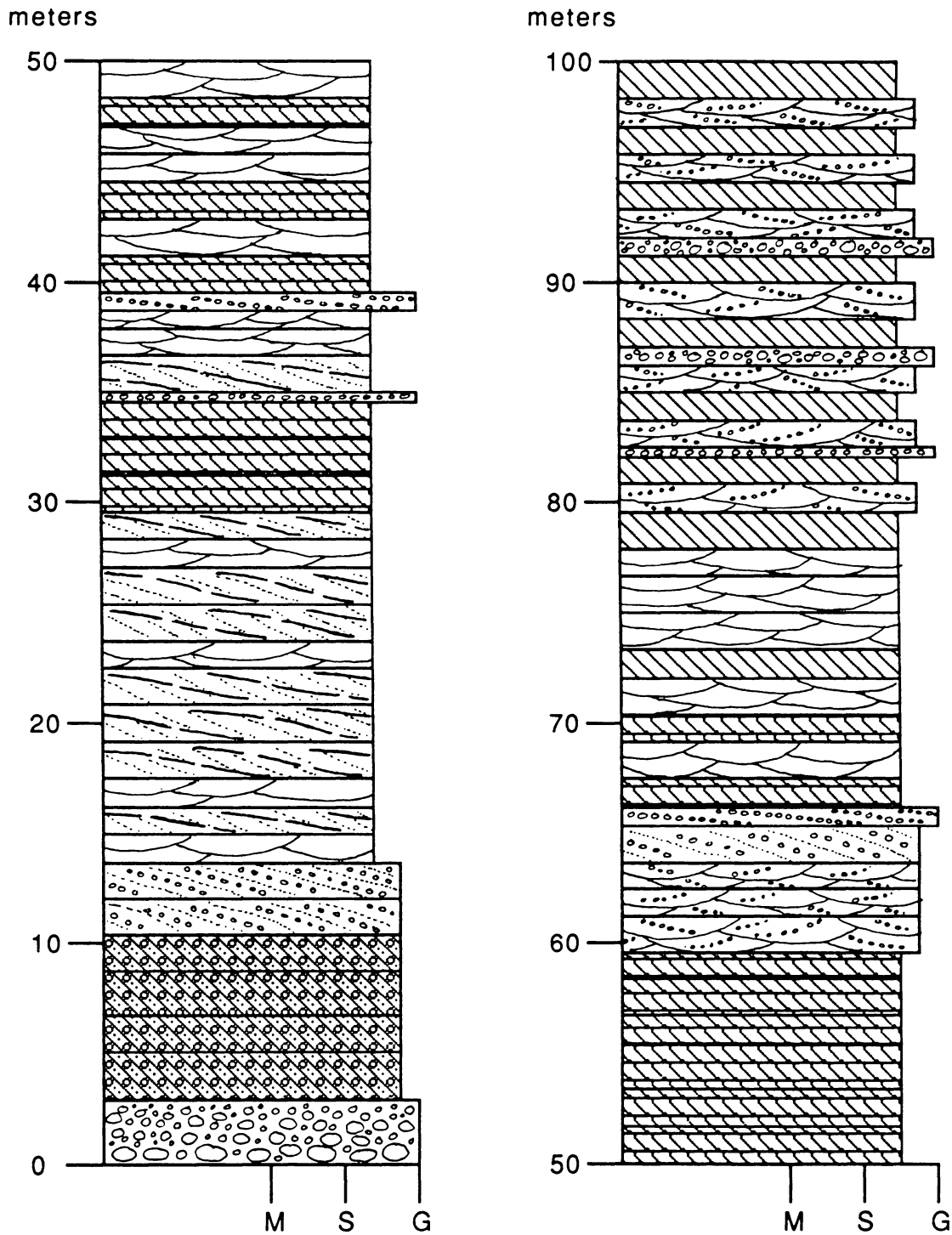

Q1 - Snowdon Peak Section CH-576-86

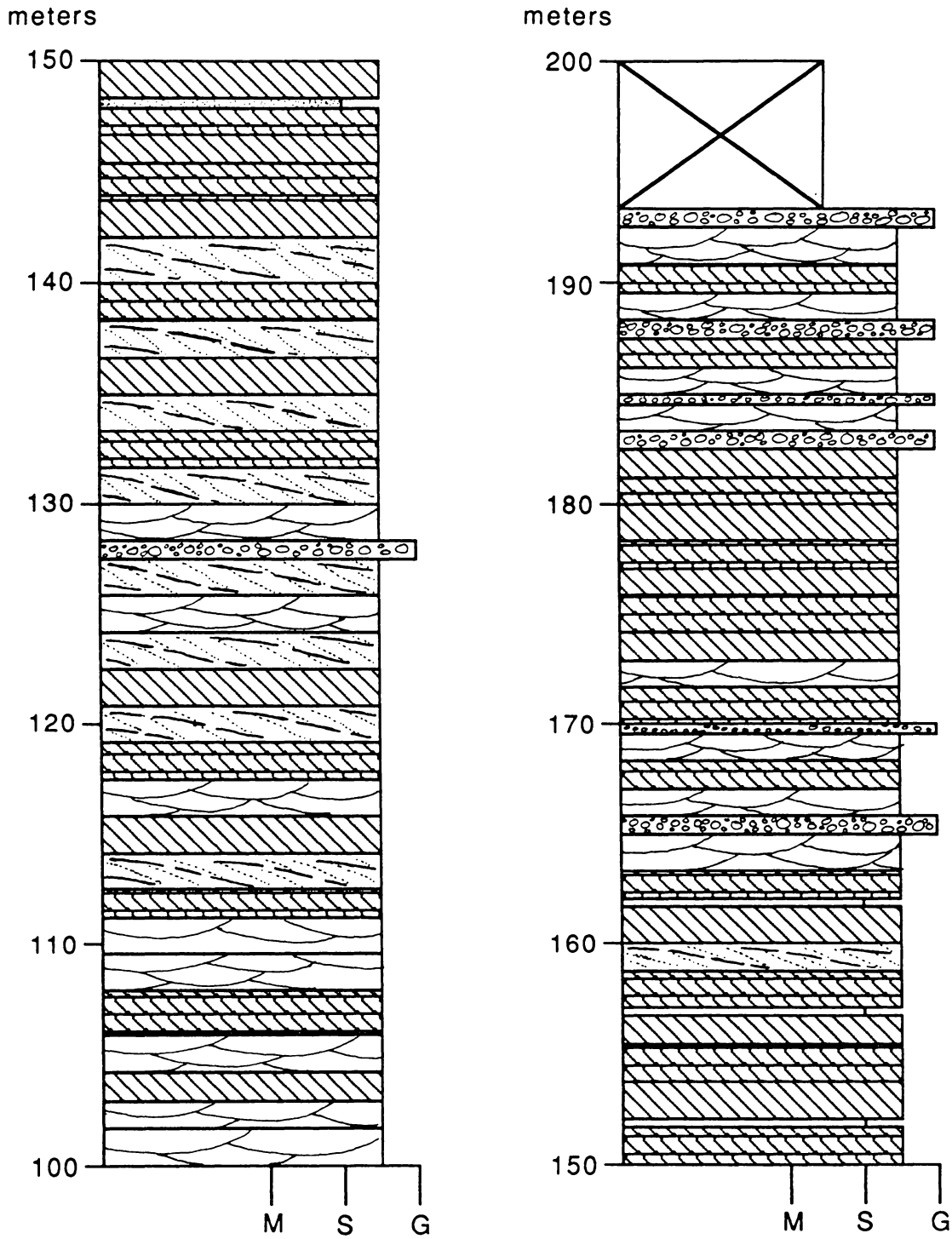

Q1 - Snowdon Peak Section CH-576-86

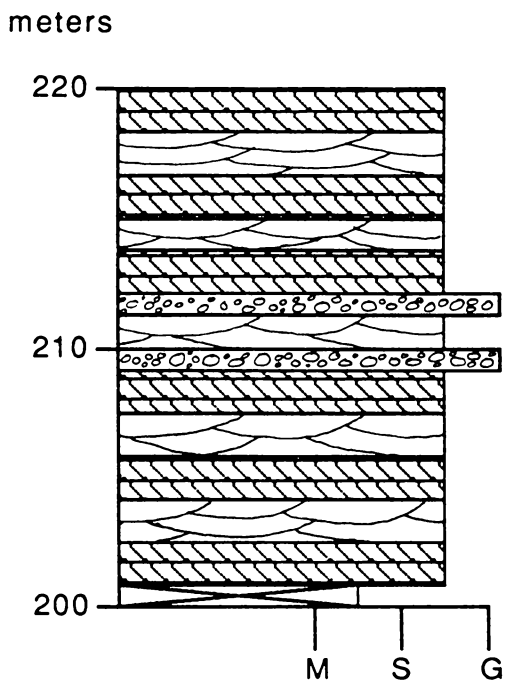

Lower Q2 - Lime Creek Section CH-87-84

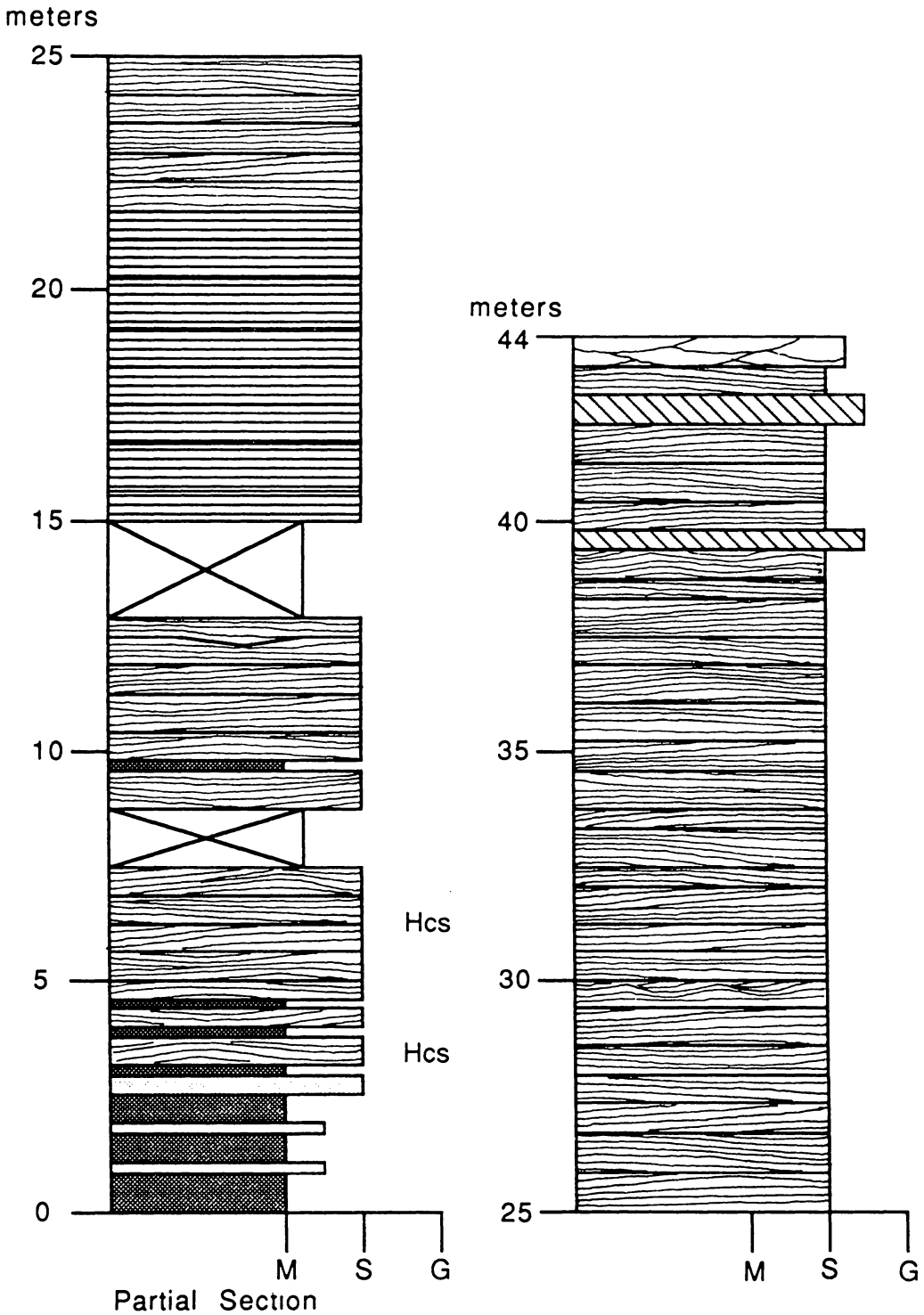

Medial Q2 - Lime Creek Section CH-88-84

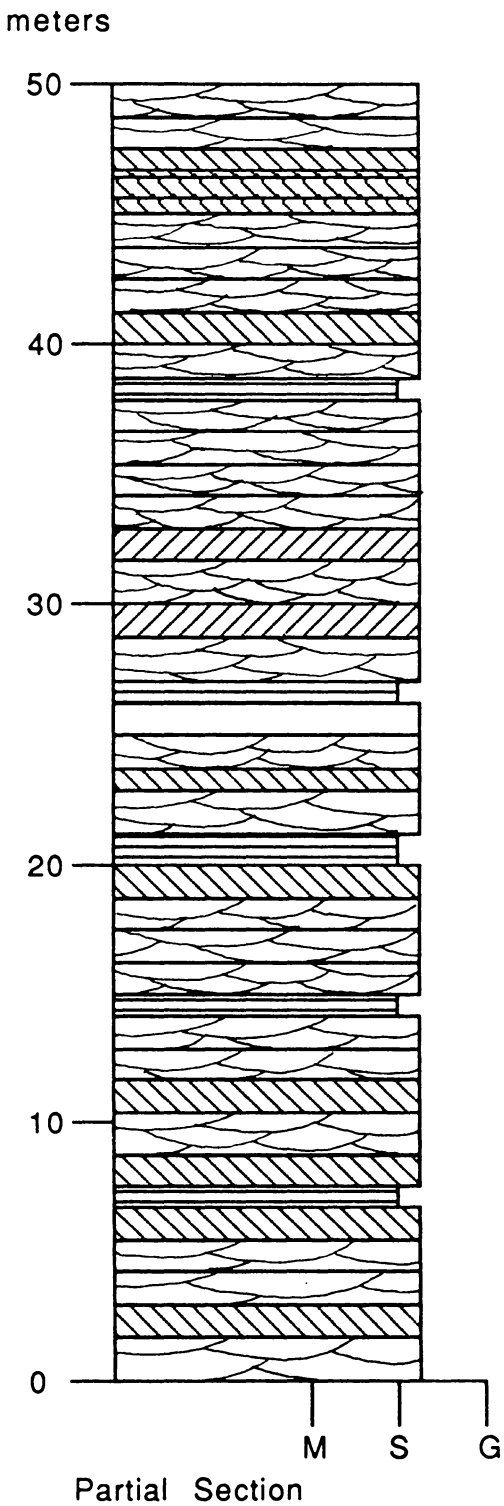

Partial Section

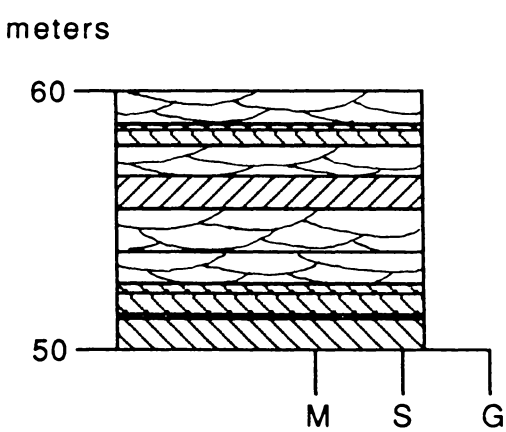

Upper Q2 - Lime Creek Section CH-36-84

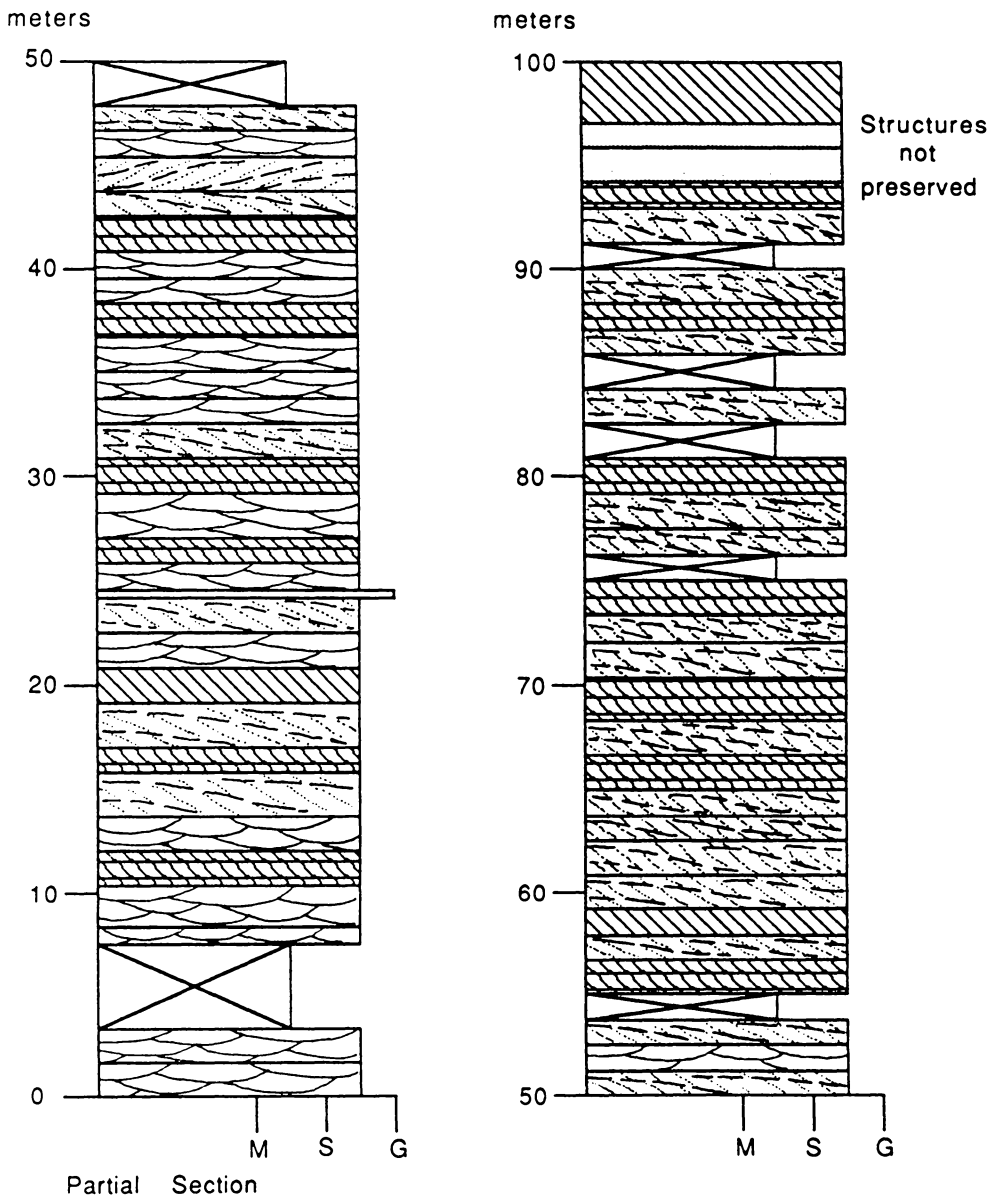

Upper Q2 - Lime Creek Section CH-36-84

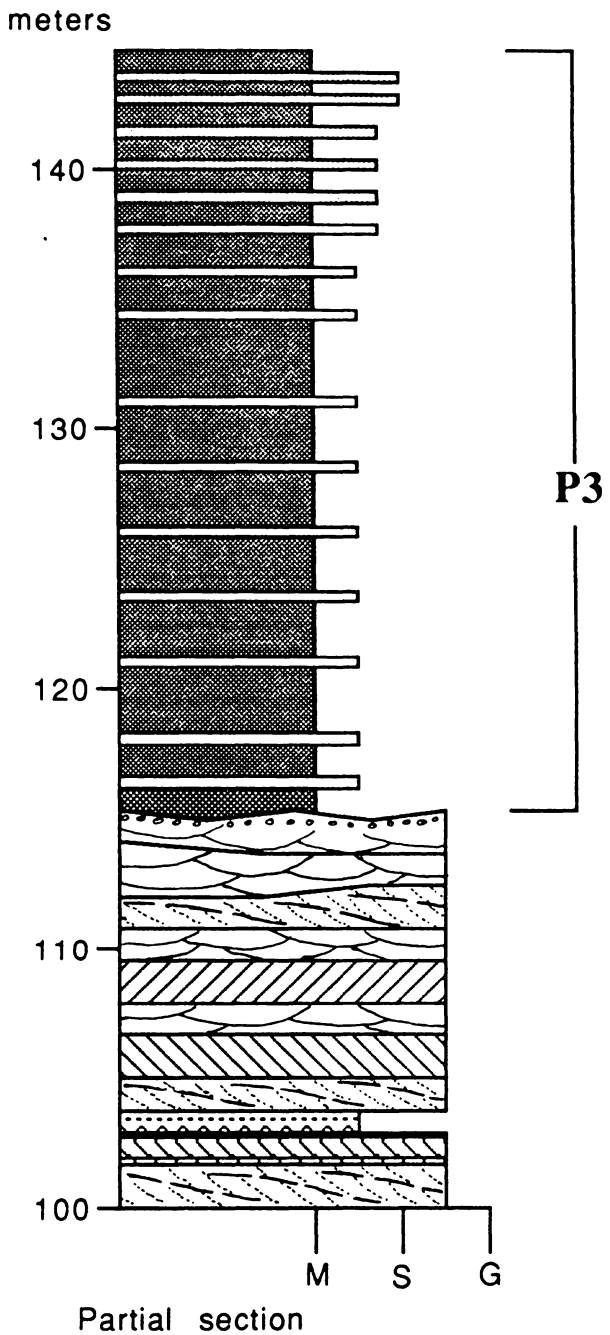

Medial Q2 - Elk Creek Section CH-567-86

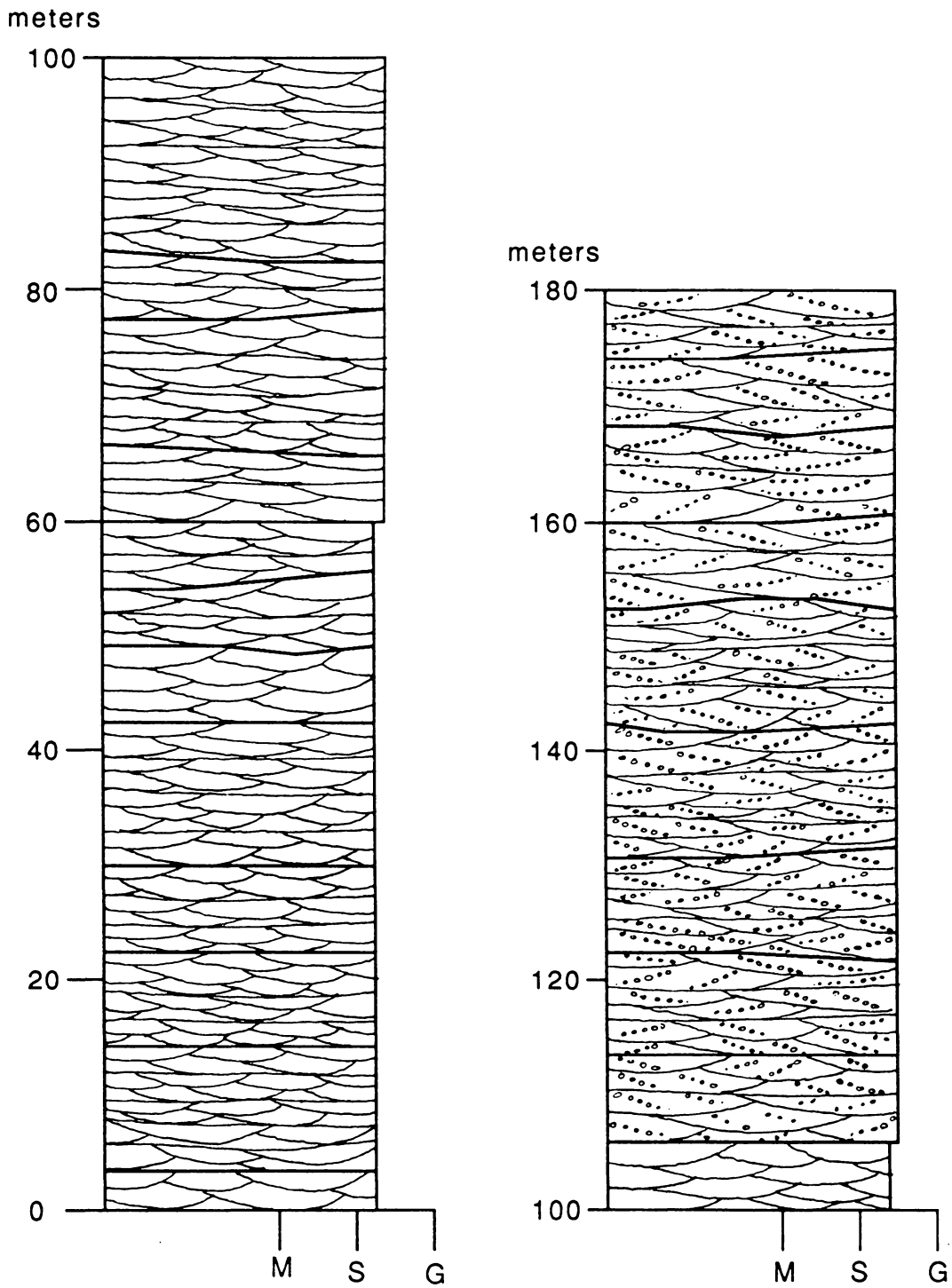

Partial Section: Base not exposed

Q3 - Three Lakes Creek Section CH-09-84

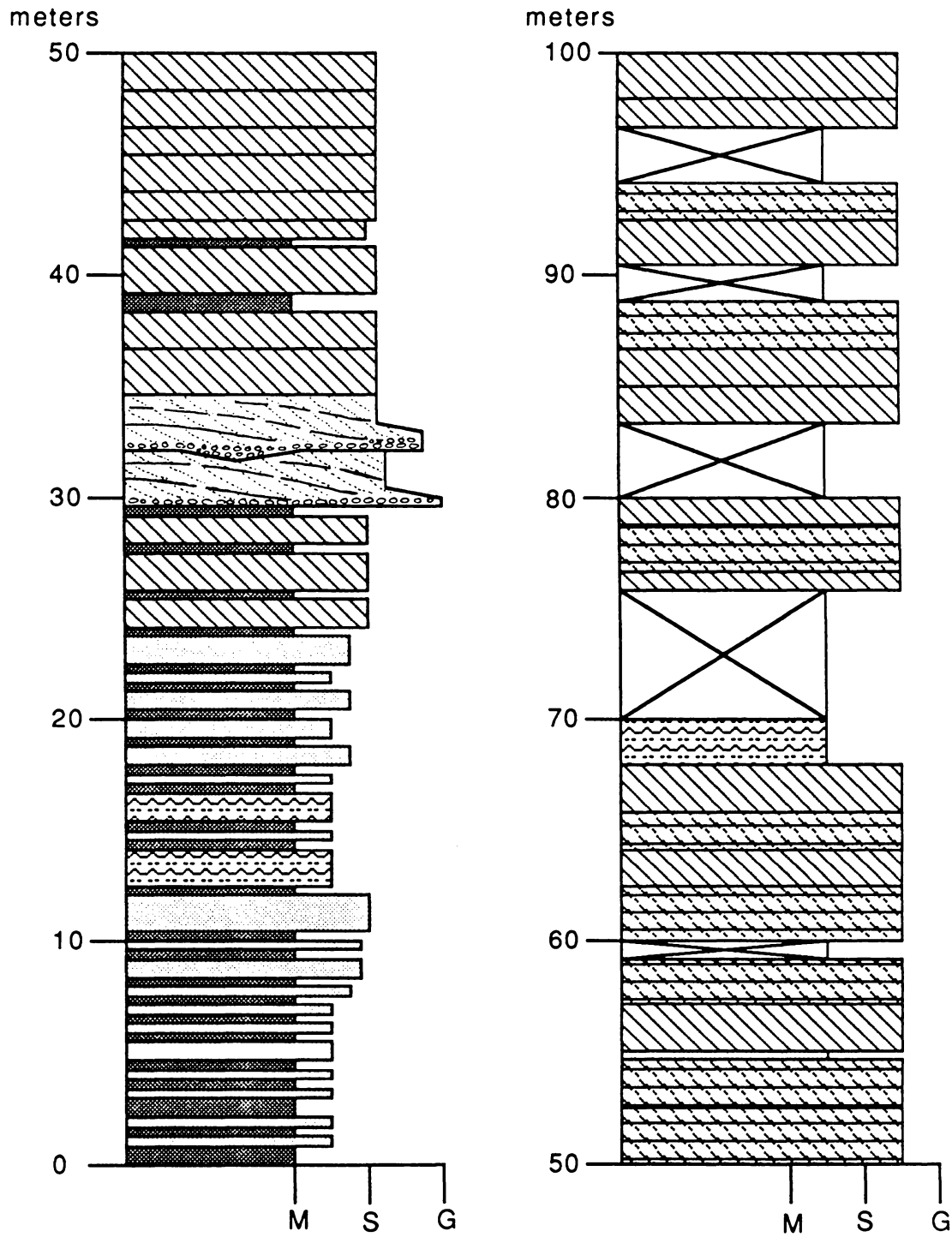

Q3 - Three Lakes Creek Section CH-09-84

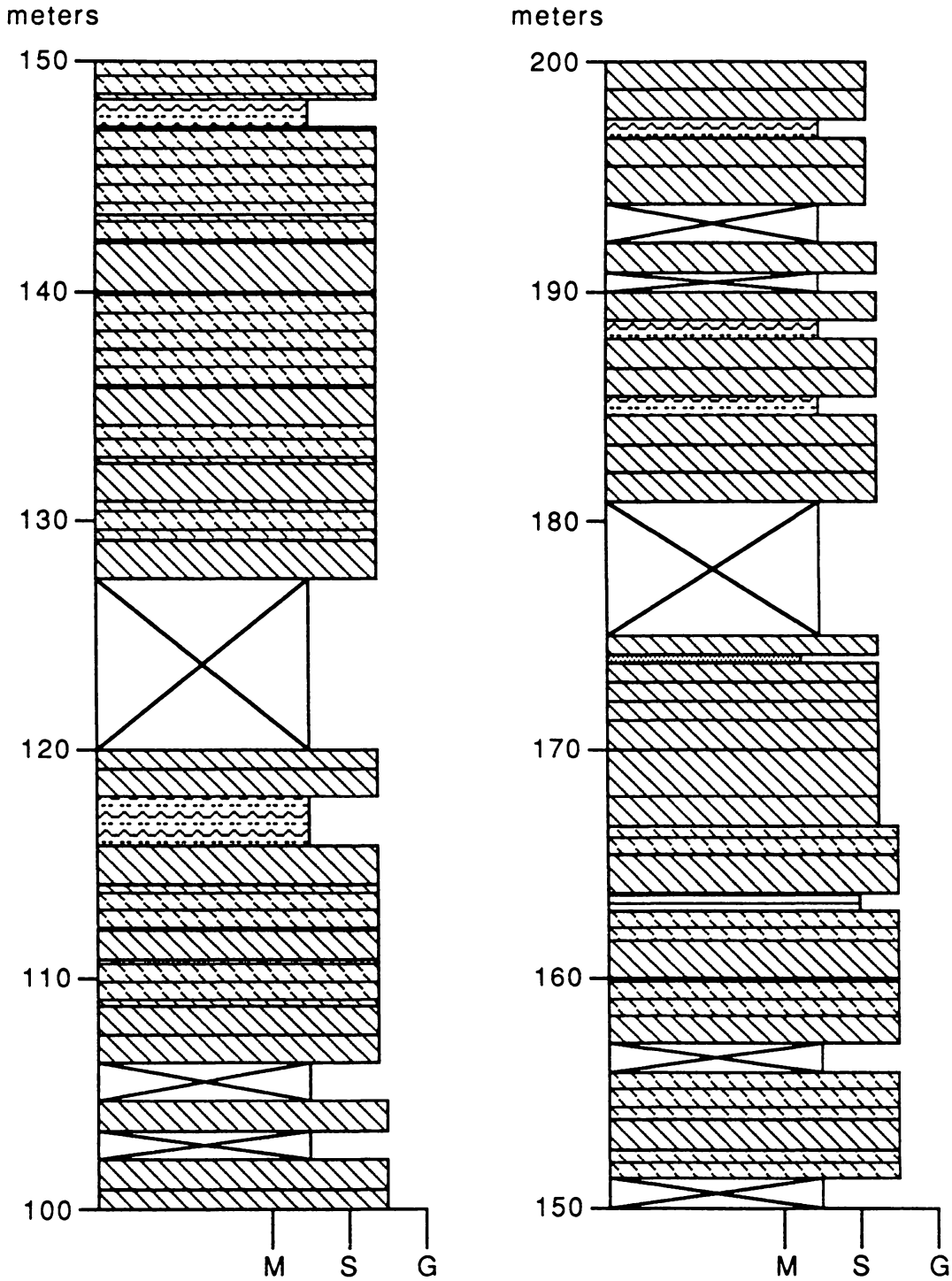

Q3 - Three Lakes Creek Section CH-09-84

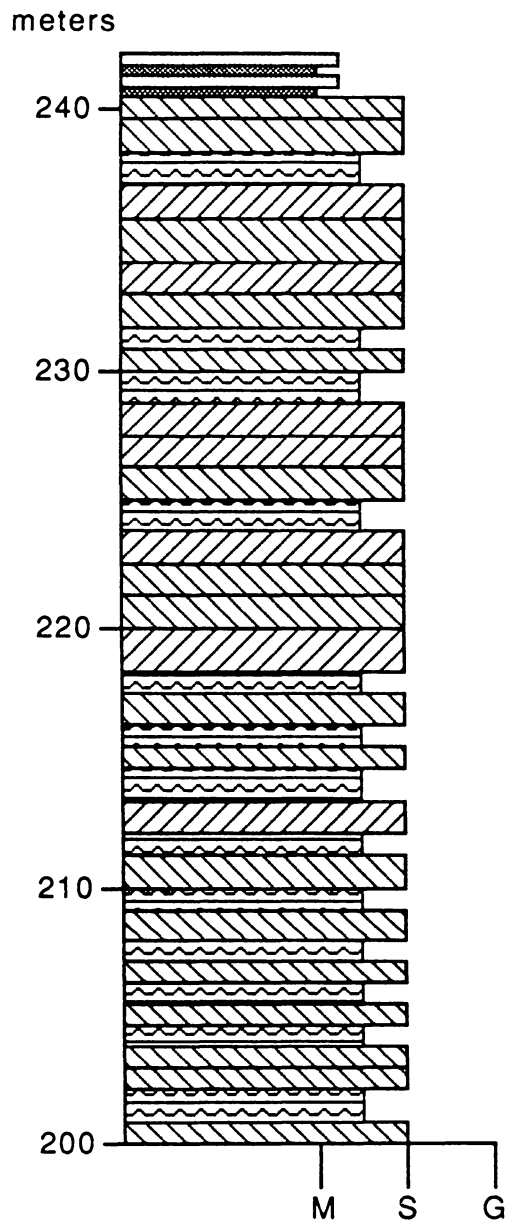

P4 - Lime Creek Section CH-5-84

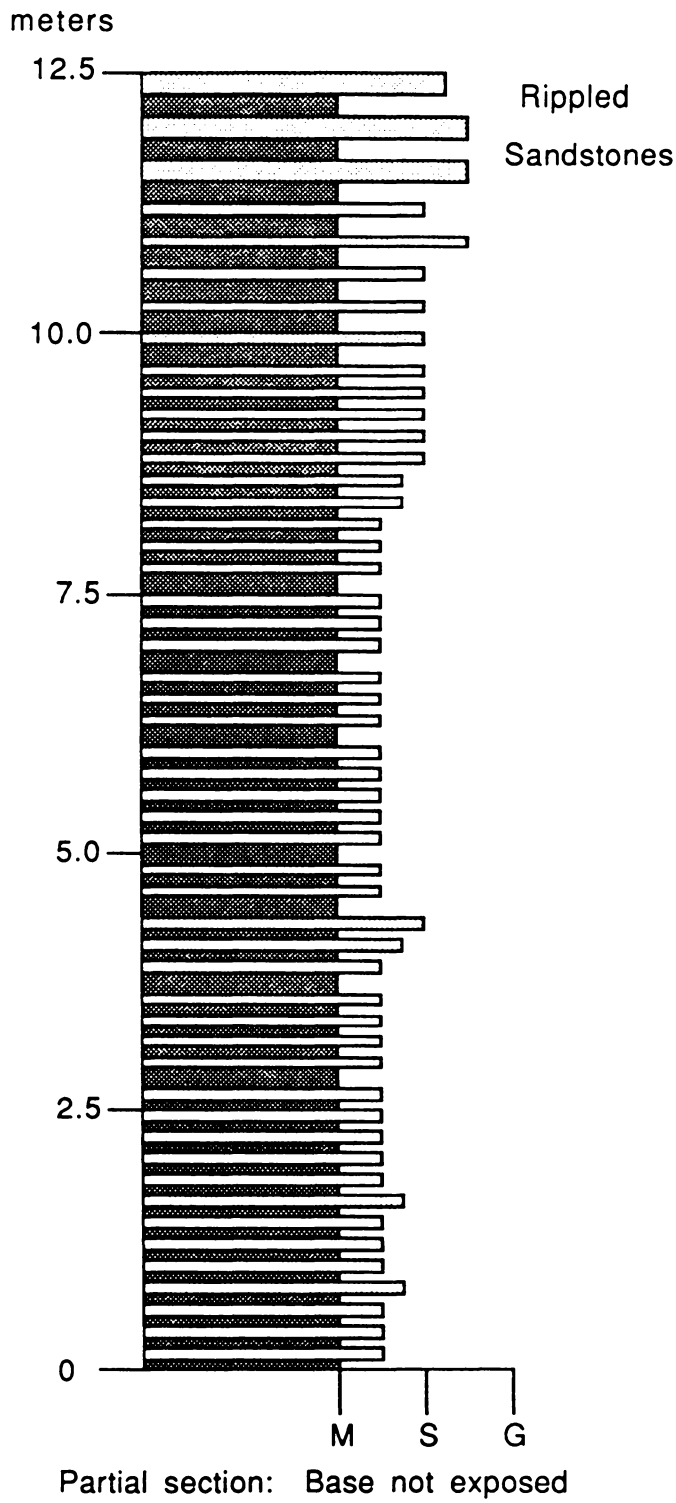

Partial section: Base not exposed

Q4 - Lime Creek Section CH-06-84

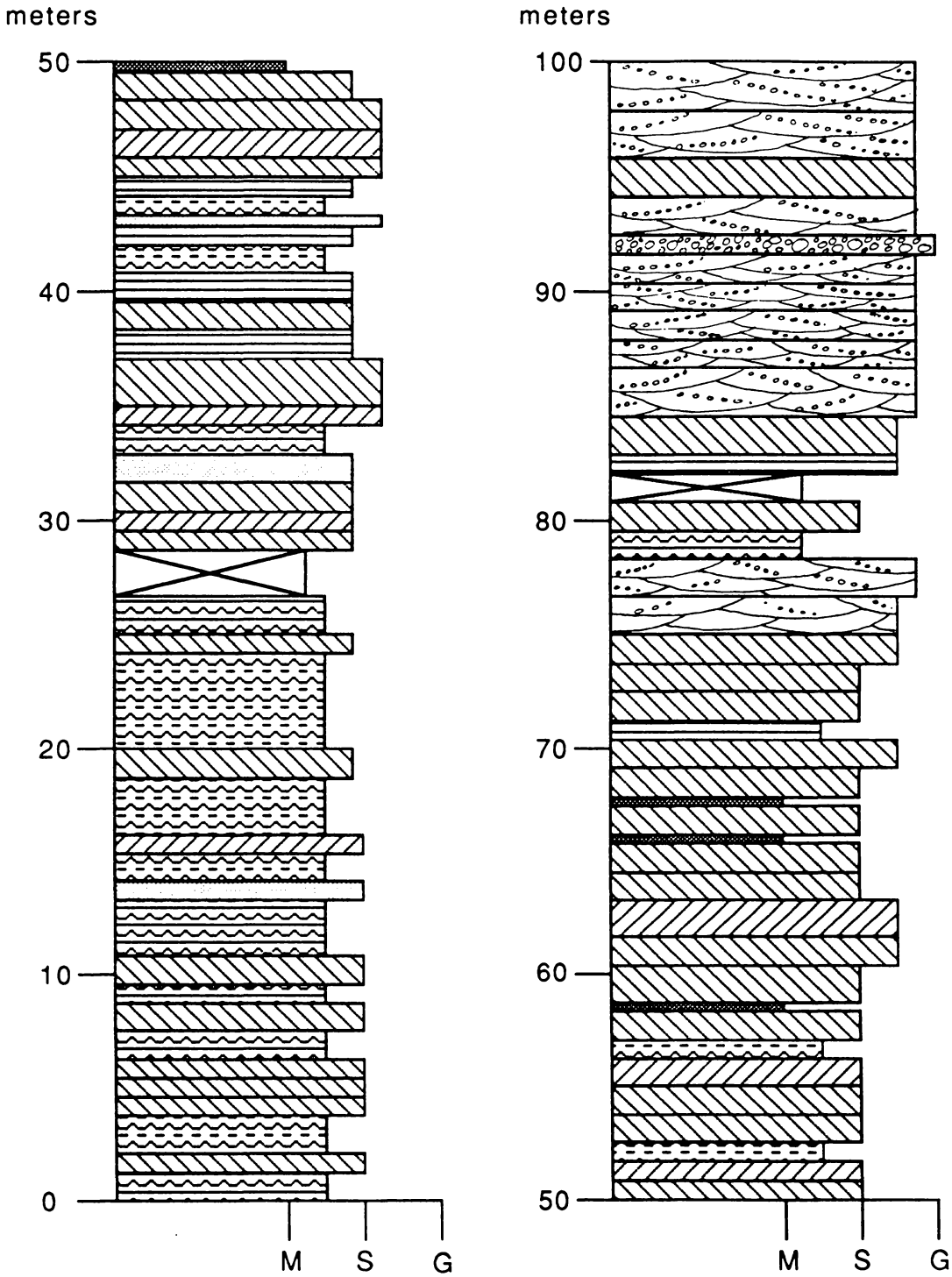

Partial Section: Base not exposed

Q4 - Lime Creek Section CH-06-84

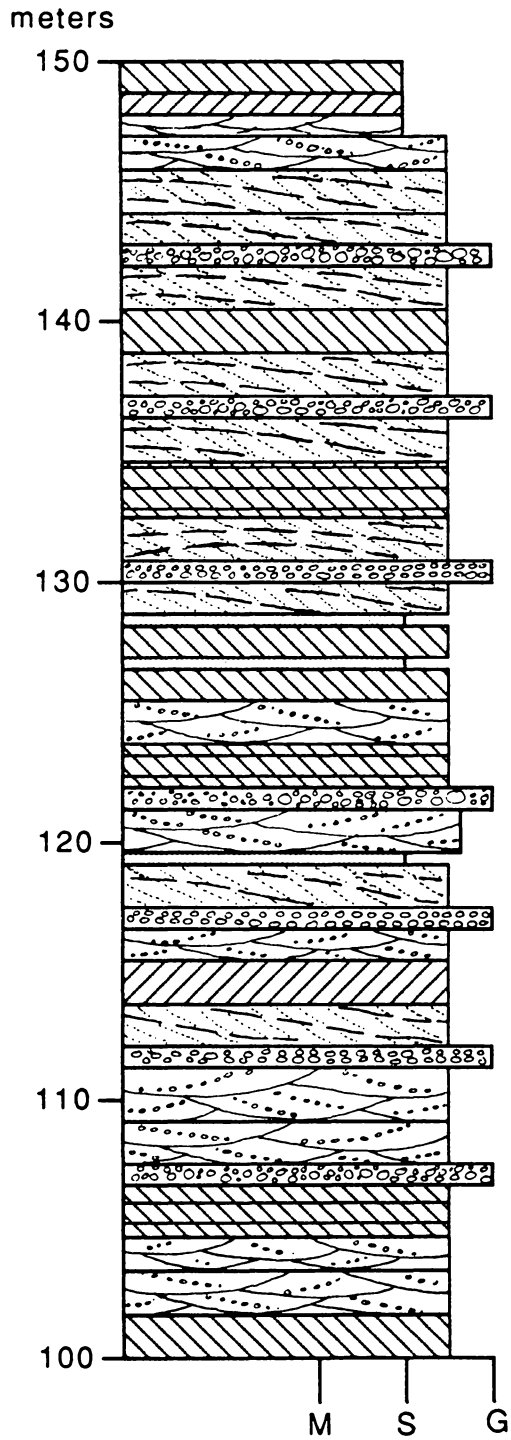

Q4 - Lime Creek Section CH-35-84

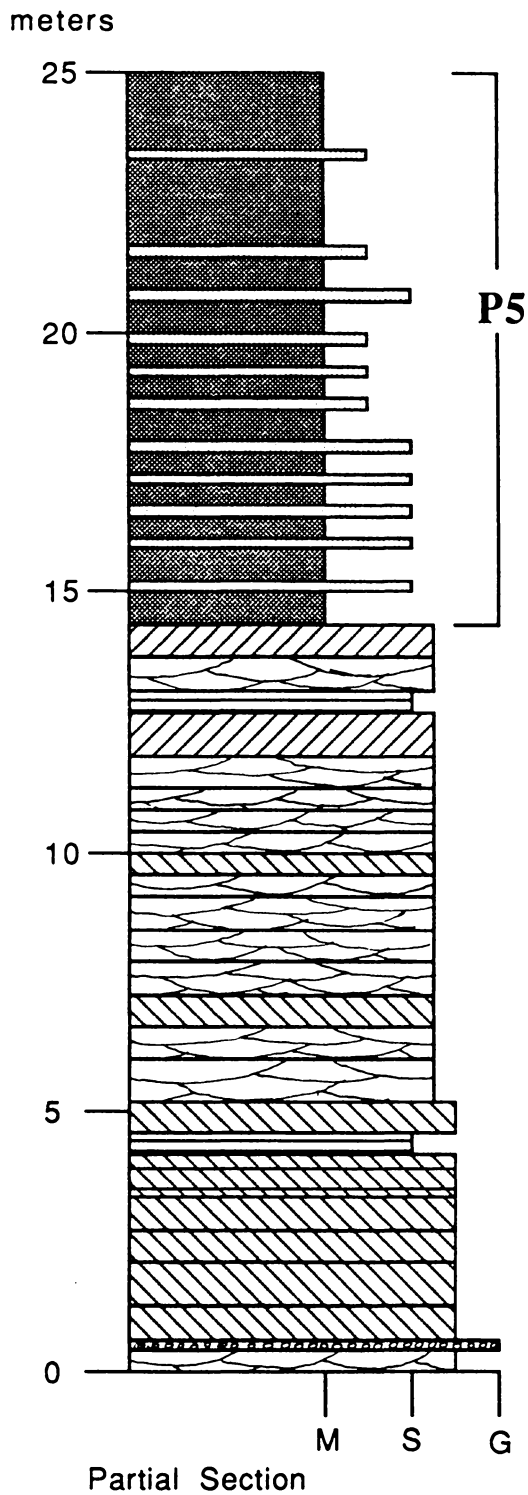

Q4 - Lime Creek Section CH-83-84

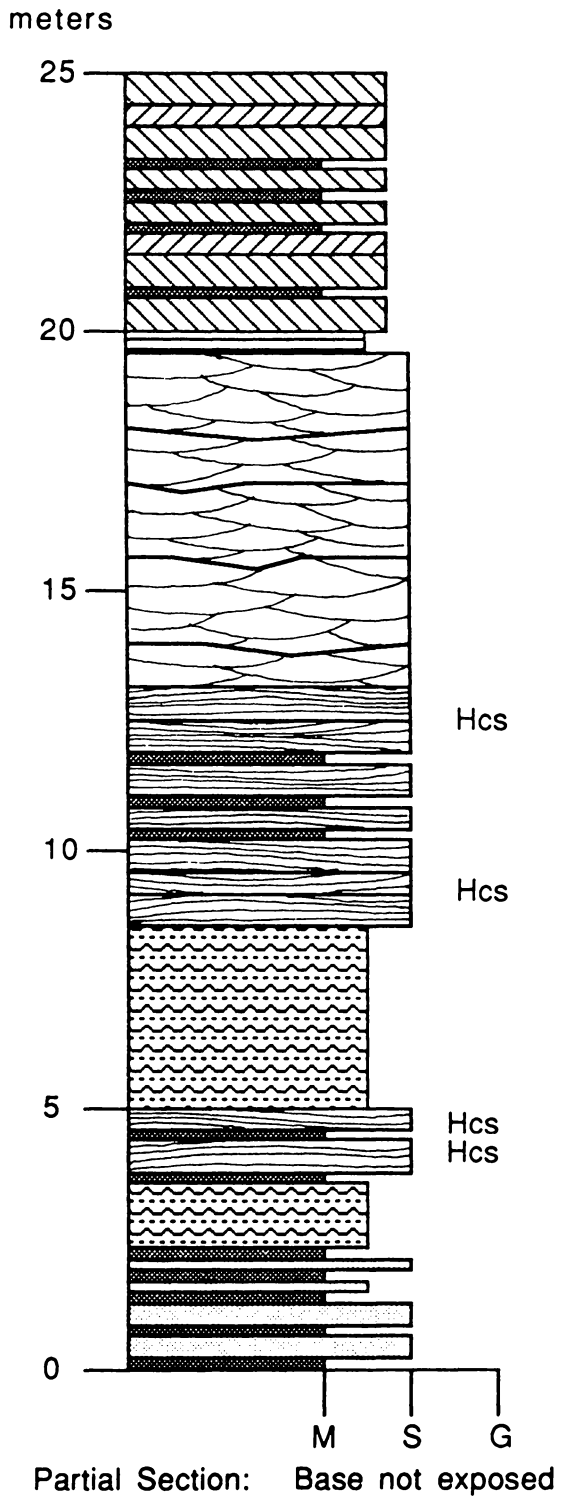

Partial Section: Base not exposed

Q4 - Coal Creek Section CH-17-84

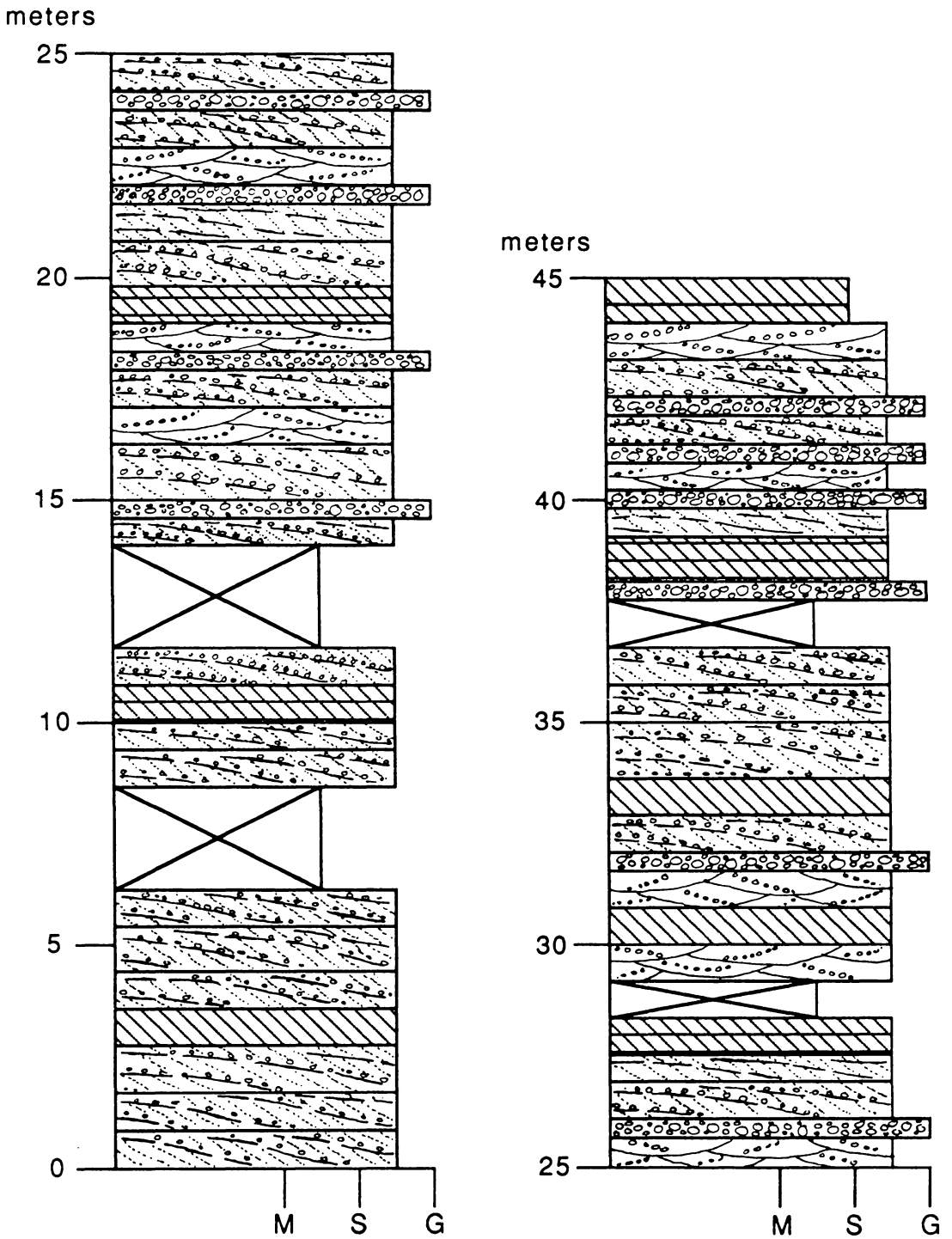

Partial Section: Base not exposed

Q4 - Coal Creek Section CH-22-84

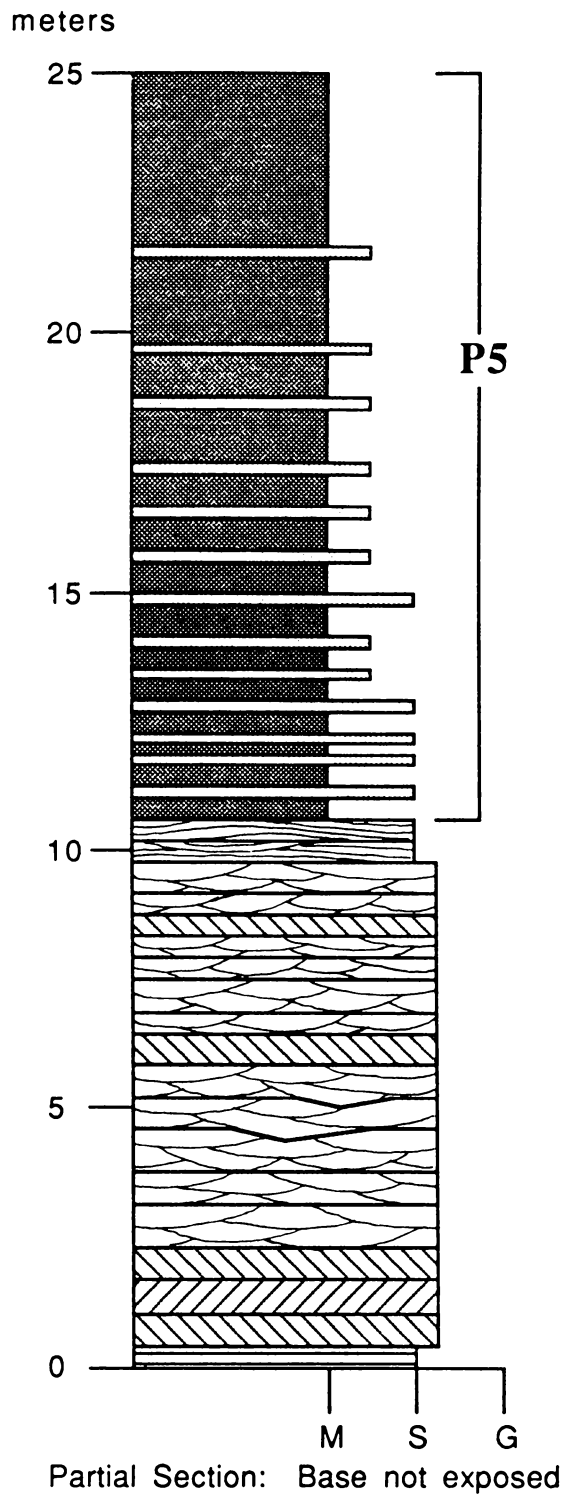

Partial Section: Base not exposed

Uncompahgre Gorge area:

Location Map and UTM Grid Coordinates

of Measured Sections

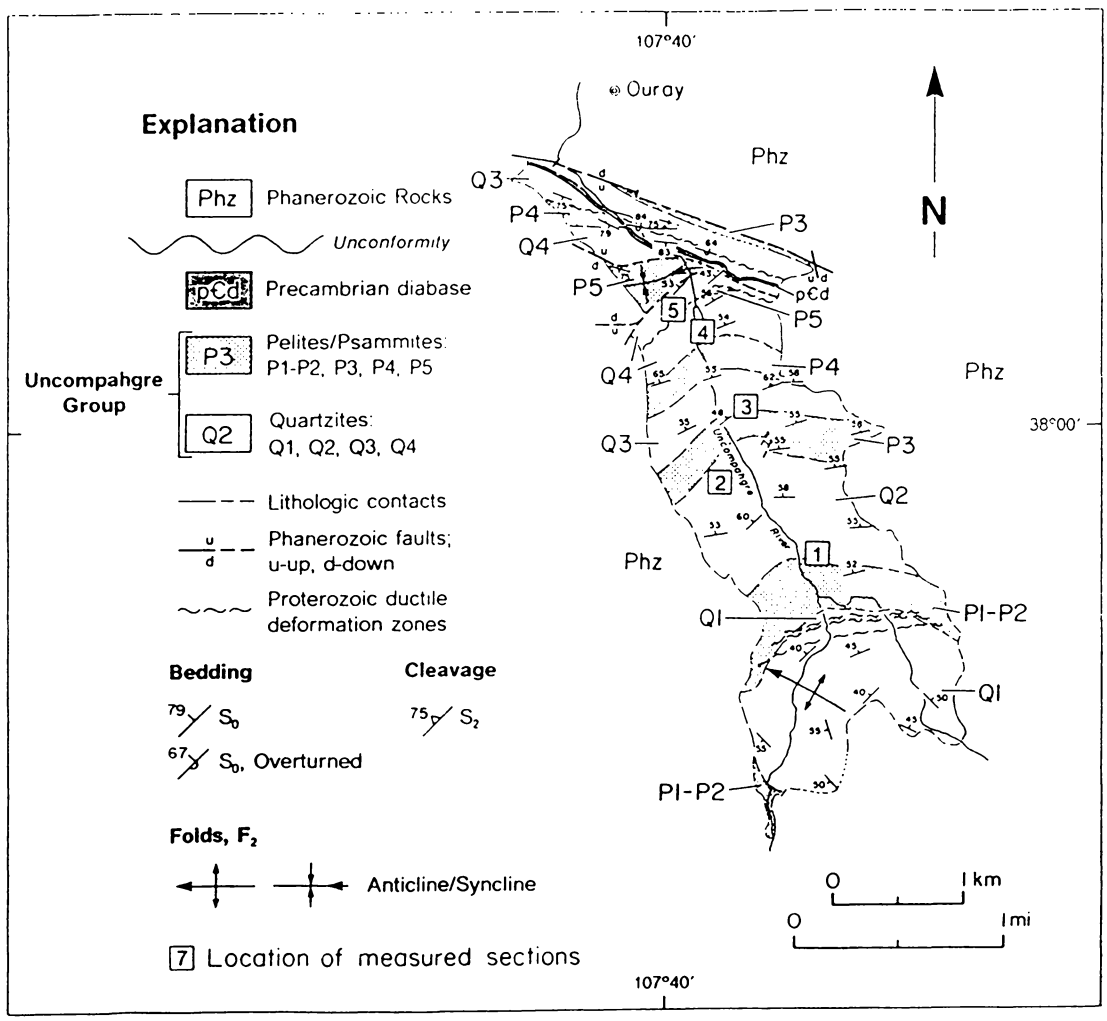

Figure B-2: Locations of measured sections in the Uncompahgre Gorge area.

Table B-2: UTM Grid Coordinates of Measured Sections.

Location	Station Number	7 1/2′ Quadrangle	UTM Grid Coordinates
1.	CH-268-85	Ironton	13SBN67460782
	CH-270-85	Ironton	13SBN67090798
2.	CH-402a-86	Ironton	13SBN66480872
	CH-402b-86	Ironton	13SBN66490878
3.	CH-109-84	Ironton	13SBN66590893
	CH-108-84	Ouray	13SBN66650919
4.	CH-91-84	Ouray	13SBN66460979
	CH-112-84	Ouray	13SBN66430982
	CH-273-85	Ouray	13SBN66210974
5.	CH-403-86	Ouray	13SBN65880989
	CH-404-86	Ouray	13SBN65860989

Upper P2 - Uncompahgre River Section CH-268-85

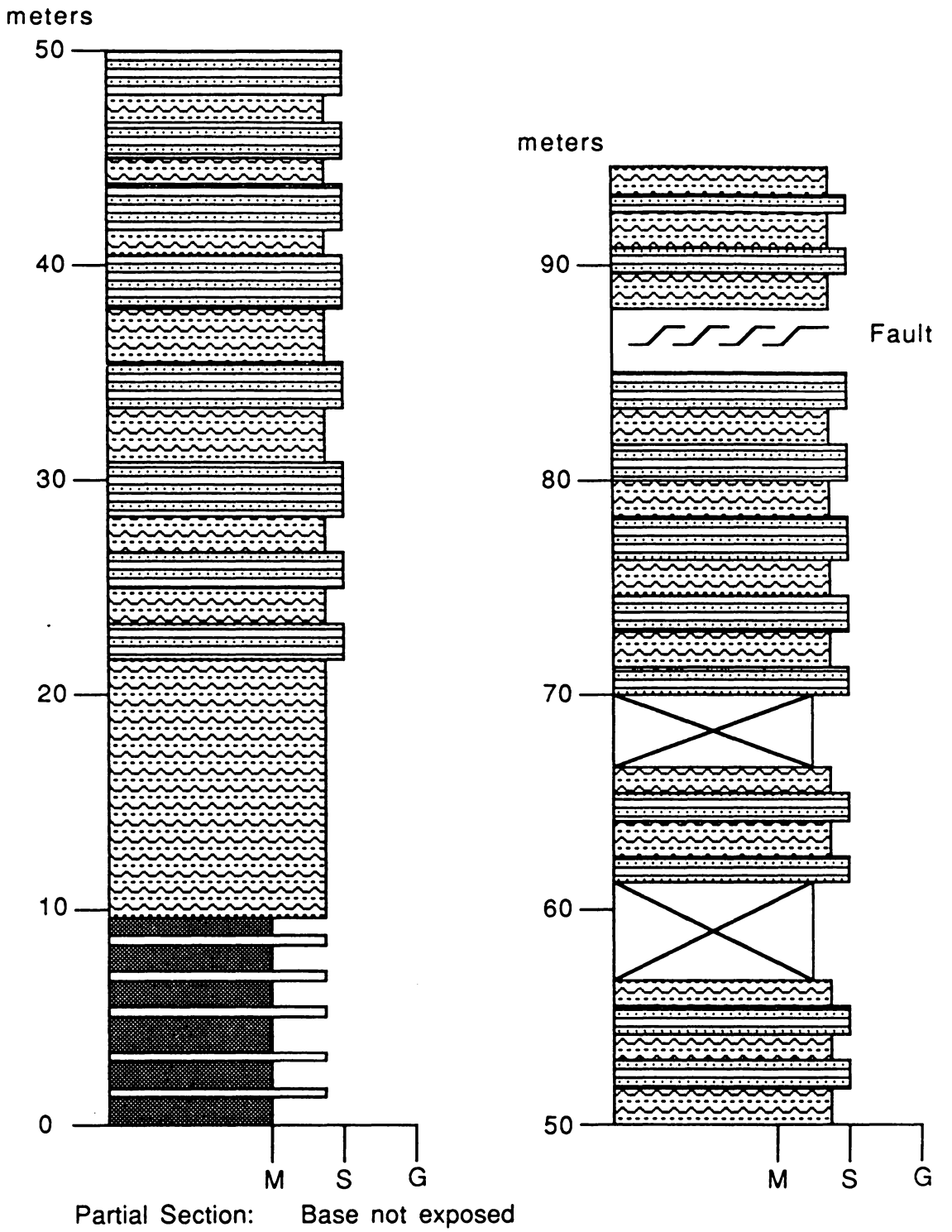

Partial Section: Base not exposed

Lower Q2 - Uncompahgre River Section CH-270-85

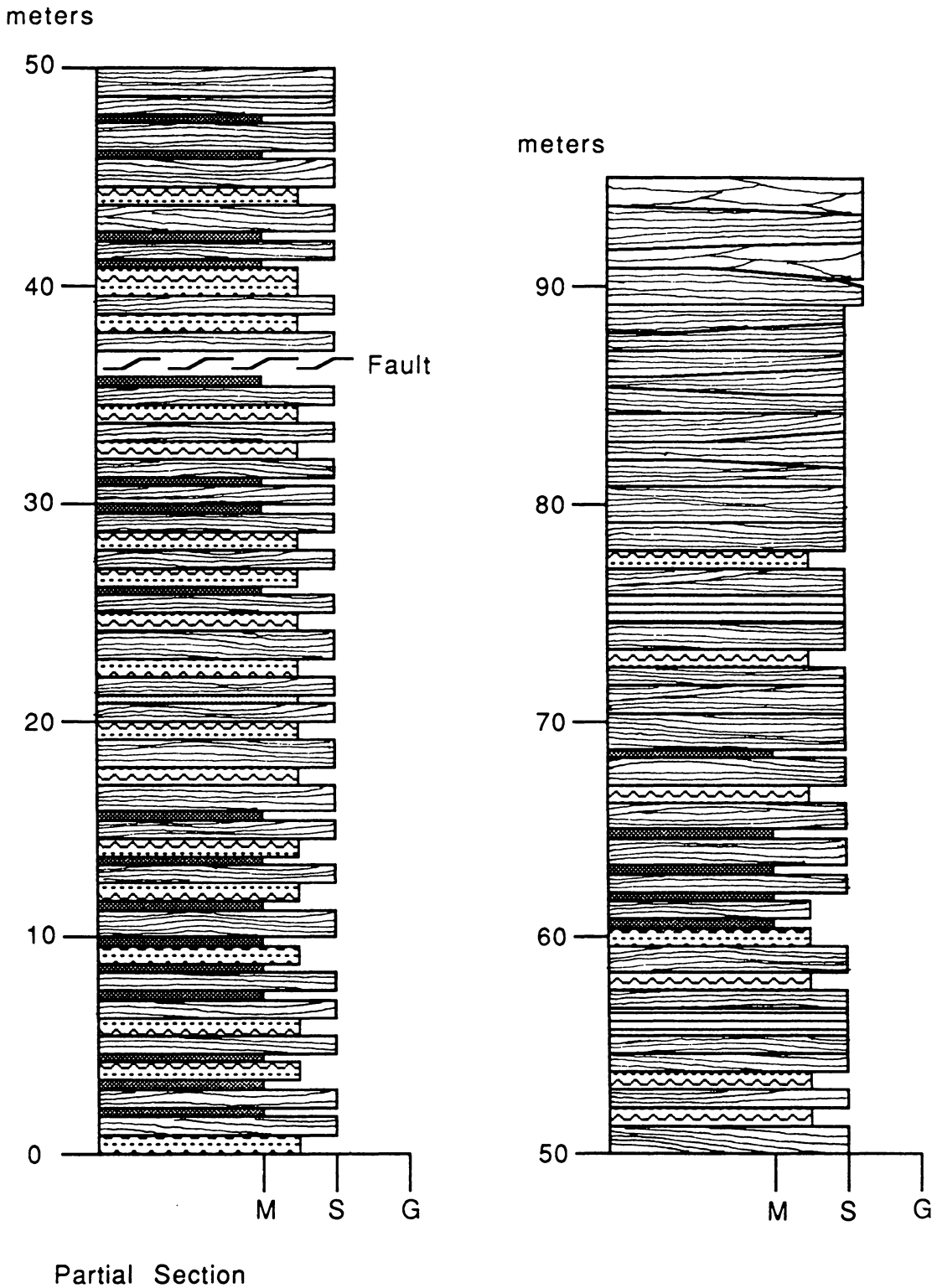

Partial Section

Upper Q2 - Uncompahgre River Section CH-402a-86

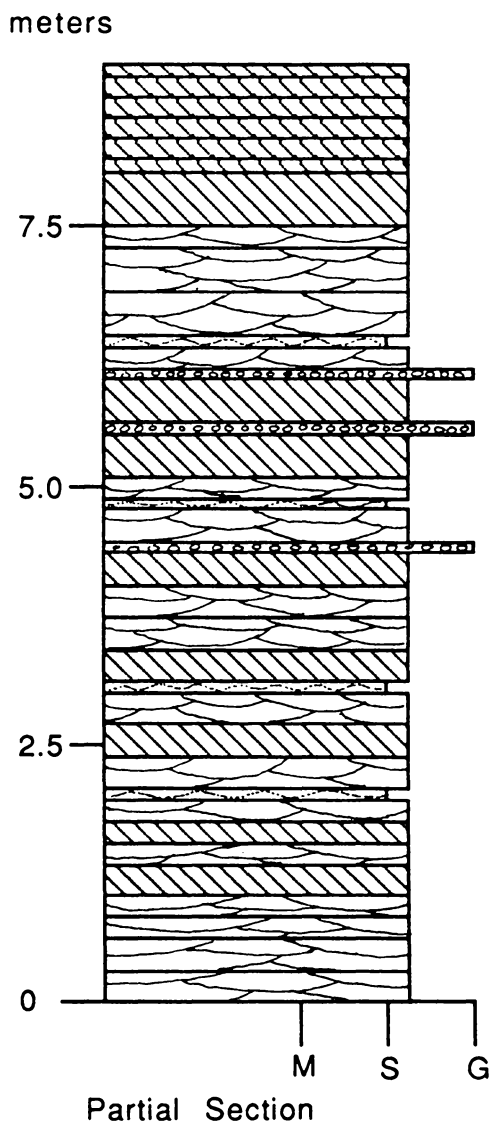

Upper Q2 - Uncompahgre River Section CH-402b-86

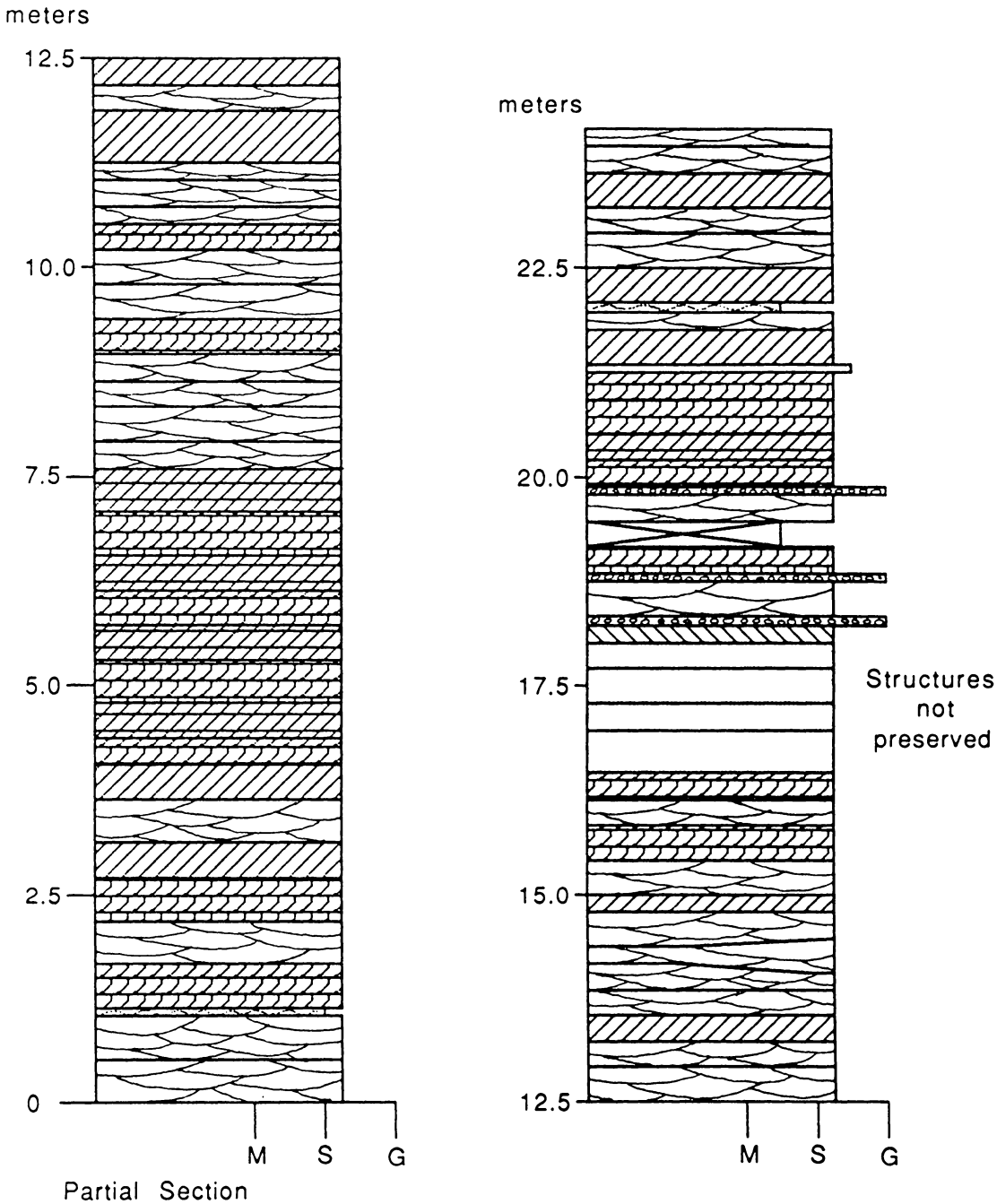

P3 - Bear Creek Section CH-109-84

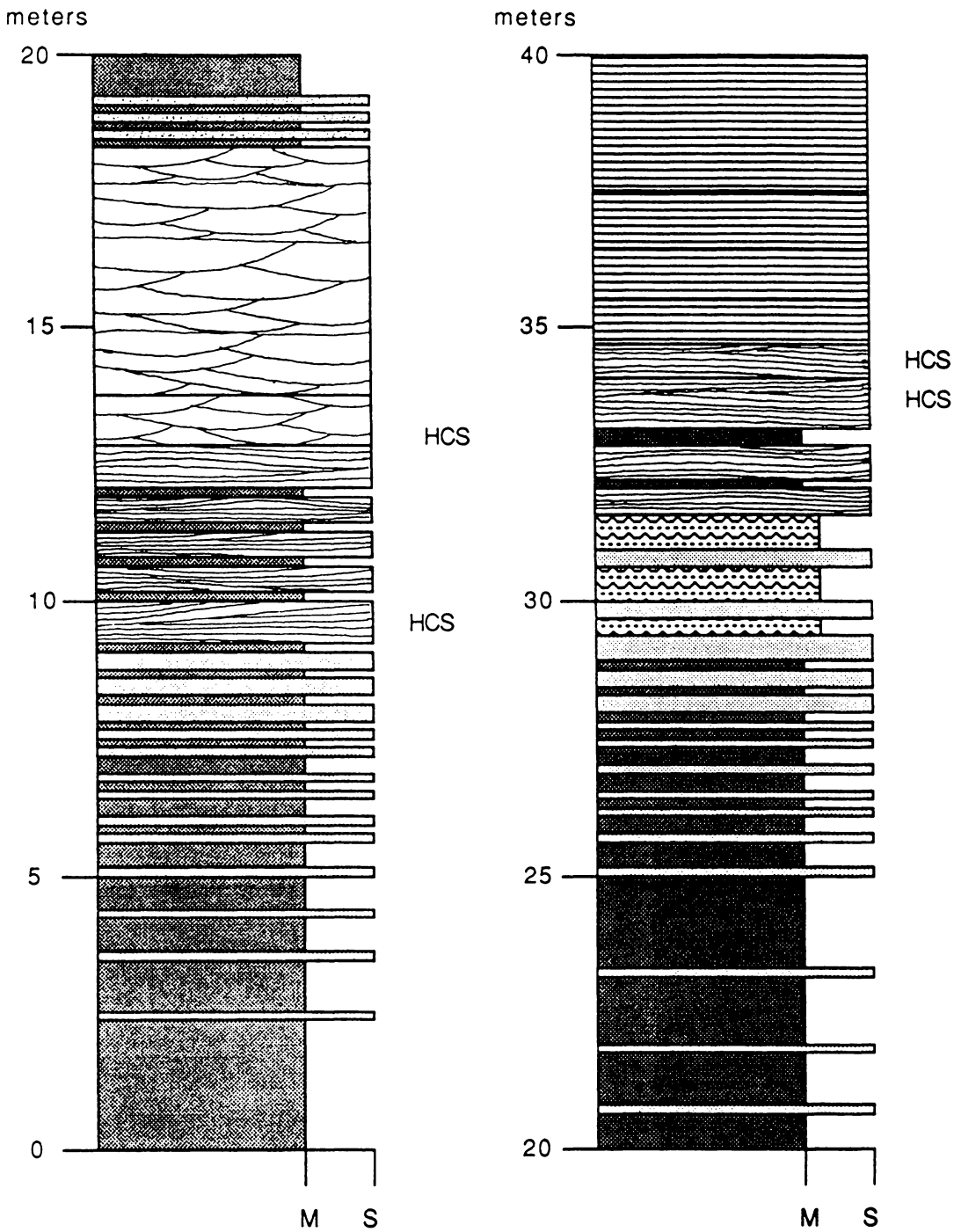

P3 - Bear Creek Section CH-109-84

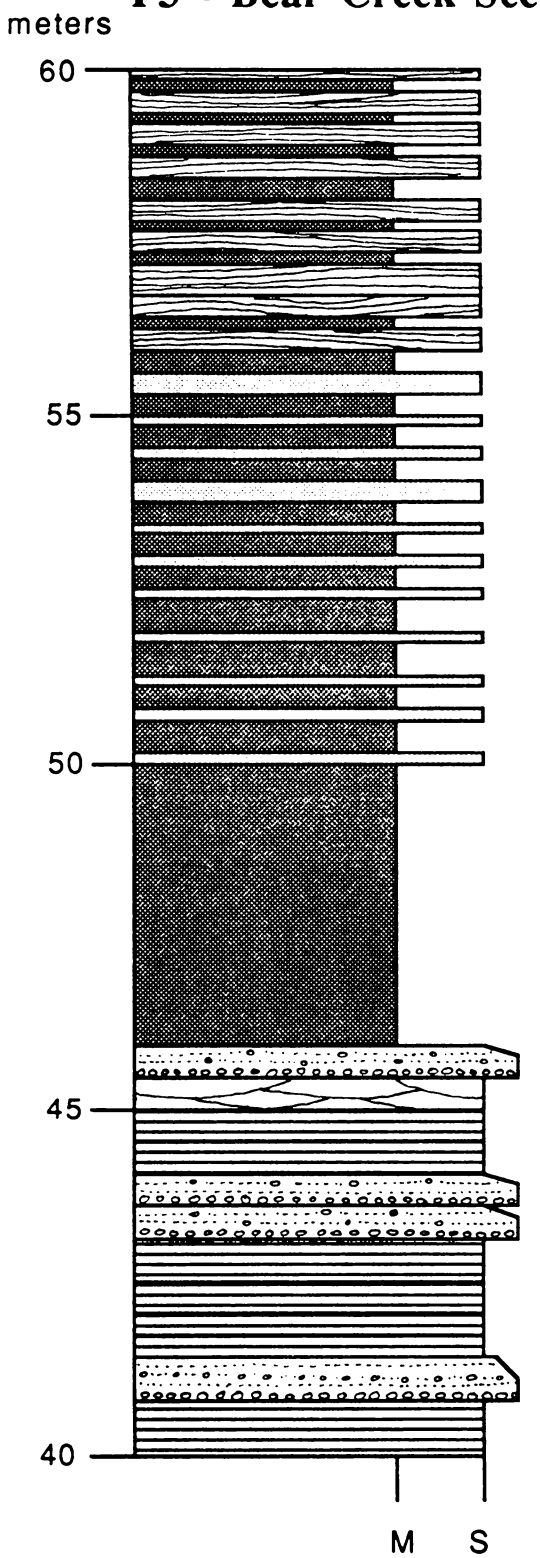

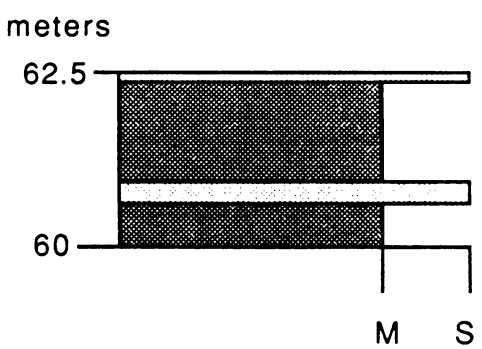

Q3 - Bear Creek Section CH-108-84

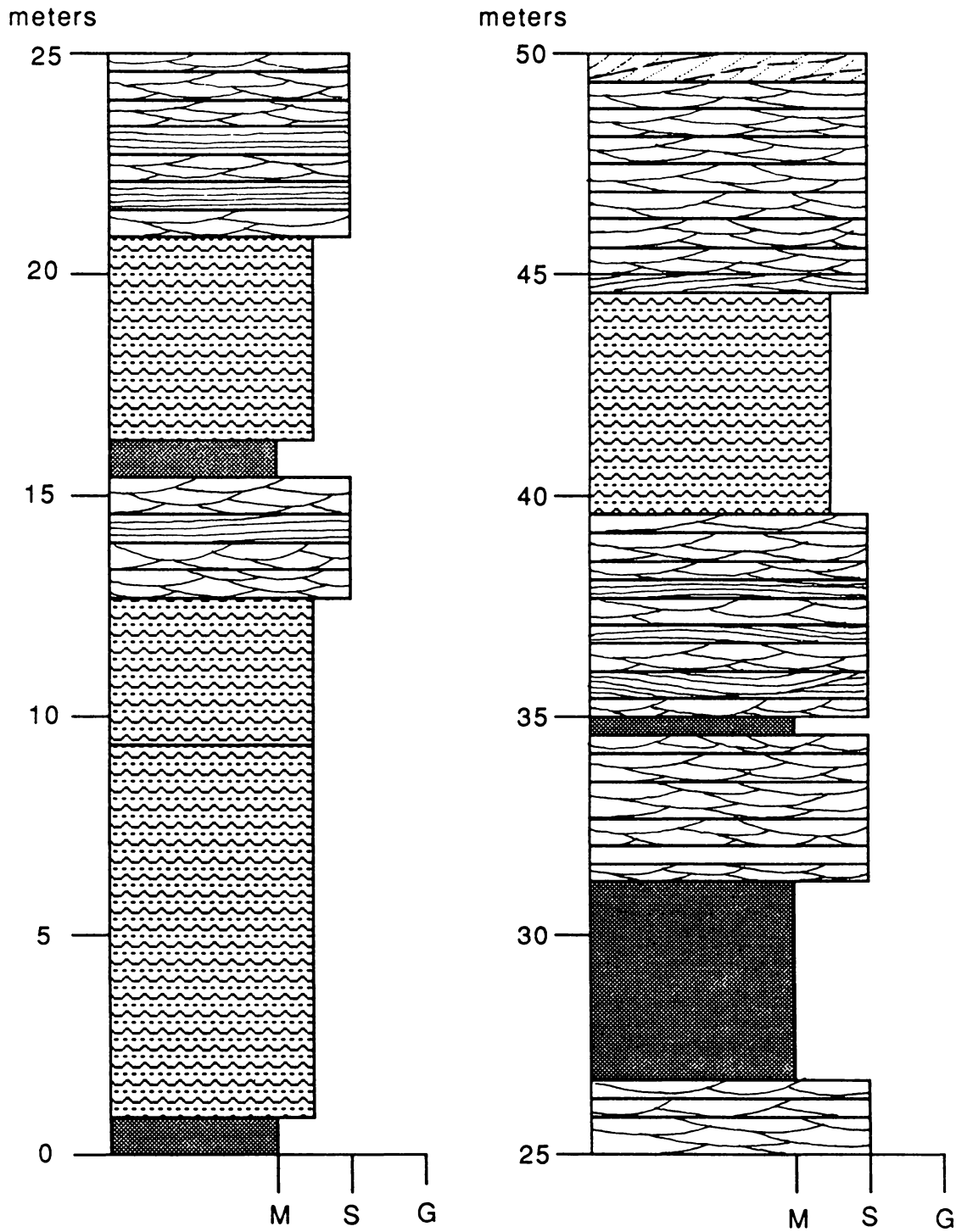

Q3 - Bear Creek Section CH-108-84

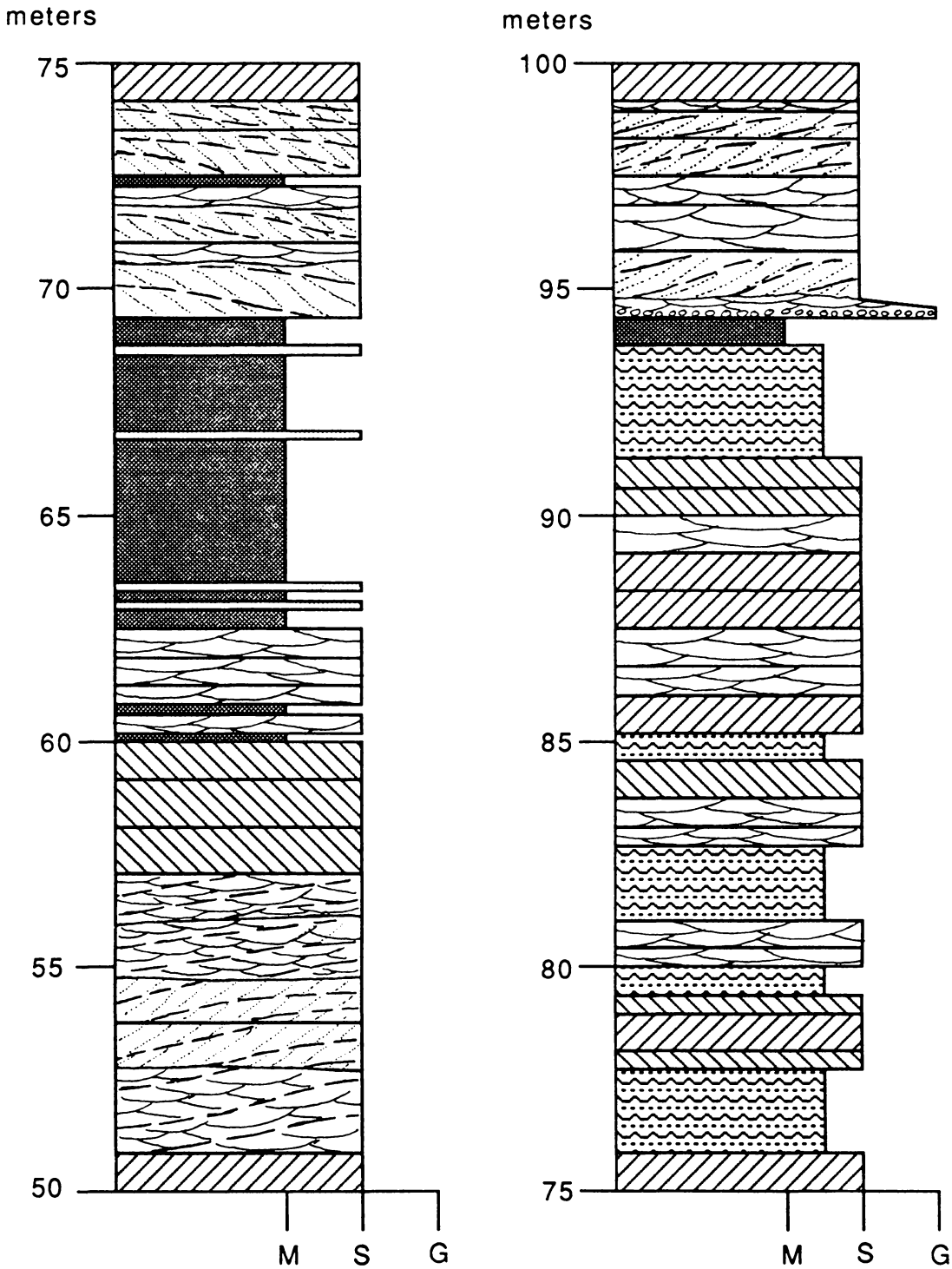

Q3 - Bear Creek Section CH-108-84

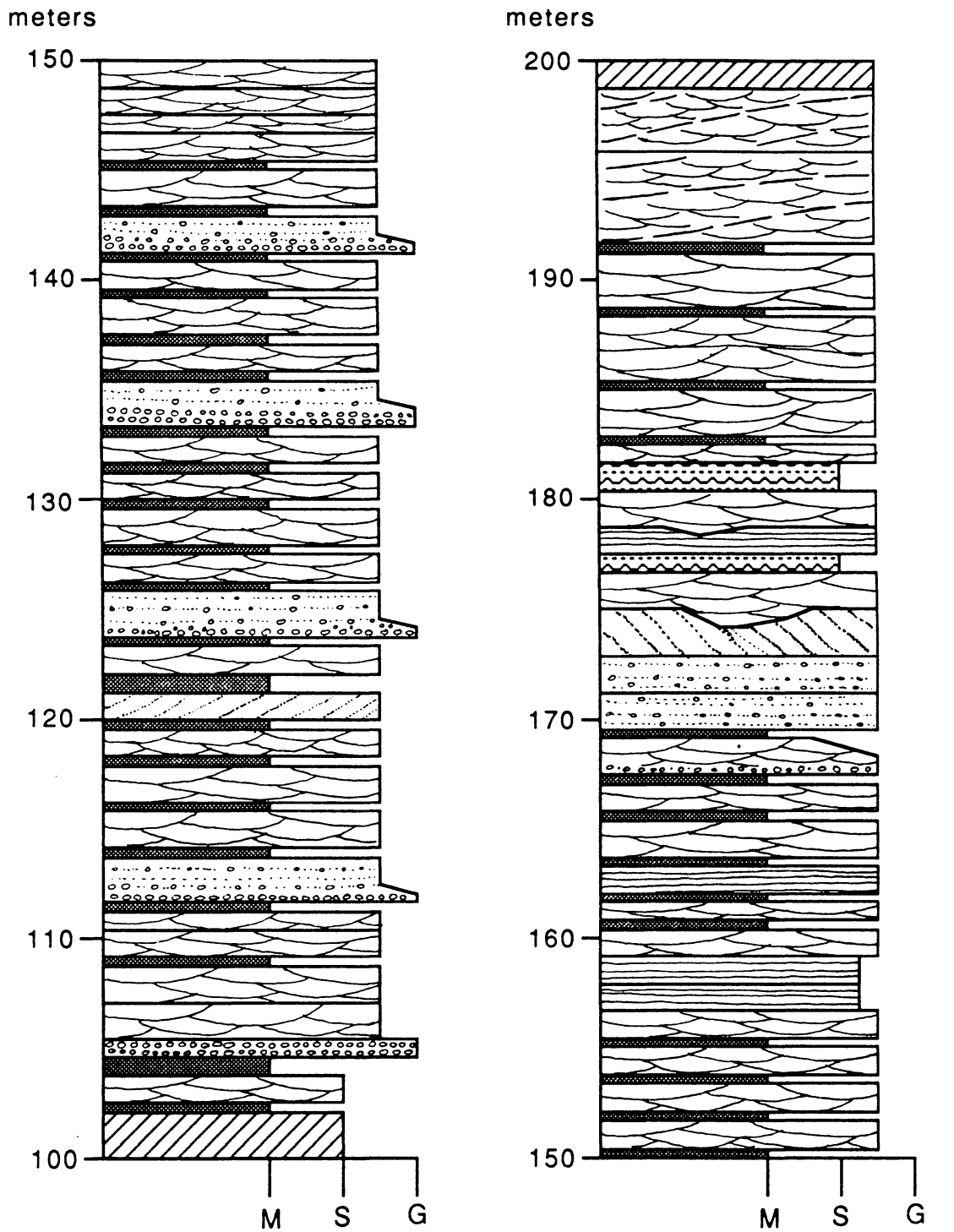

Q3 - Bear Creek Section CH-108-84

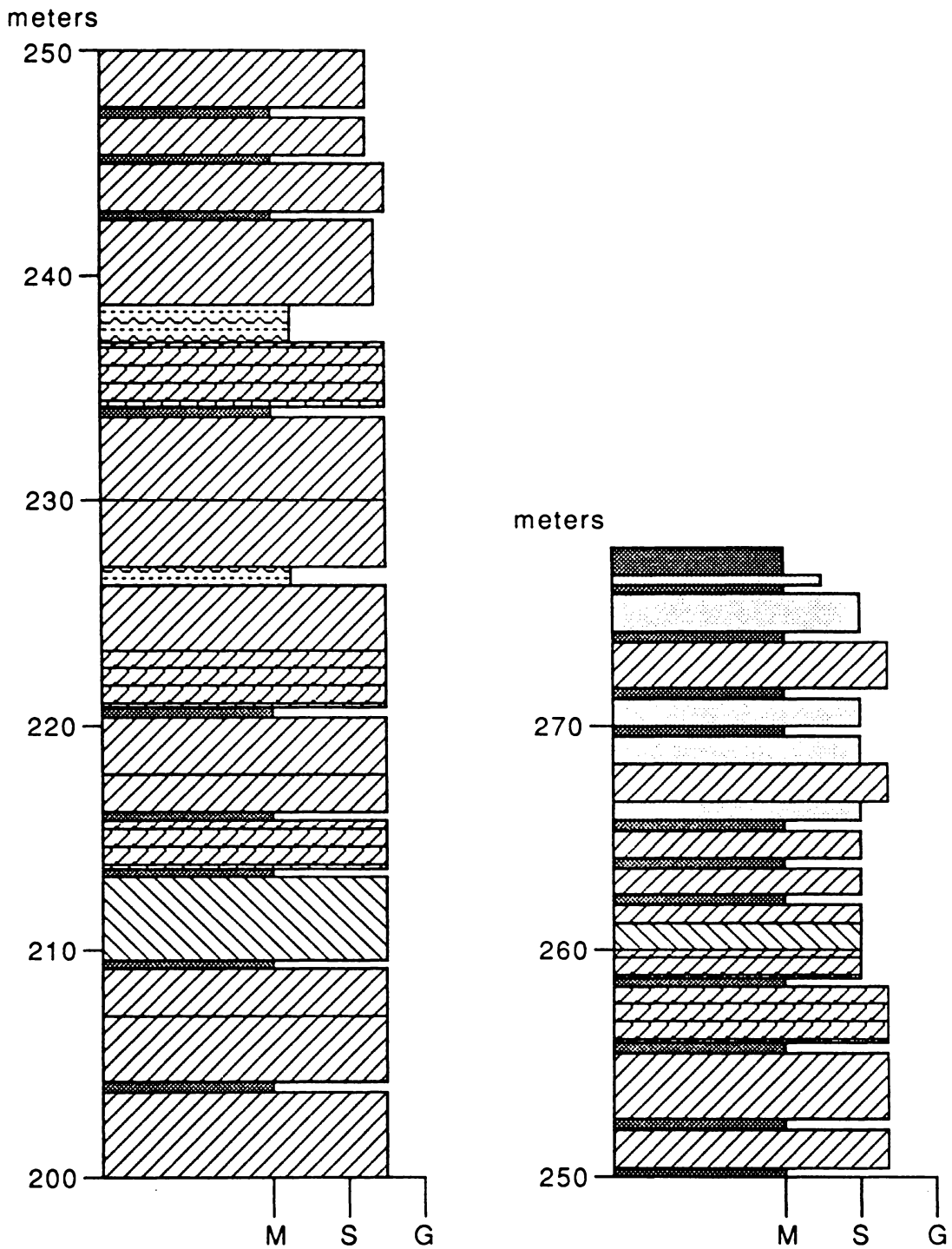

Lower Q4 - Uncompahgre River Section CH-91-84

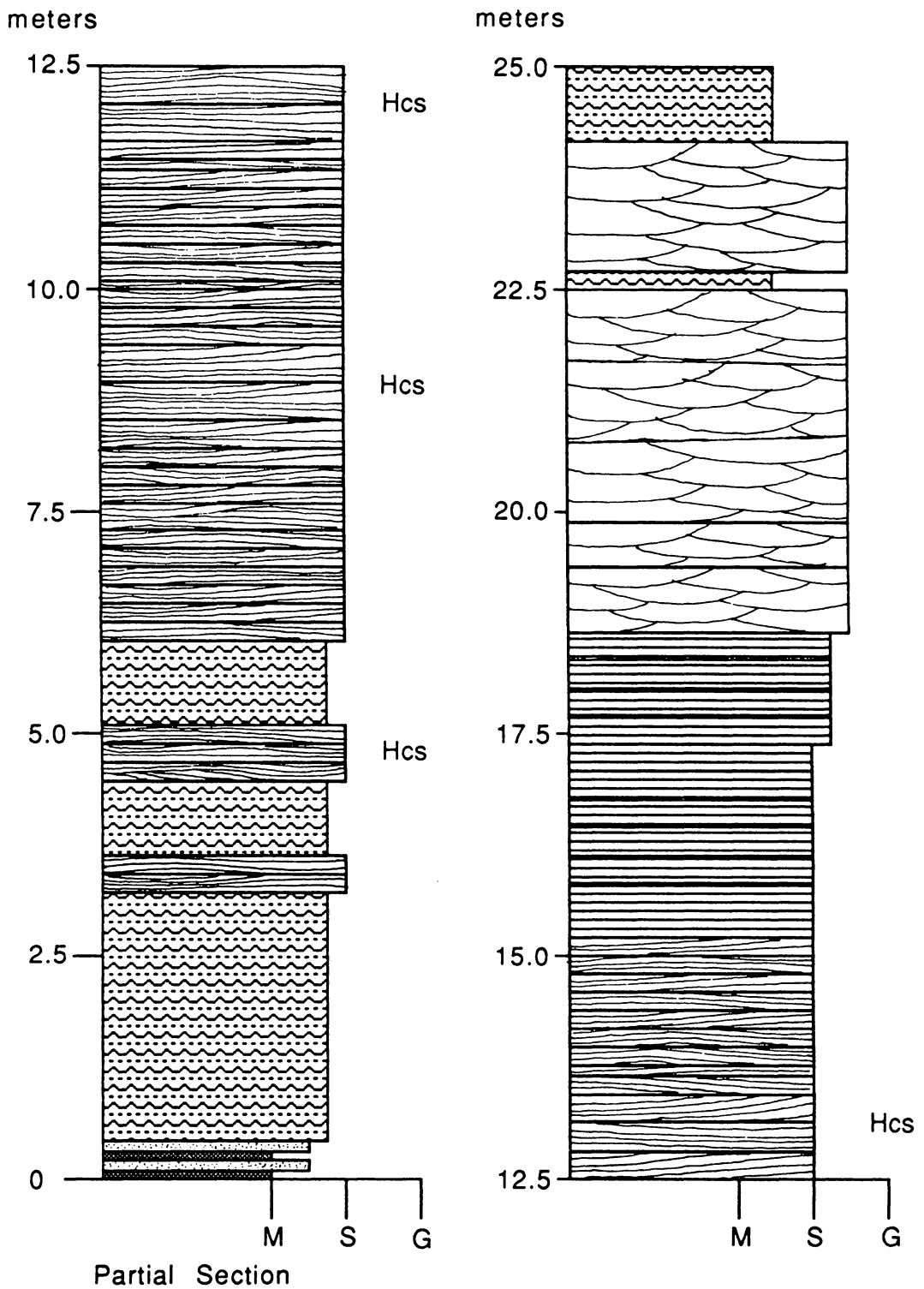

Q4 - Uncompahgre River Section CH-112-84

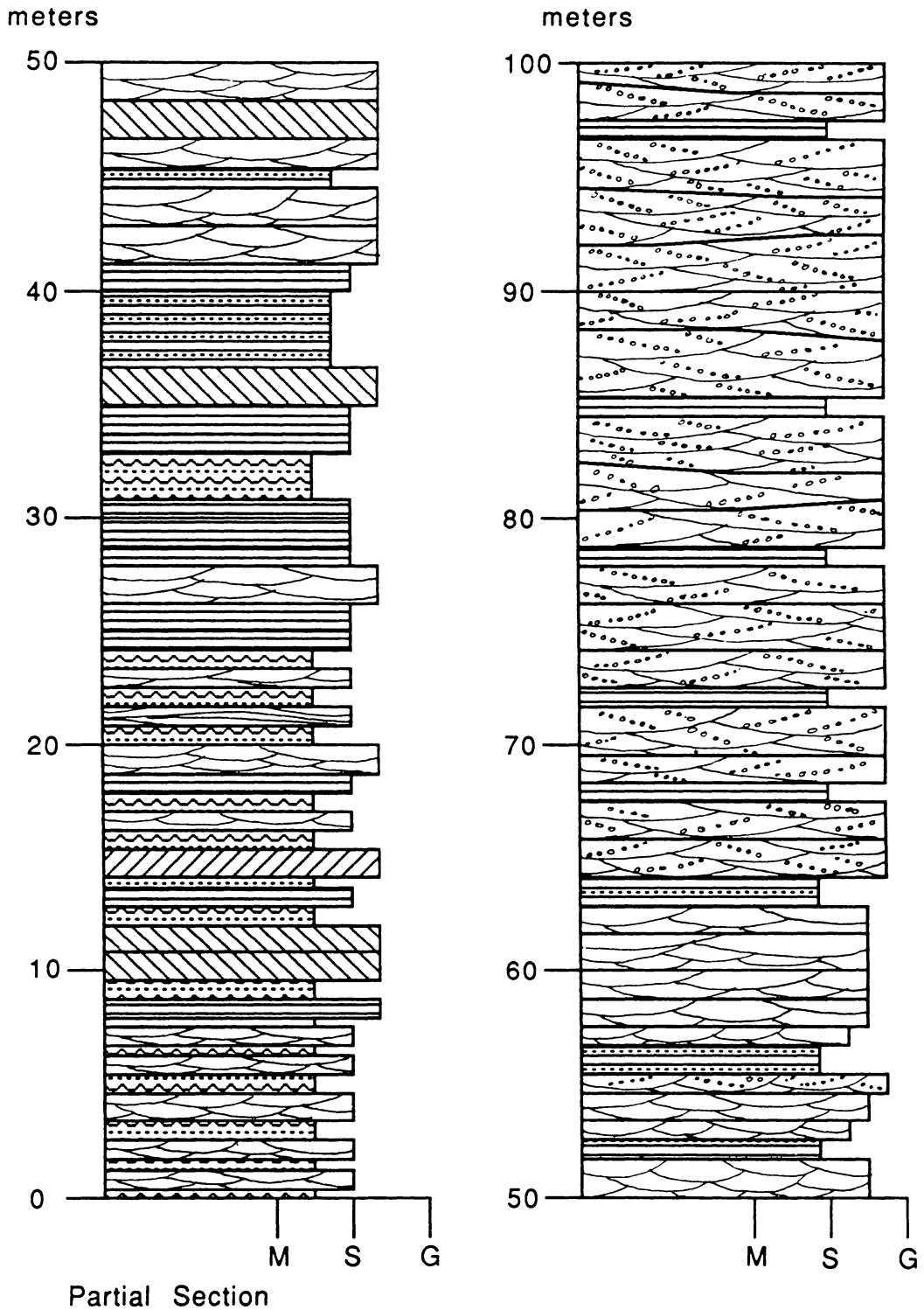

Q4 - Uncompahgre River Section CH-112-84

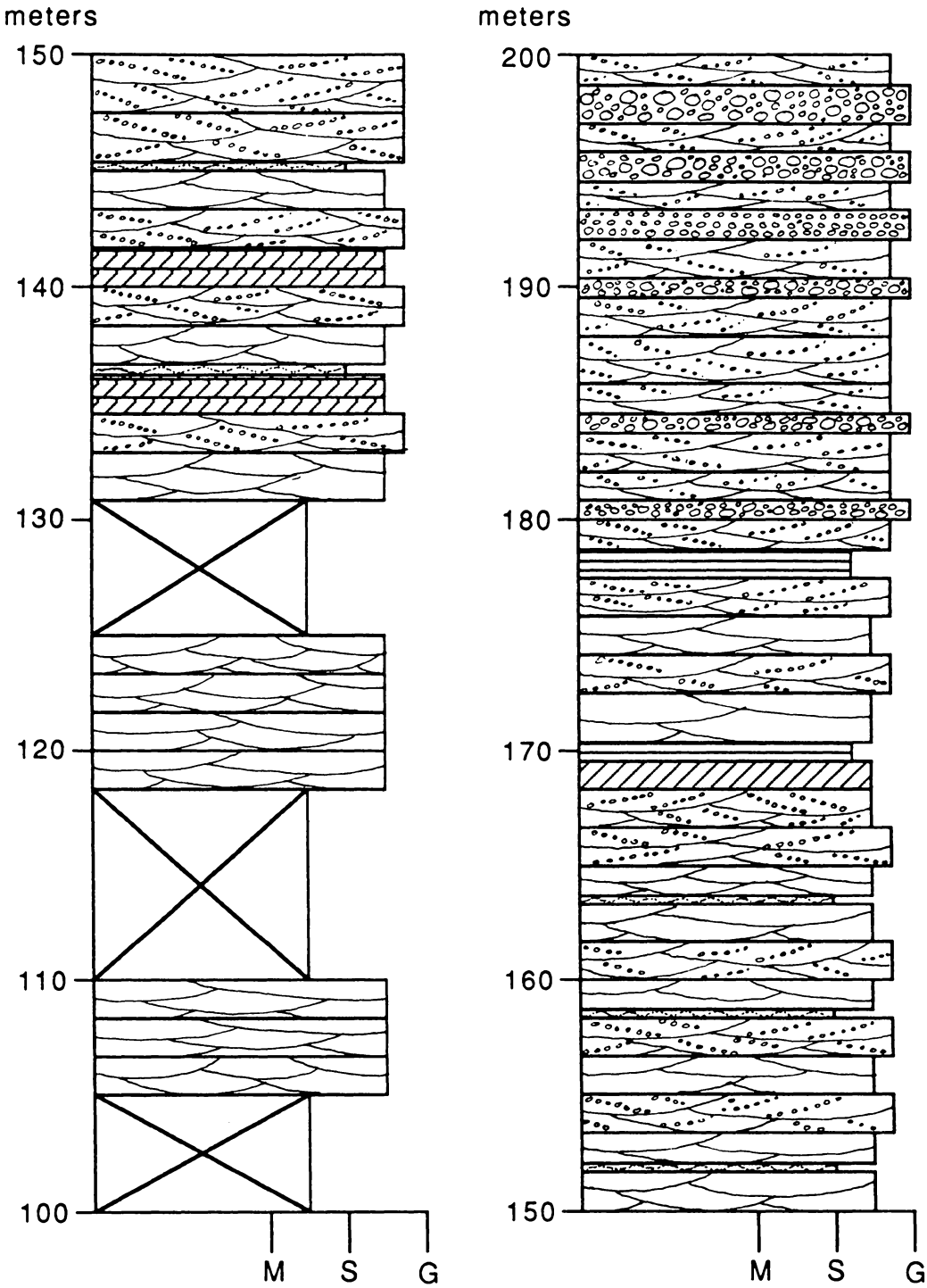

Q4 - Uncompahgre River Section CH-112-84

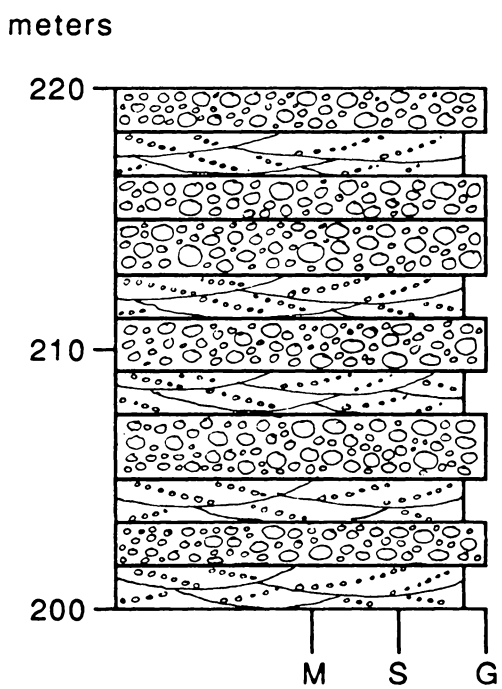

Lower Q4 - Uncompahgre River Section CH-273-85

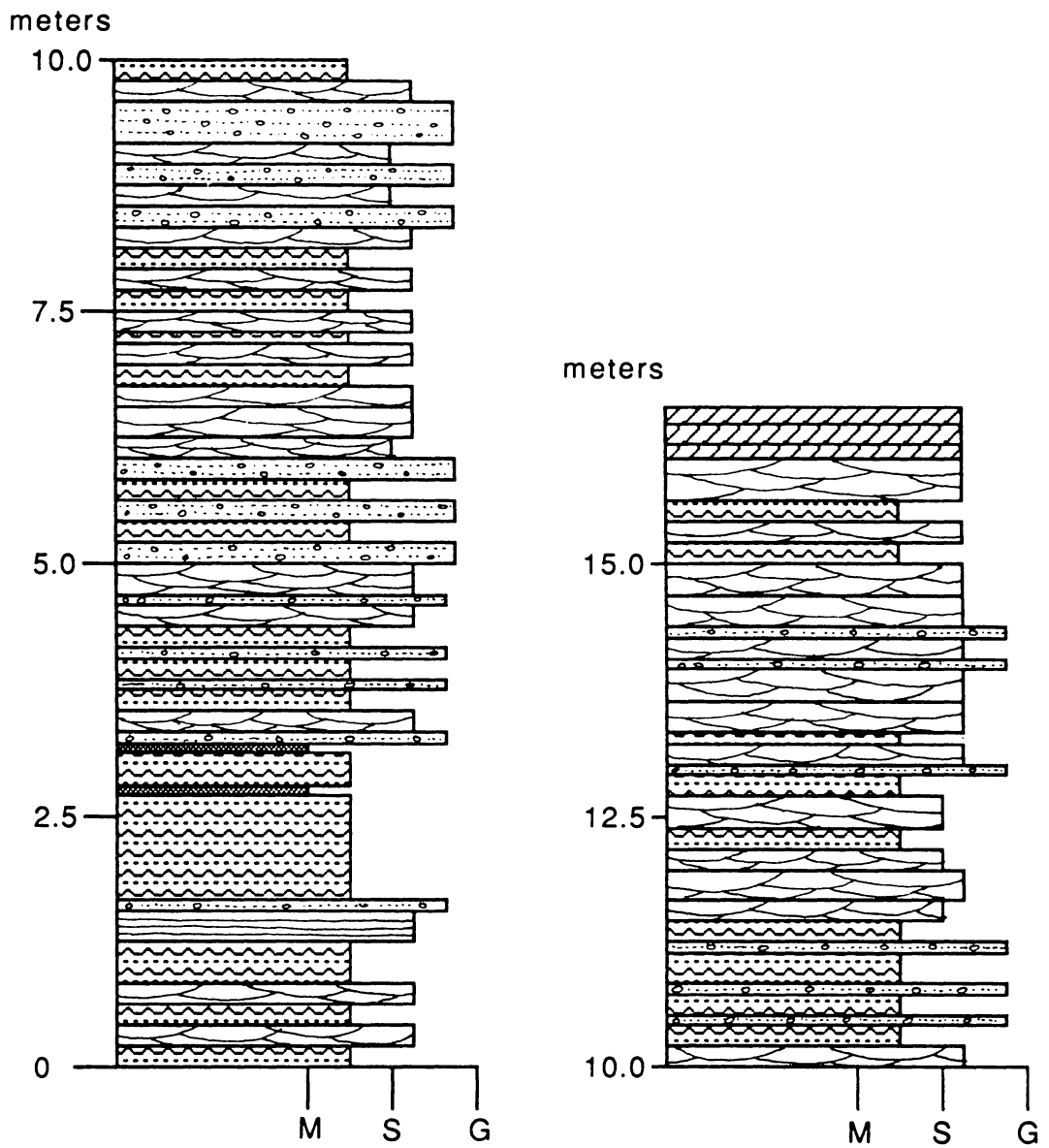

Upper Q4 - Uncompahgre River Section CH-403-86

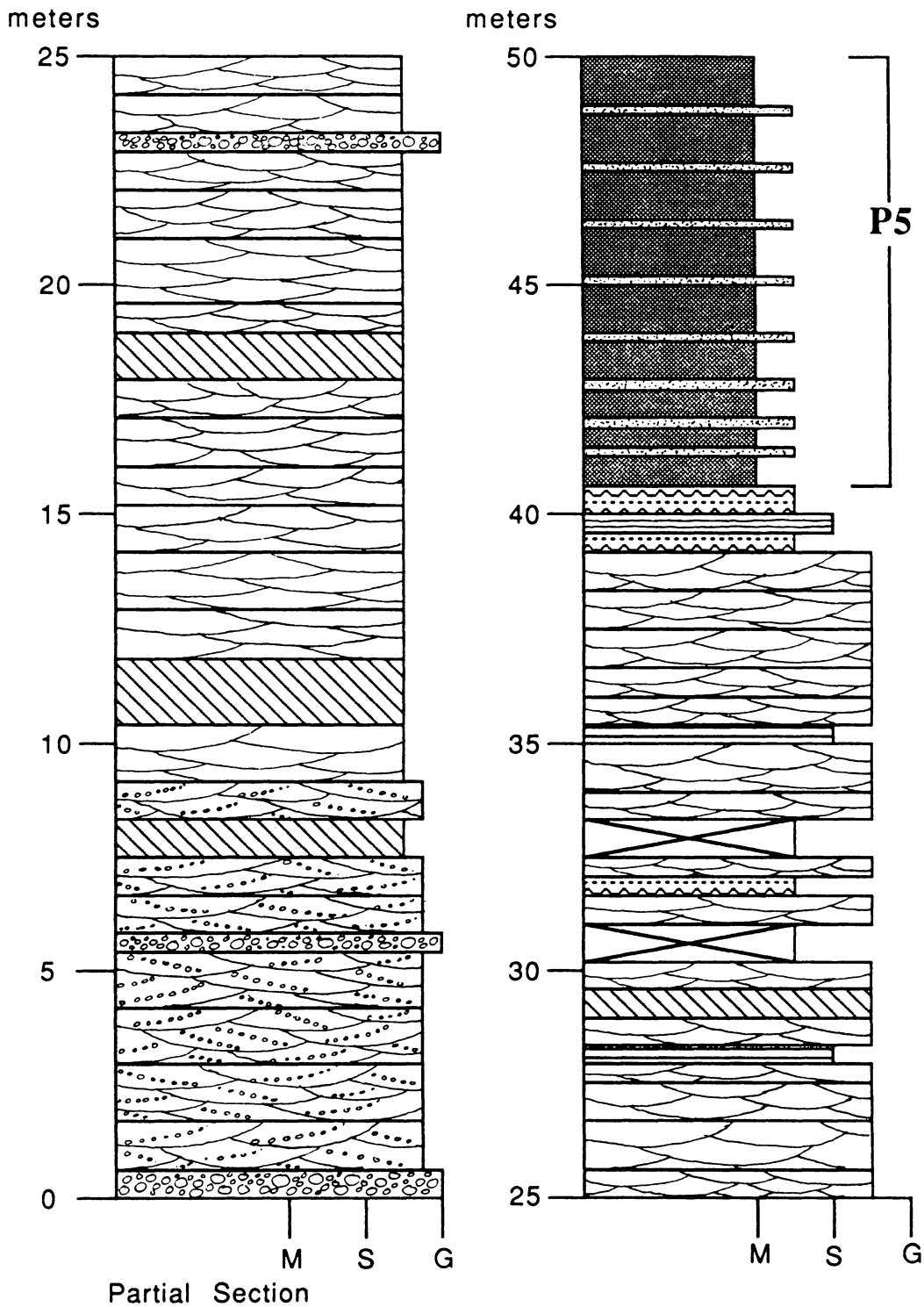

Upper Q4 - Uncompahgre River Section CH-404-86

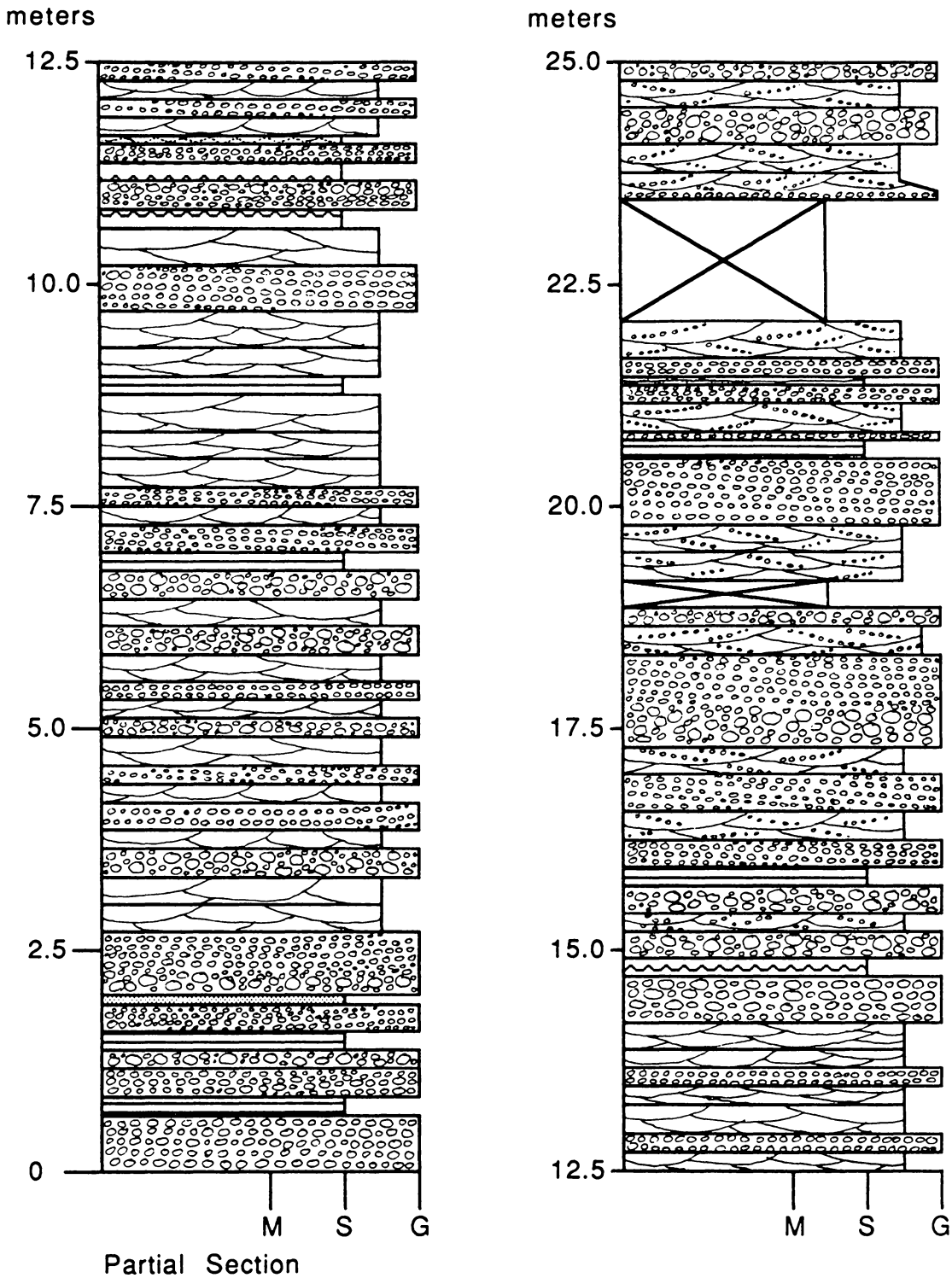

Appendix C. Paleocurrent Data

Structural data and paleocurrent rotations

A detailed meso- to macroscopic structural analysis was completed for the West Needle Mountains and Uncompahgre Gorge areas and serves as a basis for defining domains in which the macroscopic structures are homogeneous (Turner and Weiss, 1963). This information can then be employed to rotate paleocurrent data collected from these domains.

Paleocurrent Rotations

To rotate the paleocurrent data two things must be known, 1) the fold style and its effect on the orientation of planar and linear features, and 2) the orientation of fold axes, bedding and planar or linear features. At Uncompahgre Gorge and Lime Creek, slickensides perpendicualr to the fold axes are present on bedding surfaces and indicate that flexural slip served to accomodate much of the large scale folding of the quartzites. Constant orthogonal bed thickness around fold hinges indicates that the folds belong to class 1-B of Ramsay (1967). In flexural slip, parallel folds, linear and planar structures are not reoriented relative to bedding (Ramsay, 1960; 1961; 1967). Tabular-planar and -tangential cross strata and pebbles within beds of the Uncompahgre Group quartzites do not exhibit pervasive internal strain, which supports the flexural-slip model for folding. In addition, the quartzites are encased in thick pelitic and psammitic units which accomodated much of the strain. These observations suggest paleocurrent indicators in the various quartzite units can be rotated to their original position without compensation for internal strain.

Paleocurrent indicators include tabular-planar or tabular-tangential cross beds, trough cross strata, and symmetrical ripples. The data can be treated as either linear

or planar structures for geometric rotations. Tabular cross strata are plotted as poles to foresets. Upon rotation of bedding to horizontal, the current vector is the dip direction of the foresets. Linear features, plotted as the trend of a line, can yield absolute or bidirectional current vectors. Trough axes, determined from trough cross strata, yield absolute vectors, as the paleocurrent is oriented in the concave direction outlined by the intersection of the foreset and bedding plane. For symmetrical ripples the current sense is oscillatory (bidirectional vector) and is measured as a linear structure perpendicular to the ripple crests.

The rotation of paleocurrent data is outlined in stereoplots 1 through 6 in Figure C-1 (similar techniques are described in Ramsay, 1961). The example discussed is from the Lime Creek area. Four rotations are necessary on an equal area (Schmidt) net. The first rotation (stereoplot 2) brings the F_3 fold axis to vertical. The F_3 axis is rotated along a small circle to the center of the net, with the attendant movement of all other points along small circles. The limbs of the F_3 fold are then unfolded, in which all points are rotated about a vertical axis on the stereonet (stereoplot 3). The arc subtended is equal to a 50° anticlockwise rotation of all points about the perimeter of the net. Another method may be implemented at this point, and involves redefining a new North pole (N′) equivalent to the amount of rotation necessary to unfold the F_3 fold limbs. The F_2 fold axis is then brought to horizontal along a small circle (stereoplot 4) with an equivalent angular rotation of all other points along small circles. The final step involves restoring bedding to its horizontal position (stereoplot 5). The pole to bedding is rotated along the equator of the net to the center and poles to linear and planar structures are rotated along small circles an equal amount. The stereonet is then restored to its original N-S orientation (stereoplot 6) or to N′. The current azimuths can then be determined. If an F_3 fold generation is not present, as is the case at Uncompahgre Gorge or in the

Animas Canyon and Grenadier Range areas, then steps 1 and 2 of the rotation procedure can be omitted.

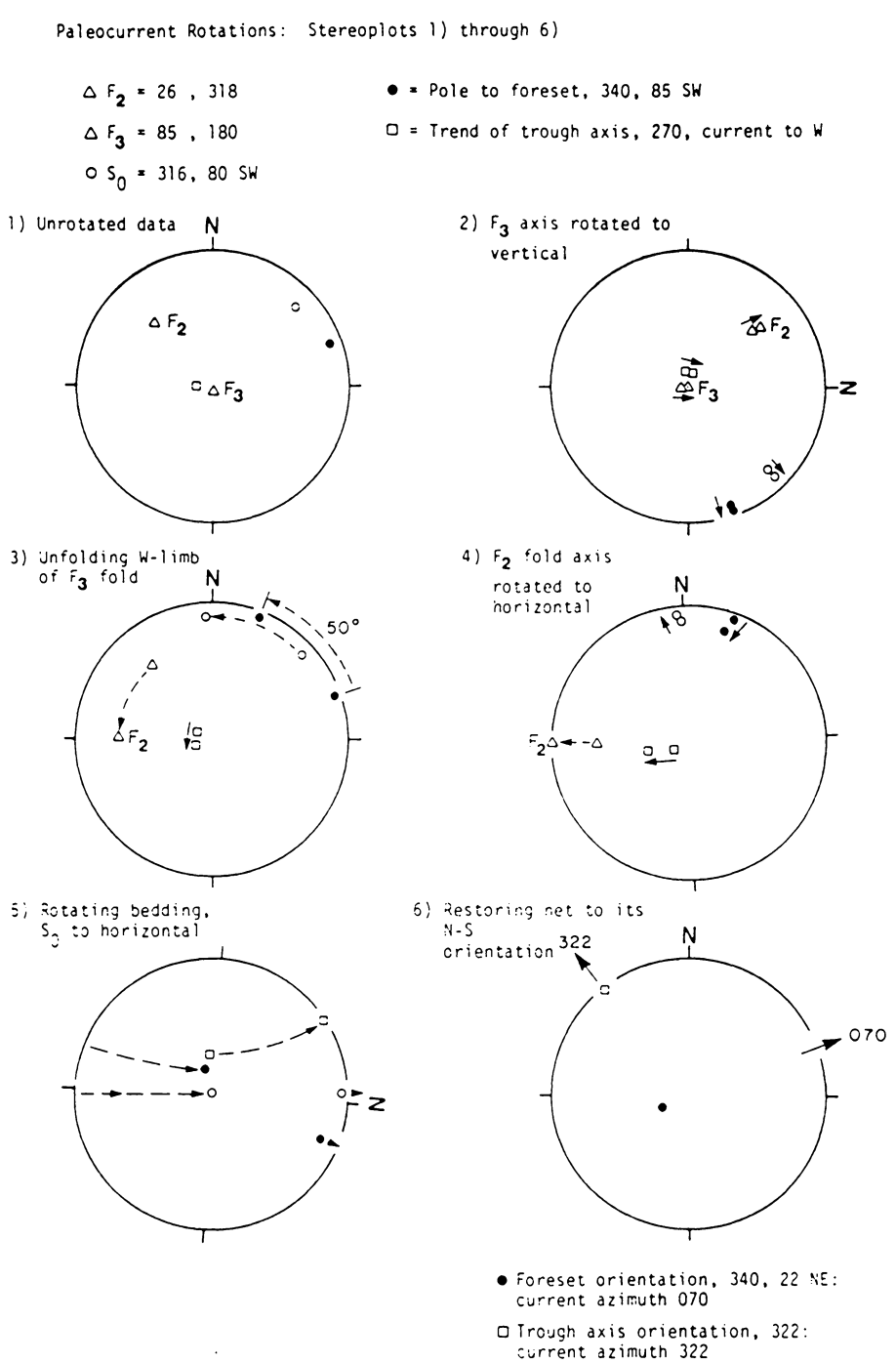

Figure C-1: Procedure for paleocurrent rotations.

MEDIAL Q1: SNOWDON PEAK

Station Number: CH-119-84
Paleocurrent data: trough axes
Plunge of F_2 fold axis: 0° 270 **Master Bedding: 086 49N**
Number of readings: N = 36 **Vector Mean: 164.3**

Unrotated Azimuth Current	Rotated Azimuth	Current Direction
1. 045 SW	037	217
2. 357 SE	356	176
3. 313 SE	321	141
4. 301 SE	305	125
5. 284 SE	290	110
6. 327 SE	333	153
7. 032 SW	024	204
8. 302 SE	311	131
9. 338 SE	342	162
10. 343 SE	346	166
11. 063 SW	057	237
12. 034 SW	026	206
13. 033 SW	025	205
14. 042 SW	034	214
15. 018 SW	012	192
16. 353 SE	354	174
17. 325 SE	332	152
18. 001 SW	360	180
19. 330 SE	336	156
20. 346 SE	348	168
21. 325 SE	332	152
22. 001 SW	360	180
23. 307 SE	316	136
24. 328 SE	334	154
25. 019 SW	014	194
26. 310 SE	318	138
27. 286 SE	293	113
28. 282 SE	288	108
29. 338 SE	342	162
30. 039 SW	031	211
31. 293 SE	289	109
32. 343 SE	346	166
33. 331 SE	337	157
34. 291 SE	298	118
35. 347 SE	349	169
36. 006 SW	003	183

MEDIAL Q1: SNOWDON PEAK

Station Number: CH-231-85
Paleocurrent data: Tangential to planar foresets
Plunge of F_2 fold axis: 0° 270
Number of readings: N = 26 **Vector Mean: 102.2**

	Bedding Strike Dip	Unrotated Strike Dip	Rotated Strike Dip	Current Direction
	273 42NE			
1.		293 42NE	018 15SE	108
2.		295 41NE	020 18SE	100
3.		292 44NE	002 13SE	092
4.		293 46NE	354 15NE	084
5.		291 52NE	333 16NE	063
6.		292 51NE	340 16NE	070
7.		292 43NE	006 14SE	096
8.		276 36NE	066 08SE	156
9.		284 35NE	042 10SE	132
10.		286 35NE	042 11SE	132
11.		294 46NE	006 16SE	096
12.		292 50NE	334 16NE	074
13.		295 48NE	009 18SE	099
14.		285 52NE	317 13NE	047
15.		288 54NE	321 17NE	051
16.		297 34NE	041 18SE	131
17.		293 37NE	031 14SE	121
18.		298 31NE	047 20SE	137
19.		296 31NE	049 18SE	139
20.		291 36NE	009 11SE	099
21.		290 36NE	008 11SE	098
22.		290 41NE	018 12SE	108
23.		298 30NE	051 19SE	141
24.		297 31NE	050 19SE	140
25.		293 47NE	349 16NE	079
26.		298 44NE	004 17SE	094

MEDIAL Q2: ANIMAS CANYON

Station Number: CH-342-85
Paleocurrent data: Trough axes
Plunge of F_2 fold axis: 15° 273 **Master Bedding: 315 22NW**
Number of readings: N = 52 **Vector Mean: 207.2**

	Unrotated Azimuth Current	Rotated Azimuth	Current Direction
1.	199 SW	204	204
2.	188 SW	192	192
3.	193 SW	196	196
4.	186 SW	190	190
5.	208 SW	211	211
6.	190 SW	194	194
7.	206 SW	209	209
8.	203 SW	207	207
9.	207 SW	210	210
10.	192 SW	196	196
11.	199 SW	204	204
12.	205 SW	208	208
13.	194 SW	198	198
14.	188 SW	192	192
15.	195 SW	200	200
16.	210 SW	213	213
17.	199 SW	204	204
18.	203 SW	207	207
19.	205 SW	208	208
20.	193 SW	196	196
21.	203 SW	207	207
22.	206 SW	209	209
23.	180 S	184	184
24.	212 SW	216	216
25.	216 SW	219	219
26.	184 SW	188	188
27.	201 SW	205	205
28.	204 SW	207	207
29.	193 SW	196	196
30.	219 SW	222	222
31.	190 SW	194	194
32.	199 SW	204	204
33.	213 SW	216	216
34.	223 SW	226	226
35.	205 SW	208	208
36.	223 SW	226	226
37.	217 SW	220	220
38.	217 SW	220	220
39.	220 SW	223	223
40.	225 SW	228	228

41.	220 SW	223	223
42.	232 SW	234	234
43.	225 SW	228	228
44.	215 SW	218	218
45.	206 SW	209	209
46.	208 SW	211	211
47.	208 SW	211	211
48.	194 SW	198	198
49.	175 SE	179	179
50.	209 SW	212	212
51.	196 SW	201	201
52.	202 SW	206	206

UPPER Q2: LIME CREEK

Station Number: CH-36-84
Paleocurrent data: Tangential to planar foresets
Plunge of F_2 fold axis: 26° 318
Plunge of F_3 fold axis: 80° 170
Number of readings: N = 77 **Vector Mean:** 59.1

	Bedding Strike Dip	Unrotated Strike Dip	Rotated Strike Dip	Current Direction
	302 88SW Overturned			
1.		322 84SW	340 22NE	070
2.		328 81SW	334 27NE	064
3.		324 85SW	341 23NE	071
4.		321 82SW	333 21NE	063
5.		324 86SW	341 23NE	071
	304 86NE			
6.		321 81SW	316 24NE	046
7.		329 86SW	334 27NE	064
8.		330 89SW	342 27NE	072
9.		331 87SW	341 28NE	071
10.		328 90	339 26NE	069
11.		326 87NE	350 23NE	080
12.		321 74SW	304 26NE	034
13.		316 77SW	298 21NE	028
14.		318 80SW	311 22NE	041
15.		314 78SW	296 20NE	026
16.		315 75SW	294 22NE	024
17.		323 81SW	318 24NE	048
18.		322 84SW	326 22NE	056
	304 90			
19.		322 72SW	208 25NE	038
20.		319 74SW	307 22NE	037
21.		319 76SW	311 20NE	041
22.		316 75SW	304 18NE	034
23.		316 74SW	300 20NE	030
24.		317 77SW	312 18NE	042
25.		321 81SW	327 20NE	057
26.		319 77SW	317 20NE	047
27.		323 77SW	319 23NE	049
28.		323 81SW	330 21NE	060
29.		320 78SW	317 20NE	047
30.		326 84SW	337 24NE	067
31.		333 86SW	343 29NE	073
32.		327 90	349 24NE	079
33.		326 88NE	359 22NE	089
34.		329 84NE	008 26SE	098
35.		330 89NE	356 26NE	086

36.		320 81NE	015 19SE	105
37.		316 86NE	016 14SE	106
38.		334 90	354 30NE	084
	301 87SW Overturned			
39.		322 90	356 22NE	086
40.		322 88SW	351 20NE	081
41.		321 87SW	346 20NE	076
42.		323 86SW	342 22NE	072
43.		325 86SW	342 24NE	072
	300 88SW Overturned			
44.		322 83SW	334 23NE	064
45.		323 78SW	325 25NE	055
46.		326 75SW	321 30NE	051
47.		325 76SW	320 28NE	050
48.		324 76SW	320 28NE	050
49.		322 79SW	326 24NE	054
50.		299 65NE	268 22SE	178
51.		328 88NE	350 26NE	080
52.		323 89SW	338 22NE	068
53.		326 90	344 24NE	074
54.		322 89NE	348 19NE	078
55.		327 89NE	346 24NE	076
56.		321 80SW	315 23NE	045
57.		323 80SW	319 24NE	049
58.		328 76SW	325 27NE	055
	296 85SW Overturned			
59.		301 58SW	271 25NE	001
60.		312 66SW	288 30NE	018
61.		303 66SW	274 18NE	004
62.		303 67SW	274 19NE	004
63.		304 68SW	098 19NE	008
64.		304 63SW	096 19NE	006

LOWER-MEDIAL Q2: LIME CREEK

Station Number: CH-88-84

	Bedding Strike Dip	Unrotated Strike Dip	Rotated Strike Dip	Current Direction
	294 83SW Overturned			
65.		323 85SW	342 28NE	072
66.		317 83SW	340 24NE	070
67.		316 82SW	340 22NE	070
68.		316 80SW	333 23NE	067
69.		324 73SW	321 31NE	051

70.	327 86SW	345 34NE	075
71.	325 81SW	336 31NE	066
72.	328 78SW	331 34NE	061
73.	324 76SW	326 31NE	056
74.	325 80SW	332 31NE	062
75.	328 84SW	341 34NE	071
76.	327 86SW	345 34NE	075
77.	324 85SW	342 30NE	072

UPPER Q2: LIME CREEK

Station Number: CH-36-84
Paleocurrent data: Tangential to planar foresets
Number of readings: N = 10 **Vector Mean: 205.9**

	Bedding Strike Dip	Unrotated Strike Dip	Rotated Strike Dip	Current Direction
	303 88NE			
1.		293 73NE	296 17SW	206
2.		296 74NE	284 15SW	194
3.		299 75NE	275 12SW	185
4.		291 76NE	301 17SW	211
5.		295 76NE	291 14SW	201
6.		296 76NE	287 13SW	197
7.		298 74NE	279 14SW	189
8.		289 78NE	315 16SW	226
9.		297 81NE	292 10SW	202
	296 85SW Overturned			
10.		296 77SW	083 08NW	253

Station Number: CH-36-84
Paleocurrent data: Tangential to planar foresets
Number of readings: N = 14 **Vector Mean: 348.0**

	Bedding Strike Dip	Unrotated Strike Dip	Rotated Strike Dip	Current Direction
	296 85SW Overturned			
1.		290 64SW	052 17NW	322
2.		295 73SW	072 13NW	342
3.		296 67SW	075 17NW	345
4.		294 66SW	068 18NW	338
5.		299 65SW	084 20NW	354
6.		300 63SW	085 22NW	355
7.		296 68SW	075 16NW	345
8.		298 71SW	083 14NW	353

9.	299 64SW	082 21NW	352
10.	300 65SW	089 16NW	359
11.	298 63SW	080 22NW	350
12.	302 62SW	088 23NW	358
13.	297 65SW	078 20NW	348
14.	298 63SW	080 22NW	350

Q3: THREE LAKES CREEK

Station Number: CH-09-84
Paleocurrent data: Tangential to planar foresets
Plunge of F_2 fold axis: 20° 075
Plunge of F_3 fold axis: 75° 164
Number of readings: N = 133 **Vector Mean:** 108.6

	Bedding Strike Dip	Unrotated Strike Dip	Rotated Strike Dip	Current Direction
	072 82SE (0-130 m) Overturned			
1.		080 86NW	073 18SE	163
2.		274 78NE	062 29SE	152
3.		080 88SE	052 10SE	142
4.		274 70SW	347 25NE	077
5.		273 63SW	334 28NE	064
6.		270 77N	071 27SE	161
7.		087 78SE	004 16NE	094
8.		085 77SE	356 14NE	086
9.		088 90	043 17SE	133
10.		086 79NW	067 24SE	157
11.		276 64SW	339 30NE	069
12.		272 60SW	329 20NE	059
13.		278 70SW	351 28NE	081
14.		278 71SW	354 28NE	084
15.		087 69SE	327 34NE	047
16.		280 68SW	352 28NE	082
17.		274 76SW	002 20NE	092
18.		274 88SW	032 24SE	122
19.		088 74NW	076 28SE	166
20.		083 85SE	030 12SE	120
	070 80SE (130-176 m) Overturned			
21.		083 82SE	028 14SE	118
22.		083 72SE	352 15NE	082
23.		084 75SE	360 15E	090
24.		073 60SE	303 19NE	033
25.		271 87SW	036 22SE	126
26.		080 79SE	020 10SE	110
27.		077 70SE	314 12NE	044
28.		082 69SE	320 15NE	050
29.		079 69SE	316 12NE	046
30.		076 67SE	308 15NE	038
31.		074 59SE	298 29NE	028
32.		083 87SE	053 14SE	143
33.		276 73SW	026 24SE	116
34.		275 65SW	008 24SE	098
35.		275 82SW	049 27SE	139

36.	274 65SW	010 23SE	100
37.	076 81SE	085 12SE	175
38.	089 70SE	024 17SE	114
39.	077 85SE	088 16SE	178
40.	085 75SE	038 14SE	128
41.	092 77SW	018 20SE	108
42.	084 72SE	028 14SE	118
43.	090 63S	338 18NE	068
44.	091 65SW	008 20SE	098
45.	091 60SW	353 22NE	083
	070 72SE		
	Overturned		
46.	083 65SE	339 15NE	079
47.	087 72SE	014 17SE	104
48.	085 68SE	001 15SE	091
49.	088 60SE	342 22NE	072
50.	090 68SE	359 20NE	089
51.	083 76SE	033 13SE	123
52.	085 50SE	324 26NE	054
53.	088 52SE	330 26NE	060
54.	084 49SE	318 27NE	048
55.	087 74SE	023 16SE	113
56.	082 72SE	012 10SE	102
57.	088 60SE	342 22NE	072
58.	091 68SW	003 22SE	093
59.	093 66SW	360 23E	090
60.	090 70S	004 18SE	094
61.	088 75SE	024 18SE	114
62.	085 62SE	345 18NE	075
63.	084 59SE	335 18NE	065
	068 76SE		
	Overturned		
64.	083 68SE	334 24NE	064
65.	084 70SE	347 21NE	077
66.	092 72SW	355 26NE	085
67.	085 64SE	336 24NE	066
68.	087 64SE	339 24NE	069
69.	083 63SE	334 24NE	064
70.	087 78SE	011 22SE	101
71.	082 81SE	023 17SE	113
72.	082 85SE	346 18NE	076
73.	089 87SE	030 25SE	120
74.	091 88NE	031 27SE	121
75.	085 87NW	048 24SE	138
76.	087 64SE	339 24NE	069
77.	092 74SW	018 20SE	108
78.	088 87SE	053 21SE	143
	073 69SE (140 m - individual sandwave)		
	Overturned		
79.	086 72SE	034 12SE	124
80.	085 70SE	018 13SE	098

81.	087 75SE	044 14SE	134
82.	084 79SE	064 17SE	154
83.	083 70SE	031 10SE	121
84.	094 70SW	022 20SE	112
85.	098 71SW	024 23SE	114
86.	091 74SW	036 17SE	126
87.	094 70SW	022 20SE	112
88.	092 73SW	030 18SE	120
89.	093 67SW	014 20SE	104
90.	093 73SW	032 17SE	122
91.	096 60SW	360 24E	090
92.	094 68SW	016 20SE	106
93.	095 64SW	005 22SE	095
96.	092 69SW	021 18SE	111
97.	093 74SW	034 18SE	124
98.	091 71SW	022 16SE	112
99.	090 68S	018 17SE	108
100.	087 65SE	005 14SE	095
101.	093 66SW	010 20SE	100
102.	094 70SW	022 20SE	112
103.	099 73SW	027 24SE	117
104.	095 67SW	019 21SE	109
075 73SE (140 m - individual sandwave) Overturned			
105.	087 74SE	032 12SE	122
106.	278 75SW	030 21SE	120
107.	272 79SW	016 18SE	106
108.	271 73SW	020 15SE	110
109.	088 76SE	044 14SE	134
110.	087 71SE	010 12SE	100
111.	272 77SW	008 17SE	098
112.	270 75SW	018 14SE	108
113.	271 76SW	030 16SE	120
070 78SE (180-215 m) Overturned			
114.	084 90	055 19SE	145
115.	086 74SE	006 16SE	096
116.	064 58SE	284 19NE	014
117.	093 76SW	010 20SE	100
118.	085 88NW	056 22SE	146
119.	087 88NW	054 24SE	144
120.	092 90	042 25SE	132
121.	094 77SW	018 24SE	108
122.	086 89NW	048 23SE	138
123.	085 87NW	055 23SE	145
124.	081 83NW	071 23SE	161
125.	082 86NW	065 21SE	155
126.	084 85SE	048 18SE	138
127.	086 89SE	049 20SE	139
072 76SE Overturned			

128.	081 83NW	083 23SE	173
129.	082 86NW	080 22SE	170
130.	080 82NW	088 22SE	178
131.	084 83NW	077 22SE	167
132.	083 84NW	076 22SE	166
133.	082 87NW	079 20SE	169

Paleocurrent data: Planar to tangential foresets
Number of readings: N = 7 **Vector Mean: 316.3**

	Bedding Strike Dip	Unrotated Strike Dip	Rotated Strike Dip	Current Direction
	072 82SE Overturned			
1.		057 88SE	003 16NW	273
2.		061 71SE	071 17NW	341
	070 72SE Overturned			
3.		048 69SE	035 20NW	305
4.		044 69SE	034 25NW	304
	070 78SE Overturned			
5.		047 72SE	036 22NW	306
6.		055 54SE	084 28NW	354
7.		056 58SE	083 21NW	353

Paleocurrent data: Tangential to planar foresets and trough axes
Number of readings: N = 7 **Vector Mean: 189.0**

	Bedding Strike Dip	Unrotated Strike Dip	Rotated Strike Dip	Currrent Direction
	072 82SE Overturned			
1.		060 89NW	340 15SW	250
2.		077 80NW	275 22SW	185
3.		079 81NW	271 24SW	181
4.		079 81NW	271 24SW	181
5.		072 78NW	286 24SW	196

Trough axes

	Unrotated Azimuth Current	Rotated Azimuth	Current Direction
1.	155 SE	022	202
2.	164 SE	024	204

UPPER Q3: LIME CREEK

Station Number: CH-24-84
Paleocurrent data: Tangential to planar foresets
Plunge of F_2 fold axis: 26° 318
Plunge of F_3 fold axis: 75° 164
Number of readings: N = 9 **Vector Mean: 56.6**

	Bedding Strike Dip	Unrotated Strike Dip	Rotated Strike Dip	Current Direction
	305 82SW Overturned			
1.		323 80SW	317 18NE	047
2.		335 81SW	318 30NE	048
3.		326 76NE	010 30SE	100
	308 82SW Overturned			
4.		342 76SW	313 34NE	043
5.		338 78SW	316 30NE	046
6.		323 77SW	307 16NE	037
7.		336 80SW	320 28NE	050
	312 85SW Overturned			
8.		337 84NE	354 28NE	084
9.		341 84SW	329 29NE	059

Paleocurrent data: Tangential to planar foresets
Number of readings: N = 8 **Vector Mean: 220.1**

	Bedding Strike Dip	Unrotated Strike Dip	Rotated Strike Dip	Current Direction
	305 82SW Overturned			
1.		293 67NE	072 33SE	162
	308 82SW Overturned			
2.		285 73NE	351 13SW	261
3.		278 71SW	360 12W	270
4.		293 84NE	279 21SW	189
	312 85SW Overturned			
5.		283 80SW	335 29SW	245
6.		289 84NE	298 26SW	208
7.		285 89NE	312 28SW	222
8.		281 83NE	293 25SW	203

Q4: LIME CREEK

Station Number: CH-06-84
Paleocurrent data: Tangential to planar foresets
Plunge of F_2 fold axis: 0° 090
Plunge of F_3 fold axis: 85° 180
Number of readings: N = 29 **Vector Mean:** 47.9

	Bedding Strike Dip	Unrotated Strike Dip	Rotated Strike Dip	Current Direction
	079 84SE Overturned			
1.		085 72SE	313 17NE	043
2.		090 76SE	335 18NE	065
	070 87NW			
3.		081 80SE	310 18NE	040
4.		088 71SE	311 29NE	041
	072 87SE Overturned			
5.		280 78SW	343 30NE	073
6.		087 75SE	326 22NE	056
7.		270 80S	340 20NE	070
8.		273 84SW	356 24NE	086
9.		087 74SE	327 20NE	057
10.		086 74SE	324 18NE	054
11.		275 76SW	335 26NE	065
	075 85SE Overturned			
12.		085 65SE	301 23NE	031
13.		080 63SE	289 24NE	019
14.		079 63SE	284 24NE	014
15.		075 74SE	090 11N	360
16.		280 73SW	336 28NE	066
17.		083 80SE	332 10NE	062
18.		089 62SE	303 27NE	033
19.		085 84SE	355 10NE	085
20.		275 84SW	358 21NE	088
21.		087 77SE	329 15NE	059
22.		087 61SE	299 27NE	029
23.		087 66SE	395 23NE	035
24.		087 69SE	309 20NE	039
25.		077 76SE	287 11NE	017
26.		272 74SW	319 24NE	049
	076 88SE Overturned			
27.		086 76SE	316 16NE	046
28.		088 76SE	319 18NE	049
29.		073 78SE	287 11NE	017

Paleocurrent data: Tangential to planar foresets
Number of readings: 15 **Vector Mean: 137.4**

	Bedding Strike Dip	Unrotated Strike Dip	Rotated Strike Dip	Current Direction
	074 84SE Overturned			
1.		078 77NW	075 20SE	165
	072 87SE Overturned			
2.		080 71NW	064 22SE	154
3.		075 74NW	077 20SE	167
4.		075 82NW	172 12SE	162
	075 85SE Overturned			
5.		272 89SW	016 18SE	106
6.		274 90	014 20SE	104
7.		279 73NW	040 33SE	130
8.		271 76NW	048 25SE	138
9.		279 71NW	046 34SE	136
10.		280 86NW	020 27SE	110
11.		075 71NW	087 25SE	177
12.		082 86NW	051 12SE	141
	076 88SE Overturned			
13.		086 82NW	041 15SE	131
14.		085 84NW	038 13SE	128
15.		087 87NW	022 13SE	112

Paleocurrent data: Tangential to planar foresets
Number of readings: 14 **Vector Mean: 215.6**

	Bedding Strike Dip	Unrotated Strike Dip	Rotated Strike Dip	Current Direction
	074 84SE Overturned			
1.		066 83NW	297 17SW	207
2.		062 72NW	295 26SW	205
3.		058 83NW	319 20SW	229
	072 87SE Overturned			
4.		060 72NW	299 23SW	209
	075 85SE Overturned			
5.		066 71NW	286 25SW	196
6.		064 67NW	288 28SW	198
7.		055 80NW	319 25SW	229
8.		049 73NW	314 35SW	224

9.		057 71NW	302 30SW	212
10.		058 75NW	304 27SW	214
11.		058 84NW	324 20SW	234
12.		068 74NW	285 23SW	195
	076 88SE Overturned			
13.		058 72NW	306 28SW	216
14.		059 86NW	342 16SW	252

Paleocurrent data: Tangential to planar foresets
Number of readings: 1 **Vector Mean: 342.0**

	Bedding Strike Dip	Unrotated Strike Dip	Rotated Strike Dip	Current Direction
	074 84SE Overturned			
1.		068 70SE	072 14NW	342

UPPER Q4: LIME CREEK

Station Number: CH-35-84
Paleocurrent data: Tangential to planar foresets
Plunge of F_2 fold axis: 20° 075
Plunge of F_3 fold axis: 85° 180
Number of readings: N = 10 **Vector Mean: 97.7**

	Bedding Strike Dip	Unrotated Strike Dip	Rotated Strike Dip	Current Direction
	O65 84SE Overturned			
1.		093 85NE	033 29SE	123
2.		091 77SW	355 27NE	085
3.		083 90	030 17SE	120
	070 88SE Overturned			
4.		082 81SE	345 15NE	075
5.		086 70SE	326 25NE	056
6.		087 79SE	347 20NE	077
7.		086 72SE	328 24NE	058
8.		084 86NW	022 17SE	112
9.		080 84NW	053 12SE	143
10.		093 83NE	038 25SE	128

Paleocurrent data: Tangential to planar foresets
Number of readings: N = 8 **Vector Mean: 290.3**

	Bedding Strike Dip	Unrotated Strike Dip	Rotated Strike Dip	Current Direction
	065 84SE Overturned			
1.		048 88NW	351 19SW	261
2.		050 80SE	032 15NW	302
	070 88SE Overturned			
3.		046 87NW	004 25NW	274
4.		046 69SE	330 32SW	240
5.		057 83NW	344 14SW	254
6.		053 79SE	046 19NW	316
7.		062 77SE	072 14NW	342
8.		055 74SE	066 21NW	336

UPPER Q4: COAL CREEK

Station Number: CH-17-84
Paleocurrent data: Tangential to planar foresets
Plunge of F_2 fold axis: 26° 318
Plunge of F_3 fold axis: 85° 180
Number of readings: N = 60 **Vector Mean: 56.8**

	Bedding Strike Dip	Unrotated Strike Dip	Rotated Strike Dip	Current Direction
	319 78SW Overturned			
1.		350 83SW	328 30NE	058
2.		332 78SW	322 14NE	052
3.		337 87SW	310 26NE	040
4.		342 85SW	331 24NE	061
5.		337 77NE	350 20NE	080
6.		338 79NE	346 23NE	076
7.		341 85NE	350 25NE	080
8.		336 88NE	318 24NE	048
9.		331 84SW	334 12NE	064
Station Number: CH-20-84				
	280 74SW Overturned			
10.		082 74SE	338 22NE	068
11.		078 72SE	325 28NE	055
	283 80SW Overturned			
12.		079 68SE	311 26NE	041
13.		076 74SE	322 26NE	052
14.		068 84SE	344 34NE	074
15.		068 78SE	336 34NE	066
	277 78SW Overturned			
16.		068 74SE	320 28NE	050
17.		073 75SE	322 24NE	052
18.		075 78SE	332 21NE	062
	280 82SW Overturned			
19.		082 84SE	347 18NE	077
	281 81SW Overturned			
20.		083 71SE	303 18NE	033
21.		082 78SE	328 18NE	058
	288 87SW Overturned			
22.		082 74SE	320 28NE	050
23.		088 78SE	322 22NE	052
	294 86SW			

	Overturned		
24.	087 79SE	342 28NE	
Station number: CH-23-84			
	316 80SW		
	Overturned		
25.	335 88NE	336 20NE	066
26.	328 89SW	334 18NE	064
27.	332 88SW	336 15NE	066
28.	340 85SW	327 24NE	057
29.	334 75SW	318 19NE	048
30.	332 74SW	316 18NE	046
31.	340 84SW	325 25NE	055
32.	336 77SW	322 20NE	052
33.	341 88NE	335 27NE	065
34.	344 87NE	336 30NE	066
35.	341 75SW	316 24NE	046
36.	332 86NE	339 17NE	069
37.	337 84SW	326 20NE	056
38.	337 83SW	324 21NE	054
39.	333 87SW	327 17NE	057
40.	334 80SW	322 19NE	052
41.	338 76SW	322 21NE	052
42.	335 85SW	334 19NE	066
43.	336 86SW	328 20NE	058
44.	336 86SW	328 20NE	058
45.	334 87SW	328 16NE	058
46.	344 84SW	325 28NE	055
47.	344 82SW	323 28NE	057
48.	342 80SW	323 26NE	057
49.	343 69SW	310 26NE	040
50.	339 67SW	306 24NE	036
51.	340 62SW	302 24NE	032
52.	334 76SW	320 18NE	050
53.	335 86SW	335 19NE	065
54.	338 71SW	313 22NE	041
55.	344 76SW	317 28NE	047
56.	342 82SW	325 25NE	055
57.	337 86SW	328 22NE	058
58.	335 88NE	337 21NE	067
59.	341 90	332 26NE	062
60.	337 88NE	338 22NE	068

Paleocurrent data: Tangential to planar foresets
Number of readings: N = 2 **Vector Mean: 231.0**

	Bedding Strike Dip	Unrotated Strike Dip	Rotated Strike Dip	Current Direction
1.		305 88NE	313 20SW	223
2.		305 78SW	329 10SW	239

UPPER Q2: UNCOMPAHGRE GORGE

Station Number: CH-402-86
Paleocurrent data: Tangential to planar foresets
Plunge of F_2 fold axis: 35° 288
Number of readings: N = 8 **Vector Mean: 239.9**

	Bedding Strike Dip	Unrotated Strike Dip	Rotated Strike Dip	Current Direction
	066 68NW			
1.		047 76NW	344 19SW	254
2.		047 74NW	337 18SW	247
3.		046 79NW	350 22SW	260
4.		046 79NW	350 22SW	260
5.		047 65NW	308 17SW	218
6.		036 70NW	320 28SW	230
7.		044 69NW	318 20SW	228
8.		047 66NW	312 17SW	222

MEDIAL Q3: UNCOMPAHGRE GORGE

Station Number: CH-103-84
Paleocurrent data: Tangential to planar foresets
Plunge of F_2 fold axis: 35° 288
Number of readings: N = 11 **Vector Mean: 206.5**

	Bedding Strike Dip	Unrotated Strike Dip	Rotated Strike Dip	Current Direction
	074 60NW			
1.		044 57NW	312 26SW	222
2.		046 51NW	297 25SW	207
3.		054 52NW	297 18SW	207
4.		053 49NW	288 20SW	198
5.		050 56NW	309 20SW	219
6.		051 51NW	296 21SW	206
7.		048 53NW	303 22SW	213
8.		050 51NW	295 22SW	205
9.		046 55NW	309 24SW	219
10.		048 40NW	275 28SW	185
11.		044 44NW	280 29SW	190

Station Number: CH-104-84
Paleocurrent data: Tangential to planar foresets
Plunge of F_2 fold axis: 35° 288
Number of readings: N = 30 **Vector Mean: 104.5**

	Bedding Strike Dip	Unrotated Strike Dip	Rotated Strike Dip	Current Direction
	O73 55NW			
1.		293 44NE	002 32SE	092
2.		291 38NE	014 32SE	104
3.		295 45NE	001 32SE	091
4.		289 46NE	359 28NE	089
5.		284 43NE	004 26SE	094
6.		287 51NE	349 27NE	079
7.		285 43NE	003 27SE	093
8.		280 41NE	014 24SE	104
9.		286 46NE	359 27NE	089
10.		280 44NE	007 23SE	097
11.		281 38NE	108 26SE	108
12.		284 41NE	011 26SE	101
13.		278 36NE	026 26SE	116
14.		275 30NE	037 28SE	127
15.		284 49NE	353 26NE	083
16.		281 44NE	007 24SE	097
17.		283 50NE	351 24NE	081

18.		284 45NE	001 26SE	091
19.		286 40NE	012 28SE	102
20.		285 45NE	355 26NE	085
	078 58NW			
21.		282 51NE	001 21SE	091
22.		283 50NE	005 22SE	095
23.		281 49NE	008 20SE	098
24.		279 50NE	006 19SE	096
	070 58NW			
25.		073 38NW	050 20SE	140
26.		074 34NW	052 24SE	142
27.		067 38NW	060 21SE	150
28.		075 34NW	050 24SE	140
29.		078 36NW	044 23SE	134
30.		078 30NW	048 28SE	138

Station Number: CH-108-84
Paleocurrent data: Tangential to planar foresets
Plunge of F_2 fold axis: 35° 288
Number of readings: N = 44 **Vector Mean: 145.9**

	Bedding Strike Dip	Unrotated Strike Dip	Rotated Strike Dip	Current Direction
	073 52NW	(70-75 m)		
1.		275 35NE	024 24SE	114
2.		276 34NE	030 25SE	120
3.		275 35NE	024 24SE	114
4.		278 25NE	038 30SE	128
5.		273 34NE	028 22SE	118
6.		276 37NE	024 23SE	114
7.		271 39NE	016 18SE	106
	073 52NW	(72.5 m)		
8.		085 40NW	029 15SE	119
9.		087 38NW	036 17SE	126
10.		089 36NW	035 20SE	125
11.		092 37NE	028 20SE	118
12.		082 32NW	043 22SE	133
13.		084 34NW	044 18SE	134
14.		085 25NW	050 29SE	140
15.		086 32NW	042 23SE	132
16.		090 38N	026 19SE	116
	073 52NW	(73.5 m)		
17.		053 51NW	318 16SW	228
18.		052 50NW	312 16SW	222
19.		048 49NW	309 20SW	219
	073 52NW	(91.0 m)		
20.		086 23NW	051 30SE	141
21.		080 34NW	050 20SE	140
22.		087 36NW	046 20SE	136

23.		097 38NE	019 22SE	109
24.		107 34NE	020 30SE	110
25.		097 36NE	023 24SE	113
	078 58NW	(100 + m)		
26.		082 35NW	058 24SE	148
27.		088 35NW	048 23SE	138
28.		058 42NW	280 22SW	190
29.		057 41NW	278 24SW	188
30.		057 39NW	275 26SW	185
31.		053 40NW	280 26SW	190
32.		058 39NW	275 24SW	185
33.		068 34NW	076 26SE	166
34.		068 30NW	073 30SE	163
35.		060 38NW	271 25SW	181
36.		073 38NW	074 21SE	164
37.		080 33NW	060 26SE	150
38.		078 37NW	062 21SE	152
39.		076 34NW	065 25SE	155
40.		079 30NW	063 29SE	153
41.		073 28NW	067 31SE	157
42.		082 30NW	058 29SE	148
43.		085 30NW	056 30SE	146
44.		080 26NW	061 32SE	151

Paleocurrent data: Tangential to planar foresets
Number of readings: N = 8 **Vector Mean: 82.6**

	Bedding Strike Dip	Unrotated Strike Dip	Rotated Strike Dip	Current Direction
	079 50NW	(176 m)		
45.		291 48NE	352 24NE	082
46.		286 47NE	354 21NE	084
47.		289 51NE	343 23NE	073
48.		288 49NE	348 22NE	078
49.		290 46NE	356 24NE	086
50.		290 47NE	353 24NE	083
51.		289 48NE	351 22NE	081
52.		284 43NE	004 27SE	094

Paleocurrent data: Tangential to planar foresets
Number of readings: N = 6 **Vector Mean: 261.0**

	Bedding Strike Dip	Unrotated Strike Dip	Rotated Strike Dip	Current Direction
	080 51NW (250 m)			
1.		051 60NW	345 25SW	255
2.		055 64NW	359 24NW	269
3.		051 63NW	353 26SW	263
4.		051 62NW	350 26SW	260
5.		048 61NW	345 28SW	255
6.		050 64NW	354 28SW	264

Station Numbers: CH-107-84, CH-108-84
Paleocurrent data: Linear elements perpendicular to symmetrical ripple crests
Number of readings: N = 6 **Vector Mean: 134.2**

	Bedding Strike Dip	Unrotated Plunge Trend	Rotated Plunge Trend	Current Direction
1.	077 56NW	55° 327	0° 315	135-315
2.	078 54NW	54° 008	0° 346	346-166
3.	072 50NW	51° 312	0° 310	310-130
4.	075 59NW	26° 278	0° 098	098-278
5.	078 54NW	43° 046	0° 014	014-194
6.	078 54NW	12° 272	0° 086	086-266

Station Number: CH-108-84
Paleocurrent data: Trough axes
Plunge of F_2 fold axis: 35° 288 **Master Bedding: 075 50NW**
Number of readings: N = 7 **Vector Mean: 218.5**

	Unrotated Azimuth Current	Rotated Azimuth	Current Direction
1.	051 SW	028	208
2.	061 SW	041	221
3.	082 SW	082	262
4.	051 SW	028	208
5.	045 SW	020	200
6.	069 SW	052	232
7.	047 SW	022	202

UPPER Q4: UNCOMPAHGRE GORGE

Station Number: CH-403-86; CH-405-86
Paleocurrent data: Tangential to planar foresets
Plunge of F_2 fold axis: 35° 288
Number of readings: N = 39 **Vector Mean:** 169.0

	Bedding Strike Dip	Unrotated Strike Dip	Rotated Strike Dip	Current Direction
	070 57NW			
1.		040 38NW	276 28SW	186
2.		058 33NW	072 24SE	162
3.		035 36NW	273 32SW	183
4.		048 40NW	273 23SW	183
5.		065 42NW	064 16SE	154
6.		043 44NW	284 24SW	194
7.		048 45NW	280 21SW	190
8.		052 44NW	274 18SW	184
9.		053 43NW	270 17S	180
	(28 m)			
10.		048 48NW	290 19SW	200
11.		055 46NW	274 16SW	184
12.		051 41NW	089 21SE	179
13.		049 43NW	276 21SW	186
14.		052 45NW	280 18SW	190
	(29 m)			
15.		052 38NW	083 22SE	173
16.		051 41NW	089 21SE	179
17.		048 46NW	284 20SW	194
18.		050 40NW	088 22SE	178
19.		046 52NW	302 20SW	212
20.		055 53NW	298 13SW	208
21.		052 43NW	271 18SW	181
22.		054 39NW	079 21SE	169
23.		052 44NW	274 18SW	184
24.		056 44NW	087 17SE	177
	063 60NW			
25.		063 38NW	051 23SE	141
26.		064 36NW	051 25SE	141
27.		068 34NW	046 27SE	136
28.		065 35NW	049 26SE	139
29.		062 44NW	054 17SE	144
30.		066 41NW	048 20SE	138
31.		072 44NW	031 18SE	121
32.		070 45NW	034 16SE	124
33.		062 42NW	055 18SE	145
34.		063 40NW	053 21SE	143
35.		064 35NW	053 26SE	143
36.		053 41NW	071 20SE	161

37.	053 51NW	271 13SW	181
38.	050 40NW	072 22SE	162
39.	053 35NW	064 26SE	154

Station Number: CH-403-86
Paleocurrent data: Trough axes
Plunge of F_2 fold axis: 35° 288 **Master Bedding: 070 57NW**
Number of readings: N = 16 **Vector Mean: 137.9**

Unrotated Azimuth Current	Rotated Azimuth	Current Direction
(4.5-5.25 m)		
1. 014 SW	358	178
2. 298 SE	300	120
3. 006 SW	342	162
4. 326 SE	318	138
(9.0-12.0 m)		
5. 354 SE	334	154
6. 352 SE	333	153
7. 034 SW	003	183
8. 291 SE	294	114
9. 286 SE	290	110
10. 039 SW	008	188
11. 286 SE	290	110
(16.0-18.0 m)		
12. 280 SE	284	104
13. 270 E	090	090
14. 343 SE	328	148
(22.5 m)		
15. 302 SE	304	124
(28.4 m)		
16. 320 SE	315	135

The vita has been removed from the scanned document

Plate 1: Proterozoic Geology of the West Needle Mountains area, San Juan County, Colorado

Explanation of Map Symbols

- Geologic contacts (known, approximate, inferred)
- Faults (known, approximate) - defined by cataclasis and brecciation; sense of movement indicated by U = up, D = down, or split arrows
- Fault zone - comprised of intensely fractured and iron-stained gneiss
- Ductile deformation zones - sense of movement indicated by U = up, D = down, or split arrows
- Bedding (inclined, overturned)

Fabric Elements

- S_{1B} in gneisses
- S_{1B} in gneisses (inclined, vertical)
- S_{3B} in granitoids (inclined, vertical)
- S_{1C} in Uncompahgre Group
- S_{1C} in Uncompahgre Group (inclined, vertical)
- S_m in ductile deformation zones
- Mineral lineation (shown in combination with previous symbols)

Macroscopic Folds

- Antiform (upright symmetric, upright with short arrow on steeper limb)
- Synform (upright symmetric, upright with short arrow on steeper limb, inclined)
- F_{2B} fold axial trace in gneisses - arrow shows plunge direction
- Axial trace of F_{3B} in gneisses and F_{3C} in Uncompahgre Group - arrow shows plunge direction
- F_{3C} fold axial trace in Uncompahgre Group - arrow shows plunge of fold axis
- Asterisk denotes endpoints and bends in section lines

GN | MN

1° 34' | 13 1/2°

1.0 0.5 0 1.0 mile

1.0 0.5 0 1.0 kilometer

Topographic base from U.S.G.S. map of San Juan County, Colorado (1975)

Explanation of Lithologic Units

- **Tp** — Tertiary granitic rocks
- **Tv** — Tertiary volcanic, volcaniclastic, and sedimentary rocks

Unconformity

- **Pz** — Paleozoic sedimentary rocks.

Unconformity

- **▲** — outcrop locations of undifferentiated dike rocks intrusive into Proterozoic lithologies - mafic varieties locally have preserved ophitic textures and primary clinopyroxene although most contain secondary amphibole, biotite, or chlorite; felsic varieties locally contain fluorite and a primary flow foliation; generally ≤ 5 m thick, subvertical, and strike nearly east-west; ages unknown but may range from Precambrian to Tertiary.
- **EG** — Eolus Granite - undeformed, medium- to coarse-grained, megacrystic quartz monzonite; U-Pb zircon age 1430±20 Ma (Silver and Barker, 1968).

Uncompahgre Group

- **P5** — dark gray to black carbonaceous pelite with intercalated very thin-bedded siltstone; preserved thickness ~ 200 m.
- **Q4** — blue gray to white quartz arenite comprising a ~ 300 m-thick, coarsening- and thickening-upward sequence; lower portion consists of thin- to medium-bedded, parallel-laminated to cross-bedded sandstone with intercalated mudstone overlain by coarse-grained to conglomeratic, cross-stratified sandstone; upper portion dominated by massive to stratified conglomerate succeeded by 30-50 m of cross-stratified sandstone.
- **P4** — blue gray to black carbonaceous pelite with interbedded very thin-bedded siltstone and quartz arenite; ~ 200 m thick.
- **Q3** — blue gray to white, medium- to thick-bedded quartz arenite comprising a ~ 250 m-thick, coarsening- and thickening-upward sequence; upper 80 m consists of thin-to medium-bedded, dark blue gray, cross-bedded and parallel-laminated quartz arenite.
- **P3** — maroon to blue-gray pelite with interbedded very thin-bedded quartz arenite; medial portion consists of 2 or 3 coarsening- and thickening-upward, quartz arenite sequences (≤ 25 m thick) overlain by dark gray to black carbonaceous pelite; total thickness ~ 150 m.
- **Q2** — coarsening- and thickening-upward sequence comprised of maroon to gray quartz arenite overlain by pink to white, thick-bedded, cross-stratified quartz arenite; upper portion contains interbedded conglomerate in Grenadier Range and Animas Canyon areas; total thickness ~ 600 m.
- **P1-P2** — maroon and bluish gray pelite with intercalated thin-bedded quartz arenite; 100-200 m thick; pelites contain abundant andalusite porphyroblasts.
- **Q1** — fining-upward sequence comprised of maroon to pinkish gray, massive basal conglomerate grading upward into cross-bedded quartz arenite with conglomerate layers; total thickness ~ 550 m.

Unconformity

WG | TG | • — **Granitoids**

U-Pb zircon age 1694±20 Ma (Silver and Barker, 1968)

WG - Whitehead Granite; complex of weakly foliated granite to quartz monzonite dikes and small intrusive bodies in northern basement domain; contains abundant screens of gneiss; mapped boundaries indicate approximate location where granite becomes predominant over gneiss.

TG - Tenmile Granite; multiphase intrusion of granite, quartz monzonite, granodiorite, and pegmatite in southern basement domain; many dikes intrude gneisses along margins of pluton; contains weak vertical, east-west striking foliation.

• - location of significant granitic pegmatite and aplite bodies intrusive into gneisses.

GBG — **Gabbroic Gneiss**

GBG - texturally homogeneous amphibolite and metagabbro; hb + pl + ttn ± ep ± grt; contacts locally truncate layering in LGm or cut mafic inclusions in GGt.

GGg | GGt | GGu | GGm — **Granitoid Gneiss**

U-Pb zircon age 1753 ± 20 Ma (Silver and Barker, 1968).

GGg - texturally homogeneous leucotonalitic and granitic gneiss; pl + qtz + bt ± ksp ± ep; often contains ellipsoidal patches of epidote.

GGt - texturally homogeneous tonalitic and granodioritic gneiss; pl + qtz + bt ± hb ± ksp ± ep ± grt; ribbony foliation; locally porphyroclastic; abundant ellipsoidal mafic inclusions elongate parallel to foliation.

GGu - undifferentiated granitoid gneiss.

GGm - GGg or GGt interlayered with amphibolite (25-75%) on outcrop scale

LGf | LGm | LGu — **Layered Gneiss**

LGf - felsic gneiss with centimeter- to meter-scale layering; pl + qtz + bt ± grt ± ms ± ksp; some porphyroblastic grt with pressure shadows; gradational into dacite porphyry, breccia, and flow-banded metadacite; locally contains quartz "eyes"

LGm - mafic gneiss with centimeter- to meter-scale layering; hb + pl ± bt ± qtz ± ep ± grt ± act; locally relict amygdules, pillow structures, and volcaniclastic textures.

LGu - mixture of LGf and LGm with coarse-grained pl + bt + ged + qtz ± cum ± grt granofels; includes broken formation zones.

Index Map

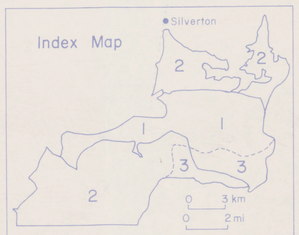

1: C.W. Harris 2: R.G. Gibson

3: F. Barker (1969), B.J. Tewksbury (1981)

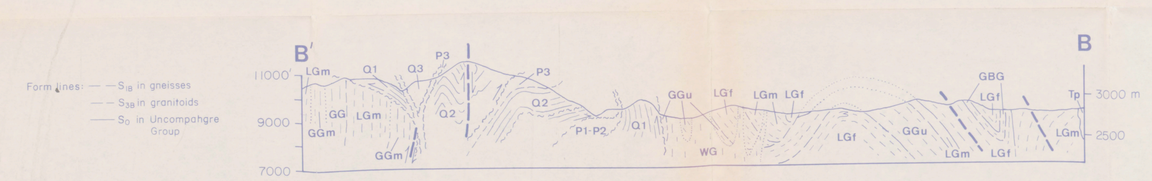

Form lines: — S_{1B} in gneisses — S_{3B} in granitoids — S_0 in Uncompahgre Group

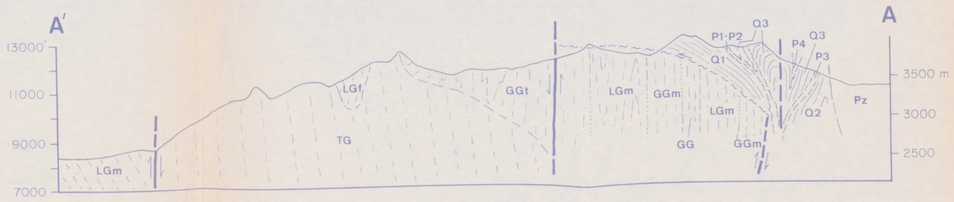

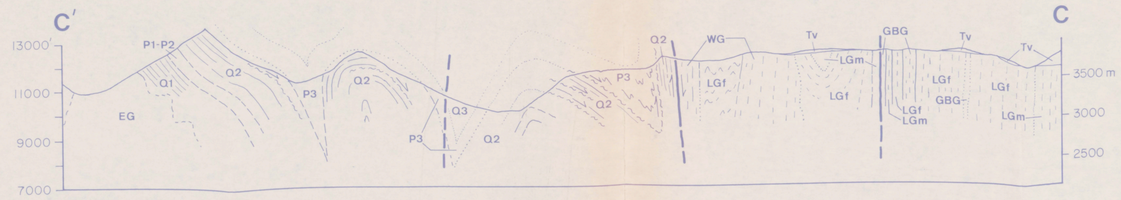

107° 37' 30" 2 70 2 75000 m E

41 75000 m N

41 85

41 80

37° 45'

41 70

107° 45' 2 55 2 60 2 65

A' B' C'

Durango (27mi, 43km)